



UNIVERSITY OF  

---

LIVERPOOL

**Analytical challenges, development and application  
of CLE-ACSV for the determination of  
the organic speciation of iron in marine waters**

Thesis submitted in accordance with the requirements of  
the University of Liverpool for the degree of Doctor in Philosophy by

**Léo Paul Mahieu**

January 2023

Faculty of Science and Engineering

School of Environmental Sciences

Department of Earth, Ocean and Ecological Sciences



*'These aren't problems,  
they're opportunities for distraction.'*  
*'If it was easy, someone else would have done it.'*

*To Adele and Vera, who Standed by me in the little good  
and big bad times and made it possible.*

# Acknowledgment

First of all, I want to thank Pascal Salaün and Stan van den Berg for the trust they placed in me for this project. I also thank Hannah Whitby who joined the supervisory team along the journey and provided so much for this project. A warm thank you to Dario Omanović for his involvement in my work and for sharing his knowledge and passion for electrochemistry, to Gabriel Dulaquais who took the time, energy, and patience to train me despite the complications met, and to Kristen Buck for her time sharing her knowledge on interpreting ligand titration time even on the last day at land before a cruise.

A special thank you for all the collaborators met during this project. It all started by a little talk with Géraldine Sarthou, Eva Bucciarelli and Hélène Planquette from LEMAR, to end up being involved in the Tonga project and participating to cruises on the Anghullas II. I want to thank Cécile Guieu and Sophie Bonnet, project investigator for the Tonga cruise, and Chloé Tilliette, Marc Tedetti, Catherine Guigue and Dominique Lefevre for their implication in my contribution. I want to thank all the great scientists and crew met on the Anghullas II, Susanne Fitz, Thato Mtshali and Alakendra Roychoudhury, and the project investigators of these cruises, Marcello Vichi and Thomas Ryan-Keogh. A very special thank you to the whole TracEx team from Stellenbosch University; exploring the Southern Ocean during winter times made these memories some of my most cherished ones. I also want to thank all the staff I met at the University of Liverpool who facilitated my PhD journey. A special thank you for Paula Houghton and Andrew Gilroy for their efficiency and kindness.

My PhD has been an intense journey, professionally and personally. From the excitement of the beginning, cruising and discovering South-Africa, to the rough times of complication in the lab and worldwide pandemic, until the crazy last year condensing most of my work in, it has been a life. And I would not have made it through without the incredible support I had along it. Thank you to the PhD students of Liverpool University and met through the Doctoral Training Program for sharing the highs and lows; to the beautiful people met in Liverpool, especially Kevin Bayley and Matthew Burk, the best music mates ever; to the raving and travelling buddies with who it has been wild, from Liverpool docks to the North of Scotland; back to France, to the wonderful collective Dose de Bonne Humeur and all

friends around it, always shining in the night even if the sun had risen already; to my beloved parents, sisters, nephews and more; and a special thank you to Meggy; I would not have make it without your unconditional support. I will hope the best for you too.









# Abstract

Iron (Fe) is an essential micronutrient for marine phytoplankton, but its poor solubility in oxic waters is responsible for limited primary production across large parts of the ocean. It has been shown that organic compounds are able to bind with Fe to keep it in the dissolved phase (DFe), thought to be the most bioavailable for phytoplankton. The compounds composing the fraction of the dissolved organic matter (DOM) able to bind with Fe are referred to as Fe-binding ligands. While > 99% of DFe is bound to Fe-binding ligands, the knowledge on their identity and cycling is limited as they represent a very small and diverse fraction of the DOM. There is a one-thousand factor difference between the range of concentrations of Fe-binding ligands and the wider DOM pool (nanomolar and micromolar, respectively), the composition and structure of which is impacted by multiple biological and physical processes. One method to investigate Fe-binding properties of the DOM is to titrate Fe-binding ligands against a calibrated added ligand at different DFe concentrations. This method is called Competitive Ligand Exchange (CLE) using Cathodic Stripping Voltammetry (ACSV). The CLE-ACSV approach allows the estimation of the Fe-binding ligand concentration ( $[L]$ ), and of their average binding strength ( $K^{\text{cond}}$ ). This approach, however, suffers from technical and practical limitations. In this work, I address several limitations of the CLE-ACSV approach and present techniques to improve accessibility for new users and minimise the risk of user subjectivity within data selection. I then apply these to samples collected from the subtropical South Pacific to assess the role of Fe-binding ligands in the distribution and cycling of DFe in waters impacted by intense diazotrophic and hydrothermal activities.

In Chapter 1, I introduce the general background of my work by reviewing the inorganic and organic aspects of DFe speciation. I present in Chapter 2 a description of the CLE-ACSV approach; the concept, the theory, the apparatus, and the technical limitations are discussed to provide general knowledge on the different aspects hampering the application of the CLE-ACSV. In Chapter 3, I address the limitation of the CLE-ACSV approach related to the pH buffering of the sample, a technical requirement of the current methods which are potentially impacting and hampering our understanding of the DFe speciation. In Chapter 4, limitations related to the interpretation and comparability of the CLE-CSV

titrations are addressed. I present a procedure developed to limit the subjectivity of the analyst on the results produced, aiming to ease the comparability of the results between laboratories. Finally, in Chapter 5, I present the application of my CLE-ACSV development on natural samples collected in the Western Tropical South Pacific. Fe-binding ligand data are combined with electrochemical and fluorescence data of the humic fraction, a known contributor to the Fe-binding ligand pool, to interpret the composition and cycling of the fraction of the DOM implicated in DFe distribution in this region. I finally conclude this thesis by sharing some thoughts about how to move forward in this challenging but important research area that marine Fe speciation is.

# Publications and contributions

## Included in the thesis

**Mahieu, L.**, Whitby, H., Omanović, D., van den Berg, C.M.G., Salaün, P.: Catalytic enhancement of the reduction current of iron bound to 1-nitroso-2-naphthol (FeNN<sub>3</sub>) in seawater by adsorptive cathodic stripping voltammetry unbuffered and with low volume requirement. To be submitted to Analytical Letters. ML performed the analysis and prepared the manuscript; WH, OD, vdBCMG and PS revised the manuscript.

**Mahieu, L.**, Whitby, H., Omanović, D., Salaün, P.: Conditioning, equilibration, voltammetric, and data treatment procedures for iron speciation in seawater using salicylaldoxime by cathodic stripping voltammetry. To be submitted to Frontiers in Marine Sciences. ML performed the analysis and prepared the manuscript; WH, OD and PS revised the manuscript.

**Mahieu, L.**, Whitby, H., Dulaquais, G., Tilliette, C., Guigue, C., Tedetti, M., Lefevre, D., Fourier, Bressac, M., P., Sarthou, G., Bonnet, S., Guieu, C., Salaün, P.: Iron-binding by dissolved organic matter in the Western Tropical South Pacific (GEOTRACES cruise GPpr14). To be submitted to Frontiers Research Topic ‘Hydrothermal and submarine volcanic activity: Impacts on ocean chemistry and plankton dynamics’. ML performed the CLE-ACSV analysis and prepared the manuscript; TC and GC provided DFe data; DG and FP provided Fe-eHS data; PG provided Mo-eHS data; GC and TM provided HS-like fluorescence data; LD provided oxygen and AOU data; SG was responsible for the sampling; all authors revised the manuscript.

## Other publications

**Mahieu, L.**, Lo Monaco, C., Metz, N., Fin, J., Mignon, C.: Variability and stability of anthropogenic CO<sub>2</sub> in Antarctic Bottom Water observed in the Indian sector of the Southern Ocean, 1978–2018. Ocean Sciences, 16, 1559–1576, <https://doi.org/10.5194/os-16-1559-2020>, 2020. ML, LMC, MN, FJ and MC sampled and analysed samples; ML prepared the manuscript; LMC and MN revised the manuscript.

Longhini, M. C., **Mahieu, L.**, Sá, F., van den Berg, C.M.G., Salaün, P., Neto, R. R.: Coastal waters contamination by mining tailings: What triggers the stability of iron in the dissolved and soluble fractions? Limnology and Oceanography, 66(1), 171-187, <https://doi.org/10.1002/lno.11595>, 2021. LCM prepared the manuscript; LCM and ML performed the analyses; LCM and SF performed the sampling; all authors revised the manuscript.

# Glossary

Fe: iron

Zn: zinc

Mn: manganese

Ni: nickel

Cu: copper

Co: cobalt

Cd: cadmium

$\mu\text{mol/mol C}$ : micromolar per mol of carbon

M: mol per litre

HNLC: high nutrient-low chlorophyll

DOM: dissolved organic matter

FeL: iron-binding ligands

pH: potential hydrogen

CO<sub>2</sub>: carbon dioxide

O<sub>2</sub>: oxygen

Fe<sup>3+</sup>: ferric ion

Fe<sup>2+</sup>: ferrous ion

CO<sub>3</sub><sup>2-</sup>: carbonate

FeCO<sub>3</sub>: iron carbonate

Fe<sup>3+</sup>OH<sub>n</sub><sup>(3-n)+</sup>: iron (oxy)hydroxides

DFe: dissolved iron

POM: particulate organic matter

EPS: exopolymeric substances

HS: humic and humic-like substances

Fe<sub>aq</sub>: aqueous iron

SFe: soluble iron

CFe: colloidal iron

PFe: particulate iron

DOC: dissolved organic carbon

L: conditional iron-binding ligands

K<sup>cond</sup>: conditional binding strength

CLE: competitive ligand exchange

AL: added ligand

ACSV: adsorptive cathodic stripping voltammetry

DHN: 2,3-dihydroxynaphthalene

TAC: 2-(2-thiazolylazo)-p-cresol

SA: salicylaldehyde

NN: 1-nitroso-2-naphthol

CDOM: chromophoric dissolved organic matter

FDOM: fluorescent dissolved organic matter

FeAL: iron-added ligand complex

$K_{FeL}^{cond}$ : conditional binding strength expressed with respect to  $Fe^{3+}$

$Fe^{3+}AL_x$ : complex of ferric ion and added ligand

MDE: mercury drop electrode

MME: multi-mode electrode

Ag/AgCl: silver chloride

PCTFE: polychlorotrifluoroethylene

KCl: potassium chloride

Ag: silver

nA: nanoampere

KBrO<sub>3</sub>: potassium bromate

H<sub>2</sub>O<sub>2</sub>: hydrogen peroxide

Hg: mercury

L: natural organic binding ligands defined by CLE-ACSV

Fe': free iron

L': free iron-binding ligands

$\alpha_{IN}$ : inorganic side reaction

$K'_{FeL}$ : conditional stability constant with respect to  $Fe^{3+}$

$\beta$ : conditional stability constant

$\alpha$ : side reaction coefficient of the iron-added ligand complex

D: detection window

S: sensitivity

$i_p$ : reductive current measured

EDTA: ethylenediamine tetraacetic acid

$i_{p/0}$ : maximal reductive current measured without ethylenediamine tetraacetic acid

$i_{p/i}$ : attenuated reductive current measured with ethylene diamine tetra acetic acid

$H^+$ : proton

MeOH: methanol

MDW: multiple detection window

h: hours

min: minutes

nMeqFe: nanomole equivalent of iron per litre

OMZ: oxygen minimum zone

HO $^-$ : hydroxides

## List of figures

Figure 1.1. Schematic view of the marine Fe and FeL cycles (black arrows) representing sources, recycling, and export. Water circulation and mixing is also represented (blue arrows). Letters (in black) are referring to table 1. Estimated annual fluxes values (in black, in petagram) are from Worsfold et al. (2014).

Figure 1.2. Schematic representation of Fe chelating bounds a) unchelated, b) in a 1:1 complex, c) in a 1:2 complex, and d) in a 3:2 complex. Black line, full triangle and hatched triangle represent plan, forward and backward bound, respectively. Grey shapes represent organic ligands.

Figure 1.3. Natural (bold black) and practical (light grey) size spectrum scattering of organic (top section) and inorganic (bottom section) forms of Fe in the marine environment. DOM for dissolved organic matter, POM for particulate organic matter, EPS for exopolymeric substances, HS for humic substances, Fe<sub>aq</sub> for aqueous Fe, sFe for soluble Fe, cFe for colloidal Fe, and pFe for particulate Fe. Adapted from Hassler et al. (2017), von der Heyden and Roychoudhoury (2015), Qiu et al. (2021) and Tagliabue et al. (2017).

Figure 1.4. Examples of a) a siderophore with enterobactin (Dertz et al., 2006), b) a HS (Stevenson, 1994) and c) an EPS with succinoglycan (Simsek et al., 2007).

Figure 2.1. Concept of the CLE approach divided in a) sample preparation, b) equilibration and c) resultant Fe partitioning. The light grey curve shows that in absence of FeL, AL complexes all the Fe. The dark grey curve represents the amount of Fe complexed by FeL, (from low to high DFe) first outcompeting the AL until they are saturate, then competing with AL, and finally when all the FeL are saturated. The red curve represents the amount of DFe complexed by the AL. The dots in the plot represent the aliquots. Proportions are only figurative.

Figure 2.2. Process of ACSV measurement (a, b, c) in the diffusion layer (black dashes) of the mercury drop (Hg, in grey) with a) concentration of the Fe<sup>3+</sup>AL<sub>x</sub> complex by application of a fixed potential, b) reduction of the Fe<sup>3+</sup>AL<sub>x</sub> complex by potential scan toward more negative values, and c) reduction of the Fe<sup>3+</sup>AL<sub>x</sub> complex and of O<sub>2</sub> into H<sub>2</sub>O<sub>2</sub> in the case of catalysis with O<sub>2</sub>, and d) recorded voltammograms for deoxygenated (black line) and oxygenated (red line) conditions.

Figure 2.3. Apparatus provided by Metrohm™ for ACSV analysis. It is composed (top, left to right) of a computer with the software NOVA (2.5.1), controlling a potentiostat (μAutolab Type III) and an IME (663) piloting the voltammetric system (663 VA Stand), the stirring, the purge, and the electrodes it is equipped with. The cell (bottom right) contains a glassy carbon auxiliary electrode (1), a stirring rod in Teflon™ (2), a capillary holding the MDE (3), and a Ag/AgCl electrode (4) in a bridge.

Figure 2.4. Screenshot of the simultaneous graphical fittings provided by the software ProMCC in the case of the titration of a seawater sampled in the Atlantic Southern Ocean titrated with 25  $\mu\text{M}$  of salicylaldoxime. The top left window shows the titration curve, the top right window the Langmuir/Gerringa fitting, the bottom left the Ruzic/van den Berg fitting, and the bottom right the Scatchard fitting.

Figure 3.1. Electrode and cell as a) initially used and b) optimised in this study, with 1) the auxiliary electrode, 2a) Teflon stirrer, 2b) home-made stirrer with a vibrator, 3) SMDE, 4a) Ag/AgCl electrode in a glass bridge and 4b) silver wire. The numbers in blue represent the range of volume of sample for each set-up. The solid grey part represents the cell holder.

Figure 3.2. Calibration curve (black line) of the spectrophotometric determination from two diluted NN-MeOH standards over 5 weeks (light grey dots), and an example of the calibration of a NN-MQ solution with 3 dilutions (black dots).

Figure 3.3.  $\text{FeNN}_3$  reduction current with (open circle) and without (filled circle) glass bridge at the auxiliary platinum electrode in CRM NASS-6 diluted in Milli-Q, 2.5 min between each scan.

Figure 3.4. Selected voltammograms of deoxygenation experiment of a UV-irradiated seawater sample at natural pH and spiked with 5  $\text{nmol.L}^{-1}$  of DFe for 30 s deposition. The highest and lowest voltammograms (black lines) correspond to the scan number 1 and 29 and higher and lower  $\text{O}_2$ , respectively. The deoxygenation steps (grey lines) correspond, from higher to lower, to the scans number 2, 5, 10, 15, and 21.

Figure 3.5.  $\text{FeNN}_3$  reduction peak in unbuffered irradiated seawater with the compact (1.5 mL of sample, home-made stirrer with vibrator and a Ag wire as reference electrode; red) and classic (5mL of sample, a Teflon<sup>TM</sup> stirrer and a Ag/AgCl reference electrode; black) systems. The difference in sensitivity is explained by the cleanliness of the mercury.

Figure 3.6. a) Relative peak height for each experiment and b) potential of the  $\text{FeNN}_3$  reduction peak in function of the pH successively alkalinised (filled symbols) and acidified (empty symbols) in UV-irradiated seawater enriched with 5  $\text{nmol.L}^{-1}$  Fe for 60 s deposition. The experiment was performed on samples oxygenated and alkalinised with  $\text{NH}_3$  while buffered with PIPES (circles) and POPSO (triangles), with NaOH with POPSO (squares) and on deoxygenated sample with  $\text{NH}_3$  and POPSO (diamonds).

Figure 3.7.  $\text{FeNN}_3$  reduction peak height in function of the DFe added in UV-irradiated seawater containing 20  $\mu\text{mol.L}^{-1}$  of NN and unbuffered to evaluate the proportionality of the reduction signal with the deposition time applied in a) a deoxygenated sample, and b) an oxygenated sample. Three scans were recorded for each deposition time and DFe addition, and the two closest retained.



Figure 4.1. Stability of the FeSA reduction signal in a buffered open-ocean seawater sample containing  $25 \mu\text{mol.L}^{-1}$  after a) overnight conditioning with  $100 \text{ nmol.L}^{-1}$  of and b) deconditioning of the cell by 15 min rinse with  $0.5 \text{ mol.L}^{-1}$  HCl. 5 scans were recorded if the peak was stable, or until the signal reached 0 nA if unstable. For each DFe addition, the first voltammogram recorded are darkest and become paler with time (90 s between voltammograms with 60 s deposition time).

Figure 4.2. Titration of the open ocean seawater used for voltammetric cell and tubes conditioning with  $25 \mu\text{mol.L}^{-1}$  of SA and buffered at 8.18 with  $10 \text{ mmol.L}^{-1}$  of borate. Duplicates were recorded with a deposition time and potential of 60 s and 0.05 V, respectively. The sample was equilibrated following the sequential procedure equilibration. The black empty dots represent the data selected to determine [L] and  $\log K_{FeL,Fe}^{cond}$  (procedure detailed hereafter). Grey dashed dots represent the discarded data, corresponding to carry-over Fe in the cell from previous analysis at the start of the titration, and saturation of the working electrode with the last aliquot.

Figure 4.3. Reduction current of the FeSA peak after 45 s deposition as a function of the deposition potential applied in a seawater sample buffered to pH 8.18 containing  $25 \mu\text{mol.L}^{-1}$  of SA. Previously published values (-0.05 V and 0.00 V) and the one selected in this study (0.05 V) are noted.

Figure 4.4. Diagram describing the procedure developed for the interpretation of ligand titration data, with n corresponding to the number of voltammograms recorded for each aliquot. RPDi is the Relative Percentage Difference.

Figure 5.1. Map of sampling station of the TONGA cruise (GPpr14) for which FeL characteristics have been measured. The colour of the stations corresponds to the region (coloured labels on the map). Geographic features (in black) such as the main islands, the Tonga trench and the location of the Late'iki islands are also noted.

Figure 5.2. Profile of  $\sigma_0$  (full line, square),  $\text{O}_2$  (full line, diamond), T (temperature, dot line, square), and S (salinity, dot line, diamond) at ST7 with the water mass separations applied in this study. The WSPCW, not present at ST7, is also mentioned to not omit any water mass investigated in this work.

Figure 5.3. Top 600 m and full depth distribution of a)  $\text{O}_2$  and b) DOC concentrations for the Tonga cruise (GEOTRACES GPpr14). The approximative water mass boundaries are defined by  $\text{O}_2$  (see Figure 5.2). The section is separated in 4 segments with, from left to right, the Melanesian basin (ST2 and ST3), the Western Lau basin (ST12, ST4, ST11), the Eastern Lau basin (ST10-T1, ST10-T2, ST10-T3) and the South Pacific gyre (ST6, ST7, ST8). See Figure 5.1 for more details on the sampling locations.

Figure 5.4. Top 600 m and full depth distribution of a) tryptophan-like FDOM, b) HS-like FDOM, and c) eHS for the Tonga cruise (GEOTRACES GPpr14). The approximative water mass boundaries are

defined by  $O_2$  (see Figure 5.2). The section is separated in 4 segments with, from left to right, the Melanesian basin (ST2 and ST3), the Western Lau basin (ST12, ST4, ST11), the Eastern Lau basin (ST10-T1, ST10-T2, ST10-T3) and the South Pacific gyre (ST6, ST7, ST8). See Figure 5.1 for more details on the sampling locations.

Figure 5.5. Top 600 m and full depth distribution of a) DFe, b) [L] and c)  $\log K_{FeL,Fe}^{cond}$  for the Tonga cruise (GEOTRACES GPpr14). The approximative water mass boundaries are defined by  $O_2$  (see Figure 5.2). The section is separated in 4 segments with, from left to right, the Melanesian basin (ST2 and ST3), the Western Lau basin (ST12, ST4, ST11), the Eastern Lau basin (ST10-T1, ST10-T2, ST10-T3) and the South Pacific gyre (ST6, ST7, ST8). See Figure 5.1 for more details on the sampling locations.

Figure 5.6. Box and Whiskers plot of a) [L] and b)  $\log K_{FeL,Fe}^{cond}$  split by the regions and water masses. The mean values of the entire dataset are represented (black dot line). Please refer to Figure 5.2 regarding the acronyms of the water masses.

Figure 5.7. Profiles with depth at a) ST2, b) ST6, and c) ST10-T3. The profiles are showing (from left to right) DFe, tryptophan-like FDOM (dotted line, open circles), HS-like FDOM (full line, open circles), eHS (full line, full circles, bottom axis), [L],  $\log K_{FeL,Fe}^{cond}$ , AOU (open circles), and DOC (full circles, bottom axis).

Figure 5.8. Reduction potential (E) of the Fe-SA complex with depth for a) the entire water column and b) 200 m.

## List of tables

Table 1.1. Notes and references describing Fe and FeL sourcing in the ocean. Letters are referring to Figure 1.1.

Table 2.1. Specificities of the ALs in use for the investigation of FeL by CLE-ACSV.

Table 3.1. Voltammetric set up and procedure of the classic NN method and proposed NN-Air approach to investigate Fe in seawater.

Table 3.2. Buffer used in this study.

Table 3.3. Reproducibility of the mercury drop formation and oxygenation of the sample as shown by the stability of the H<sub>2</sub>O<sub>2</sub> reduction current peak.

Table 4.1. Typical AL concentrations and corresponding detection windows (log D) for the different ALs in use to investigate FeL by CLE-ACSV.  $n$ ,  $K_{FeAL,FeI}^{cond}$  or  $\beta_{FeAL,FeI}^{cond}$  used for the calculation of D were taken in the references.

Table 4.2. DFe concentrations in nmol.L<sup>-1</sup> to be added in 5 mL of seawater sample with 25  $\mu$ M of SA and 10 mM of borate buffer for conditioning of Metal Free (Labcon<sup>TM</sup>) tubes and ligand titration as used in this study. Note that recommendations are different for voltammetric cells.

Table 4.3. Differences in [L] and  $\log K_{FeL,FeI}^{cond}$  on duplicate analyses due to the definition of the sensitivity during titration data fitting. The dispersion corresponds to the standard deviation divided by the mean [L] for  $\Delta[L]$ , and by the acknowledged range covered by a single detection window for  $\Delta \log K_{FeL,FeI}^{cond}$  (2; Apte et al., 1988; Gerringa et al., 2014).

Table 4.4. FeL characteristics of duplicate samples from the Western South Tropical Pacific prepared following the sequential equilibration procedure. The QF is defined as in Section 4.3.4.

Table 4.5. Comparison of the sequential and overnight equilibration procedure on FeL characteristics. The determination of the QF is detailed in Section 4.3.4.

Table 5.1. Table of the Spearman rank correlation ( $\rho$ ) of investigated parameters for the Tonga transect. Blue corresponds to negative correlation, red to positive correlation, and white to absence of correlation. The intensity of the color is proportional to the strength of the correlation. Bold values correspond to  $p < 0.0001$  (higher level of confidence compared to studies discussing Spearman correlation matrixes and including Fe-binding ligands data, e.g. Genovese et al., 2018; Heller et al., 2013).

Table 5.2. Mean values of DFe, extremum ability of eHS to bind DFe, and [L] for the mixed layer and deeper waters.

Table 5.3. Values in surface sample (depth < 20 m) with distance to the hydrothermal site.

# Table of content

Abstract.....	1
Publications and contributions .....	3
Glossary.....	4
List of figures.....	7
List of tables.....	11
Table of content.....	13
<b>1. Introduction.....</b>	<b>19</b>
1.1. The role of iron in the ocean.....	19
1.2. Iron chemistry in the ocean .....	20
1.3. Iron-binding ligands.....	23
1.4. Investigation of iron-binding ligands by voltammetry .....	26
1.5. References .....	27
<b>2. Introducing the CLE-ACSV method .....</b>	<b>39</b>
2.1. Presentation .....	39
2.1.1. Concept of the competitive ligand exchange approach .....	39
2.1.2. ACSV measurement .....	40
2.2. Theory of the CLE.....	43
2.2.1. Calculation of [L] and $\log K_{FeLcond}$ .....	44
2.2.2. Calibration .....	46
2.2.3. Graphical fitting .....	47
2.3. Characteristics of the ALs .....	49

<b>2.4.</b>	<b>Assumption and consideration</b> .....	<b>52</b>
2.4.1.	Sample preparation .....	53
2.4.2.	Chemical and constant assumptions .....	54
2.4.3.	Laboratory vs <i>in situ</i> conditions .....	55
<b>2.5.</b>	<b>Aims of the PhD thesis</b> .....	<b>57</b>
<b>2.6.</b>	<b>References</b> .....	<b>59</b>
	Note for the reader .....	72
<b>3.</b>	<b>Catalytic enhancement of the reduction current of iron bound to 1-nitroso-2-naphthol (FeNN<sub>3</sub>) in seawater by adsorptive cathodic stripping voltammetry unbuffered and with low volume requirement</b> .....	<b>73</b>
	Abstract .....	73
<b>3.1.</b>	<b>Introduction</b> .....	<b>74</b>
<b>3.2.</b>	<b>Method</b> .....	<b>77</b>
3.2.1.	Voltammetric apparatus and procedure .....	77
3.2.2.	Determination of DFe in test waters .....	79
3.2.3.	Reagents .....	79
<b>3.3.</b>	<b>Results and discussion</b> .....	<b>81</b>
3.3.1.	Spectrophotometric determination of the NN stock concentration.....	81
3.3.2.	O <sub>2</sub> catalysis and oxygenation of the sample.....	83
3.3.3.	Voltammetric system adjustment for the NN-Air method.....	84
3.3.4.	Comparison between oxygenated and deoxygenated sample .....	86
3.3.5.	Comparison between compact and classic set up .....	87
3.3.6.	Impact of buffers and pH on Fe-NN <sub>3</sub> signal in presence of O <sub>2</sub> .....	88
3.3.7.	The NN-Air limitation: peak height vs deposition time .....	91
3.3.8.	Suggestions for future work investigating the impact of pH on Fe organic speciation .....	93
<b>3.4.</b>	<b>Conclusion</b> .....	<b>94</b>
<b>3.5.</b>	<b>References</b> .....	<b>95</b>

Note for the reader .....	108
<b>4. Conditioning, equilibration, voltammetric, and data treatment</b>	
<b>procedures for iron speciation in seawater using salicylaldoxime by</b>	
<b>cathodic stripping voltammetry.....</b>	<b>109</b>
<b>Abstract.....</b>	<b>109</b>
<b>4.1. Introduction .....</b>	<b>110</b>
4.1.1. The CLE-ACSV approach.....	111
4.1.2. Added ligand and detection window .....	112
4.1.3. Sample preparation and technical limitations .....	114
<b>4.2. Method.....</b>	<b>116</b>
4.2.1. Apparatus.....	116
4.2.2. Voltammetric procedure.....	117
4.2.3. Reagent preparation.....	117
4.2.4. Sample preparation .....	118
4.2.5. Peak height extraction from voltammetric measurements .....	119
<b>4.3. Result and discussion .....</b>	<b>119</b>
4.3.1. Conditioning procedure for cell and tubes .....	119
4.3.2. Effect of the deposition potential.....	123
4.3.3. Procedure for the interpretation of ligand titrations .....	125
4.3.4. Automated determination of the quality flag within the spreadsheet .....	128
4.3.5. Reproducibility of ligand titrations.....	129
4.3.6. Comparison of equilibration procedure .....	132
<b>4.4. Conclusion.....</b>	<b>136</b>
<b>4.5. References .....</b>	<b>137</b>
<b>Note for the reader .....</b>	<b>143</b>

<b>5. Iron-binding by dissolved organic matter in the Western Tropical South Pacific (GEOTRACES cruise GPpr14)</b> .....	<b>144</b>
<b>Abstract</b> .....	<b>144</b>
<b>5.1. Introduction</b> .....	<b>145</b>
<b>5.2. Material and methods</b> .....	<b>149</b>
5.2.1. Sampling strategy during the TONGA cruise.....	149
5.2.2. Sample collection and storage .....	150
5.2.3. Analyses.....	151
5.2.3.1. <i>O<sub>2</sub> and AOU</i> .....	151
5.2.3.2. <i>DOC</i> .....	151
5.2.3.3. <i>FDOM</i> .....	152
5.2.3.4. <i>Iron-binding ligands</i> .....	152
5.2.4. Statistical treatment .....	154
<b>5.3. Results</b> .....	<b>155</b>
5.3.1. Hydrography.....	155
5.3.2. DOC.....	156
5.3.3. FDOM.....	157
5.3.4. eHS.....	160
5.3.5. DFe.....	160
5.3.1. Iron-binding ligands.....	162
<b>5.4. Discussion</b> .....	<b>163</b>
5.4.1. Comparison of the Fe-binding ligand characteristics with basin scale transects.....	163
5.4.2. Correlation within the dataset and DFe stabilization .....	165
5.4.3. Humic contribution to the Fe-binding ligand pool .....	167
5.4.4. Interpretation of [L] enhancements .....	169
5.4.5. Future and perspective for Fe-binding ligands detection .....	173
5.4.5.1. <i>In hydrothermal waters</i> .....	173
5.4.5.2. <i>Deposition potential with depth and by basins</i> .....	174



5.4.5.3. <i>An unexplored role of iron-sulphides in volcanic arc systems</i> .....	176
<b>5.5. Conclusion</b> .....	<b>178</b>
<b>5.6. References</b> .....	<b>180</b>
<b>6. Conclusion</b> .....	<b>192</b>
6.1. <b>Summary of my findings</b> .....	<b>192</b>
6.2. <b>Future and perspectives</b> .....	<b>194</b>
6.3. <b>References</b> .....	<b>197</b>
<b>7. Annexs</b> .....	<b>199</b>



# Chapter 1

## 1. Introduction

### 1.1. The role of iron in the ocean

Marine phytoplankton is responsible for about half of the worldwide photosynthetic carbon fixation (Field et al., 1998; Friedlingstein et al., 2019). Part of the carbon fixed is exported to the deep ocean, but the export is limited by microbial remineralisation of sinking particles (Bar-On et al., 2018; Friedlingstein et al., 2019). Because microbial activity is dependent on the supply of trace metals, trace metal cycling is an indirect but essential aspect of the carbon cycle (Sunda, 2012).

The trace metals implicated in physiological phytoplankton processes are iron (Fe), zinc (Zn), manganese (Mn), nickel (Ni), copper (Cu), cobalt (Co) and cadmium (Cd; de Baar et al., 2017; Morel and Price, 2003), with Fe being involved in most enzymatic processes (Twining and Baines, 2013). The importance of Fe has been demonstrated by its presence in proteins involved in processes such as photosynthesis and respiration (94 % of the intracellular Fe; Tortell et al., 1999), nitrate and nitrite reduction, detoxification of reactive oxygen, and so on (Twining and Baines, 2013). Consequently, phytoplankton intracellular Fe concentration is about 50 micromole per mol of carbon ( $\mu\text{mol/mol C}$ ), corresponding to about  $1 \mu\text{mol.L}^{-1}$  ( $\mu\text{M}$ ; Morel and Price, 2003), 1,000 to 10,000-fold more than ambient seawater concentration (Liu and Millero, 2002).

The disequilibrium between Fe availability and cellular demand leads to limited phytoplankton growth and carbon export (Tortell et al., 1996), notably in high nutrient-low chlorophyll (HNLC) regions (Moore et al., 2013). There, major macronutrients (i.e. nitrate, phosphate and silicate) are in ample abundance in surface waters, yet phytoplankton abundance (proxied by chlorophyll *a*) is very low (Chisholm and Morel, 1991). The major HNLC regions are the Southern Ocean, the Subarctic North Pacific, and the equatorial Pacific. The relation between Fe and phytoplankton growth was thoroughly investigated in those regions through fertilisation experiments (de Baar et al., 2005; Laglera et al.,

2019), but at first in bottle incubation experiments (Buma et al., 1991; Coale, 1991; de Baar et al., 1990; Martin et al., 1990, 1989; Martin and Fitzwater, 1988). Bottle experiments are still widely used notably to investigate co-limitations with other major nutrients (i.e. Bertrand et al., 2007; Browning et al., 2021; Schoffman et al., 2016), and to investigate the link between dissolved organic matter (DOM), Fe availability, and phytoplanktonic carbon and nitrogen fixation (Avendaño et al., 2016; Gledhill et al., 2015; Hoppe et al., 2013; Mills et al., 2004; Schuback et al., 2015; Shi et al., 2010). These incubation experiments highlighted that Fe concentration in seawater and bioavailability to microbes is dependent on its chemical speciation. While the inorganic speciation of Fe is relatively well understood, there are still a lot of unknowns in the role of dissolved organic matter (DOM) in Fe organic speciation due the complexity of the DOM pool (Dittmar et al., 2021; Mentges et al., 2017; Millero, 2001). This Chapter will provide a comprehensive review of the chemistry responsible for the Fe distribution in the ocean.

## **1.2. Iron chemistry in the ocean**

Fe is the fourth most concentrated element in the Earth crust (5.6 %; Millero, 2001; Taylor, 1964). It is naturally extracted from the Earth crust by erosion, and release within hydrothermal fluids. Fe sources to the ocean are atmospheric deposition, river runoff, sediment exchange, sea-ice melting, and hydrothermal input (Blazevic et al., 2016; Cheize et al., 2019; Dale et al., 2015; Findlay et al., 2019; Hopwood et al., 2019; Krachler et al., 2015; Lannuzel et al., 2016; Mahowald et al., 2009; Poulton and Raiswell, 2002; Tagliabue et al., 2010; Tagliabue, 2014; Tagliabue et al., 2014a; Tagliabue and Resing, 2016). Recycling and re-supply processes include microbial remineralisation and water mixing (Boyd et al., 2010; Tagliabue et al., 2014b), while the main Fe sink is the burial of particulate Fe in sediments (Ingall et al., 2013). The processes driving Fe distribution in the ocean (Table 1.1) are tightly linked to those distributing Fe-binding organic ligands (FeL; Table 1.1). The FeL cycle and composition is developed in Section 1.3.

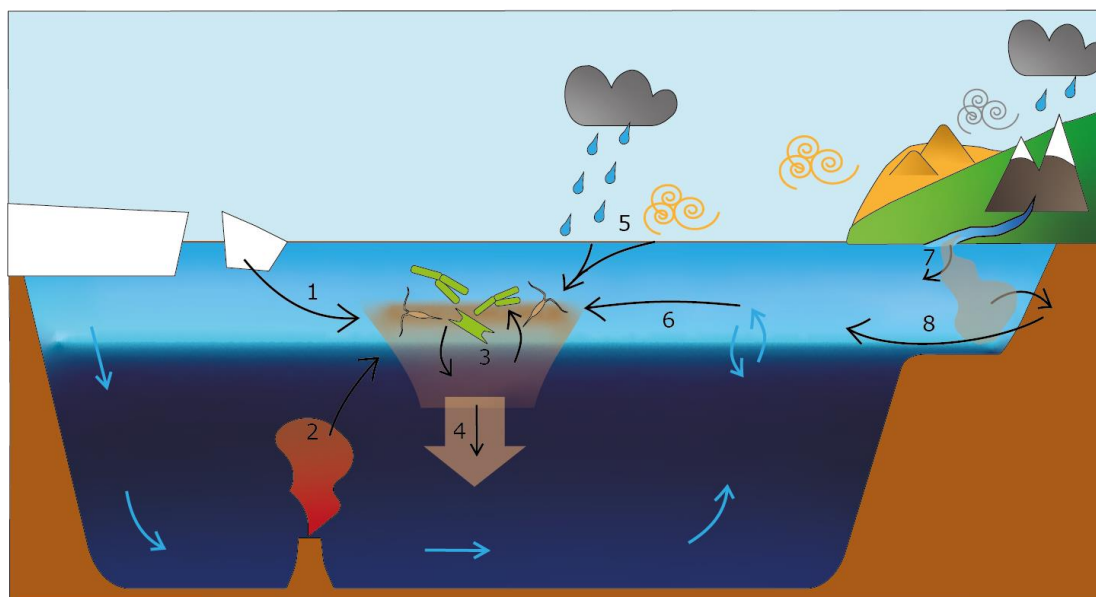


Figure 1.2. Schematic view of the marine Fe and FeL cycles (black arrows) representing sources, recycling, and export. Water circulation and mixing is also represented (blue arrows). Letters (in black) are referring to table 1.1.

Table 1.1. Notes and references describing Fe and FeL sourcing in the ocean. Letters are referring to Figure 1.1.

Number and name of the process	Notes and references for DFe	Notes and references for FeL
1 – Sea-ice melting	Only at high latitude Hopwood et al., 2019; Lannuzel et al., 2016	Only at high latitude Genovese et al., 2018; Janssens et al., 2018
2 – Hydrothermal input	Findlay et al., 2019; Tagliabue, 2014; Tagliabue et al., 2010; Tagliabue and Resing, 2016	Hawkes et al., 2013; Kleint et al., 2016; Wang et al., 2022
3 – Microbial remineralisation	Boyd et al., 2010	Boiteau et al., 2016; Raymond et al., 2015; Velasquez et al., 2016; Whitby et al., 2020
4 – Particulate burial	Ingall et al., 2013	
5 – Atmospheric deposition	Mainly through dust deposition from arid regions Mahowald et al., 2009	Observed in rainwater Cheize et al., 2012; Fitzsimmons et al., 2015
6 – Mixing re-supply	Tagliabue et al., 2014b	Hassler et al., 2019
7 – River runoff	Blazevic et al., 2016; Krachler et al., 2015; Poulton and Raiswell, 2002	Krachler et al., 2015; Slagter et al., 2017; Williford et al., 2021
8 – Sediment exchange	Cheize et al., 2019; Dale et al., 2015	Bundy et al., 2014

The potential hydrogen (pH) range and redox potential of the ocean, driven by dissolved carbon dioxide (CO<sub>2</sub>) and oxygen (O<sub>2</sub>), respectively, are responsible for the low solubility of Fe in oxic seawater. Free cationic forms of Fe, mostly ferric ion (Fe<sup>3+</sup>) but also ferrous (Fe<sup>2+</sup>), are very reactive in the presence of O<sub>2</sub> at seawater pH. They are stabilised by chelation, the sharing of electrons with surrounding compounds to reach a lower level of energy. The diversity of those chelates, also known as complexes, is infinite in terms of geometry and chelating agents (Figure 1.2; Burgess and Twigg, 2006; Cotton, 1972), but a simplified view of Fe chemistry in the ocean can be depicted (Figure 1.3). On the inorganic side, Fe<sup>2+</sup> reacts with carbonate (CO<sub>3</sub><sup>2-</sup>) to form iron carbonate (FeCO<sub>3</sub>) and with sulphur compounds and sulphides (Rickard and Luther, 2007), while the most abundant Fe<sup>3+</sup> is hydrolysed and forms Fe (oxy)hydroxides (Fe<sup>3+</sup>OH<sub>n</sub><sup>(3-n)+</sup>). Fe sulfoxides aggregate into Fe sulphides solid (Rickard and Luther, 2007) while Fe (oxy)hydroxides aggregate into colloidal form or adsorb onto particulate material, both being ultimately exported to the sediment (Liu and Millero, 2002). This essential process is known as scavenging. Inorganic Fe chelates are essential for phytoplankton growth in some oceanic regions (Chen and Wang, 2001; McQuaid et al., 2018; Morel et al., 2008), but are not enough to explain phytoplankton growth in most of the ocean. The introduction of the Fe organic chelation, or organic speciation, is necessary to explain microbial activity (Lis et al., 2015; Shaked et al., 2020). The most stable and, therefore, abundant geometry of Fe<sup>3+</sup> organic chelates is octahedral, which consists of 6 bonds with Fe binding sites that can be found on one or several organic chelators (Figure 1.2).

Those organic chelators, called ligands, have a virtually infinite diversity with a recent estimation of up to 600,000 different compounds of low molecular weight, keeping Fe in the dissolved phase (DFe; Dittmar et al., 2021), which is defined as the fraction passing through filters with a porosity of 0.2 µm or 0.45 µm. The investigation of trace metal chemistry is eased by decomposition into different size fractions (Figure 1.3). Most of the organically-complexed Fe is in the dissolved phase, which is also considered the bioavailable fraction, justifying the focus on the DFe fraction (Worsfold et al., 2014). In open ocean waters where anthropogenic impacts are limited, DFe concentration presents a nutrient-like profile, with low subsurface concentrations due to phytoplankton uptake, an increase inversely proportional to O<sub>2</sub> concentrations due to a supply from microbial remineralisation, and below the O<sub>2</sub>

minimum, a relative equilibrium between decrease with depth due to scavenging and increase with remineralisation, balanced by the Fe solubility of the studied seawater (Johnson et al., 1997).

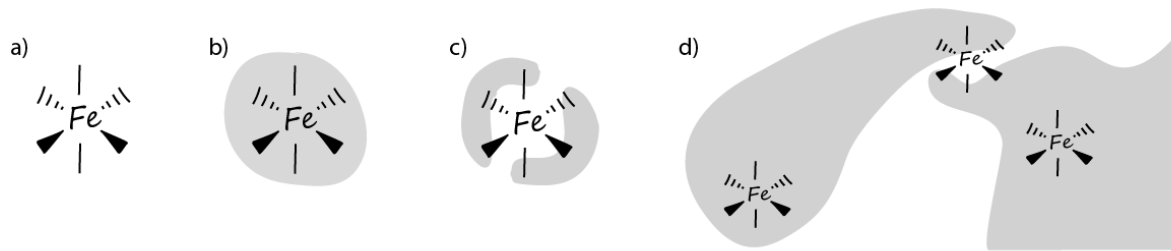


Figure 1.3. Schematic representation of Fe chelating bonds a) unchelated, b) in a 1:1 complex, c) in a 1:2 complex, and d) in a 3:2 complex. Black line, full triangle and hatched triangle represent plan, forward and backward bond, respectively. Grey shapes represent organic ligands.

In open-ocean waters, DFe concentrations range between 0.02-2 nM (Tagliabue et al., 2012), while Fe solubility has been shown to be only of 0.01 nM in artificial seawater without organic ligands (Liu and Millero, 2002). In fact, ligands have been shown to bind more than 99% of the DFe pool in most ocean regions (as listed by Mohamed et al., 2011). The capability of ligands to limit Fe hydrolysis is demonstrated by the enhancement of DFe solubility by a factor of 2 to 200 times, and in specific cases, reaching up to 10,000 times. Indeed, concentrations of tens to even thousands of nM of DFe were measured in coastal waters impacted by human activities (Longhini et al., 2021; Su et al., 2016). These extremely high concentrations, related to the presence of anthropogenic FeL, illustrate the potential of organic compounds to enhance Fe solubility. The expected subsequent phytoplankton growth is, however, dependent on the bioavailability of the chelated Fe, which in turn, depends on the chemistry of the seawater, on the physiology of the cell, and on the chelator chemical structure.

### 1.3. Iron-binding ligands

Despite its crucial importance in the Fe cycle, our understanding of organic DFe speciation is limited by the chemical diversity of DOM (Dittmar et al., 2021; Mentges et al., 2017) and the difficulty to isolate distinct compounds within DOM, limiting the identification of FeL (Dulaquais et al., 2018; Laglera et al., 2011). Yet, three major types of ligand are commonly used to describe FeL distribution in the ocean (Hassler et al., 2017). These ligands are siderophores, humic and humic-like substances (HS), and exopolymeric substances (EPS; Figure 1.4). Siderophores are strong Fe-binding molecules

with low molecular weight produced by bacteria to help them reach their Fe requirement (Hopkinson and Morel, 2009). Part of the siderophores are photo-reactive, and their breakdown leads to the reduction of  $\text{Fe}^{3+}$  into  $\text{Fe}^{2+}$ , which can potentially be oxidized back into  $\text{Fe}^{3+}$  and chelated by siderophore photoproducts (Barbeau et al., 2001). Despite their relatively low concentrations throughout the water column, siderophores can substantially sustain DFe requirements where microbial production occurs (Bundy et al., 2018; Hassler et al., 2015; Hopkinson and Morel, 2009; Norman et al., 2015). They have a relatively low diversity compared to the two other main classes of FeL, but even for this simpler ligand class, many distinct siderophore compounds exist and biological uptake processes are highly diverse (Amin et al., 2012, 2009; Raymond et al., 2015).

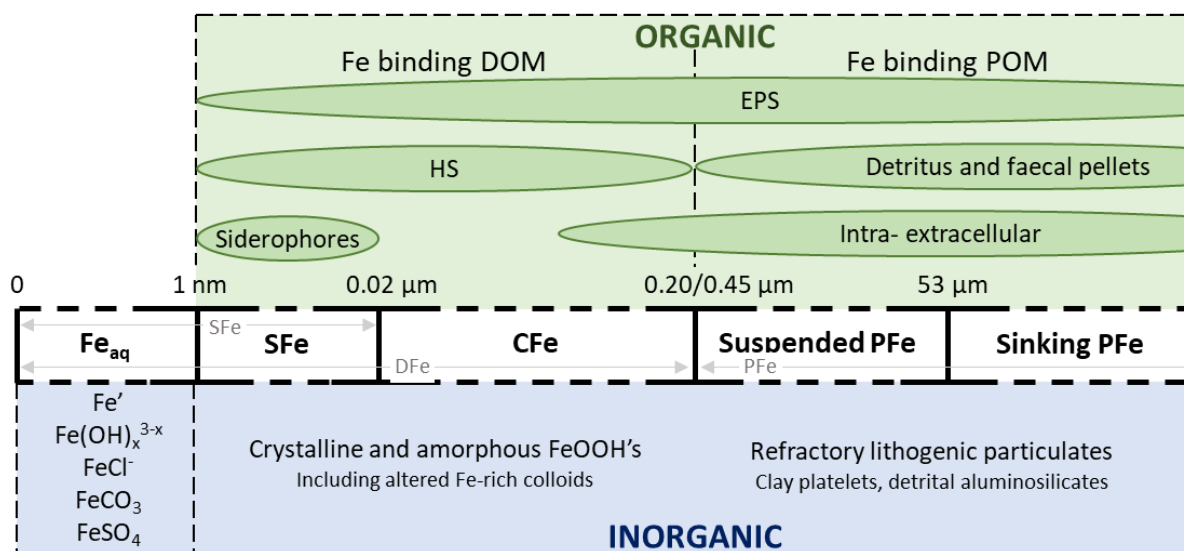


Figure 1.4. Natural (bold black) and practical (light grey) size spectrum scattering of organic (top section) and inorganic (bottom section) forms of Fe in the marine environment. DOM for dissolved organic matter, POM for particulate organic matter, EPS for exopolymers, HS for humic substances, Fe<sub>aq</sub> for aqueous Fe, SFe for soluble Fe, CFe for colloidal Fe, and PFe for particulate Fe. Adapted from Hassler et al. (2017), von der Heyden and Roychoudhury (2015), Qiu et al. (2021) and Tagliabue et al. (2017).

HS are produced by the decomposition of terrestrial as well as oceanic organic matter. HS have significant control on DFe distribution in deep and coastal waters (Whitby et al., 2020). HS represent around 50% of the entire dissolved organic carbon (DOC) pool (Zigah et al., 2017). Some HS can bind Fe and (part of) this fraction can be quantified by voltammetry, referred to as electroactive HS (eHS), representing around 5% of DOC (Dulaquais et al., 2018; Laglera et al., 2011). HS composition and characteristics are poorly constrained because of the almost infinite breakdown and agglomeration pathways they experience. Yet, the definition of reference material has helped develop methodologies



to estimate the amount and binding ability of the metal-binding eHS fraction (Abualhaija et al., 2015; Laglera et al., 2007; Pernet-Coudrier et al., 2013; Quentel et al., 1987; Sukekava et al., 2018; Whitby and van den Berg, 2015). A combination of those approaches, with complementary analysis such as fluorescence, separation and extraction techniques are a step forward in the understanding of the composition of the Fe-binding fraction of DOM (Fourrier et al., 2022), even if the characterised fraction may differ between the different techniques applied.

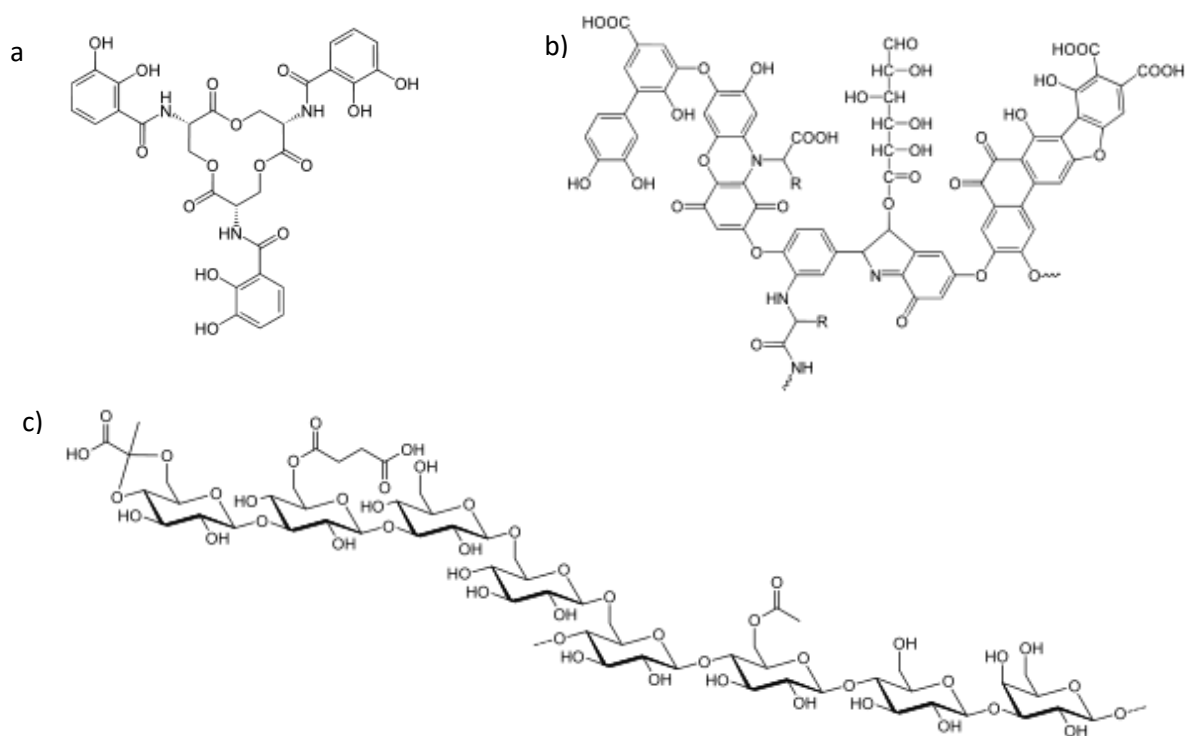


Figure 1.5. Examples of a) a siderophore with enterobactin (Dertz et al., 2006), b) a HS (Stevenson, 1994) and c) an EPS with succinoglycan (Simsek et al., 2007).

The term EPS is used to classify marine organism exudate material, composed mostly of polysaccharides but also amino acids and protein (Nichols et al., 2005). EPS form a sticky layer rich in micro and macronutrients kept at the surface of living organisms that enhances biological Fe uptake (Hassler et al., 2015). EPS represent around 50% of the DOC pool (Benner et al., 1992), but the EPS and HS pools may overlap (Figure 1.3). Some EPS can be made of combined HS, and EPS degradation can contribute to HS formation. Isolated EPS have been shown to contain high levels of bioavailable Fe (Hassler et al., 2015; Norman et al., 2015). EPS are, therefore, a major pathway to store and provide nutrients to microorganisms and their predators.

## 1.4. Investigation of iron-binding ligands by voltammetry

The complexes formed by Fe and its chelators are characterized by the strength of the electrostatic interaction binding them. In line with the DOM diversity, the virtually unlimited chelation possibilities of unique binding strengths challenge the separation and characterisation of the different chelates. The most widely used approach to investigate trace metal organic speciation allows the estimation of the conditional iron-binding ligand concentration ( $[L]$ ) and conditional binding strength ( $K^{\text{cond}}$ ) of the FeL bulk by electrochemical analysis. This approach consists of competitive ligand exchange (CLE) against an added ligand (AL) followed by cathodic stripping voltammetry of the adsorbed compound (ACSV). There are currently four ALs in use: 2,3-dihydroxynaphthalene (DHN; Sanvito and Monticelli, 2020; van den Berg, 2006), 2-(2-thiazolylazo)-p-cresol (TAC; Croot and Johansson, 2000), salicylaldoxime (SA; Abualhaija and van den Berg, 2014; Buck et al., 2007; Rue and Bruland, 1995), and 1-nitroso-2-naphthol (NN; Gledhill and van den Berg, 1994; van den Berg, 1995). All require slightly different methods of implementation and experience specific limitations. The use of the different AL shows limited agreement (Ardiningsih et al., 2021; Buck et al., 2012; Genovese et al., 2022; Gerringa et al., 2021) because of practical and chemical limitations for the application of the CLE-ACSV approach. The CLE-ACSV approach and its limitations are detailed in the next Chapter.

## 1.5. References

- Abualhaija, M.M., van den Berg, C.M.G., 2014. Chemical speciation of iron in seawater using catalytic cathodic stripping voltammetry with ligand competition against salicylaldehyde. *Mar. Chem.* 164, 60–74. <https://doi.org/10.1016/j.marchem.2014.06.005>
- Abualhaija, M.M., Whitby, H., van den Berg, C.M.G., 2015. Competition between copper and iron for humic ligands in estuarine waters. *Mar. Chem.* 172, 46–56. <https://doi.org/10.1016/j.marchem.2014.06.00510.1016/j.marchem.2015.03.010>
- Aldrich, A.P., van den Berg, C.M.G., 1998. Determination of Iron and Its Redox Speciation in Seawater Using Catalytic Cathodic Stripping Voltammetry. *Electroanalysis* 10, 369–373. [https://doi.org/10.1002/\(SICI\)1521-4109\(199805\)10:6<369::AID-ELAN369>3.0.CO;2-W](https://doi.org/10.1002/(SICI)1521-4109(199805)10:6<369::AID-ELAN369>3.0.CO;2-W)
- Altmann, R.S., Buffle, J., 1988. The use of differential equilibrium functions for interpretation of metal binding in complex ligand systems: Its relation to site occupation and site affinity distributions. *Geochim. Cosmochim. Acta* 52, 1505–1519. [https://doi.org/10.1016/0016-7037\(88\)90221-9](https://doi.org/10.1016/0016-7037(88)90221-9)
- Amin, S.A., Green, D.H., Gärdes, A., Romano, A., Trimble, L., Carrano, C.J., 2012. Siderophore-mediated iron uptake in two clades of *Marinobacter* spp. associated with phytoplankton: the role of light. *BioMetals* 25, 181–192. <https://doi.org/10.1007/s10534-011-9495-5>
- Amin, S.A., Green, D.H., Hart, M.C., Küpper, F.C., Sunda, W.G., Carrano, C.J., 2009. Photolysis of iron–siderophore chelates promotes bacterial–algal mutualism. *Proc. Natl. Acad. Sci.* 106, 17071–17076. <https://doi.org/10.1073/pnas.0905512106>
- Apte, S.C., Gardner, M.J., Ravenscroft, J.E., 1988. An evaluation of voltammetric titration procedures for the determination of trace metal complexation in natural waters by use of computers simulation. *Anal. Chim. Acta* 212, 1–21. [https://doi.org/10.1016/S0003-2670\(00\)84124-0](https://doi.org/10.1016/S0003-2670(00)84124-0)
- Ardiningsih, I., Zhu, K., Lodeiro, P., Gledhill, M., Reichart, G.-J., Achterberg, E.P., Middag, R., Gerringa, L.J.A., 2021. Iron Speciation in Fram Strait and Over the Northeast Greenland Shelf: An Inter-Comparison Study of Voltammetric Methods. *Front. Mar. Sci.* 7. <https://doi.org/10.3389/fmars.2020.609379>
- Avendaño, L., Gledhill, M., Achterberg, E.P., Rérolle, V.M.C., Schlosser, C., 2016. Influence of Ocean Acidification on the Organic Complexation of Iron and Copper in Northwest European Shelf Seas; a Combined Observational and Model Study. *Front. Mar. Sci.* 3. <https://doi.org/10.3389/fmars.2016.00058>
- Barbeau, K., Rue, E.L., Bruland, K.W., Butler, A., 2001. Photochemical cycling of iron in the surface ocean mediated by microbial iron(III)-binding ligands. *Nature* 413, 409–413. <https://doi.org/10.1038/35096545>
- Bar-On, Y.M., Phillips, R., Milo, R., 2018. The biomass distribution on Earth. *Proc. Natl. Acad. Sci.* 115, 6506–6511. <https://doi.org/10.1073/pnas.1711842115>
- Benner, R., Pakulski, J.D., Mccarthy, M., Hedges, J.I., Hatcher, P.G., 1992. Bulk Chemical Characteristics of Dissolved Organic Matter in the Ocean. *Science* 255, 1561–1564. <https://doi.org/10.1126/science.255.5051.1561>
- Bertrand, E.M., Saito, M.A., Rose, J.M., Riesselman, C.R., Lohan, M.C., Noble, A.E., Lee, P.A., DiTullio, G.R., 2007. Vitamin B12 and iron colimitation of phytoplankton growth in the Ross Sea. *Limnol. Oceanogr.* 52, 1079–1093. <https://doi.org/10.4319/lo.2007.52.3.1079>
- Blazevic, A., Orłowska, E., Kandioller, W., Jirsa, F., Keppler, B.K., Tafili-Kryeziu, M., Linert, W., Krachler, R.F., Krachler, R., Rompel, A., 2016. Photoreduction of Terrigenous Fe-Humic Substances Leads to Bioavailable Iron in Oceans. *Angew. Chem. Int. Ed.* 55, 6417–6422. <https://doi.org/10.1002/anie.201600852>
- Boiteau, R.M., Mende, D.R., Hawco, N.J., McIlvin, M.R., Fitzsimmons, J.N., Saito, M.A., Sedwick, P.N., DeLong, E.F., Repeta, D.J., 2016. Siderophore-based microbial adaptations to iron scarcity across the eastern Pacific Ocean. *Proc. Natl. Acad. Sci.* 113, 14237–14242. <https://doi.org/10/f9fvs4>

- Bondietti, G., Sinniger, J., Stumm, W., 1993. The reactivity of FE(III) (hydr)oxides: Effects of ligands in inhibiting the dissolution. *Colloids Surf. Physicochem. Eng. Asp.* 79, 157–167. [https://doi.org/10.1016/0927-7757\(93\)80171-A](https://doi.org/10.1016/0927-7757(93)80171-A)
- Boyd, P.W., Ibsanmi, E., Sander, S.G., Hunter, K.A., Jackson, G.A., 2010. Remineralization of upper ocean particles: Implications for iron biogeochemistry. *Limnol. Oceanogr.* 55, 1271–1288. <https://doi.org/10.4319/lo.2010.55.3.1271>
- Boye, M., van den Berg, C.M.G., de Jong, J.T.M., Leach, H., Croot, P., de Baar, H.J.W., 2001. Organic complexation of iron in the Southern Ocean. *Deep Sea Res. Part Oceanogr. Res. Pap.* 48, 1477–1497. [https://doi.org/10.1016/S0967-0637\(00\)00099-6](https://doi.org/10.1016/S0967-0637(00)00099-6)
- Browning, T.J., Achterberg, E.P., Engel, A., Mawji, E., 2021. Manganese co-limitation of phytoplankton growth and major nutrient drawdown in the Southern Ocean. *Nat. Commun.* 12, 884. <https://doi.org/10.1038/s41467-021-21122-6>
- Buck, K.N., Lohan, M.C., Berger, C.J.M., Bruland, K.W., 2007. Dissolved iron speciation in two distinct river plumes and an estuary: Implications for riverine iron supply. *Limnol. Oceanogr.* 52, 843–855. <https://doi.org/10.4319/lo.2007.52.2.0843>
- Buck, K.N., Moffett, J., Barbeau, K.A., Bundy, R.M., Kondo, Y., Wu, J., 2012. The organic complexation of iron and copper: an intercomparison of competitive ligand exchange-adsorptive cathodic stripping voltammetry (CLE-ACSV) techniques. *Limnol. Oceanogr. Methods* 10, 496–515. <https://doi.org/10.4319/lom.2012.10.496>
- Buck, K.N., Sedwick, P.N., Sohst, B., Carlson, C.A., 2018. Organic complexation of iron in the eastern tropical South Pacific: Results from US GEOTRACES Eastern Pacific Zonal Transect (GEOTRACES cruise GP16). *Mar. Chem., The U.S. GEOTRACES Eastern Tropical Pacific Transect (GP16)* 201, 229–241. <https://doi.org/10.1016/j.marchem.2017.11.007>
- Buck, K.N., Sohst, B., Sedwick, P.N., 2015. The organic complexation of dissolved iron along the U.S. GEOTRACES (GA03) North Atlantic Section. *Deep Sea Res. Part II Top. Stud. Oceanogr.* 116, 152–165. <https://doi.org/10.1016/j.dsr2.2014.11.016>
- Buma, A.G.J., de Baar, H.J.W., Nolting, R.F., van Bennekom, A.J., 1991. Metal enrichment experiments in the Weddell-Scotia Seas: Effects of iron and manganese on various plankton communities. *Limnol. Oceanogr.* 36, 1865–1878. <https://doi.org/10.4319/lo.1991.36.8.1865>
- Bundy, R.M., Biller, D.V., Buck, K.N., Bruland, K.W., Barbeau, K.A., 2014. Distinct pools of dissolved iron-binding ligands in the surface and benthic boundary layer of the California Current. *Limnol. Oceanogr.* 59, 769–787. <https://doi.org/10.4319/lo.2014.59.3.0769>
- Bundy, R.M., Boiteau, R.M., McLean, C., Turk-Kubo, K.A., McIlvin, M.R., Saito, M.A., Van Mooy, B.A.S., Repeta, D.J., 2018. Distinct Siderophores Contribute to Iron Cycling in the Mesopelagic at Station ALOHA. *Front. Mar. Sci.* 5. <https://doi.org/10.3389/fmars.2018.00061>
- Burgess, J., Twigg, M.V., 2006. Iron: Inorganic & Coordination Chemistry Based in part on the article Iron: Inorganic & Coordination Chemistry by Pelham N. Hawker & Martyn V. Twigg which appeared in the Encyclopedia of Inorganic Chemistry, First Edition., in: *Encyclopedia of Inorganic Chemistry*. John Wiley & Sons, Ltd. <https://doi.org/10.1002/0470862106.ia108>
- Caprara, S., Buck, K.N., Gerringa, L.J.A., Rijkenberg, M.J.A., Monticelli, D., 2016. A Compilation of Iron Speciation Data for Open Oceanic Waters. *Front. Mar. Sci.* 3. <https://doi.org/10.3389/fmars.2016.00221>
- Caprara, S., Laglera, L.M., Monticelli, D., 2015. Ultrasensitive and Fast Voltammetric Determination of Iron in Seawater by Atmospheric Oxygen Catalysis in 500  $\mu$ L Samples. *Anal. Chem.* 87, 6357–6363. <https://doi.org/10.1021/acs.analchem.5b01239>
- Cheize, M., Planquette, H.F., Fitzsimmons, J.N., Pelleter, E., Sherrell, R.M., Lambert, C., Bucciarelli, E., Sarthou, G., Le Goff, M., Liorzou, C., Chéron, S., Viollier, E., Gayet, N., 2019. Contribution of resuspended sedimentary particles to dissolved iron and manganese in the ocean: An experimental study. *Chem. Geol.* 511, 389–415. <https://doi.org/10.1016/j.chemgeo.2018.10.003>

- Cheize, M., Sarthou, G., Croot, P.L., Bucciarelli, E., Baudoux, A.-C., Baker, A.R., 2012. Iron organic speciation determination in rainwater using cathodic stripping voltammetry. *Anal. Chim. Acta* 736, 45–54. <https://doi.org/10.1016/j.aca.2012.05.011>
- Chen, M., Wang, W.-X., 2001. Bioavailability of natural colloid-bound iron to marine plankton: Influences of colloidal size and aging. *Limnol. Oceanogr.* 46, 1956–1967. <https://doi.org/10.4319/lo.2001.46.8.1956>
- Chisholm, S.W., Morel, F.M., 1991. *Limnology and Oceanography*, Volume 36, Number 8, December 1991. What Controls Phytoplankton Production in Nutrient-Rich Areas of the Open Sea?
- Cloete, R., Loock, J.C., van Horsten, N.R., Menzel Barraqueta, J.-L., Fietz, S., Mtshali, T.N., Planquette, H., García-Ibáñez, M.I., Roychoudhury, A.N., 2021. Winter dissolved and particulate zinc in the Indian Sector of the Southern Ocean: Distribution and relation to major nutrients (GEOTRACES G1pr07 transect). *Mar. Chem.* 236, 104031. <https://doi.org/10.1016/j.marchem.2021.104031>
- Coale, K., 1991. Effects of Iron, Manganese, Copper, and Zinc Enrichments on Productivity and Biomass in the Sub-Arctic Pacific. *Limnol. Oceanogr.* 36, 1851–1864. <https://doi.org/10.4319/lo.1991.36.8.1851>
- Cotton, S.A., 1972. Some aspects of the coordination chemistry of iron(III). *Coord. Chem. Rev.* 8, 185–223. [https://doi.org/10.1016/S0010-8545\(00\)80028-4](https://doi.org/10.1016/S0010-8545(00)80028-4)
- Croot, P.L., Andersson, K., Öztürk, M., Turner, D.R., 2004. The distribution and speciation of iron along 6°E in the Southern Ocean. *Deep Sea Res. Part II Top. Stud. Oceanogr., The SWEDARP 1997/98 Expedition 51*, 2857–2879. <https://doi.org/10.1016/j.dsr2.2003.10.012>
- Croot, P.L., Johansson, M., 2000. Determination of Iron Speciation by Cathodic Stripping Voltammetry in Seawater Using the Competing Ligand 2-(2-Thiazolylazo)-p-cresol (TAC). *Electroanalysis* 12, 565–576. [https://doi.org/10.1002/\(SICI\)1521-4109\(200005\)12:8<565::AID-ELAN565>3.0.CO;2-L](https://doi.org/10.1002/(SICI)1521-4109(200005)12:8<565::AID-ELAN565>3.0.CO;2-L)
- Dale, A.W., Nickelsen, L., Scholz, F., Hensen, C., Oschlies, A., Wallmann, K., 2015. A revised global estimate of dissolved iron fluxes from marine sediments. *Glob. Biogeochem. Cycles* 29, 691–707. <https://doi.org/10.1002/2014GB005017>
- de Baar, H.J.W., Boyd, P.W., Coale, K.H., Landry, M.R., Tsuda, A., Assmy, P., Bakker, D.C.E., Bozec, Y., Barber, R.T., Brzezinski, M.A., Buesseler, K.O., Boyé, M., Croot, P.L., Gervais, F., Gorbunov, M.Y., Harrison, P.J., Hiscock, W.T., Laan, P., Lancelot, C., Law, C.S., Levasseur, M., Marchetti, A., Millero, F.J., Nishioka, J., Nojiri, Y., van Oijen, T., Riebesell, U., Rijkenberg, M.J.A., Saito, H., Takeda, S., Timmermans, K.R., Veldhuis, M.J.W., Waite, A.M., Wong, C.-S., 2005. Synthesis of iron fertilization experiments: From the Iron Age in the Age of Enlightenment. *J. Geophys. Res. Oceans* 110. <https://doi.org/10.1029/2004JC002601>
- de Baar, H.J.W., Buma, A.G.J., Nolting, R.F., Cadée, G.C., Jacques, G., Tréguer, P.J., 1990. On iron limitation of the Southern Ocean: experimental observations in the Weddell and Scotia Seas. *Mar. Ecol. Prog. Ser.* 65, 105–122.
- de Baar, H.J.W., van Heuven, S.M.A.C., Abouchami, W., Xue, Z., Galer, S.J.G., Rehkämper, M., Middag, R., van Ooijen, J., 2017. Interactions of dissolved CO<sub>2</sub> with cadmium isotopes in the Southern Ocean. *Mar. Chem., SI: Honoring Frank Millero* 195, 105–121. <https://doi.org/10.1016/j.marchem.2017.06.010>
- Dertz, E.A., Xu, J., Stintzi, A., Raymond, K.N., 2006. Bacillibactin-Mediated Iron Transport in *Bacillus subtilis*. *J. Am. Chem. Soc.* 128, 22–23. <https://doi.org/10.1021/ja055898c>
- Dittmar, T., Lennartz, S.T., Buck-Wiese, H., Hansell, D.A., Santinelli, C., Vanni, C., Blasius, B., Hehemann, J.-H., 2021. Enigmatic persistence of dissolved organic matter in the ocean. *Nat. Rev. Earth Environ.* 2, 570–583. <https://doi.org/10.1038/s43017-021-00183-7>
- Dulaquais, G., Waeles, M., Gerringa, L.J.A., Middag, R., Rijkenberg, M.J.A., Riso, R., 2018. The Biogeochemistry of Electroactive Humic Substances and Its Connection to Iron Chemistry in the North East Atlantic and the Western Mediterranean Sea. *J. Geophys. Res. Oceans* 123, 5481–5499. <https://doi.org/10/gd8db3>

- Fenton, H.J.H., 1894. LXXIII.—Oxidation of tartaric acid in presence of iron. *J. Chem. Soc. Trans.* 65, 899–910. <https://doi.org/10.1039/CT8946500899>
- Field, C.B., Behrenfeld, M.J., Randerson, J.T., Falkowski, P., 1998. Primary Production of the Biosphere: Integrating Terrestrial and Oceanic Components. *Science* 281, 237–240. <https://doi.org/10.1126/science.281.5374.237>
- Findlay, A.J., Estes, E.R., Gartman, A., Yücel, M., Kamyshny, A., Luther, G.W., 2019. Iron and sulfide nanoparticle formation and transport in nascent hydrothermal vent plumes. *Nat. Commun.* 10, 1–7. <https://doi.org/10.1038/s41467-019-09580-5>
- Fitzsimmons, J.N., Bundy, R.M., Al-Subiaï, S.N., Barbeau, K.A., Boyle, E.A., 2015. The composition of dissolved iron in the dusty surface ocean: An exploration using size-fractionated iron-binding ligands. *Mar. Chem., SCOR WG 139: Organic Ligands – A Key Control on Trace Metal Biogeochemistry in the Ocean* 173, 125–135. <https://doi.org/10/f7fc99>
- Fourrier, P., Dulaquais, G., Guigue, C., Giamarchi, P., Sarthou, G., Whitby, H., Riso, R., 2022. Characterization of the vertical size distribution, composition and chemical properties of dissolved organic matter in the (ultra)oligotrophic Pacific Ocean through a multi-detection approach. *Mar. Chem.* 240, 104068. <https://doi.org/10.1016/j.marchem.2021.104068>
- Friedlingstein, P., Jones, M.W., O’Sullivan, M., Andrew, R.M., Hauck, J., Peters, G.P., Peters, W., Pongratz, J., Sitch, S., Quéré, C.L., Bakker, D.C.E., Canadell, J.G., Ciais, P., Jackson, R.B., Anthoni, P., Barbero, L., Bastos, A., Bastrikov, V., Becker, M., Bopp, L., Buitenhuis, E., Chandra, N., Chevallier, F., Chini, L.P., Currie, K.I., Feely, R.A., Gehlen, M., Gilfillan, D., Gkritzalis, T., Goll, D.S., Gruber, N., Gutekunst, S., Harris, I., Haverd, V., Houghton, R.A., Hurtt, G., Ilyina, T., Jain, A.K., Joetzjer, E., Kaplan, J.O., Kato, E., Klein Goldewijk, K., Korsbakken, J.I., Landschützer, P., Lauvset, S.K., Lefèvre, N., Lenton, A., Lienert, S., Lombardozzi, D., Marland, G., McGuire, P.C., Melton, J.R., Metzl, N., Munro, D.R., Nabel, J.E.M.S., Nakaoka, S.-I., Neill, C., Omar, A.M., Ono, T., Pregon, A., Pierrot, D., Poulter, B., Rehder, G., Resplandy, L., Robertson, E., Rödenbeck, C., Séférian, R., Schwinger, J., Smith, N., Tans, P.P., Tian, H., Tilbrook, B., Tubiello, F.N., Werf, G.R. van der, Wiltshire, A.J., Zaehle, S., 2019. Global Carbon Budget 2019. *Earth Syst. Sci. Data* 11, 1783–1838. <https://doi.org/10.5194/essd-11-1783-2019>
- Gattuso, J.-P., Magnan, A., Billé, R., Cheung, W.W.L., Howes, E.L., Joos, F., Allemand, D., Bopp, L., Cooley, S.R., Eakin, C.M., Hoegh-Guldberg, O., Kelly, R.P., Pörtner, H.-O., Rogers, A.D., Baxter, J.M., Laffoley, D., Osborn, D., Rankovic, A., Rochette, J., Sumaila, U.R., Treyer, S., Turley, C., 2015. Contrasting futures for ocean and society from different anthropogenic CO2 emissions scenarios. *Science* 349. <https://doi.org/10.1126/science.aac4722>
- Genovese, C., Grotti, M., Ardini, F., Wuttig, K., Vivado, D., Cabanes, D., Townsend, A., Hassler, C., Lannuzel, D., 2022. Effect of salinity and temperature on the determination of dissolved iron-binding organic ligands in the polar marine environment. *Mar. Chem.* 238, 104051. <https://doi.org/10.1016/j.marchem.2021.104051>
- Genovese, C., Grotti, M., Pittaluga, J., Ardini, F., Janssens, J., Wuttig, K., Moreau, S., Lannuzel, D., 2018. Influence of organic complexation on dissolved iron distribution in East Antarctic pack ice. *Mar. Chem.* 203, 28–37. <https://doi.org/10.1016/j.marchem.2018.04.005>
- Gerringa, L.J.A., Gledhill, M., Ardiningsih, I., Muntjewerf, N., Laglera, L.M., 2021. Comparing CLE-AdCSV applications using SA and TAC to determine the Fe-binding characteristics of model ligands in seawater. *Biogeosciences* 18, 5265–5289. <https://doi.org/10.5194/bg-18-5265-2021>
- Gerringa, L.J.A., Herman, P.M.J., Poortvliet, T.C.W., 1995. Comparison of the linear Van den Berg/Ružić transformation and a non-linear fit of the Langmuir isotherm applied to Cu speciation data in the estuarine environment. *Mar. Chem.* 48, 131–142. [https://doi.org/10.1016/0304-4203\(94\)00041-B](https://doi.org/10.1016/0304-4203(94)00041-B)
- Gerringa, L.J.A., Rijkenberg, M.J.A., Schoemann, V., Laan, P., de Baar, H.J.W., 2015. Organic complexation of iron in the West Atlantic Ocean. *Mar. Chem., Cycles of metals and carbon in the oceans - A tribute to the work stimulated by Hein de Baar* 177, 434–446. <https://doi.org/10.1016/j.marchem.2015.04.007>

- Gerringa, L.J.A., Rijkenberg, M.J.A., Thuróczy, C.-E., Maas, L.R.M., 2014. A critical look at the calculation of the binding characteristics and concentration of iron complexing ligands in seawater with suggested improvements. *Environ. Chem.* 11, 114–136. <https://doi.org/10/f52sbv>
- Gledhill, M., Achterberg, E.P., Li, K., Mohamed, K.N., Rijkenberg, M.J.A., 2015. Influence of ocean acidification on the complexation of iron and copper by organic ligands in estuarine waters. *Mar. Chem., Cycles of metals and carbon in the oceans - A tribute to the work stimulated by Hein de Baar* 177, 421–433. <https://doi.org/10.1016/j.marchem.2015.03.016>
- Gledhill, M., Buck, K.N., 2012. The Organic Complexation of Iron in the Marine Environment: A Review. *Front. Microbiol.* 3. <https://doi.org/10.3389/fmicb.2012.00069>
- Gledhill, M., van den Berg, C.M.G., 1994. Determination of complexation of iron(III) with natural organic complexing ligands in seawater using cathodic stripping voltammetry. *Mar. Chem.* 47, 41–54. [https://doi.org/10.1016/0304-4203\(94\)90012-4](https://doi.org/10.1016/0304-4203(94)90012-4)
- Gupta, B.S., Taha, M., Lee, M.-J., 2013. Stability Constants for the Equilibrium Models of Iron(III) with Several Biological Buffers in Aqueous Solutions. *J. Solut. Chem.* 42, 2296–2309. <https://doi.org/10.1007/s10953-013-0107-6>
- Hassler, C., Cabanes, D., Blanco-Ameijeiras, S., Sander, S.G., Benner, R., Hassler, C., Cabanes, D., Blanco-Ameijeiras, S., Sander, S.G., Benner, R., 2019. Importance of refractory ligands and their photodegradation for iron oceanic inventories and cycling. *Mar. Freshw. Res.* 71, 311–320. <https://doi.org/10.1071/MF19213>
- Hassler, C.S., Berg, V.D., G, C.M., Boyd, P.W., 2017. Toward a Regional Classification to Provide a More Inclusive Examination of the Ocean Biogeochemistry of Iron-Binding Ligands. *Front. Mar. Sci.* 4. <https://doi.org/10.3389/fmars.2017.00019>
- Hassler, C.S., Legiret, F.-E., Butler, E.C.V., 2013. Measurement of iron chemical speciation in seawater at 4°C: The use of competitive ligand exchange–adsorptive cathodic stripping voltammetry. *Mar. Chem.* 149, 63–73. <https://doi.org/10.1016/j.marchem.2012.12.007>
- Hassler, C.S., Norman, L., Mancuso Nichols, C.A., Clementson, L.A., Robinson, C., Schoemann, V., Watson, R.J., Doblin, M.A., 2015. Iron associated with exopolymeric substances is highly bioavailable to oceanic phytoplankton. *Mar. Chem., SCOR WG 139: Organic Ligands – A Key Control on Trace Metal Biogeochemistry in the Ocean* 173, 136–147. <https://doi.org/10.1016/j.marchem.2014.10.002>
- Hawkes, J. A., Connelly, D.P., Gledhill, M., Achterberg, E.P., 2013. The stabilisation and transportation of dissolved iron from high temperature hydrothermal vent systems. *Earth Planet. Sci. Lett.* 375, 280–290. <https://doi.org/10.1016/j.epsl.2013.05.047>
- Hawkes, Jeffrey A., Gledhill, M., Connelly, D.P., Achterberg, E.P., 2013. Characterisation of iron binding ligands in seawater by reverse titration. *Anal. Chim. Acta* 766, 53–60. <https://doi.org/10.1016/j.aca.2012.12.048>
- Hayyan, M., Hashim, M.A., AlNashef, I.M., 2016. Superoxide Ion: Generation and Chemical Implications. *Chem. Rev.* 116, 3029–3085. <https://doi.org/10.1021/acs.chemrev.5b00407>
- Hiemstra, T., van Riemsdijk, W.H., 2006. Biogeochemical speciation of Fe in ocean water. *Mar. Chem.* 102, 181–197. <https://doi.org/10.1016/j.marchem.2006.03.008>
- Ho, P., Lee, J.-M., Heller, M.I., Lam, P.J., Shiller, A.M., 2018. The distribution of dissolved and particulate Mo and V along the U.S. GEOTRACES East Pacific Zonal Transect (GP16): The roles of oxides and biogenic particles in their distributions in the oxygen deficient zone and the hydrothermal plume. *Mar. Chem., The U.S.GEOTRACES Eastern Tropical Pacific Transect (GP16)* 201, 242–255. <https://doi.org/10.1016/j.marchem.2017.12.003>
- Hoffmann, L.J., Breitbarth, E., Boyd, P.W., Hunter, K.A., 2012. Influence of ocean warming and acidification on trace metal biogeochemistry. *Mar. Ecol. Prog. Ser.* 470, 191–205. <https://doi.org/10.3354/meps10082>
- Hogle, S.L., Hackl, T., Bundy, R.M., Park, J., Satinsky, B., Satinsky, B., Hiltunen, T., Biller, S., Berube, P.M., Chisholm, S.W., 2021. Siderophores as an iron source for *Prochlorococcus* in deep

- chlorophyll maximum layers of the oligotrophic ocean.  
<https://doi.org/10.1101/2021.11.13.468467>
- Hopkinson, B.M., Morel, F.M.M., 2009. The role of siderophores in iron acquisition by photosynthetic marine microorganisms. *BioMetals* 22, 659–669. <https://doi.org/10.1007/s10534-009-9235-2>
- Hoppe, C.J.M., Hassler, C.S., Payne, C.D., Tortell, P.D., Rost, B., Trimborn, S., 2013. Iron Limitation Modulates Ocean Acidification Effects on Southern Ocean Phytoplankton Communities. *PLoS ONE* 8. <https://doi.org/10.1371/journal.pone.0079890>
- Hopwood, M.J., Carroll, D., Höfer, J., Achterberg, E.P., Meire, L., Le Moigne, F.A.C., Bach, L.T., Eich, C., Sutherland, D.A., González, H.E., 2019. Highly variable iron content modulates iceberg-ocean fertilisation and potential carbon export. *Nat. Commun.* 10, 1–10. <https://doi.org/10.1038/s41467-019-13231-0>
- Hunter, K.A., 2005. Comment on ‘Measuring Marine Iron(III) Complexes by CLE-AdSV.’ *Environ. Chem.* 2, 85–87. <https://doi.org/10.1071/EN05030>
- Hutchins, D.A., Boyd, P.W., 2016. Marine phytoplankton and the changing ocean iron cycle. *Nat. Clim. Change* 6, 1072–1079. <https://doi.org/10.1038/nclimate3147>
- Ingall, E.D., Diaz, J.M., Longo, A.F., Oakes, M., Finney, L., Vogt, S., Lai, B., Yager, P.L., Twining, B.S., Brandes, J.A., 2013. Role of biogenic silica in the removal of iron from the Antarctic seas. *Nat. Commun.* 4, 1981. <https://doi.org/10.1038/ncomms2981>
- Janssens, J., Meiners, K.M., Townsend, A.T., Lannuzel, D., 2018. Organic Matter Controls of Iron Incorporation in Growing Sea Ice. *Front. Earth Sci.* 6.
- Johnson, K.S., Gordon, R.M., Coale, K.H., 1997. What controls dissolved iron concentrations in the world ocean? *Mar. Chem.* 57, 137–161. [https://doi.org/10.1016/S0304-4203\(97\)00043-1](https://doi.org/10.1016/S0304-4203(97)00043-1)
- Kleint, C., Hawkes, J.A., Sander, S.G., Koschinsky, A., 2016. Voltammetric Investigation of Hydrothermal Iron Speciation. *Front. Mar. Sci.* 3, UNSP 75. <https://doi.org/10.3389/fmars.2016.00075>
- Krachler, R., Krachler, R.F., Wallner, G., Hann, S., Laux, M., Cervantes Recalde, M.F., Jirsa, F., Neubauer, E., von der Kammer, F., Hofmann, T., Keppler, B.K., 2015. River-derived humic substances as iron chelators in seawater. *Mar. Chem.* 174, 85–93. <https://doi.org/10.1016/j.marchem.2015.05.009>
- Kuma, K., Nishioka, J., Matsunaga, K., 1996. Controls on iron(III) hydroxide solubility in seawater: The influence of pH and natural organic chelators. *Limnol. Oceanogr.* 41, 396–407. <https://doi.org/10.4319/lo.1996.41.3.0396>
- Laglera, L.M., Battaglia, G., van den Berg, C.M.G., 2011. Effect of humic substances on the iron speciation in natural waters by CLE/CSV. *Mar. Chem.* 127, 134–143. <https://doi.org/10.1016/j.marchem.2011.09.003>
- Laglera, L.M., Battaglia, G., van den Berg, C.M.G., 2007. Determination of humic substances in natural waters by cathodic stripping voltammetry of their complexes with iron. *Anal. Chim. Acta* 599, 58–66. <https://doi.org/10.1016/j.aca.2007.07.059>
- Laglera, L.M., Caprara, S., Monticelli, D., 2016. Towards a zero-blank, preconcentration-free voltammetric method for iron analysis at picomolar concentrations in unbuffered seawater. *Talanta* 150, 449–454. <https://doi.org/10.1016/j.talanta.2015.12.060>
- Laglera, L.M., Monticelli, D., 2017. Iron detection and speciation in natural waters by electrochemical techniques: A critical review. *Curr. Opin. Electrochem.* 3, 123–129. <https://doi.org/10.1016/j.coelec.2017.07.007>
- Laglera, L.M., Tovar-Sanchez, A., Sukekava, C.F., Naik, H., Naqvi, S.W.A., Wolf-Gladrow, D.A., 2019. Iron organic speciation during the LOHAFEX experiment: Iron ligands release under biomass control by copepod grazing. *J. Mar. Syst.* 103151. <https://doi.org/10.1016/j.jmarsys.2019.02.002>
- Langmuir, I., 1916. THE CONSTITUTION AND FUNDAMENTAL PROPERTIES OF SOLIDS AND LIQUIDS. PART I. SOLIDS. *J. Am. Chem. Soc.* 38, 2221–2295. <https://doi.org/10.1021/ja02268a002>



- Lannuzel, D., Vancoppenolle, M., van der Merwe, P., de Jong, J., Meiners, K.M., Grotti, M., Nishioka, J., Schoemann, V., 2016. Iron in sea ice: Review and new insights. *Elem. Sci. Anthr.* 4, 000130. <https://doi.org/10.12952/journal.elementa.000130>
- Lis, H., Shaked, Y., Kranzler, C., Keren, N., Morel, F.M.M., 2015. Iron bioavailability to phytoplankton: an empirical approach. *ISME J.* 9, 1003–1013. <https://doi.org/10.1038/ismej.2014.199>
- Liu, X., Millero, F.J., 2002. The solubility of iron in seawater. *Mar. Chem.* 77, 43–54. [https://doi.org/10.1016/S0304-4203\(01\)00074-3](https://doi.org/10.1016/S0304-4203(01)00074-3)
- Lodeiro, P., Rey-Castro, C., David, C., Achterberg, E.P., Puy, J., Gledhill, M., 2020. Acid-base properties of dissolved organic matter extracted from the marine environment. *Sci. Total Environ.* 729, 138437. <https://doi.org/10.1016/j.scitotenv.2020.138437>
- Lohan, M.C., Aguilar-Islas, A.M., Bruland, K.W., 2006. Direct determination of iron in acidified (pH 1.7) seawater samples by flow injection analysis with catalytic spectrophotometric detection: Application and intercomparison. *Limnol. Oceanogr. Methods* 4, 164–171. <https://doi.org/10.4319/lom.2006.4.164>
- Longhini, C.M., Mahieu, L., Sá, F., van den Berg, C.M.G., Salaün, P., Neto, R.R., 2021. Coastal waters contamination by mining tailings: What triggers the stability of iron in the dissolved and soluble fractions? *Limnol. Oceanogr.* 66, 171–187. <https://doi.org/10.1002/lno.11595>
- Louis, Y., Garnier, C., Lenoble, V., Omanović, D., Mounier, S., Pižeta, I., 2009. Characterisation and modelling of marine dissolved organic matter interactions with major and trace cations. *Mar. Environ. Res.* 67, 100–107. <https://doi.org/10.1016/j.marenvres.2008.12.002>
- Mahmood, A., Abualhaija, M.M., van den Berg, C.M.G., Sander, S.G., 2015. Organic speciation of dissolved iron in estuarine and coastal waters at multiple analytical windows. *Mar. Chem.* 177, 706–719. <https://doi.org/10.1016/j.marchem.2015.11.001>
- Mahowald, N., Engelstaedter, S., Luo, C., Sealy, A., Artaxo, P., Benitez-Nelson, C., Bonnet, S., Chen, Y., Chuang, P., Cohen, D., Dulac, F., Herut, B., Johansen, A., Kubilay, N., Losno, R., Maenhaut, W., Paytan, A., Prospero, J., Shank, L., Siefert, R., 2009. Atmospheric Iron Deposition: Global Distribution, Variability, and Human Perturbations. *Annu. Rev. Mar. Sci.* 1. <https://doi.org/10.1146/annurev.marine.010908.163727>
- Martin, J.H., Fitzwater, S.E., 1988. Iron deficiency limits phytoplankton growth in the north-east Pacific subarctic. *Nature* 331, 341–343. <https://doi.org/10.1038/331341a0>
- Martin, J.H., Fitzwater, S.E., Gordon, R.M., 1990. Iron deficiency limits phytoplankton growth in Antarctic waters. *Glob. Biogeochem. Cycles* 4, 5–12. <https://doi.org/10.1029/GB004i001p00005>
- Martin, J.H., Gordon, R.M., Fitzwater, S., Broenkow, W.W., 1989. Vertex: phytoplankton/iron studies in the Gulf of Alaska. *Deep Sea Res. Part Oceanogr. Res. Pap.* 36, 649–680. [https://doi.org/10.1016/0198-0149\(89\)90144-1](https://doi.org/10.1016/0198-0149(89)90144-1)
- McQuaid, J.B., Kustka, A.B., Oborník, M., Horák, A., McCrow, J.P., Karas, B.J., Zheng, H., Kindeberg, T., Andersson, A.J., Barbeau, K.A., Allen, A.E., 2018. Carbonate-sensitive phytoferritin controls high-affinity iron uptake in diatoms. *Nature* 555, 534–537. <https://doi.org/10.1038/nature25982>
- Mentges, A., Feenders, C., Seibt, M., Blasius, B., Dittmar, T., 2017. Functional Molecular Diversity of Marine Dissolved Organic Matter Is Reduced during Degradation. *Front. Mar. Sci.* 4. <https://doi.org/10.3389/fmars.2017.00194>
- Millero, F., 2001. Speciation of metals in natural waters. *Geochem. Trans.* 2, 56–64. <https://doi.org/10.1039/B104809K>
- Millero, F.J., Woosley, R., Ditrolio, B., Waters, J., 2009. Effect of Ocean Acidification on the Speciation of Metals in Seawater. *Oceanography* 22, 72–85. <https://doi.org/10.5670/oceanog.2009.98>

- Mills, M.M., Ridame, C., Davey, M., La Roche, J., Geider, R.J., 2004. Iron and phosphorus co-limit nitrogen fixation in the eastern tropical North Atlantic. *Nature* 429, 292–294. <https://doi.org/10.1038/nature02550>
- Mohamed, K.N., Steigenberger, S., Nielsdottir, M.C., Gledhill, M., Achterberg, E.P., 2011. Dissolved iron(III) speciation in the high latitude North Atlantic Ocean. *Deep Sea Res. Part Oceanogr. Res. Pap.* 58, 1049–1059. <https://doi.org/10.1016/j.dsr.2011.08.011>
- Moore, C.M., Mills, M.M., Arrigo, K.R., Berman-Frank, I., Bopp, L., Boyd, P.W., Galbraith, E.D., Geider, R.J., Guieu, C., Jaccard, S.L., Jickells, T.D., La Roche, J., Lenton, T.M., Mahowald, N.M., Marañón, E., Marinov, I., Moore, J.K., Nakatsuka, T., Oschlies, A., Saito, M.A., Thingstad, T.F., Tsuda, A., Ulloa, O., 2013. Processes and patterns of oceanic nutrient limitation. *Nat. Geosci.* 6, 701–710. <https://www.nature.com/articles/ngeo1765>
- Morel, F.M.M., Kustka, A.B., Shaked, Y., 2008. The role of unchelated Fe in the iron nutrition of phytoplankton. *Limnol. Oceanogr.* 53, 400–404. <https://doi.org/10.4319/lo.2008.53.1.0400>
- Morel, F.M.M., Price, N.M., 2003. The Biogeochemical Cycles of Trace Metals in the Oceans. *Science* 300, 944–947. <https://doi.org/10.1126/science.1083545>
- Nagai, T., Imai, A., Matsushige, K., Yokoi, K., Fukushima, T., 2004. Voltammetric determination of dissolved iron and its speciation in freshwater. *Limnology* 5, 87–94. <https://doi.org/10.1007/s10201-004-0121-x>
- Nichols, C.M., Lardière, S.G., Bowman, J.P., Nichols, P.D., A E Gibson, J., Guézennec, J., 2005. Chemical characterization of exopolysaccharides from Antarctic marine bacteria. *Microb. Ecol.* 49, 578–589. <https://doi.org/10.1007/s00248-004-0093-8>
- Nolting, R.F., Gerringa, L.J.A., Swagerman, M.J.W., Timmermans, K.R., de Baar, H.J.W., 1998. Fe (III) speciation in the high nutrient, low chlorophyll Pacific region of the Southern Ocean. *Mar. Chem.* 62, 335–352. [https://doi.org/10.1016/S0304-4203\(98\)00046-2](https://doi.org/10.1016/S0304-4203(98)00046-2)
- Norman, L., Worms, I.A.M., Angles, E., Bowie, A.R., Nichols, C.M., Ninh Pham, A., Slaveykova, V.I., Townsend, A.T., David Waite, T., Hassler, C.S., 2015. The role of bacterial and algal exopolymeric substances in iron chemistry. *Mar. Chem., SCOR WG 139: Organic Ligands – A Key Control on Trace Metal Biogeochemistry in the Ocean* 173, 148–161. <https://doi.org/10.1016/j.marchem.2015.03.015>
- Obata, H., van den Berg, C.M.G., 2001. Determination of Picomolar Levels of Iron in Seawater Using Catalytic Cathodic Stripping Voltammetry. *Anal. Chem.* 73, 2522–2528. <https://doi.org/10.1021/ac001495d>
- Obata, Hajime., Karatani, Hajime., Nakayama, Eiichiro., 1993. Automated determination of iron in seawater by chelating resin concentration and chemiluminescence detection. *Anal. Chem.* 65, 1524–1528. <https://doi.org/10.1021/ac00059a007>
- Omanović, D., Garnier, C., Pižeta, I., 2015. ProMCC: An all-in-one tool for trace metal complexation studies. *Mar. Chem., SCOR WG 139: Organic Ligands – A Key Control on Trace Metal Biogeochemistry in the Ocean* 173, 25–39. <https://doi.org/10.1016/j.marchem.2014.10.011>
- Pernet-Coudrier, B., Waeles, M., Filella, M., Quentel, F., Riso, R.D., 2013. Simple and simultaneous determination of glutathione, thioacetamide and refractory organic matter in natural waters by DP-CSV. *Sci. Total Environ.* 463–464, 997–1005. <https://doi.org/10.1016/j.scitotenv.2013.06.053>
- Pižeta, I., Sander, S.G., Hudson, R.J.M., Omanović, D., Baars, O., Barbeau, K.A., Buck, K.N., Bundy, R.M., Carrasco, G., Croot, P.L., Garnier, C., Gerringa, L.J.A., Gledhill, M., Hirose, K., Kondo, Y., Laglera, L.M., Nuester, J., Rijkenberg, M.J.A., Takeda, S., Twining, B.S., Wells, M., 2015. Interpretation of complexometric titration data: An intercomparison of methods for estimating models of trace metal complexation by natural organic ligands. *Mar. Chem., SCOR WG 139: Organic Ligands – A Key Control on Trace Metal Biogeochemistry in the Ocean* 173, 3–24. <https://doi.org/10.1016/j.marchem.2015.03.006>

- Poulton, S.W., Raiswell, R., 2002. The low-temperature geochemical cycle of iron: From continental fluxes to marine sediment deposition. *Am. J. Sci.* 302, 774–805. <https://doi.org/10.2475/ajs.302.9.774>
- Qiu, G.-W., Koedooder, C., Qiu, B.-S., Shaked, Y., Keren, N., 2021. Iron transport in cyanobacteria – from molecules to communities. *Trends Microbiol.* <https://doi.org/10.1016/j.tim.2021.06.001>
- Quentel, F., Madec, C., Courtot-coupez, J., 1987. Determination of Humic Substances in Seawater by Electrochemistry (Mechanisms). *Anal. Lett.* 20, 47–62. <https://doi.org/10.1080/00032718708082236>
- Raspor, B., Nürnberg, H.W., Valenta, P., Branica, M., 1980. Kinetics and mechanism of trace metal chelation in sea water. *J. Electroanal. Chem. Interfacial Electrochem.* 115, 293–308. [https://doi.org/10.1016/S0022-0728\(80\)80333-0](https://doi.org/10.1016/S0022-0728(80)80333-0)
- Raymond, K.N., Allred, B.E., Sia, A.K., 2015. Coordination Chemistry of Microbial Iron Transport. *Acc. Chem. Res.* 48, 2496–2505. <https://doi.org/10.1021/acs.accounts.5b00301>
- Rickard, D., Luther, G.W., 2007. Chemistry of Iron Sulfides. *Chem. Rev.* 107, 514–562. <https://doi.org/10.1021/cr0503658>
- Roshan, S., DeVries, T., 2021. Global Contrasts Between Oceanic Cycling of Cadmium and Phosphate. *Glob. Biogeochem. Cycles* 35, e2021GB006952. <https://doi.org/10.1029/2021GB006952>
- Rue, E.L., Bruland, K.W., 1997. The role of organic complexation on ambient iron chemistry in the equatorial Pacific Ocean and the response of a mesoscale iron addition experiment. *Limnol. Oceanogr.* 42, 901–910. <https://doi.org/10.4319/lo.1997.42.5.0901>
- Rue, E.L., Bruland, K.W., 1995. Complexation of iron(III) by natural organic ligands in the Central North Pacific as determined by a new competitive ligand equilibration/adsorptive cathodic stripping voltammetric method. *Mar. Chem., The Chemistry of Iron in Seawater and its Interaction with Phytoplankton* 50, 117–138. [https://doi.org/10.1016/0304-4203\(95\)00031-L](https://doi.org/10.1016/0304-4203(95)00031-L)
- Ružić, I., 1982. Theoretical aspects of the direct titration of natural waters and its information yield for trace metal speciation. *Anal. Chim. Acta* 140, 99–113. [https://doi.org/10.1016/S0003-2670\(01\)95456-X](https://doi.org/10.1016/S0003-2670(01)95456-X)
- Sanvito, F., Monticelli, D., 2021. Exploring bufferless iron speciation in seawater by Competitive Ligand Equilibration-Cathodic Stripping Voltammetry: Does pH control really matter? *Talanta* 229, 122300. <https://doi.org/10.1016/j.talanta.2021.122300>
- Sanvito, F., Monticelli, D., 2020. Fast iron speciation in seawater by catalytic Competitive Ligand Equilibration-Cathodic Stripping Voltammetry with tenfold sample size reduction. *Anal. Chim. Acta* 1113, 9–17. <https://doi.org/10.1016/j.aca.2020.04.002>
- Sanvito, F., Pacileo, L., Monticelli, D., 2019. Fostering and Understanding Iron Detection at the Ultratrace Level by Adsorptive Stripping Voltammetry with Catalytic Enhancement. *Electroanalysis* 31, 212–216. <https://doi.org/10.1002/elan.201800675>
- Scatchard, G., 1949. The Attractions of Proteins for Small Molecules and Ions. *Ann. N. Y. Acad. Sci.* 51, 660–672. <https://doi.org/10.1111/j.1749-6632.1949.tb27297.x>
- Schoffman, H., Lis, H., Shaked, Y., Keren, N., 2016. Iron–Nutrient Interactions within Phytoplankton. *Front. Plant Sci.* 7.
- Schuback, N., Schallenberg, C., Duckham, C., Maldonado, M.T., Tortell, P.D., 2015. Interacting Effects of Light and Iron Availability on the Coupling of Photosynthetic Electron Transport and CO<sub>2</sub>-Assimilation in Marine Phytoplankton. *PLOS ONE* 10, e0133235. <https://doi.org/10.1371/journal.pone.0133235>
- Shaked, Y., Buck, K.N., Mellett, T., Maldonado, M.T., 2020. Insights into the bioavailability of oceanic dissolved Fe from phytoplankton uptake kinetics. *ISME J.* 14, 1182–1193. <https://doi.org/10.3389/fmicb.2012.00204>
- Shi, D., Xu, Y., Hopkinson, B.M., Morel, F.M.M., 2010. Effect of Ocean Acidification on Iron Availability to Marine Phytoplankton. *Science* 327, 676–679. <https://doi.org/10.1126/science.1183517>

- Simsek, S., Ojanen-Reuhs, T., Stephens, S.B., Reuhs, B.L., 2007. Strain-ecotype specificity in *Sinorhizobium meliloti*-*Medicago truncatula* symbiosis is correlated to succinoglycan oligosaccharide structure. *J. Bacteriol.* 189, 7733–7740. <https://doi.org/10.1128/JB.00739-07>
- Slagter, H.A., Reader, H.E., Rijkenberg, M.J.A., Rutgers van der Loeff, M., de Baar, H.J.W., Gerringa, L.J.A., 2017. Organic Fe speciation in the Eurasian Basins of the Arctic Ocean and its relation to terrestrial DOM. *Mar. Chem.* 197, 11–25. <https://doi.org/10.1016/j.marchem.2017.10.005>
- Stevenson, F.J., 1994. *Humus Chemistry: Genesis, Composition, Reactions*. John Wiley & Sons.
- Stockdale, A., Tipping, E., Lofts, S., Mortimer, R.J.G., 2016. Effect of Ocean Acidification on Organic and Inorganic Speciation of Trace Metals. *Environ. Sci. Technol.* 50, 1906–1913. <https://doi.org/10.1021/acs.est.5b05624>
- Su, H., Yang, R., Pižeta, I., Omanović, D., Wang, S., Li, Y., 2016. Distribution and Speciation of Dissolved Iron in Jiaozhou Bay (Yellow Sea, China). *Front. Mar. Sci.* 3. <https://doi.org/10.3389/fmars.2016.00099>
- Sukekava, C., Downes, J., Slagter, H.A., Gerringa, L.J.A., Laglera, L.M., 2018. Determination of the contribution of humic substances to iron complexation in seawater by catalytic cathodic stripping voltammetry. *Talanta* 189, 359–364. <https://doi.org/10.1016/j.talanta.2018.07.021>
- Sunda, W.G., 2012. Feedback Interactions between Trace Metal Nutrients and Phytoplankton in the Ocean. *Front. Microbiol.* 3. <https://doi.org/10.3389/fmicb.2012.00204>
- Tagliabue, A., 2014. More to hydrothermal iron input than meets the eye. *Proc. Natl. Acad. Sci.* 111, 16641–16642. <https://doi.org/10.1073/pnas.1419829111>
- Tagliabue, A., Aumont, O., Bopp, L., 2014a. The impact of different external sources of iron on the global carbon cycle. *Geophys. Res. Lett.* 41, 920–926. <https://doi.org/10.1002/2013GL059059>
- Tagliabue, A., Aumont, O., DeAth, R., Dunne, J.P., Dutkiewicz, S., Galbraith, E., Misumi, K., Moore, J.K., Ridgwell, A., Sherman, E., Stock, C., Vichi, M., Völker, C., Yool, A., 2016. How well do global ocean biogeochemistry models simulate dissolved iron distributions?: GLOBAL IRON MODELS. *Glob. Biogeochem. Cycles* 30, 149–174. <https://doi.org/10.1002/2015GB005289>
- Tagliabue, A., Bopp, L., Dutay, J.-C., Bowie, A.R., Chaver, F., Jean-Baptiste, P., Bucciarelli, E., Lannuzel, D., Remenyi, T., Sarthou, G., Aumont, O., Gehlen, M., Jeandel, C., 2010. Hydrothermal contribution to the oceanic dissolved iron inventory. *Nat. Geosci.* 3, 252–256. <https://doi.org/10.1038/ngeo818>
- Tagliabue, A., Mtshali, T., Aumont, O., Bowie, A.R., Klunder, M.B., Roychoudhury, A.N., Swart, S., 2012. A global compilation of dissolved iron measurements: focus on distributions and processes in the Southern Ocean 17. <https://doi.org/10.5194/bg-9-2333-2012>
- Tagliabue, A., Resing, J., 2016. Impact of hydrothermalism on the ocean iron cycle. *Philos. Trans. R. Soc. Math. Phys. Eng. Sci.* 374, 20150291. <https://doi.org/10.1098/rsta.2015.0291>
- Tagliabue, A., Sallée, J.-B., Bowie, A.R., Lévy, M., Swart, S., Boyd, P.W., 2014b. Surface-water iron supplies in the Southern Ocean sustained by deep winter mixing. *Nat. Geosci.* 7, 314–320. <https://doi.org/10.1038/ngeo2101>
- Tagliabue, A., Bowie, A.R., Boyd, P.W., Buck, K.N., Johnson, K.S., Saito, M.A., 2017. The integral role of iron in ocean biogeochemistry. *Nature* 543, 51. <https://doi.org/10.1038/nature21058>
- Taylor, S.R., 1964. Abundance of chemical elements in the continental crust: a new table. *Geochim. Cosmochim. Acta* 28, 1273–1285. [https://doi.org/10.1016/0016-7037\(64\)90129-2](https://doi.org/10.1016/0016-7037(64)90129-2)
- Tortell, P.D., Maldonado, M.T., Granger, J., Price, N.M., 1999. Marine bacteria and biogeochemical cycling of iron in the oceans. *FEMS Microbiol. Ecol.* 29, 1–11. <https://doi.org/10.1111/j.1574-6941.1999.tb00593.x>
- Tortell, P.D., Maldonado, M.T., Price, N.M., 1996. The role of heterotrophic bacteria in iron-limited ocean ecosystems. *Nature* 383, 330–332. <https://doi.org/10.1038/383330a0>
- Town, R.M., van Leeuwen, H.P., 2005. Measuring Marine Iron(III) Complexes by CLE-AdSV. *Environ. Chem.* 2, 80–84. <https://doi.org/10.1071/EN05021>

- Twining, B.S., Baines, S.B., 2013. The Trace Metal Composition of Marine Phytoplankton. *Annu. Rev. Mar. Sci.* 5, 191–215. <https://doi.org/10.1146/annurev-marine-121211-172322>
- van den Berg, C.M.G., 2006. Chemical Speciation of Iron in Seawater by Cathodic Stripping Voltammetry with Dihydroxynaphthalene. *Anal. Chem.* 78, 156–163. <https://doi.org/10.1021/ac051441+>
- van den Berg, C.M.G., 2005. Organic Iron Complexation Is Real, The Theory Is Used Incorrectly. Comment on “Measuring Marine Iron(III) Complexes by CLE-AdSV.” *Environ. Chem.* 2, 88. <https://doi.org/10.1071/EN05029>
- van den Berg, C.M.G., 1995. Evidence for organic complexation of iron in seawater. *Mar. Chem., The Chemistry of Iron in Seawater and its Interaction with Phytoplankton* 50, 139–157. [https://doi.org/10.1016/0304-4203\(95\)00032-M](https://doi.org/10.1016/0304-4203(95)00032-M)
- van den Berg, C.M.G., 1982. Determination of copper complexation with natural organic ligands in seawater by equilibration with MnO<sub>2</sub> II. Experimental procedures and application to surface seawater. *Mar. Chem.* 11, 323–342. [https://doi.org/10.1016/0304-4203\(82\)90029-9](https://doi.org/10.1016/0304-4203(82)90029-9)
- Van den Berg, C.M.G., Huang, Z.Qiang., 1984. Direct electrochemical determination of dissolved vanadium in seawater by cathodic stripping voltammetry with the hanging mercury drop electrode. *Anal. Chem.* 56, 2383–2386. <https://doi.org/10.1021/ac00277a028>
- van den Berg, C.M.G., Nimmo, M., Daly, P., Turner, D.R., 1990. Effects of the detection window on the determination of organic copper speciation in estuarine waters. *Anal. Chim. Acta* 232, 149–159. [https://doi.org/10.1016/S0003-2670\(00\)81231-3](https://doi.org/10.1016/S0003-2670(00)81231-3)
- Velasquez, I.B., Ibisani, E., Maas, E.W., Boyd, P.W., Nodder, S., Sander, S.G., 2016. Ferrioxamine Siderophores Detected amongst Iron Binding Ligands Produced during the Remineralization of Marine Particles. *Front. Mar. Sci.* 3. <https://doi.org/10.3389/fmars.2016.00172>
- von der Heyden, B.P., Roychoudhury, A.N., 2015. A review of colloidal iron partitioning and distribution in the open ocean. *Mar. Chem., Biogeochemistry of trace elements and their isotopes* 177, 9–19. <https://doi.org/10.1016/j.marchem.2015.09.003>
- Walczak, M.M., Dryer, D.A., Jacobson, D.D., Foss, M.G., Flynn, N.T., 1997. pH Dependent Redox Couple: An Illustration of the Nernst Equation. *J. Chem. Educ.* 74, 1195. <https://doi.org/10.1021/ed074p1195>
- Wang, H., Wang, W., Liu, M., Zhou, H., Ellwood, M.J., Butterfield, D.A., Buck, N.J., Resing, J.A., 2022. Iron ligands and isotopes in hydrothermal plumes over backarc volcanoes in the Northeast Lau Basin, Southwest Pacific Ocean. *Geochim. Cosmochim. Acta* 336, 341–352. <https://doi.org/10.1016/j.gca.2022.09.026>
- Wang, P., Ding, Y., Liang, Y., Liu, M., Lin, X., Ye, Q., Shi, Z., 2021. Linking molecular composition to proton and copper binding ability of fulvic acid: A theoretical modeling approach based on FT-ICR-MS analysis. *Geochim. Cosmochim. Acta* 312, 279–298. <https://doi.org/10.1016/j.gca.2021.07.019>
- Welch, K.D., Davis, T.Z., Aust, S.D., 2002. Iron Autoxidation and Free Radical Generation: Effects of Buffers, Ligands, and Chelators. *Arch. Biochem. Biophys.* 397, 360–369. <https://doi.org/10.1006/abbi.2001.2694>
- Wells, M., Buck, K.N., Sander, S.G., 2013. New approach to analysis of voltammetric ligand titration data improves understanding of metal speciation in natural waters. *Limnol. Oceanogr. Methods* 11, 450–465. <https://doi.org/10.4319/lom.2013.11.450>
- Whitby, H., Planquette, H., Cassar, N., Bucciarelli, E., Osburn, C.L., Janssen, D.J., Cullen, J.T., González, A.G., Völker, C., Sarthou, G., 2020. A call for refining the role of humic-like substances in the oceanic iron cycle. *Sci. Rep.* 10, 1–12. <https://doi.org/10.1038/s41598-020-62266-7>
- Whitby, H., van den Berg, C.M.G., 2015. Evidence for copper-binding humic substances in seawater. *Mar. Chem., SCOR WG 139: Organic Ligands – A Key Control on Trace Metal Biogeochemistry in the Ocean* 173, 282–290. <https://doi.org/10.1016/j.marchem.2014.09.011>

- Williford, T., Amon, R.M.W., Benner, R., Kaiser, K., Bauch, D., Stedmon, C., Yan, G., Walker, S.A., van der Loeff, M.R., Klunder, M.B., 2021. Insights into the origins, molecular characteristics and distribution of iron-binding ligands in the Arctic Ocean. *Mar. Chem.* 231, 103936. <https://doi.org/10.1016/j.marchem.2021.103936>
- Worsfold, P.J., Lohan, M.C., Ussher, S.J., Bowie, A.R., 2014. Determination of dissolved iron in seawater: A historical review. *Mar. Chem.* 166, 25–35. <https://doi.org/10.1016/j.marchem.2014.08.009>
- Wu, J., Luther, G.W., 1995. Complexation of Fe(III) by natural organic ligands in the Northwest Atlantic Ocean by a competitive ligand equilibration method and a kinetic approach. *Mar. Chem., The Chemistry of Iron in Seawater and its Interaction with Phytoplankton* 50, 159–177. [https://doi.org/10.1016/0304-4203\(95\)00033-N](https://doi.org/10.1016/0304-4203(95)00033-N)
- Wu, S., He, M., Hu, B., Jiang, Z., 2007. Determination of trace rare earth elements in natural water by electrothermal vaporization ICP-MS with pivaloyltrifluoroacetone as chemical modifier. *Microchim. Acta* 159, 269–275. <https://doi.org/10.1007/s00604-007-0764-5>
- Yun, J., Choi, H., 2000. Micellar colorimetric determination of iron, cobalt, nickel and copper using 1-nitroso-2-naphthol. *Talanta* 52, 893–902. <https://doi.org/10/fnrgn7>
- Zhu, K., Hopwood, M.J., Groenenberg, J.E., Engel, A., Achterberg, E.P., Gledhill, M., 2021. Influence of pH and Dissolved Organic Matter on Iron Speciation and Apparent Iron Solubility in the Peruvian Shelf and Slope Region. *Environ. Sci. Technol.* 55, 9372–9383. <https://doi.org/10.1021/acs.est.1c02477>
- Zigah, P.K., McNichol, A.P., Xu, L., Johnson, C., Santinelli, C., Karl, D.M., Repeta, D.J., 2017. Allochthonous sources and dynamic cycling of ocean dissolved organic carbon revealed by carbon isotopes. *Geophys. Res. Lett.* 44, 2407–2415. <https://doi.org/10.1002/2016GL071348>

# **Chapter 2**

## **2. Introducing the CLE-ACSV method**

### **2.1. Presentation**

#### **2.1.1. Concept of the competitive ligand exchange approach**

The CLE approach consists of the addition of an AL forming an electroactive complex with the metal of interest, here Fe (Figure 2.1a). Because of its ability to complex Fe, the AL creates a new equilibrium between free Fe ( $Fe'$ ), Fe bond to natural Fe-binding ligand (FeL), and Fe bond to AL. The analysis relies on the competition between FeL and AL along a gradient of DFe concentration. At least 10 aliquots of the same sample are prepared, in which an increasing amount of DFe is spiked. Once the aliquots have been left to compete until thermodynamic equilibrium is reached (Figure 2.1b), the stronger FeL have complexed most of the DFe at low DFe concentration, and FeL are progressively saturated until complete saturation with increasing DFe (Figure 2.1c). The progressive saturation of FeL is indirectly followed by the electrochemical quantification of the Fe-AL complex (FeAL; Figure 2.1c; Figure 2.3). The section of the titration for which FeL are saturated and the amount of FeAL increases linearly allows the estimation of the FeL concentration ( $[L]$ ), while the curvature section for which FeL and AL are competing for DFe allows the estimation of the binding constant  $K^{cond}$  expressed as a logarithmic value relative to FeL ( $\log K_{FeL}^{cond}$ ).

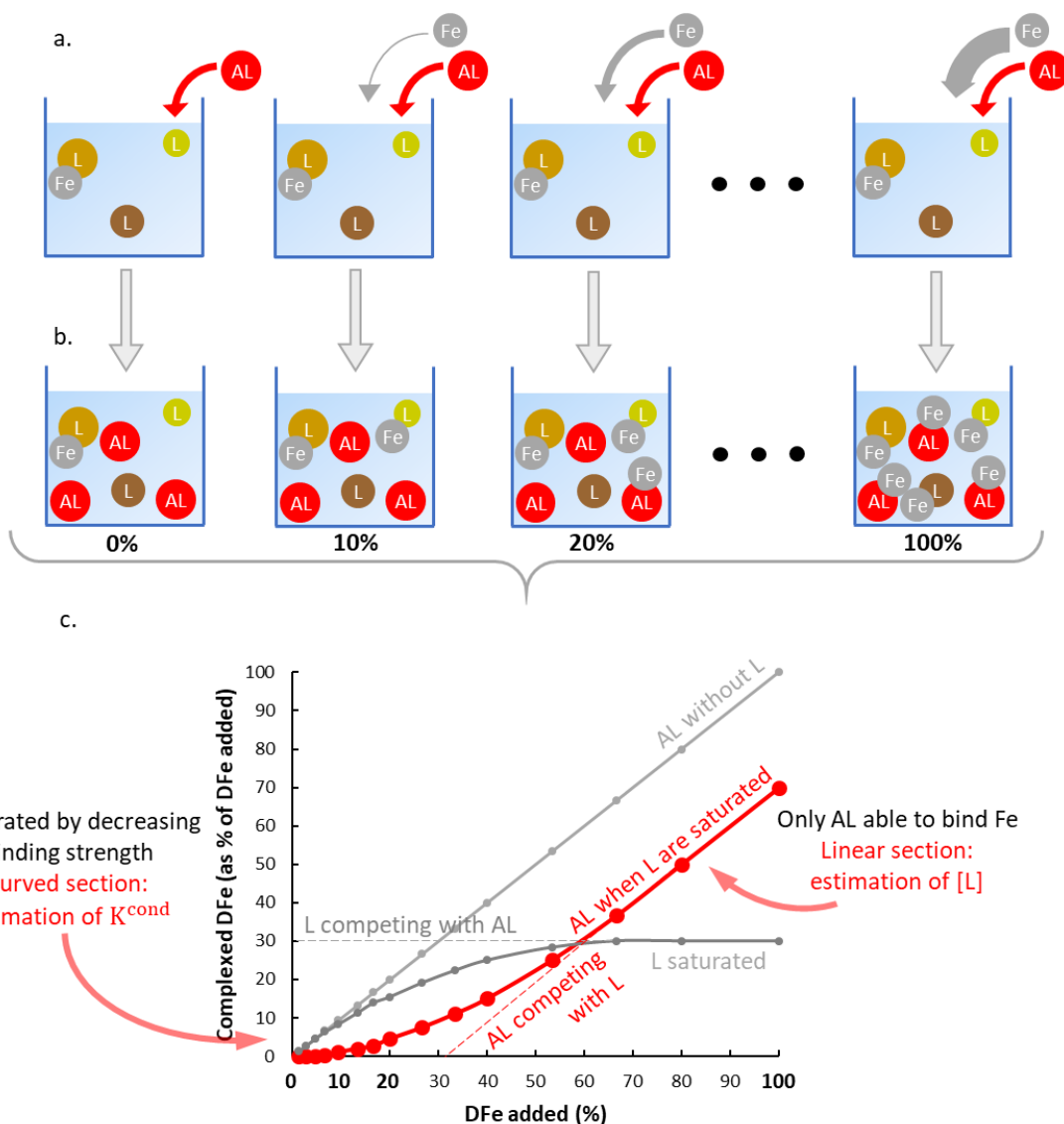


Figure 2.1. Concept of the CLE approach divided in a) sample preparation, b) equilibration and c) resultant Fe partitioning. The light grey curve shows that in absence of FeL, AL complexes all the Fe. The dark grey curve represents the amount of Fe complexed by FeL, (from low to high DFe) first outcompeting the AL until they are saturate, then competing with AL, and finally when all the FeL are saturated. The red curve represents the amount of DFe complexed by the AL. The dots in the plot represent the aliquots. Proportions are only figurative.

### 2.1.2. ACSV measurement

The electrochemical quantification of DFe bound as FeAL by ACSV consists of, first, the accumulation of the chelated Fe<sup>3+</sup> by the AL (FeAL or Fe<sup>3+</sup>AL<sub>x</sub> in Figure 2.2) onto a mercury drop electrode (MDE; working electrode) at a fixed potential. After this pre-concentration step, the quantification is performed by the reduction of Fe<sup>3+</sup> to Fe<sup>2+</sup> during a cathodic scan, where the potential is scanned from positive to more negative values, called the stripping step (Figure 2.2). In the case of our set up provided by the brand Metrohm™ (Figure 2.3), the voltammetric system consists of a 663 VA Stand, Metrohm™, a



potentiostat  $\mu$ Autolab Type III (to impose and measure potential and current at the electrodes), and of an interface (IME 663, Metrohm<sup>TM</sup>) which controls the formation of fresh mercury drops, and the stirring and purge of the solution (Figure 2.3). The voltammetric system is piloted using the software NOVA (version 2.5.1, Metrohm<sup>TM</sup>; Figure 2.3) and requires gas supply, either 1 bar of nitrogen ( $N_2$ ), oxygen ( $O_2$ ) or a mix of  $O_2$  and  $CO_2$  depending on the application. ACSV analysis requires a 3-electrode system (Figure 2.2). The working electrode, where the consumption of electrons by reduction happens (cathode), is a single-use MDE. It requires a specific device for reproducible formation of the drops, composed of a multi-mode electrode (MME, Metrohm<sup>TM</sup>; Figure 2.2) and of a glass capillary (Metrohm<sup>TM</sup>; Figure 2.3). The auxiliary electrode, classically a glassy carbon or platinum rod in ACSV applications, completes the electrical circuit and accepts electrons (anode). The control of the potential requires the presence of a reference electrode. Most applications use a silver-silver chloride electrode (Ag/AgCl; Metrohm<sup>TM</sup>; Figure 2.3), isolated from the solution by a saline bridge, composed of a ceramic junction and of either a polychlorotrifluoroethylene (PCTFE) or glass reservoir, filled with a saturated potassium chloride solution (3 M KCl).

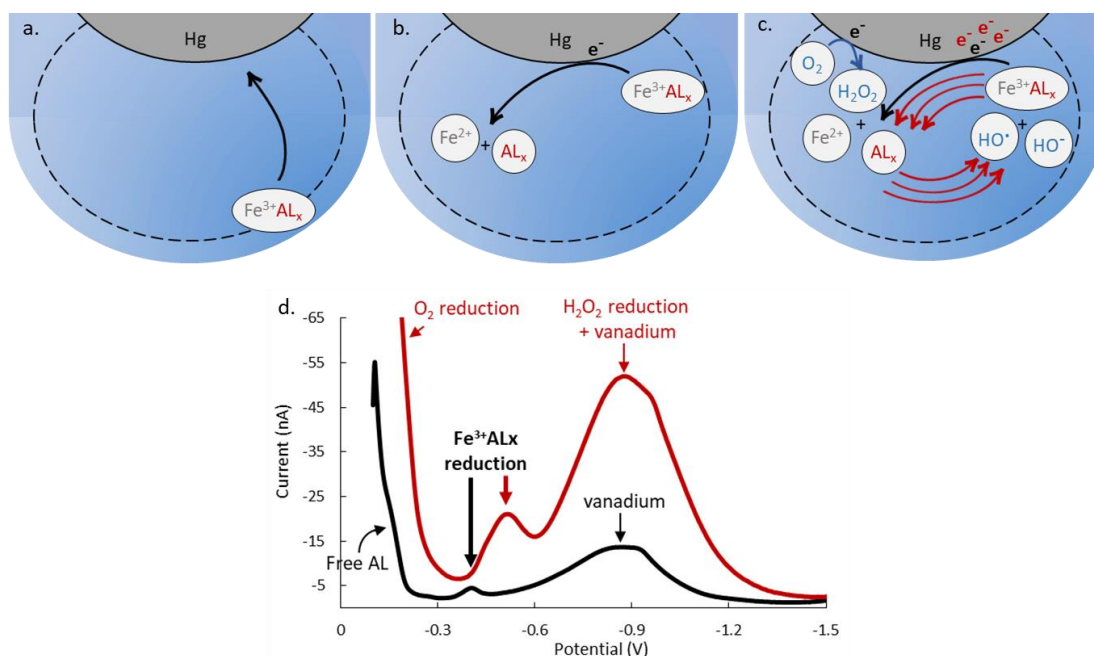


Figure 2.2. Process of ACSV measurement (a, b, c) in the diffusion layer (black dashes) of the mercury drop (Hg, in grey) with a) concentration of the  $Fe^{3+}AL_x$  complex by application of a fixed potential, b) reduction of the  $Fe^{3+}AL_x$  complex by potential scan toward more negative values in deoxygenated solution, and c) reduction of the  $Fe^{3+}AL_x$  complex and of  $O_2$  into  $H_2O_2$  in the case of catalysis with  $O_2$ , and d) recorded voltammograms for deoxygenated (black line) and oxygenated (red line) conditions.

The stripping and reduction of FeAL (Figure 2.2b) generate a reductive peak current (in nanoampere; nA) proportional to the amount of Fe<sup>3+</sup> reduced (Figure 2.2d). Some CLE-ACSV applications use a catalytic process to enhance the reduction signal measured, increasing the sensitivity and lowering the analysis time (Figure 2.2c; Table 1). The catalysis is based on the addition or *in-situ* production of a super-oxidant at the working electrode, which is able to instantly oxidise the freshly reduced Fe<sup>2+</sup> into Fe<sup>3+</sup>, that forms back the FeAL complex. The speed of this reaction is such that it allows the metal of interest to be reduced several times during the stripping step, and thus enhance considerably the reduction signal. The super oxidant necessary for this catalytic process can be directly added to the sample, as previously done with potassium bromate (KBrO<sub>3</sub>) and hydrogen peroxide (H<sub>2</sub>O<sub>2</sub>) (Kolthoff and Parry, 1951; Pospíšil, 1953; Yokoi and van den Berg, 1992). Recently, the *in-situ* formation of H<sub>2</sub>O<sub>2</sub> at the working electrode surface by the reduction of the O<sub>2</sub> naturally present in the sample has known an increasing interest as it limits the number of reagents to add to the sample and the risk of oxidation of the DOM present in the sample. This method is based on the Fenton (1894) reaction, naturally occurring for photosynthesis and commonly used in wastewater treatments (Haber and Willstätter, 1931). Here at the MDE, H<sub>2</sub>O<sub>2</sub> is formed and the Fe<sup>3+</sup> bound to the AL is reduced into Fe<sup>2+</sup>. Then, the H<sub>2</sub>O<sub>2</sub> and Fe<sup>2+</sup> reduce and oxidise each other, respectively, and the regenerated Fe<sup>3+</sup> can be chelated again by the AL, giving rise to an enhanced sensitivity through this catalytic effect.

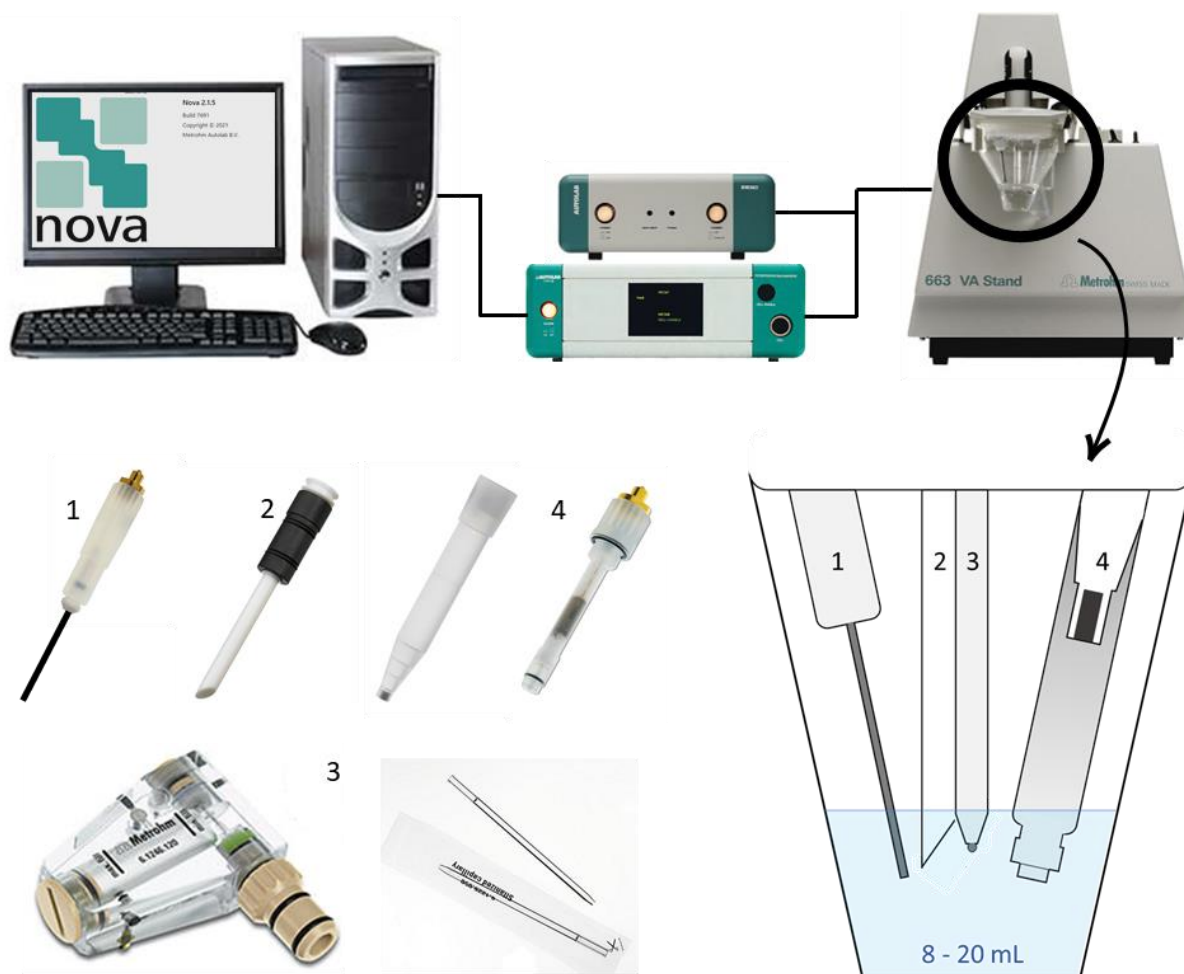


Figure 2.3. Apparatus provided by Metrohm™ for ACSV analysis. It is composed (top, left to right) of a computer with the software NOVA (2.5.1), controlling a potentiostat ( $\mu$ Autolab Type III) and an IME (663) piloting the voltammetric system (663 VA Stand), the stirring, the purge, and the electrodes it is equipped with. The cell (bottom right) contains a glassy carbon auxiliary electrode (1), a stirring rod in Teflon™ (2), a capillary holding the MDE (3), and an Ag/AgCl electrode (4) in a bridge.

## 2.2. Theory of the CLE

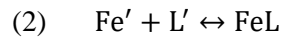
In the following section, a differentiation is made between the organically chelated DFe (FeL) and the natural organic binding ligands defined by CLE-ACSV (L) because [L] corresponds to the maximal ability of the DOM to bind DFe in the given analytical conditions, which generally exceeds the DFe measured in seawater samples (e.g. Buck et al., 2018, 2015; Gerringa et al., 2015).

### 2.2.1. Calculation of [L] and $\log K_{FeL}^{cond}$

All species mentioned into brackets correspond to concentrations, generally in  $\text{nmol.L}^{-1}$ . In seawater, the DFe speciation can be summarized as the sum of the inorganic and free Fe ( $\text{Fe}'$ ) and of the organically chelated forms (FeL):

$$(1) \quad [\text{DFe}] = [\text{Fe}'] + [\text{FeL}]$$

The chemical equilibrium of the association/dissociation of  $\text{Fe}'$  with the free iron-binding ligands ( $\text{L}'$ ) into FeL complexes (FeL) is expressed as:



With its conditional stability constant being:

$$(3) \quad K_{FeL}^{cond} = \frac{[\text{L}]}{[\text{Fe}'][\text{L}']}$$

This conditional stability constant includes all inorganic DFe forms. However, the most DFe forms susceptible to be chelated are its free forms, the predominant one being  $\text{Fe}^{3+}$ . The introduction of the inorganic side reaction coefficient ( $\alpha_{IN}$ ) allows expression of the conditional stability constant with respect to  $\text{Fe}^{3+}$  ( $K'_{FeL}$ ):

$$(4) \quad \alpha_{IN} = \frac{[\text{Fe}']}{[\text{Fe}^{3+}]}$$

$$(5) \quad K_{FeL}^{cond} = \alpha_{IN} K'_{FeL}$$

The CLE-ACSV method is based on the addition of AL in excess, leading to the new speciation equation:

$$(6) \quad [\text{dFe}] = [\text{Fe}'] + [\text{FeL}] + [\text{FeAL}_n]$$

With n the stoichiometry of the AL to complex Fe. The corresponding conditional stability constant between Fe and the added ligand is:

$$(7) \quad \beta_1 = \frac{[\text{FeAL}_n]}{[\text{Fe}'][\text{AL}]^n}$$

The coefficient  $\beta_1$  is determined by the calibration of the artificial ligand. The related procedure and calculation are explained from Eq.(13). The side reaction coefficient of the  $\text{FeAL}_n$  complex ( $\alpha_1$ ) can then be expressed as a function of Eq.(7):

$$(8) \quad \alpha_1 = \frac{[\text{FeAL}_n]}{[\text{Fe}']} = \beta_1 [\text{AL}]^n$$

$\alpha_1$  is also called detection window (D), sometimes expressed as a logarithmic value ( $\log D$ ; Ardiningsih et al., 2021). The reason of the definition of D is that if  $\text{FeL}$  are considered as a continuum of  $K_{\text{FeL}}^{\text{cond}}$ , the AL used will be able to compete with only a certain range of them. The only unknown variable in Eq.(8) is  $[\text{Fe}']$  but it can be calculated by introducing the notion of sensitivity S (in,  $\text{A}/(\text{mol.L}^{-1})$  with A meaning amper) which is the ratio between the reductive current measured ( $i_p$ , in nA) and the amount of  $\text{FeAL}_n$  (in  $\text{nmol.L}^{-1}$ ) formed:

$$(9) \quad S = \frac{i_p}{[\text{FeAL}_n]}$$

This value is defined using the linear end section of the titration (Figure 2.1), when the natural ligands are saturated and  $\text{FeAL}_n$  only depends on the amount of Fe added. Therefore Eq.(8) and Eq.(9) can be rearranged as:

$$(10) \quad [\text{Fe}'] = \frac{i_p}{S\alpha_1}$$

The only remaining unknown component to solve Eq.(6) is  $\text{FeL}$ . This term is defined by its equilibrium constant  $K_0$  and its side reaction coefficient  $\alpha_0$ . The latter can be determined by reorganizing Eq.(8) and Eq.(6). By expressing each dFe components by the variable  $\text{Fe}'$  (from Eq.(3) and (8)), the following expression is obtained:

$$(11) \quad \frac{[\text{FeAL}_n]}{[\text{dFe}]} = \frac{\beta_1 [\text{AL}]^n}{1 + K_{\text{Fe}'\text{L}}^{\text{cond}} [\text{L}'] + \beta_1 [\text{AL}]^n} = \frac{\alpha_1}{1 + \alpha_0 + \alpha_1}$$

Those equations consider only one class of ligand. Eq.(11) can be extended to different classes by replacing the terms  $K_{Fe'L}^{cond}$  [L'] by  $\sum K^{cond}L$ . A simple expression can be defined to determine this variable by reversing Eq.(11) and injecting Eq.(8):

$$(12) \quad \frac{[Fe']}{[dFe]-[FeAL_n]} = \frac{1}{1+\sum K^{cond}L}$$

To solve Eq.(4) of which depends Eq.(12), the Fe' overall side reaction ( $\alpha_{IN}$ ) is also necessary. This value is still debated, however, the value  $10^{10}$  (Rue and Bruland, 1995b) is commonly used for the convenience of the conversion. Values of  $10^{11}$  (Rue and Bruland, 1997),  $10^{11.6}$  (Gledhill and van den Berg, 1994), and  $10^{11.9}$  (Nolting et al., 1998) have also been used.

### 2.2.2. Calibration

The calibration of the AL is necessary to determine  $\alpha_1$  and  $\beta_1$ . The calibration of the AL is very similar to the investigation of the natural one: a compound known to form very strong mono-complexes with trace metals, such as the ethylene diamine tetra acetic acid (EDTA), is added in at least 10 aliquots of seawater free of natural ligands but containing a known artificial ligand concentration, such as:

$$(13) \quad [dFe] = [FeAL_n] + [FeEDTA]$$

In seawater free of natural ligands with only the artificial ligand, the reduction current is maximum and proportional to the amount of FeAL<sub>n</sub> complex formed:

$$(14) \quad i_{p/0} = S[FeAL_n] = S([dFe] - [Fe'])$$

In presence of EDTA, the attenuation of the signal is proportional to the amount of FeEDTA complexes formed:

$$(15) \quad i_{p/i} = S([dFe] - [Fe'] - [FeEDTA])$$

The ratio of these reductive current can be expressed as:

$$(16) \quad X = \frac{i_{p/i}}{i_{p/0}} = \frac{\beta_1[AL]^n}{K_{FeEDTA}[EDTA'] + \beta_1[AL]^n}$$

With:

$$(17) \quad [\text{EDTA}'] = [\text{EDTA}_T] - (1 - X)[\text{DFe}]$$

Finally, this expression can be rearranged to determine the value of the equilibrium constant of the artificial ligand:

$$(18) \quad \beta_1 = \frac{XK_{\text{FeEDTA}}[\text{EDTA}']}{[\text{AL}]^n - X[\text{AL}]^n}$$

To calculate  $K_{\text{FeEDTA}}$  and solve Eq.(16), EDTA overall side reaction ( $\alpha_{\text{EDTA}}$ ) is necessary. This constant is classically defined with respect to the major cations and proton concentrations as assembled by Martell and Smith (1982).

### 2.2.3. Graphical fitting

After recording the reduction signal of the FeAL in the aliquots of a seawater sample, the titration needs to be interpreted. Several mathematical approaches have been developed to interpret the CLE-ACSV titration results. With the aim of limiting human error and subjectivity by user, tools were developed to simultaneously constrain the titration data following the most commonly used fittings, such as the software ProMCC (Omanović et al., 2015). Multiple publications present comparison of the mathematical approaches and their limitations (Gerringa et al., 2014, 1995; Omanović et al., 2015; Pižeta et al., 2015). Hereafter is presented a simplified overview of the methods compared in the software ProMCC.

The determination of the constants  $K^{\text{cond}}$  and  $[\text{L}]$  is usually made by fitting the data to a mathematical expression similar to the Langmuir isotherm (Langmuir, 1916), by the use of a linear or non-linear rearrangement of Eq.(12). The (Scatchard, 1949) and Ruzic/van den Berg (Ružić, 1982; van den Berg, 1982) linearization (Eq.(19) and Eq.(20), respectively) are the two most famous linear fittings because of their simplicity:

$$(19) \quad \frac{[\text{FeL}]}{[\text{Fe}']} = -K^{\text{cond}}[\text{FeL}] + K^{\text{cond}}[\text{L}']$$

$$(20) \quad \frac{[\text{Fe}']}{[\text{FeL}]} = \frac{[\text{Fe}']}{[\text{L}']} + \frac{1}{K^{\text{cond}}[\text{L}']}$$

These two expressions are fairly similar, however the dependence of the 2 right members to  $K^{\text{cond}}$  instead of  $[L]$  in Eq. 19 allows the qualification of more than 1 ligand class:

$$(21) \quad \frac{[Fe']}{\sum[FeL_i]} = 1 / \sum \left( \frac{[L_i]}{[Fe'] + 1/K_i^{\text{cond}}} \right)$$

Details of the non-linear calculation have been presented by Gerringa et al. (2014), and compared with the other fittings by (Pižeta et al., 2015). The particularity of the commonly called Langmuir/Gerringa method is the solvation of a one-member equation (Gerringa et al., 2014b):

$$(22) \quad [FeL] = \frac{K^{\text{cond}}[L][Fe']}{1 + K^{\text{cond}}[Fe']}$$

Originally, the consideration of more than one ligand class was made by using the Ruzic/van den Berg expressions (Eq. 21; (Gerringa et al., 1995). In the latest revision of the method, the exchange of the dependent (L) and independent (Fe') variables in the expression allows to decompose  $[FeL]$  as (Gerringa et al., 2014b; Omanović et al., 2015):

$$(23) \quad \sum[FeL_i] = \sum \frac{K_i^{\text{cond}}[L_i][Fe']}{1 + K_i^{\text{cond}}[Fe']}$$

To be noticed that in those expressions, FeL could already be replaced by L as the fitting of those equations results in determining the potential of the DOM to bind DFe. The equations above are popularly used because of their relative simplicity, but they are not fully satisfying as X and Y axes are dependent (Omanović et al., 2015). The calculation concepts are however well explained from those, and more complex solutions behind these solutions have been presented in the literature as listed by (Omanović et al., 2015). As a simplified tool for the estimation of  $K^{\text{cond}}$  and  $[L]$ , the software ProMCC compile the graphical fittings presented above in 4 distinct windows (Figure 2.4). The top left one is the initial data, to verify if the shape corresponds to the progressive saturation of the natural ligands and often used to define S. The top right one and bottom left are the Langmuir/Gerringa non-linear (Eq. 23) and Ruzic/van den Berg linear solutions respectively, which can both be used to estimate  $K^{\text{cond}}$  and  $[L]$ . The bottom right plot is the Scatchard plot, which is used to verify the presence of 1 (linear plot) or 2 (curvature plot) ligand class.



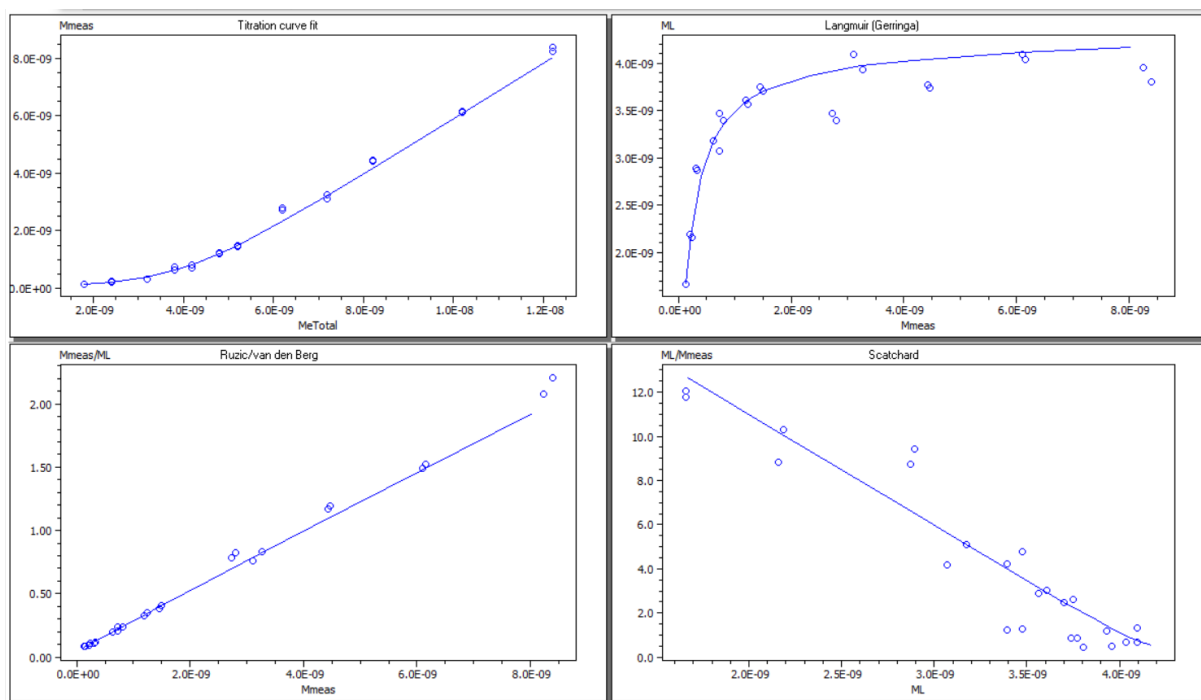


Figure 2.4. Screenshot of the simultaneous graphical fittings provided by the software ProMCC in the case of the titration of a seawater sampled in the Atlantic Southern Ocean titrated with 25  $\mu\text{M}$  of salicylaldoxime. The top left window shows the titration curve, the top right window the Langmuir/Gerringa fitting, the bottom left the Ruzic/van den Berg fitting, and the bottom right the Scatchard fitting.

### 2.3. Characteristics of the ALs

The artificial ligands adapted to investigate iron ligands by CLE-ACSV are displayed in Table 2.1: 2,3-dihydroxynaphthalene (DHN; Sanvito and Monticelli, 2020; van den Berg 2006), 2-(2-thiazolylazo)-p-cresol (TAC; (Croot and Johansson, 2000), salicylaldoxime (SA; Abualhaija and van den Berg, 2014; Buck et al., 2007; Rue and Bruland, 1995), and 1-nitroso-2-naphthol (NN; Gledhill and van den Berg, 1994; van den Berg, 1995). NN is the ligand with the broader range of application. The latter has been used in different matrix (and pH) such as seawater (pH 6.9 and 8.0; Gledhill and van den Berg, 1994; van den Berg, 1995), freshwater (pH 8.1; Nagai et al., 2004), and rainwater (pH from 5.5 to 6.2; Cheize et al., 2012), but can show an interfering signal limiting the interpretation of the voltammograms (e.g. Boye et al., 2001; Croot et al., 2004). An alternative method to the classic ligand titration was developed with NN to titrate FeL when DFe is in excess, relying on the addition of NN instead of DFe (Hawkes et al., 2013a). This method is of specific interest to titrate FeL in hydrothermal systems (e.g. Hawkes et al., 2013b; Wang et al., 2022, 2021). NN was, however, shown to outcompete HS in the range of concentration (Laglera et al., 2011). Other ligands are not flexible in pH, but somehow TAC seems

more straightforward to use, which is why it has been more widely applied (see Table 1 in Caprara et al., 2016). Each AL requires specific attention from preparing the solution to interpreting data.

SA and DHN solutions are easily prepared by dilution in Milli-Q water. They are stored acidified to avoid their progressive oxidation over time. In the case of DHN, the oxidation happens in the order of minutes at room temperature which drastically constrains its use (Sanvito and Monticelli, 2020). On the other hand, the preparation of TAC and NN is restricted by the need to dissolve them in methanol (MeOH). MeOH requires a purification step by triple distillation to avoid Fe contamination. Also, MeOH is a volatile solvent of low surface tension. Therefore, the concentration of TAC and NN solutions can vary in time, and the pipetting can be less accurate because of leaching from the pipette tip.

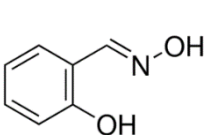
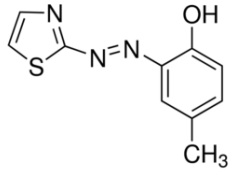
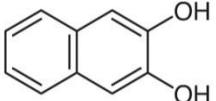
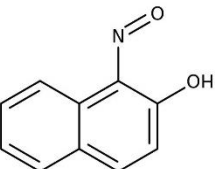
It is essential to know exactly the stoichiometry of  $\text{Fe}^{3+}$  complexation by artificial ligands to estimate  $[\text{L}]$  and  $\log K_{\text{FeL}}^{\text{cond}}$ . It is also essential to be sure that the electroactive complex is the major FeAL chelate formed. If not, the natural ligands would be competing for Fe with other species than the detectable one and both  $[\text{L}]$  and  $\log K_{\text{FeL}}^{\text{cond}}$  would be overestimated. In the case of SA, it has been shown that the high concentration used in the first applications (Buck et al., 2007; Rue and Bruland, 1995) were favouring the formation of a non-electroactive complex  $\text{Fe}(\text{SA})_2$  over time (Abualhaija and van den Berg, 2014). The presence of both species  $\text{FeTAC}$  and  $\text{FeTAC}_2$  has been observed in previous work (Croot and Johansson, 2000) but the  $\text{FeTAC}$  complex did not interfere with the determination of  $[\text{L}]$  and  $\log K_{\text{FeL}}^{\text{cond}}$ . No interfering complexes has been referenced for NN and DHN.

Together with the stoichiometry of the artificial ligand-complex formed, AL concentration and  $\beta_1$  define the analytical window  $D$  or  $\alpha_{\text{Fe}^{\text{AL}}}$  (Section 2.2.1.; Ardiningsih et al., 2021). The term  $D$  comes from the fact that the binding ligands present are very diverse, so it is unlikely that the AL is competing with all of them at a single concentration. Indeed, if  $\text{FeL}$  are strong and at low concentration, the competition only happens on the few first aliquots (or not at all), which is not enough to allow their determination (Apte et al., 1988). In the meantime, a detection window too high will outcompete weak ligands. The importance of  $D$  was illustrated by van den Berg (1995) who observed decreasing  $[\text{L}]$  and

increasing  $K^{\text{cond}}$  with increasing detection window with the ligand NN. Tests on the CLE-ACSV method shown that the natural ligand detected have  $\log \alpha_{\text{Fe}^{\text{L}}}$  values encompassed by  $\log D \pm 1$  (Apte et al., 1988; van den Berg et al., 1990) up to  $\log D \pm 2$  (Gerringa et al., 2014), while measured  $\log K_{\text{FeL}}^{\text{cond}}$  generally encompass a range of 2 to 4 units.

The choice in the AL used drives to different CLE-ACSV outputs. Two classes of ligand are often detected using SA while only one is detected with TAC and NN (Ardiningsih et al., 2021; Buck et al., 2012). More recently, thorough comparison of SA, TAC and NN showed a strong lack of agreement in the resulting [L] and  $\log K_{\text{FeL}}^{\text{cond}}$  (Ardiningsih et al., 2021; Gerringa et al., 2021). It has been suggested that the implementation of multiple detection window (MDW) could help resolve the differences observed between methods (Pižeta et al., 2015). MDW consists of performing several titrations at different AL concentrations (therefore, different D), and has been shown to reveal the presence of different ligand classes (e.g. Bundy et al., 2014; Mahmood et al., 2015; Wells et al., 2013), but it is not a common approach due the number of aliquots involved, implicating longer analysis time, harder data interpretation, and larger volume requirement of the sample.

Table 2.1. Specificities of the ALs in use for the investigation of FeL by CLE-ACSV.

Ligand	SA	TAC	DHN	NN
References	Abualhaija and van den Berg, 2014; Buck et al., 2007; Rue and Bruland, 1995	Croot et al., 2004; Croot and Johansson, 2000; Laglera et al., 2011	Laglera et al., 2011; Sanvito and Monticelli, 2020; van den Berg, 2006	Aldrich and van den Berg, 1998; Boye et al., 2001; Gledhill and van den Berg, 1994
Dissolution	Acidified Milli-Q MeOH	Acidified Milli-Q	MeOH	MeOH
Compound chemistry				
Electroactive Fe chelate	FeSA	Fe(TAC) <sub>2</sub>	FeDHN	Fe(NN) <sub>3</sub>
Interfering Fe chelate	Fe(SA) <sub>2</sub>	None	None	None

Other interfering chelates	Refractory HS in bottom samples?	HS?	HS?	HS or glutathione-like in Southern Ocean water
Catalysis	Dissolved O <sub>2</sub>	None	Dissolved O <sub>2</sub>	Hydrogen peroxide (1.7mM) with 5 ppm SDS None
pH (buffer)	8.18 (borate)	8.0 (EPPS)	8.0 (HEPPS)	6.9 (PIPES) 8.1 (Tris, HEPPS)
Identified interfering buffer	None	None	Borate	None
Detection windows as log $\alpha_{FeAL}$	1.2 for 5 $\mu$ M 1.8 for 27.5 $\mu$ M 1.9 for 25 $\mu$ M	2.4 for 10 $\mu$ M	2.7 for 0.5 $\mu$ M 3.2 for 1 $\mu$ M 4.0 for 5 $\mu$ M 4.2 for 10 $\mu$ M	1.5 for 1 $\mu$ M 2.4 for 2 $\mu$ M 4.0 for 7 $\mu$ M 4.3 for 8.7 $\mu$ M 5.0 for 15 $\mu$ M
Voltammetric method	Differential pulse Adsorption/step potential: 0V/6mV Modulation/interval time: 0.004 s/0.1 s Modulation amplitude: 50 mV	Linear sweep wave Adsorption/step potential: -0.4 V/2 mV Scan rate: 10.12 V/s	Square-wave Adsorption/step potential: -0.4 V/5mV Scan rate: 50 mV/s Frequency: 10 Hz	Sampled-DC mode Adsorption potential: -0.05 V Scan rate: 50 mV/s Linear sweep wave Adsorption/step potential: -0.15 V/4 mV Scan rate: 40 mV/s
Maximum deposition time used	600 s	600 s	30 s	300 s

## 2.4. Assumption and consideration

The CLE-ACSV theory relies on several assumptions and requires technical considerations which have not evolved much over the last decade (Gerringa et al., 2014; Omanović et al., 2015; Pižeta et al., 2015).

One should bear in mind these limitations while applying the method and interpreting the data.

### 2.4.1. Sample preparation

Up to date, most systems require a volume of 10 mL per aliquots. Counting a duplicate for the initial point of the titration, and a minimum requirement of 10 aliquots, a total of 12 aliquots is advised (Gledhill and Buck, 2012), with the minimum volume requirement being of 120 mL. Some applications include up to 3 conditionings of the vials, increasing further the volume requirement for CLE-ACSV application (i.e. Abualhaija and van den Berg, 2014; Croot and Johansson, 2000; Gerringa et al., 2021). This is a limiting factor when it comes to share the precious water collected in the field. However, solutions are emerging to limit the amount of water needed. Recently, a CLE-ACSV set up to perform analysis in volume as low as 0.5 mL as been proposed (Sanvito et al., 2019; Sanvito and Monticelli, 2020).

The CLE-ACSV method relies on the dynamic competitive equilibrium between FeL and AL toward the metal of interest. This equilibrium is dependent on the temperature and pH of the sample, concentration of the ligands and concentration of the cations competing for the binding-sites of the ligands (including non-metallic salts; Abualhaija et al., 2015; Louis et al., 2009; Raspor et al., 1980). The kinetic (e.g. time dependence) of the equilibrium is a limiting aspect of the CLE-ACSV and a subject of contention. As an extreme example, a historical conflict happened in 2005 about the validity of the CLE-ACSV approach, with Town and van Leeuwen (2005) stating that the method measures an artefact of hydroxide complexation, motivating answers from the community to state the veracity of the existence of organic complexation (Hunter, 2005) and to explicitly re-explain further the theory behind CLE-ACSV (van den Berg, 2005). Another good example of discord about the kinetic of the chemical equilibrium is the equilibration time use for the investigation of copper (Cu) speciation with the ligand SA, with a minimum equilibration time of the sample established to be either 2 hours (h; Louis et al., 2009), 1 h (Abualhaija et al., 2015) or 15 min (Buck et al., 2012). With regard to Fe, the two equilibration procedures applied with SA are still debated. Abualhaija and van den Berg (2014) showed that overnight equilibration is necessary when SA is added at the same time as DFe, while Rue and Bruland (1995) applied the sequential equilibration method, letting FeL equilibrate with the DFe added during 2 h before spiking with SA, leaving equilibrate with FeL for 15 min before analysis. It has been

suggested that a shorter equilibration time could lead to an overestimation of the sensitivity, and so of [L] and  $\log K_{\text{FeL}}^{\text{cond}}$ , as weak FeL would not have the time to fully equilibrate. To our knowledge, the comparison of these two equilibration procedures has not been published.

#### 2.4.2. Chemical and constant assumptions

The calculation presented in Section 2.2 to determine complexometric variables relies on several assumptions. These assumptions have been thoroughly described by Gerringa et al. (2014) and Pižeta et al. (2015). Firstly, the equilibrium between FeL and FeAL assumes an equivalence between binding sites, which has been shown to not explain fully the Fe complexation in the seawater system (Hiemstra and van Riemsdijk, 2006). Indeed, in view of the hypothesised continuum of the DOM in size and binding sites strength (Altmann and Buffle, 1988), it is unlikely that a 1:1 model represents adequately DFe partitioning between ligands. This is the reason why [L] is expressed as nmol equivalent of Fe added per litre (nMeqFe). Because both [L] and  $\log K_{\text{FeL}}^{\text{cond}}$  are determined by the fitting of a single equation, the stoichiometry of the binding sites impacts  $\log K_{\text{FeL}}^{\text{cond}}$  as well. Secondly, the ability of the AL to compete with all FeL is not ensured. This can be due to the AL used, defining D, which has been shown in the case of NN to outcompete HS (Laglera et al., 2011), and thus underestimate [L] and  $\log K_{\text{FeL}}^{\text{cond}}$ . In contrast, it is likely that some of the DFe is complexed in an irreversible way, prohibiting the competition with the AL. If the DFe is not accessible to the AL and is not corrected from the DFe used to fit the titration data, it would result in an overestimation of the [L] and  $\log K_{\text{FeL}}^{\text{cond}}$ . This phenomenon has been highlighted in hydrothermal samples (Kleint et al., 2016), where the DFe is known to be present at high concentration under inorganic and colloidal forms. The consideration of DFe lability in the determination of [L] and  $\log K_{\text{FeL}}^{\text{cond}}$  is a limiting aspect of the method, specifically in sample showing high DFe concentrations with high proportion of inaccessible inorganic and colloidal DFe such as in coastal and hydrothermal environments. Finally, potential competition with other trace metals for the FeL binding sites can impact the determination of [L] and  $\log K_{\text{FeL}}^{\text{cond}}$  (Abualhaija et al., 2015; Gerringa et al., 2014). Indeed, in the case of an increasing (or decreasing) concentration of a competing element with depth, the calculation considering the metal of interest would result in a decrease (or increase) in

[L], which is true with regard to the metal of interest but not a complete view of the reality. Therefore, it is still essential to consider multidisciplinary approaches while investigating trace metal biogeochemical cycles.

### 2.4.3. Laboratory vs *in situ* conditions

Fe speciation is known to be influenced by thermodynamic conditions (temperature), ionic strength (salinity) and pH of the matrix, with  $\log K_{\text{FeL}}^{\text{cond}}$  and probably [L] being conditional to these parameters. The impact of changes of these parameters on the inorganic Fe speciation has been documented by thorough experimental and modelling work (Millero et al., 2009): temperature increase and decrease of pH and  $[\text{CO}_3^{2-}]$  (i.e. warming and acidification, respectively) will lead to the increase in Fe solubility and stability of the  $\text{Fe}^{2+}$  and so of the Fe' pool, while the concentrations of carbonated and oxyhydroxide Fe will decrease. However, little is known about temperature and pH changes on Fe organic speciation.

In view of the diversity of temperature observed in the ocean (from  $-2\text{ }^\circ\text{C}$  to  $30\text{ }^\circ\text{C}$ ), it would be tedious and time consuming to control and match *in-situ* values. Instead, the AL calibration and FeL titrations are performed at room temperature. Because all measurements are performed the same way, results can still be compared, despite the fact that this could lead to a shift in  $\log K_{\text{FeL}}^{\text{cond}}$  and [L] proportional to the gap between the laboratory and *in-situ* temperature. However, from modelling work that combines all the knowledge about chemical equilibrium as known in seawater, the temperature effect is expected to be negligible (Hiemstra and van Riemsdijk, 2006). Experimental work concluded that the shift could be potentially quantified and corrected (Hassler et al., 2013). More recent modelling work, however, are showing that the evaluation of changes in Fe speciation with temperature or pH is still unclear (Zhu et al., 2021).

The pH of the sample is a critical aspect of the speciation of trace metals and Fe. Surface waters have an average pH of 8.1, however, the pH of deep ocean and oxygen minimum zone (OMZ) is much lower, (as low as 7.8 and 7.5 from the GLODAPv2.2019 database, in the South Atlantic Southern Ocean and in the Pacific OMZ, respectively). Therefore,  $[\text{H}^+]$  varies significantly in the ocean. It plays on Fe

inorganic speciation by defining its solubility (Liu and Millero, 2002), which can be easily corrected for in view of the knowledge of trace metal inorganic speciation (Millero, 2001; Millero et al., 2009). The impact of pH changes and of the  $H^+$  concentration on the Fe organic speciation is, however, unclear (Millero et al., 2009). The structural and chemical diversity of the DOM implies that the functional groups able to bind Fe can be differently impacted by the pH. The acid/base properties of the DOM are rather complicated to investigate notably because the concentration methods used are potentially selective on the fraction of the DOM they are able to isolate, but the results highlight the need to consider DOM protonation to evaluate its ability to bind DFe (Lodeiro et al., 2020). It has been suggested that Fe bioavailability would decrease with pH and ocean acidification, potentially because of an increase in  $\log K_{FeL}^{cond}$  (Shi et al., 2010). Some authors have attempted to verify this hypothesis by CLE-ACSV using NN at different pH, but these studies could not confidently conclude on the consequences of pH changes on Fe organic speciation because of the limited sensitivity of the method (Avendaño et al., 2016; Gledhill et al., 2015). While NN can be used at various pH values but lacks sensitivity, the application using other AL have not been adapted to pH lower than 8.0 (Table 2.1). The development of CLE-ACSV methods focusing on the pH range from 8.0 to 8.2 was motivated by the need to ensure the good representation of Fe organic speciation where its bioavailability matters the most, so in surface waters where primary production happens. Also, the sensitivity of most ALs decreases quickly with decreasing pH (i.e. (Laglera et al., 2016)). Therefore, the impact of the pH adjustment for deep water samples is still to be assessed and can be partly responsible of the lack of accuracy in global Fe cycling modelling (Tagliabue et al., 2016).

The pH of the samples analysed by CLE-ACSV is fixed by the addition of a buffer. The buffering requirement is a controversial step for two reasons. First, the buffers commonly used are organics and have Fe binding properties (Gupta et al., 2013; Welch et al., 2002), potentially overestimating the ability of the DOM to bind DFe. This could be responsible for an overestimation of [L] and  $\log K_{FeL}^{cond}$ . Inorganic buffers can also be used, with the supplementary advantage that they can be ensured free of organic surfactants by UV-irradiation. However, the inorganic ligands matching the natural pH range have a lower buffering power than organic buffers. It was recently shown that the AL DHN could be



used unbuffered, providing satisfactory results in oxygenated and carbonated seawater samples (Sanvito and Monticelli, 2021). During ACSV measurement in the absence of strong buffering, the pH changes in the diffusion layer of the WE during the stripping step, and has been estimated to reach a pH value of 9 by the production of hydroxides from oxygen reduction ( $\text{HO}^-$ ; Laglera et al., 2016). The pH change experienced by the sample is, therefore, restrained to few hundreds of  $\mu\text{m}$  close to the electrodes, and the natural pH of the sample is poorly impacted. The absence of buffering would be more representative of the *in-situ* conditions for deep water samples, as it would not impact the protonation of the DOM, its ability to bind with Fe, and the competition for binding sites between metals.

## 2.5. Aims of the PhD thesis

The CLE-ACSV approach and the methods based on it, despite being the most used tools to investigate FeL in seawater, is still controversial even after 40 years of development. Advances have been made to standardise sample collection and handling (GEOTRACES) and data interpretation, however, there is still room for improvement. This thesis aims to reduce the divergence between CLE-ACSV applications by proposing methodological development, detailed application of the methods, and by proposing a standardised interpretation procedure to further standardise data interpretation and limit user subjectivity.

Firstly, Chapter 3 is devoted to the development of an original method using the AL NN in presence of air. The development also includes optimisation of the experimental set up in terms of volume, sensitivity and pH, and an experimental approach proposed to investigate the impact of pH on the organic speciation of DFe. Chapter 4 presents a new procedure and tools specifically developed to limit the impact of the analyst on the interpretation of titration data. Specific aspects regarding the use of the AL SA are also presented, notably a conditioning procedure that solves the issue of the systematic signal decrease experienced by Gerringa et al. (2021), together with optimisation and comparison of the previously published SA applications. Finally, Chapter 5 presents the application of the optimised SA method and interpretation procedure in seawater samples collected in the Western South Tropical Pacific. The FeL characteristics data are compared to electrochemical and fluorescent determination of

HS to constrain FeL composition and DFe distribution. The summary of my findings, future of the CLE-ACSV and further perspectives are concluding this thesis.

## 2.6. References

- Abualhaija, M.M., van den Berg, C.M.G., 2014. Chemical speciation of iron in seawater using catalytic cathodic stripping voltammetry with ligand competition against salicylaldehyde. *Mar. Chem.* 164, 60–74. <https://doi.org/10.1016/j.marchem.2014.06.005>
- Abualhaija, M.M., Whitby, H., van den Berg, C.M.G., 2015. Competition between copper and iron for humic ligands in estuarine waters. *Mar. Chem.* 172, 46–56. <https://doi.org/10.1016/j.marchem.2014.06.00510.1016/j.marchem.2015.03.010>
- Aldrich, A.P., van den Berg, C.M.G., 1998. Determination of Iron and Its Redox Speciation in Seawater Using Catalytic Cathodic Stripping Voltammetry. *Electroanalysis* 10, 369–373. [https://doi.org/10.1002/\(SICI\)1521-4109\(199805\)10:6<369::AID-ELAN369>3.0.CO;2-W](https://doi.org/10.1002/(SICI)1521-4109(199805)10:6<369::AID-ELAN369>3.0.CO;2-W)
- Altmann, R.S., Buffle, J., 1988. The use of differential equilibrium functions for interpretation of metal binding in complex ligand systems: Its relation to site occupation and site affinity distributions. *Geochim. Cosmochim. Acta* 52, 1505–1519. [https://doi.org/10.1016/0016-7037\(88\)90221-9](https://doi.org/10.1016/0016-7037(88)90221-9)
- Amin, S.A., Green, D.H., Gärdes, A., Romano, A., Trimble, L., Carrano, C.J., 2012. Siderophore-mediated iron uptake in two clades of *Marinobacter* spp. associated with phytoplankton: the role of light. *BioMetals* 25, 181–192. <https://doi.org/10.1007/s10534-011-9495-5>
- Amin, S.A., Green, D.H., Hart, M.C., Küpper, F.C., Sunda, W.G., Carrano, C.J., 2009. Photolysis of iron–siderophore chelates promotes bacterial–algal mutualism. *Proc. Natl. Acad. Sci.* 106, 17071–17076. <https://doi.org/10.1073/pnas.0905512106>
- Apte, S.C., Gardner, M.J., Ravenscroft, J.E., 1988. An evaluation of voltammetric titration procedures for the determination of trace metal complexation in natural waters by use of computers simulation. *Anal. Chim. Acta* 212, 1–21. [https://doi.org/10.1016/S0003-2670\(00\)84124-0](https://doi.org/10.1016/S0003-2670(00)84124-0)
- Ardiningsih, I., Zhu, K., Lodeiro, P., Gledhill, M., Reichart, G.-J., Achterberg, E.P., Middag, R., Gerringa, L.J.A., 2021. Iron Speciation in Fram Strait and Over the Northeast Greenland Shelf: An Inter-Comparison Study of Voltammetric Methods. *Front. Mar. Sci.* 7. <https://doi.org/10.3389/fmars.2020.609379>
- Avendaño, L., Gledhill, M., Achterberg, E.P., Rérolle, V.M.C., Schlosser, C., 2016. Influence of Ocean Acidification on the Organic Complexation of Iron and Copper in Northwest European Shelf Seas; a Combined Observational and Model Study. *Front. Mar. Sci.* 3. <https://doi.org/10.3389/fmars.2016.00058>
- Barbeau, K., Rue, E.L., Bruland, K.W., Butler, A., 2001. Photochemical cycling of iron in the surface ocean mediated by microbial iron(III)-binding ligands. *Nature* 413, 409–413. <https://doi.org/10.1038/35096545>
- Bar-On, Y.M., Phillips, R., Milo, R., 2018. The biomass distribution on Earth. *Proc. Natl. Acad. Sci.* 115, 6506–6511. <https://doi.org/10.1073/pnas.1711842115>
- Benner, R., Pakulski, J.D., Mccarthy, M., Hedges, J.I., Hatcher, P.G., 1992. Bulk Chemical Characteristics of Dissolved Organic Matter in the Ocean. *Science* 255, 1561–1564. <https://doi.org/10.1126/science.255.5051.1561>
- Bertrand, E.M., Saito, M.A., Rose, J.M., Riesselman, C.R., Lohan, M.C., Noble, A.E., Lee, P.A., DiTullio, G.R., 2007. Vitamin B12 and iron colimitation of phytoplankton growth in the Ross Sea. *Limnol. Oceanogr.* 52, 1079–1093. <https://doi.org/10.4319/lo.2007.52.3.1079>
- Blazevic, A., Orłowska, E., Kandioller, W., Jirsa, F., Keppler, B.K., Tafili-Kryeziu, M., Linert, W., Krachler, R.F., Krachler, R., Rompel, A., 2016. Photoreduction of Terrigenous Fe-Humic Substances Leads to Bioavailable Iron in Oceans. *Angew. Chem. Int. Ed.* 55, 6417–6422. <https://doi.org/10.1002/anie.201600852>
- Boiteau, R.M., Mende, D.R., Hawco, N.J., McIlvin, M.R., Fitzsimmons, J.N., Saito, M.A., Sedwick, P.N., DeLong, E.F., Repeta, D.J., 2016. Siderophore-based microbial adaptations to iron scarcity across the eastern Pacific Ocean. *Proc. Natl. Acad. Sci.* 113, 14237–14242. <https://doi.org/10/f9fvs4>

- Bondietti, G., Sinniger, J., Stumm, W., 1993. The reactivity of FE(III) (hydr)oxides: Effects of ligands in inhibiting the dissolution. *Colloids Surf. Physicochem. Eng. Asp.* 79, 157–167. [https://doi.org/10.1016/0927-7757\(93\)80171-A](https://doi.org/10.1016/0927-7757(93)80171-A)
- Boyd, P.W., Ibsanmi, E., Sander, S.G., Hunter, K.A., Jackson, G.A., 2010. Remineralization of upper ocean particles: Implications for iron biogeochemistry. *Limnol. Oceanogr.* 55, 1271–1288. <https://doi.org/10.4319/lo.2010.55.3.1271>
- Boye, M., van den Berg, C.M.G., de Jong, J.T.M., Leach, H., Croot, P., de Baar, H.J.W., 2001. Organic complexation of iron in the Southern Ocean. *Deep Sea Res. Part Oceanogr. Res. Pap.* 48, 1477–1497. [https://doi.org/10.1016/S0967-0637\(00\)00099-6](https://doi.org/10.1016/S0967-0637(00)00099-6)
- Browning, T.J., Achterberg, E.P., Engel, A., Mawji, E., 2021. Manganese co-limitation of phytoplankton growth and major nutrient drawdown in the Southern Ocean. *Nat. Commun.* 12, 884. <https://doi.org/10.1038/s41467-021-21122-6>
- Buck, K.N., Lohan, M.C., Berger, C.J.M., Bruland, K.W., 2007. Dissolved iron speciation in two distinct river plumes and an estuary: Implications for riverine iron supply. *Limnol. Oceanogr.* 52, 843–855. <https://doi.org/10.4319/lo.2007.52.2.0843>
- Buck, K.N., Moffett, J., Barbeau, K.A., Bundy, R.M., Kondo, Y., Wu, J., 2012. The organic complexation of iron and copper: an intercomparison of competitive ligand exchange-adsorptive cathodic stripping voltammetry (CLE-ACSV) techniques. *Limnol. Oceanogr. Methods* 10, 496–515. <https://doi.org/10.4319/lom.2012.10.496>
- Buck, K.N., Sedwick, P.N., Sohst, B., Carlson, C.A., 2018. Organic complexation of iron in the eastern tropical South Pacific: Results from US GEOTRACES Eastern Pacific Zonal Transect (GEOTRACES cruise GP16). *Mar. Chem., The U.S. GEOTRACES Eastern Tropical Pacific Transect (GP16)* 201, 229–241. <https://doi.org/10.1016/j.marchem.2017.11.007>
- Buck, K.N., Sohst, B., Sedwick, P.N., 2015. The organic complexation of dissolved iron along the U.S. GEOTRACES (GA03) North Atlantic Section. *Deep Sea Res. Part II Top. Stud. Oceanogr.* 116, 152–165. <https://doi.org/10.1016/j.dsr2.2014.11.016>
- Buma, A.G.J., de Baar, H.J.W., Nolting, R.F., van Bennekom, A.J., 1991. Metal enrichment experiments in the Weddell-Scotia Seas: Effects of iron and manganese on various plankton communities. *Limnol. Oceanogr.* 36, 1865–1878. <https://doi.org/10.4319/lo.1991.36.8.1865>
- Bundy, R.M., Biller, D.V., Buck, K.N., Bruland, K.W., Barbeau, K.A., 2014. Distinct pools of dissolved iron-binding ligands in the surface and benthic boundary layer of the California Current. *Limnol. Oceanogr.* 59, 769–787. <https://doi.org/10.4319/lo.2014.59.3.0769>
- Bundy, R.M., Boiteau, R.M., McLean, C., Turk-Kubo, K.A., McIlvin, M.R., Saito, M.A., Van Mooy, B.A.S., Repeta, D.J., 2018. Distinct Siderophores Contribute to Iron Cycling in the Mesopelagic at Station ALOHA. *Front. Mar. Sci.* 5. <https://doi.org/10.3389/fmars.2018.00061>
- Burgess, J., Twigg, M.V., 2006. Iron: Inorganic & Coordination Chemistry Based in part on the article Iron: Inorganic & Coordination Chemistry by Pelham N. Hawker & Martyn V. Twigg which appeared in the Encyclopedia of Inorganic Chemistry, First Edition., in: *Encyclopedia of Inorganic Chemistry*. John Wiley & Sons, Ltd. <https://doi.org/10.1002/0470862106.ia108>
- Caprara, S., Buck, K.N., Gerringa, L.J.A., Rijkenberg, M.J.A., Monticelli, D., 2016. A Compilation of Iron Speciation Data for Open Oceanic Waters. *Front. Mar. Sci.* 3. <https://doi.org/10.3389/fmars.2016.00221>
- Caprara, S., Laglera, L.M., Monticelli, D., 2015. Ultrasensitive and Fast Voltammetric Determination of Iron in Seawater by Atmospheric Oxygen Catalysis in 500  $\mu$ L Samples. *Anal. Chem.* 87, 6357–6363. <https://doi.org/10.1021/acs.analchem.5b01239>
- Cheize, M., Planquette, H.F., Fitzsimmons, J.N., Pelleter, E., Sherrell, R.M., Lambert, C., Bucciarelli, E., Sarthou, G., Le Goff, M., Liorzou, C., Chéron, S., Viollier, E., Gayet, N., 2019. Contribution of resuspended sedimentary particles to dissolved iron and manganese in the ocean: An experimental study. *Chem. Geol.* 511, 389–415. <https://doi.org/10.1016/j.chemgeo.2018.10.003>

- Cheize, M., Sarthou, G., Croot, P.L., Bucciarelli, E., Baudoux, A.-C., Baker, A.R., 2012. Iron organic speciation determination in rainwater using cathodic stripping voltammetry. *Anal. Chim. Acta* 736, 45–54. <https://doi.org/10.1016/j.aca.2012.05.011>
- Chen, M., Wang, W.-X., 2001. Bioavailability of natural colloid-bound iron to marine plankton: Influences of colloidal size and aging. *Limnol. Oceanogr.* 46, 1956–1967. <https://doi.org/10.4319/lo.2001.46.8.1956>
- Chisholm, S.W., Morel, F.M., 1991. *Limnology and Oceanography*, Volume 36, Number 8, December 1991. What Controls Phytoplankton Production in Nutrient-Rich Areas of the Open Sea?
- Cloete, R., Loock, J.C., van Horsten, N.R., Menzel Barraqueta, J.-L., Fietz, S., Mtshali, T.N., Planquette, H., García-Ibáñez, M.I., Roychoudhury, A.N., 2021. Winter dissolved and particulate zinc in the Indian Sector of the Southern Ocean: Distribution and relation to major nutrients (GEOTRACES G1pr07 transect). *Mar. Chem.* 236, 104031. <https://doi.org/10.1016/j.marchem.2021.104031>
- Coale, K., 1991. Effects of Iron, Manganese, Copper, and Zinc Enrichments on Productivity and Biomass in the Sub-Arctic Pacific. *Limnol. Oceanogr.* 36, 1851–1864. <https://doi.org/10.4319/lo.1991.36.8.1851>
- Cotton, S.A., 1972. Some aspects of the coordination chemistry of iron(III). *Coord. Chem. Rev.* 8, 185–223. [https://doi.org/10.1016/S0010-8545\(00\)80028-4](https://doi.org/10.1016/S0010-8545(00)80028-4)
- Croot, P.L., Andersson, K., Öztürk, M., Turner, D.R., 2004. The distribution and speciation of iron along 6°E in the Southern Ocean. *Deep Sea Res. Part II Top. Stud. Oceanogr.*, The SWEDARP 1997/98 Expedition 51, 2857–2879. <https://doi.org/10.1016/j.dsr2.2003.10.012>
- Croot, P.L., Johansson, M., 2000. Determination of Iron Speciation by Cathodic Stripping Voltammetry in Seawater Using the Competing Ligand 2-(2-Thiazolylazo)-p-cresol (TAC). *Electroanalysis* 12, 565–576. [https://doi.org/10.1002/\(SICI\)1521-4109\(200005\)12:8<565::AID-ELAN565>3.0.CO;2-L](https://doi.org/10.1002/(SICI)1521-4109(200005)12:8<565::AID-ELAN565>3.0.CO;2-L)
- Dale, A.W., Nickelsen, L., Scholz, F., Hensen, C., Oschlies, A., Wallmann, K., 2015. A revised global estimate of dissolved iron fluxes from marine sediments. *Glob. Biogeochem. Cycles* 29, 691–707. <https://doi.org/10.1002/2014GB005017>
- de Baar, H.J.W., Boyd, P.W., Coale, K.H., Landry, M.R., Tsuda, A., Assmy, P., Bakker, D.C.E., Bozec, Y., Barber, R.T., Brzezinski, M.A., Buesseler, K.O., Boyé, M., Croot, P.L., Gervais, F., Gorbunov, M.Y., Harrison, P.J., Hiscock, W.T., Laan, P., Lancelot, C., Law, C.S., Levasseur, M., Marchetti, A., Millero, F.J., Nishioka, J., Nojiri, Y., van Oijen, T., Riebesell, U., Rijkenberg, M.J.A., Saito, H., Takeda, S., Timmermans, K.R., Veldhuis, M.J.W., Waite, A.M., Wong, C.-S., 2005. Synthesis of iron fertilization experiments: From the Iron Age in the Age of Enlightenment. *J. Geophys. Res. Oceans* 110. <https://doi.org/10.1029/2004JC002601>
- de Baar, H.J.W., Buma, A.G.J., Nolting, R.F., Cadée, G.C., Jacques, G., Tréguer, P.J., 1990. On iron limitation of the Southern Ocean: experimental observations in the Weddell and Scotia Seas. *Mar. Ecol. Prog. Ser.* 65, 105–122.
- de Baar, H.J.W., van Heuven, S.M.A.C., Abouchami, W., Xue, Z., Galer, S.J.G., Rehkämper, M., Middag, R., van Ooijen, J., 2017. Interactions of dissolved CO<sub>2</sub> with cadmium isotopes in the Southern Ocean. *Mar. Chem.*, SI: Honoring Frank Millero 195, 105–121. <https://doi.org/10.1016/j.marchem.2017.06.010>
- Dittmar, T., Lennartz, S.T., Buck-Wiese, H., Hansell, D.A., Santinelli, C., Vanni, C., Blasius, B., Hehemann, J.-H., 2021. Enigmatic persistence of dissolved organic matter in the ocean. *Nat. Rev. Earth Environ.* 2, 570–583. <https://doi.org/10.1038/s43017-021-00183-7>
- Dulaquais, G., Waeles, M., Gerringa, L.J.A., Middag, R., Rijkenberg, M.J.A., Riso, R., 2018. The Biogeochemistry of Electroactive Humic Substances and Its Connection to Iron Chemistry in the North East Atlantic and the Western Mediterranean Sea. *J. Geophys. Res. Oceans* 123, 5481–5499. <https://doi.org/10/gd8db3>
- Fenton, H.J.H., 1894. LXXIII.—Oxidation of tartaric acid in presence of iron. *J. Chem. Soc. Trans.* 65, 899–910. <https://doi.org/10.1039/CT8946500899>

- Field, C.B., Behrenfeld, M.J., Randerson, J.T., Falkowski, P., 1998. Primary Production of the Biosphere: Integrating Terrestrial and Oceanic Components. *Science* 281, 237–240. <https://doi.org/10.1126/science.281.5374.237>
- Findlay, A.J., Estes, E.R., Gartman, A., Yücel, M., Kamyshny, A., Luther, G.W., 2019. Iron and sulfide nanoparticle formation and transport in nascent hydrothermal vent plumes. *Nat. Commun.* 10, 1–7. <https://doi.org/10.1038/s41467-019-09580-5>
- Fitzsimmons, J.N., Bundy, R.M., Al-Subiai, S.N., Barbeau, K.A., Boyle, E.A., 2015. The composition of dissolved iron in the dusty surface ocean: An exploration using size-fractionated iron-binding ligands. *Mar. Chem., SCOR WG 139: Organic Ligands – A Key Control on Trace Metal Biogeochemistry in the Ocean* 173, 125–135. <https://doi.org/10/f7fc99>
- Fourrier, P., Dulaquais, G., Guigue, C., Giamarchi, P., Sarthou, G., Whitby, H., Riso, R., 2022. Characterization of the vertical size distribution, composition and chemical properties of dissolved organic matter in the (ultra)oligotrophic Pacific Ocean through a multi-detection approach. *Mar. Chem.* 240, 104068. <https://doi.org/10.1016/j.marchem.2021.104068>
- Friedlingstein, P., Jones, M.W., O’Sullivan, M., Andrew, R.M., Hauck, J., Peters, G.P., Peters, W., Pongratz, J., Sitch, S., Quéré, C.L., Bakker, D.C.E., Canadell, J.G., Ciais, P., Jackson, R.B., Anthoni, P., Barbero, L., Bastos, A., Bastrikov, V., Becker, M., Bopp, L., Buitenhuis, E., Chandra, N., Chevallier, F., Chini, L.P., Currie, K.I., Feely, R.A., Gehlen, M., Gilfillan, D., Gkritzalis, T., Goll, D.S., Gruber, N., Gutekunst, S., Harris, I., Haverd, V., Houghton, R.A., Hurtt, G., Ilyina, T., Jain, A.K., Joetzjer, E., Kaplan, J.O., Kato, E., Klein Goldewijk, K., Korsbakken, J.I., Landschützer, P., Lauvset, S.K., Lefèvre, N., Lenton, A., Lienert, S., Lombardozzi, D., Marland, G., McGuire, P.C., Melton, J.R., Metzl, N., Munro, D.R., Nabel, J.E.M.S., Nakaoka, S.-I., Neill, C., Omar, A.M., Ono, T., Pregon, A., Pierrot, D., Poulter, B., Rehder, G., Resplandy, L., Robertson, E., Rödenbeck, C., Séférian, R., Schwinger, J., Smith, N., Tans, P.P., Tian, H., Tilbrook, B., Tubiello, F.N., Werf, G.R. van der, Wiltshire, A.J., Zaehle, S., 2019. Global Carbon Budget 2019. *Earth Syst. Sci. Data* 11, 1783–1838. <https://doi.org/10.5194/essd-11-1783-2019>
- Gattuso, J.-P., Magnan, A., Billé, R., Cheung, W.W.L., Howes, E.L., Joos, F., Allemand, D., Bopp, L., Cooley, S.R., Eakin, C.M., Hoegh-Guldberg, O., Kelly, R.P., Pörtner, H.-O., Rogers, A.D., Baxter, J.M., Laffoley, D., Osborn, D., Rankovic, A., Rochette, J., Sumaila, U.R., Treyer, S., Turley, C., 2015. Contrasting futures for ocean and society from different anthropogenic CO<sub>2</sub> emissions scenarios. *Science* 349. <https://doi.org/10.1126/science.aac4722>
- Genovese, C., Grotti, M., Ardini, F., Wuttig, K., Vivado, D., Cabanes, D., Townsend, A., Hassler, C., Lannuzel, D., 2022. Effect of salinity and temperature on the determination of dissolved iron-binding organic ligands in the polar marine environment. *Mar. Chem.* 238, 104051. <https://doi.org/10.1016/j.marchem.2021.104051>
- Genovese, C., Grotti, M., Pittaluga, J., Ardini, F., Janssens, J., Wuttig, K., Moreau, S., Lannuzel, D., 2018. Influence of organic complexation on dissolved iron distribution in East Antarctic pack ice. *Mar. Chem.* 203, 28–37. <https://doi.org/10.1016/j.marchem.2018.04.005>
- Gerringa, L.J.A., Gledhill, M., Ardiningsih, I., Muntjewerf, N., Laglera, L.M., 2021. Comparing CLE-AdCSV applications using SA and TAC to determine the Fe-binding characteristics of model ligands in seawater. *Biogeosciences* 18, 5265–5289. <https://doi.org/10.5194/bg-18-5265-2021>
- Gerringa, L.J.A., Herman, P.M.J., Poortvliet, T.C.W., 1995. Comparison of the linear Van den Berg/Ružić transformation and a non-linear fit of the Langmuir isotherm applied to Cu speciation data in the estuarine environment. *Mar. Chem.* 48, 131–142. [https://doi.org/10.1016/0304-4203\(94\)00041-B](https://doi.org/10.1016/0304-4203(94)00041-B)
- Gerringa, L.J.A., Rijkenberg, M.J.A., Schoemann, V., Laan, P., de Baar, H.J.W., 2015. Organic complexation of iron in the West Atlantic Ocean. *Mar. Chem., Cycles of metals and carbon in the oceans - A tribute to the work stimulated by Hein de Baar* 177, 434–446. <https://doi.org/10.1016/j.marchem.2015.04.007>

- Gerringa, L.J.A., Rijkenberg, M.J.A., Thuróczy, C.-E., Maas, L.R.M., 2014. A critical look at the calculation of the binding characteristics and concentration of iron complexing ligands in seawater with suggested improvements. *Environ. Chem.* 11, 114–136. <https://doi.org/10/f52sbv>
- Gledhill, M., Achterberg, E.P., Li, K., Mohamed, K.N., Rijkenberg, M.J.A., 2015. Influence of ocean acidification on the complexation of iron and copper by organic ligands in estuarine waters. *Mar. Chem., Cycles of metals and carbon in the oceans - A tribute to the work stimulated by Hein de Baar* 177, 421–433. <https://doi.org/10.1016/j.marchem.2015.03.016>
- Gledhill, M., Buck, K.N., 2012. The Organic Complexation of Iron in the Marine Environment: A Review. *Front. Microbiol.* 3. <https://doi.org/10.3389/fmicb.2012.00069>
- Gledhill, M., van den Berg, C.M.G., 1994. Determination of complexation of iron(III) with natural organic complexing ligands in seawater using cathodic stripping voltammetry. *Mar. Chem.* 47, 41–54. [https://doi.org/10.1016/0304-4203\(94\)90012-4](https://doi.org/10.1016/0304-4203(94)90012-4)
- Gupta, B.S., Taha, M., Lee, M.-J., 2013. Stability Constants for the Equilibrium Models of Iron(III) with Several Biological Buffers in Aqueous Solutions. *J. Solut. Chem.* 42, 2296–2309. <https://doi.org/10.1007/s10953-013-0107-6>
- Hassler, C., Cabanes, D., Blanco-Ameijeiras, S., Sander, S.G., Benner, R., Hassler, C., Cabanes, D., Blanco-Ameijeiras, S., Sander, S.G., Benner, R., 2019. Importance of refractory ligands and their photodegradation for iron oceanic inventories and cycling. *Mar. Freshw. Res.* 71, 311–320. <https://doi.org/10.1071/MF19213>
- Hassler, C.S., Berg, V.D., G, C.M., Boyd, P.W., 2017. Toward a Regional Classification to Provide a More Inclusive Examination of the Ocean Biogeochemistry of Iron-Binding Ligands. *Front. Mar. Sci.* 4. <https://doi.org/10.3389/fmars.2017.00019>
- Hassler, C.S., Legiret, F.-E., Butler, E.C.V., 2013. Measurement of iron chemical speciation in seawater at 4°C: The use of competitive ligand exchange–adsorptive cathodic stripping voltammetry. *Mar. Chem.* 149, 63–73. <https://doi.org/10.1016/j.marchem.2012.12.007>
- Hassler, C.S., Norman, L., Mancuso Nichols, C.A., Clementson, L.A., Robinson, C., Schoemann, V., Watson, R.J., Doblin, M.A., 2015. Iron associated with exopolymeric substances is highly bioavailable to oceanic phytoplankton. *Mar. Chem., SCOR WG 139: Organic Ligands – A Key Control on Trace Metal Biogeochemistry in the Ocean* 173, 136–147. <https://doi.org/10.1016/j.marchem.2014.10.002>
- Hawkes, J. A., Gledhill, M., Connelly, D.P., Achterberg, E.P., 2013a. Characterisation of iron binding ligands in seawater by reverse titration. *Anal. Chim. Acta* 766, 53–60. <https://doi.org/10.1016/j.aca.2012.12.048>
- Hawkes, J. A., Connelly, D.P., Gledhill, M., Achterberg, E.P., 2013b. The stabilisation and transportation of dissolved iron from high temperature hydrothermal vent systems. *Earth Planet. Sci. Lett.* 375, 280–290. <https://doi.org/10.1016/j.epsl.2013.05.047>
- Hayyan, M., Hashim, M.A., AlNashef, I.M., 2016. Superoxide Ion: Generation and Chemical Implications. *Chem. Rev.* 116, 3029–3085. <https://doi.org/10.1021/acs.chemrev.5b00407>
- Hiemstra, T., van Riemsdijk, W.H., 2006. Biogeochemical speciation of Fe in ocean water. *Mar. Chem.* 102, 181–197. <https://doi.org/10.1016/j.marchem.2006.03.008>
- Ho, P., Lee, J.-M., Heller, M.I., Lam, P.J., Shiller, A.M., 2018. The distribution of dissolved and particulate Mo and V along the U.S. GEOTRACES East Pacific Zonal Transect (GP16): The roles of oxides and biogenic particles in their distributions in the oxygen deficient zone and the hydrothermal plume. *Mar. Chem., The U.S. GEOTRACES Eastern Tropical Pacific Transect (GP16)* 201, 242–255. <https://doi.org/10.1016/j.marchem.2017.12.003>
- Hoffmann, L.J., Breitbarth, E., Boyd, P.W., Hunter, K.A., 2012. Influence of ocean warming and acidification on trace metal biogeochemistry. *Mar. Ecol. Prog. Ser.* 470, 191–205. <https://doi.org/10.3354/meps10082>
- Hogle, S.L., Hackl, T., Bundy, R.M., Park, J., Satinsky, B., Satinsky, B., Hiltunen, T., Biller, S., Berube, P.M., Chisholm, S.W., 2021. Siderophores as an iron source for *Prochlorococcus* in deep

- chlorophyll maximum layers of the oligotrophic ocean.  
<https://doi.org/10.1101/2021.11.13.468467>
- Hopkinson, B.M., Morel, F.M.M., 2009. The role of siderophores in iron acquisition by photosynthetic marine microorganisms. *BioMetals* 22, 659–669. <https://doi.org/10.1007/s10534-009-9235-2>
- Hoppe, C.J.M., Hassler, C.S., Payne, C.D., Tortell, P.D., Rost, B., Trimborn, S., 2013. Iron Limitation Modulates Ocean Acidification Effects on Southern Ocean Phytoplankton Communities. *PLoS ONE* 8. <https://doi.org/10.1371/journal.pone.0079890>
- Hopwood, M.J., Carroll, D., Höfer, J., Achterberg, E.P., Meire, L., Le Moigne, F.A.C., Bach, L.T., Eich, C., Sutherland, D.A., González, H.E., 2019. Highly variable iron content modulates iceberg-ocean fertilisation and potential carbon export. *Nat. Commun.* 10, 1–10. <https://doi.org/10.1038/s41467-019-13231-0>
- Hunter, K.A., 2005. Comment on ‘Measuring Marine Iron(III) Complexes by CLE-AdSV.’ *Environ. Chem.* 2, 85–87. <https://doi.org/10.1071/EN05030>
- Hutchins, D.A., Boyd, P.W., 2016. Marine phytoplankton and the changing ocean iron cycle. *Nat. Clim. Change* 6, 1072–1079. <https://doi.org/10.1038/nclimate3147>
- Ingall, E.D., Diaz, J.M., Longo, A.F., Oakes, M., Finney, L., Vogt, S., Lai, B., Yager, P.L., Twining, B.S., Brandes, J.A., 2013. Role of biogenic silica in the removal of iron from the Antarctic seas. *Nat. Commun.* 4, 1981. <https://doi.org/10.1038/ncomms2981>
- Janssens, J., Meiners, K.M., Townsend, A.T., Lannuzel, D., 2018. Organic Matter Controls of Iron Incorporation in Growing Sea Ice. *Front. Earth Sci.* 6.
- Johnson, K.S., Gordon, R.M., Coale, K.H., 1997. What controls dissolved iron concentrations in the world ocean? *Mar. Chem.* 57, 137–161. [https://doi.org/10.1016/S0304-4203\(97\)00043-1](https://doi.org/10.1016/S0304-4203(97)00043-1)
- Kleint, C., Hawkes, J.A., Sander, S.G., Koschinsky, A., 2016. Voltammetric Investigation of Hydrothermal Iron Speciation. *Front. Mar. Sci.* 3, UNSP 75. <https://doi.org/10.3389/fmars.2016.00075>
- Krachler, R., Krachler, R.F., Wallner, G., Hann, S., Laux, M., Cervantes Recalde, M.F., Jirsa, F., Neubauer, E., von der Kammer, F., Hofmann, T., Keppler, B.K., 2015. River-derived humic substances as iron chelators in seawater. *Mar. Chem.* 174, 85–93. <https://doi.org/10.1016/j.marchem.2015.05.009>
- Kuma, K., Nishioka, J., Matsunaga, K., 1996. Controls on iron(III) hydroxide solubility in seawater: The influence of pH and natural organic chelators. *Limnol. Oceanogr.* 41, 396–407. <https://doi.org/10.4319/lo.1996.41.3.0396>
- Laglera, L.M., Battaglia, G., van den Berg, C.M.G., 2011. Effect of humic substances on the iron speciation in natural waters by CLE/CSV. *Mar. Chem.* 127, 134–143. <https://doi.org/10.1016/j.marchem.2011.09.003>
- Laglera, L.M., Battaglia, G., van den Berg, C.M.G., 2007. Determination of humic substances in natural waters by cathodic stripping voltammetry of their complexes with iron. *Anal. Chim. Acta* 599, 58–66. <https://doi.org/10.1016/j.aca.2007.07.059>
- Laglera, L.M., Caprara, S., Monticelli, D., 2016. Towards a zero-blank, preconcentration-free voltammetric method for iron analysis at picomolar concentrations in unbuffered seawater. *Talanta* 150, 449–454. <https://doi.org/10.1016/j.talanta.2015.12.060>
- Laglera, L.M., Monticelli, D., 2017. Iron detection and speciation in natural waters by electrochemical techniques: A critical review. *Curr. Opin. Electrochem.* 3, 123–129. <https://doi.org/10.1016/j.coelec.2017.07.007>
- Laglera, L.M., Tovar-Sanchez, A., Sukekava, C.F., Naik, H., Naqvi, S.W.A., Wolf-Gladrow, D.A., 2019. Iron organic speciation during the LOHAFEX experiment: Iron ligands release under biomass control by copepod grazing. *J. Mar. Syst.* 103151. <https://doi.org/10.1016/j.jmarsys.2019.02.002>
- Langmuir, I., 1916. THE CONSTITUTION AND FUNDAMENTAL PROPERTIES OF SOLIDS AND LIQUIDS. PART I. SOLIDS. *J. Am. Chem. Soc.* 38, 2221–2295. <https://doi.org/10.1021/ja02268a002>



- Lannuzel, D., Vancoppenolle, M., van der Merwe, P., de Jong, J., Meiners, K.M., Grotti, M., Nishioka, J., Schoemann, V., 2016. Iron in sea ice: Review and new insights. *Elem. Sci. Anthr.* 4, 000130. <https://doi.org/10.12952/journal.elementa.000130>
- Lis, H., Shaked, Y., Kranzler, C., Keren, N., Morel, F.M.M., 2015. Iron bioavailability to phytoplankton: an empirical approach. *ISME J.* 9, 1003–1013. <https://doi.org/10.1038/ismej.2014.199>
- Liu, X., Millero, F.J., 2002. The solubility of iron in seawater. *Mar. Chem.* 77, 43–54. [https://doi.org/10.1016/S0304-4203\(01\)00074-3](https://doi.org/10.1016/S0304-4203(01)00074-3)
- Lodeiro, P., Rey-Castro, C., David, C., Achterberg, E.P., Puy, J., Gledhill, M., 2020. Acid-base properties of dissolved organic matter extracted from the marine environment. *Sci. Total Environ.* 729, 138437. <https://doi.org/10.1016/j.scitotenv.2020.138437>
- Lohan, M.C., Aguilar-Islas, A.M., Bruland, K.W., 2006. Direct determination of iron in acidified (pH 1.7) seawater samples by flow injection analysis with catalytic spectrophotometric detection: Application and intercomparison. *Limnol. Oceanogr. Methods* 4, 164–171. <https://doi.org/10.4319/lom.2006.4.164>
- Longhini, C.M., Mahieu, L., Sá, F., van den Berg, C.M.G., Salaün, P., Neto, R.R., 2021. Coastal waters contamination by mining tailings: What triggers the stability of iron in the dissolved and soluble fractions? *Limnol. Oceanogr.* 66, 171–187. <https://doi.org/10.1002/lno.11595>
- Louis, Y., Garnier, C., Lenoble, V., Omanović, D., Mounier, S., Pižeta, I., 2009. Characterisation and modelling of marine dissolved organic matter interactions with major and trace cations. *Mar. Environ. Res.* 67, 100–107. <https://doi.org/10.1016/j.marenvres.2008.12.002>
- Mahmood, A., Abualhaija, M.M., van den Berg, C.M.G., Sander, S.G., 2015. Organic speciation of dissolved iron in estuarine and coastal waters at multiple analytical windows. *Mar. Chem.* 177, 706–719. <https://doi.org/10.1016/j.marchem.2015.11.001>
- Mahowald, N., Engelstaedter, S., Luo, C., Sealy, A., Artaxo, P., Benitez-Nelson, C., Bonnet, S., Chen, Y., Chuang, P., Cohen, D., Dulac, F., Herut, B., Johansen, A., Kubilay, N., Losno, R., Maenhaut, W., Paytan, A., Prospero, J., Shank, L., Siefert, R., 2009. Atmospheric Iron Deposition: Global Distribution, Variability, and Human Perturbations. *Annu. Rev. Mar. Sci.* 1. <https://doi.org/10.1146/annurev.marine.010908.163727>
- Martin, J.H., Fitzwater, S.E., 1988. Iron deficiency limits phytoplankton growth in the north-east Pacific subarctic. *Nature* 331, 341–343. <https://doi.org/10.1038/331341a0>
- Martin, J.H., Fitzwater, S.E., Gordon, R.M., 1990. Iron deficiency limits phytoplankton growth in Antarctic waters. *Glob. Biogeochem. Cycles* 4, 5–12. <https://doi.org/10.1029/GB004i001p00005>
- Martin, J.H., Gordon, R.M., Fitzwater, S., Broenkow, W.W., 1989. Vertex: phytoplankton/iron studies in the Gulf of Alaska. *Deep Sea Res. Part Oceanogr. Res. Pap.* 36, 649–680. [https://doi.org/10.1016/0198-0149\(89\)90144-1](https://doi.org/10.1016/0198-0149(89)90144-1)
- McQuaid, J.B., Kustka, A.B., Oborník, M., Horák, A., McCrow, J.P., Karas, B.J., Zheng, H., Kindeberg, T., Andersson, A.J., Barbeau, K.A., Allen, A.E., 2018. Carbonate-sensitive phytotransferrin controls high-affinity iron uptake in diatoms. *Nature* 555, 534–537. <https://doi.org/10.1038/nature25982>
- Mentges, A., Feenders, C., Seibt, M., Blasius, B., Dittmar, T., 2017. Functional Molecular Diversity of Marine Dissolved Organic Matter Is Reduced during Degradation. *Front. Mar. Sci.* 4. <https://doi.org/10.3389/fmars.2017.00194>
- Millero, F., 2001. Speciation of metals in natural waters. *Geochem. Trans.* 2, 56–64. <https://doi.org/10.1039/B104809K>
- Millero, F.J., Woosley, R., Ditrolio, B., Waters, J., 2009. Effect of Ocean Acidification on the Speciation of Metals in Seawater. *Oceanography* 22, 72–85. <https://doi.org/10.5670/oceanog.2009.98>

- Mills, M.M., Ridame, C., Davey, M., La Roche, J., Geider, R.J., 2004. Iron and phosphorus co-limit nitrogen fixation in the eastern tropical North Atlantic. *Nature* 429, 292–294. <https://doi.org/10.1038/nature02550>
- Mohamed, K.N., Steigenberger, S., Nielsdottir, M.C., Gledhill, M., Achterberg, E.P., 2011. Dissolved iron(III) speciation in the high latitude North Atlantic Ocean. *Deep Sea Res. Part Oceanogr. Res. Pap.* 58, 1049–1059. <https://doi.org/10.1016/j.dsr.2011.08.011>
- Moore, C.M., Mills, M.M., Arrigo, K.R., Berman-Frank, I., Bopp, L., Boyd, P.W., Galbraith, E.D., Geider, R.J., Guieu, C., Jaccard, S.L., Jickells, T.D., La Roche, J., Lenton, T.M., Mahowald, N.M., Marañón, E., Marinov, I., Moore, J.K., Nakatsuka, T., Oschlies, A., Saito, M.A., Thingstad, T.F., Tsuda, A., Ulloa, O., 2013. Processes and patterns of oceanic nutrient limitation. *Nat. Geosci.* 6, 701–710. <https://www.nature.com/articles/ngeo1765>
- Morel, F.M.M., Kustka, A.B., Shaked, Y., 2008. The role of unchelated Fe in the iron nutrition of phytoplankton. *Limnol. Oceanogr.* 53, 400–404. <https://doi.org/10.4319/lo.2008.53.1.0400>
- Morel, F.M.M., Price, N.M., 2003. The Biogeochemical Cycles of Trace Metals in the Oceans. *Science* 300, 944–947. <https://doi.org/10.1126/science.1083545>
- Nagai, T., Imai, A., Matsushige, K., Yokoi, K., Fukushima, T., 2004. Voltammetric determination of dissolved iron and its speciation in freshwater. *Limnology* 5, 87–94. <https://doi.org/10.1007/s10201-004-0121-x>
- Nichols, C.M., Lardièrre, S.G., Bowman, J.P., Nichols, P.D., A E Gibson, J., Guézennec, J., 2005. Chemical characterization of exopolysaccharides from Antarctic marine bacteria. *Microb. Ecol.* 49, 578–589. <https://doi.org/10.1007/s00248-004-0093-8>
- Nolting, R.F., Gerringa, L.J.A., Swagerman, M.J.W., Timmermans, K.R., de Baar, H.J.W., 1998. Fe (III) speciation in the high nutrient, low chlorophyll Pacific region of the Southern Ocean. *Mar. Chem.* 62, 335–352. [https://doi.org/10.1016/S0304-4203\(98\)00046-2](https://doi.org/10.1016/S0304-4203(98)00046-2)
- Norman, L., Worms, I.A.M., Angles, E., Bowie, A.R., Nichols, C.M., Ninh Pham, A., Slaveykova, V.I., Townsend, A.T., David Waite, T., Hassler, C.S., 2015. The role of bacterial and algal exopolymeric substances in iron chemistry. *Mar. Chem., SCOR WG 139: Organic Ligands – A Key Control on Trace Metal Biogeochemistry in the Ocean* 173, 148–161. <https://doi.org/10.1016/j.marchem.2015.03.015>
- Obata, H., van den Berg, C.M.G., 2001. Determination of Picomolar Levels of Iron in Seawater Using Catalytic Cathodic Stripping Voltammetry. *Anal. Chem.* 73, 2522–2528. <https://doi.org/10.1021/ac001495d>
- Obata, Hajime., Karatani, Hajime., Nakayama, Eiichiro., 1993. Automated determination of iron in seawater by chelating resin concentration and chemiluminescence detection. *Anal. Chem.* 65, 1524–1528. <https://doi.org/10.1021/ac00059a007>
- Omanović, D., Garnier, C., Pižeta, I., 2015. ProMCC: An all-in-one tool for trace metal complexation studies. *Mar. Chem., SCOR WG 139: Organic Ligands – A Key Control on Trace Metal Biogeochemistry in the Ocean* 173, 25–39. <https://doi.org/10.1016/j.marchem.2014.10.011>
- Pernet-Coudrier, B., Waeles, M., Filella, M., Quentel, F., Riso, R.D., 2013. Simple and simultaneous determination of glutathione, thioacetamide and refractory organic matter in natural waters by DP-CSV. *Sci. Total Environ.* 463–464, 997–1005. <https://doi.org/10.1016/j.scitotenv.2013.06.053>
- Pižeta, I., Sander, S.G., Hudson, R.J.M., Omanović, D., Baars, O., Barbeau, K.A., Buck, K.N., Bundy, R.M., Carrasco, G., Croot, P.L., Garnier, C., Gerringa, L.J.A., Gledhill, M., Hirose, K., Kondo, Y., Laglera, L.M., Nuester, J., Rijkenberg, M.J.A., Takeda, S., Twining, B.S., Wells, M., 2015. Interpretation of complexometric titration data: An intercomparison of methods for estimating models of trace metal complexation by natural organic ligands. *Mar. Chem., SCOR WG 139: Organic Ligands – A Key Control on Trace Metal Biogeochemistry in the Ocean* 173, 3–24. <https://doi.org/10.1016/j.marchem.2015.03.006>

- Poulton, S.W., Raiswell, R., 2002. The low-temperature geochemical cycle of iron: From continental fluxes to marine sediment deposition. *Am. J. Sci.* 302, 774–805. <https://doi.org/10.2475/ajs.302.9.774>
- Quentel, F., Madec, C., Courtot-coupez, J., 1987. Determination of Humic Substances in Seawater by Electrochemistry (Mechanisms). *Anal. Lett.* 20, 47–62. <https://doi.org/10.1080/00032718708082236>
- Raspor, B., Nürnberg, H.W., Valenta, P., Branica, M., 1980. Kinetics and mechanism of trace metal chelation in sea water. *J. Electroanal. Chem. Interfacial Electrochem.* 115, 293–308. [https://doi.org/10.1016/S0022-0728\(80\)80333-0](https://doi.org/10.1016/S0022-0728(80)80333-0)
- Raymond, K.N., Allred, B.E., Sia, A.K., 2015. Coordination Chemistry of Microbial Iron Transport. *Acc. Chem. Res.* 48, 2496–2505. <https://doi.org/10.1021/acs.accounts.5b00301>
- Rickard, D., Luther, G.W., 2007. Chemistry of Iron Sulfides. *Chem. Rev.* 107, 514–562. <https://doi.org/10.1021/cr0503658>
- Roshan, S., DeVries, T., 2021. Global Contrasts Between Oceanic Cycling of Cadmium and Phosphate. *Glob. Biogeochem. Cycles* 35, e2021GB006952. <https://doi.org/10.1029/2021GB006952>
- Rue, E.L., Bruland, K.W., 1997. The role of organic complexation on ambient iron chemistry in the equatorial Pacific Ocean and the response of a mesoscale iron addition experiment. *Limnol. Oceanogr.* 42, 901–910. <https://doi.org/10.4319/lo.1997.42.5.0901>
- Rue, E.L., Bruland, K.W., 1995. Complexation of iron(III) by natural organic ligands in the Central North Pacific as determined by a new competitive ligand equilibration/adsorptive cathodic stripping voltammetric method. *Mar. Chem., The Chemistry of Iron in Seawater and its Interaction with Phytoplankton* 50, 117–138. [https://doi.org/10.1016/0304-4203\(95\)00031-L](https://doi.org/10.1016/0304-4203(95)00031-L)
- Ružić, I., 1982. Theoretical aspects of the direct titration of natural waters and its information yield for trace metal speciation. *Anal. Chim. Acta* 140, 99–113. [https://doi.org/10.1016/S0003-2670\(01\)95456-X](https://doi.org/10.1016/S0003-2670(01)95456-X)
- Sanvito, F., Monticelli, D., 2021. Exploring bufferless iron speciation in seawater by Competitive Ligand Equilibration-Cathodic Stripping Voltammetry: Does pH control really matter? *Talanta* 229, 122300. <https://doi.org/10.1016/j.talanta.2021.122300>
- Sanvito, F., Monticelli, D., 2020. Fast iron speciation in seawater by catalytic Competitive Ligand Equilibration-Cathodic Stripping Voltammetry with tenfold sample size reduction. *Anal. Chim. Acta* 1113, 9–17. <https://doi.org/10.1016/j.aca.2020.04.002>
- Sanvito, F., Pacileo, L., Monticelli, D., 2019. Fostering and Understanding Iron Detection at the Ultratrace Level by Adsorptive Stripping Voltammetry with Catalytic Enhancement. *Electroanalysis* 31, 212–216. <https://doi.org/10.1002/elan.201800675>
- Scatchard, G., 1949. The Attractions of Proteins for Small Molecules and Ions. *Ann. N. Y. Acad. Sci.* 51, 660–672. <https://doi.org/10.1111/j.1749-6632.1949.tb27297.x>
- Schoffman, H., Lis, H., Shaked, Y., Keren, N., 2016. Iron–Nutrient Interactions within Phytoplankton. *Front. Plant Sci.* 7.
- Schuback, N., Schallenberg, C., Duckham, C., Maldonado, M.T., Tortell, P.D., 2015. Interacting Effects of Light and Iron Availability on the Coupling of Photosynthetic Electron Transport and CO<sub>2</sub>-Assimilation in Marine Phytoplankton. *PLOS ONE* 10, e0133235. <https://doi.org/10.1371/journal.pone.0133235>
- Shaked, Y., Buck, K.N., Mellett, T., Maldonado, M.T., 2020. Insights into the bioavailability of oceanic dissolved Fe from phytoplankton uptake kinetics. *ISME J.* 14, 1182–1193. <https://doi.org/10.3389/fmicb.2020.00204>
- Shi, D., Xu, Y., Hopkinson, B.M., Morel, F.M.M., 2010. Effect of Ocean Acidification on Iron Availability to Marine Phytoplankton. *Science* 327, 676–679. <https://doi.org/10.1126/science.1183517>
- Slagter, H.A., Reader, H.E., Rijkenberg, M.J.A., Rutgers van der Loeff, M., de Baar, H.J.W., Gerringa, L.J.A., 2017. Organic Fe speciation in the Eurasian Basins of the Arctic Ocean and its relation to terrestrial DOM. *Mar. Chem.* 197, 11–25. <https://doi.org/10.1016/j.marchem.2017.10.005>

- Stockdale, A., Tipping, E., Lofts, S., Mortimer, R.J.G., 2016. Effect of Ocean Acidification on Organic and Inorganic Speciation of Trace Metals. *Environ. Sci. Technol.* 50, 1906–1913. <https://doi.org/10.1021/acs.est.5b05624>
- Su, H., Yang, R., Pižeta, I., Omanović, D., Wang, S., Li, Y., 2016. Distribution and Speciation of Dissolved Iron in Jiaozhou Bay (Yellow Sea, China). *Front. Mar. Sci.* 3. <https://doi.org/10.3389/fmars.2016.00099>
- Sukekava, C., Downes, J., Slagter, H.A., Gerringa, L.J.A., Laglera, L.M., 2018. Determination of the contribution of humic substances to iron complexation in seawater by catalytic cathodic stripping voltammetry. *Talanta* 189, 359–364. <https://doi.org/10.1016/j.talanta.2018.07.021>
- Sunda, W.G., 2012. Feedback Interactions between Trace Metal Nutrients and Phytoplankton in the Ocean. *Front. Microbiol.* 3. <https://doi.org/10.3389/fmicb.2012.00204>
- Tagliabue, A., 2014. More to hydrothermal iron input than meets the eye. *Proc. Natl. Acad. Sci.* 111, 16641–16642. <https://doi.org/10.1073/pnas.1419829111>
- Tagliabue, A., Aumont, O., Bopp, L., 2014a. The impact of different external sources of iron on the global carbon cycle. *Geophys. Res. Lett.* 41, 920–926. <https://doi.org/10.1002/2013GL059059>
- Tagliabue, A., Aumont, O., DeAth, R., Dunne, J.P., Dutkiewicz, S., Galbraith, E., Misumi, K., Moore, J.K., Ridgwell, A., Sherman, E., Stock, C., Vichi, M., Völker, C., Yool, A., 2016. How well do global ocean biogeochemistry models simulate dissolved iron distributions?: GLOBAL IRON MODELS. *Glob. Biogeochem. Cycles* 30, 149–174. <https://doi.org/10.1002/2015GB005289>
- Tagliabue, A., Bopp, L., Dutay, J.-C., Bowie, A.R., Chever, F., Jean-Baptiste, P., Bucciarelli, E., Lannuzel, D., Remenyi, T., Sarthou, G., Aumont, O., Gehlen, M., Jeandel, C., 2010. Hydrothermal contribution to the oceanic dissolved iron inventory. *Nat. Geosci.* 3, 252–256. <https://doi.org/10.1038/ngeo818>
- Tagliabue, A., Mtshali, T., Aumont, O., Bowie, A.R., Klunder, M.B., Roychoudhury, A.N., Swart, S., 2012. A global compilation of dissolved iron measurements: focus on distributions and processes in the Southern Ocean 17. <https://doi.org/10.5194/bg-9-2333-2012>
- Tagliabue, A., Resing, J., 2016. Impact of hydrothermalism on the ocean iron cycle. *Philos. Trans. R. Soc. Math. Phys. Eng. Sci.* 374, 20150291. <https://doi.org/10.1098/rsta.2015.0291>
- Tagliabue, A., Sallée, J.-B., Bowie, A.R., Lévy, M., Swart, S., Boyd, P.W., 2014b. Surface-water iron supplies in the Southern Ocean sustained by deep winter mixing. *Nat. Geosci.* 7, 314–320. <https://doi.org/10.1038/ngeo2101>
- Taylor, S.R., 1964. Abundance of chemical elements in the continental crust: a new table. *Geochim. Cosmochim. Acta* 28, 1273–1285. [https://doi.org/10.1016/0016-7037\(64\)90129-2](https://doi.org/10.1016/0016-7037(64)90129-2)
- Tortell, P.D., Maldonado, M.T., Granger, J., Price, N.M., 1999. Marine bacteria and biogeochemical cycling of iron in the oceans. *FEMS Microbiol. Ecol.* 29, 1–11. <https://doi.org/10.1111/j.1574-6941.1999.tb00593.x>
- Tortell, P.D., Maldonado, M.T., Price, N.M., 1996. The role of heterotrophic bacteria in iron-limited ocean ecosystems. *Nature* 383, 330–332. <https://doi.org/10.1038/383330a0>
- Town, R.M., van Leeuwen, H.P., 2005. Measuring Marine Iron(III) Complexes by CLE-AdSV. *Environ. Chem.* 2, 80–84. <https://doi.org/10.1071/EN05021>
- Twining, B.S., Baines, S.B., 2013. The Trace Metal Composition of Marine Phytoplankton. *Annu. Rev. Mar. Sci.* 5, 191–215. <https://doi.org/10.1146/annurev-marine-121211-172322>
- van den Berg, C.M.G., 2006. Chemical Speciation of Iron in Seawater by Cathodic Stripping Voltammetry with Dihydroxynaphthalene. *Anal. Chem.* 78, 156–163. <https://doi.org/10.1021/ac051441+>
- van den Berg, C.M.G., 2005. Organic Iron Complexation Is Real, The Theory Is Used Incorrectly. Comment on “Measuring Marine Iron(III) Complexes by CLE-AdSV.” *Environ. Chem.* 2, 88. <https://doi.org/10.1071/EN05029>

- van den Berg, C.M.G., 1995. Evidence for organic complexation of iron in seawater. *Mar. Chem., The Chemistry of Iron in Seawater and its Interaction with Phytoplankton* 50, 139–157. [https://doi.org/10.1016/0304-4203\(95\)00032-M](https://doi.org/10.1016/0304-4203(95)00032-M)
- van den Berg, C.M.G., 1982. Determination of copper complexation with natural organic ligands in seawater by equilibration with MnO<sub>2</sub> II. Experimental procedures and application to surface seawater. *Mar. Chem.* 11, 323–342. [https://doi.org/10.1016/0304-4203\(82\)90029-9](https://doi.org/10.1016/0304-4203(82)90029-9)
- Van den Berg, C.M.G., Huang, Z.Qiang., 1984. Direct electrochemical determination of dissolved vanadium in seawater by cathodic stripping voltammetry with the hanging mercury drop electrode. *Anal. Chem.* 56, 2383–2386. <https://doi.org/10.1021/ac00277a028>
- van den Berg, C.M.G., Nimmo, M., Daly, P., Turner, D.R., 1990. Effects of the detection window on the determination of organic copper speciation in estuarine waters. *Anal. Chim. Acta* 232, 149–159. [https://doi.org/10.1016/S0003-2670\(00\)81231-3](https://doi.org/10.1016/S0003-2670(00)81231-3)
- Velasquez, I.B., Ibisani, E., Maas, E.W., Boyd, P.W., Nodder, S., Sander, S.G., 2016. Ferrioxamine Siderophores Detected amongst Iron Binding Ligands Produced during the Remineralization of Marine Particles. *Front. Mar. Sci.* 3. <https://doi.org/10.3389/fmars.2016.00172>
- Walczak, M.M., Dryer, D.A., Jacobson, D.D., Foss, M.G., Flynn, N.T., 1997. pH Dependent Redox Couple: An Illustration of the Nernst Equation. *J. Chem. Educ.* 74, 1195. <https://doi.org/10.1021/ed074p1195>
- Wang, H., Wang, W., Liu, M., Zhou, H., Ellwood, M.J., Butterfield, D.A., Buck, N.J., Resing, J.A., 2022. Iron ligands and isotopes in hydrothermal plumes over backarc volcanoes in the Northeast Lau Basin, Southwest Pacific Ocean. *Geochim. Cosmochim. Acta* 336, 341–352. <https://doi.org/10.1016/j.gca.2022.09.026>
- Wang, P., Ding, Y., Liang, Y., Liu, M., Lin, X., Ye, Q., Shi, Z., 2021. Linking molecular composition to proton and copper binding ability of fulvic acid: A theoretical modeling approach based on FT-ICR-MS analysis. *Geochim. Cosmochim. Acta* 312, 279–298. <https://doi.org/10.1016/j.gca.2021.07.019>
- Welch, K.D., Davis, T.Z., Aust, S.D., 2002. Iron Autoxidation and Free Radical Generation: Effects of Buffers, Ligands, and Chelators. *Arch. Biochem. Biophys.* 397, 360–369. <https://doi.org/10.1006/abbi.2001.2694>
- Wells, M., Buck, K.N., Sander, S.G., 2013. New approach to analysis of voltammetric ligand titration data improves understanding of metal speciation in natural waters. *Limnol. Oceanogr. Methods* 11, 450–465. <https://doi.org/10.4319/lom.2013.11.450>
- Whitby, H., Planquette, H., Cassar, N., Bucciarelli, E., Osburn, C.L., Janssen, D.J., Cullen, J.T., González, A.G., Völker, C., Sarthou, G., 2020. A call for refining the role of humic-like substances in the oceanic iron cycle. *Sci. Rep.* 10, 1–12. <https://doi.org/10.1038/s41598-020-62266-7>
- Whitby, H., van den Berg, C.M.G., 2015. Evidence for copper-binding humic substances in seawater. *Mar. Chem., SCOR WG 139: Organic Ligands – A Key Control on Trace Metal Biogeochemistry in the Ocean* 173, 282–290. <https://doi.org/10.1016/j.marchem.2014.09.011>
- Williford, T., Amon, R.M.W., Benner, R., Kaiser, K., Bauch, D., Stedmon, C., Yan, G., Walker, S.A., van der Loeff, M.R., Klunder, M.B., 2021. Insights into the origins, molecular characteristics and distribution of iron-binding ligands in the Arctic Ocean. *Mar. Chem.* 231, 103936. <https://doi.org/10.1016/j.marchem.2021.103936>
- Worsfold, P.J., Lohan, M.C., Ussher, S.J., Bowie, A.R., 2014. Determination of dissolved iron in seawater: A historical review. *Mar. Chem.* 166, 25–35. <https://doi.org/10.1016/j.marchem.2014.08.009>
- Wu, J., Luther, G.W., 1995. Complexation of Fe(III) by natural organic ligands in the Northwest Atlantic Ocean by a competitive ligand equilibration method and a kinetic approach. *Mar. Chem., The Chemistry of Iron in Seawater and its Interaction with Phytoplankton* 50, 159–177. [https://doi.org/10.1016/0304-4203\(95\)00033-N](https://doi.org/10.1016/0304-4203(95)00033-N)

- Wu, S., He, M., Hu, B., Jiang, Z., 2007. Determination of trace rare earth elements in natural water by electrothermal vaporization ICP-MS with pivaloyltrifluoroacetone as chemical modifier. *Microchim. Acta* 159, 269–275. <https://doi.org/10.1007/s00604-007-0764-5>
- Yun, J., Choi, H., 2000. Micellar colorimetric determination of iron, cobalt, nickel and copper using 1-nitroso-2-naphthol. *Talanta* 52, 893–902. <https://doi.org/10/fnrgrn7>
- Zhu, K., Hopwood, M.J., Groenenberg, J.E., Engel, A., Achterberg, E.P., Gledhill, M., 2021. Influence of pH and Dissolved Organic Matter on Iron Speciation and Apparent Iron Solubility in the Peruvian Shelf and Slope Region. *Environ. Sci. Technol.* 55, 9372–9383. <https://doi.org/10.1021/acs.est.1c02477>
- Zigah, P.K., McNichol, A.P., Xu, L., Johnson, C., Santinelli, C., Karl, D.M., Repeta, D.J., 2017. Allochthonous sources and dynamic cycling of ocean dissolved organic carbon revealed by carbon isotopes. *Geophys. Res. Lett.* 44, 2407–2415. <https://doi.org/10.1002/2016GL071348>



## Note for the reader

The following Chapter is in final stage of preparation for publication and is nearly ready for submission to the journal Analytical Letters. This might explain repetitions regarding the description of the methodological context and of the scientific background. This paper is co-authored by D. Omanović and C.M.G. van den Berg, and the supervisory team of this Thesis.

To be submitted as: **Mahieu, L.**, Whitby, H., Omanović, D., van den Berg, C.M.G., Salaün, P.: Catalytic enhancement of the reduction current of iron bound to 1-nitroso-2-naphthol ( $\text{FeNN}_3$ ) in seawater by adsorptive cathodic stripping voltammetry unbuffered and with low volume requirement.



## **Chapter 3**

### **3. Catalytic enhancement of the reduction current of iron bound to 1-nitroso-2-naphthol ( $\text{FeNN}_3$ ) in seawater by adsorptive cathodic stripping voltammetry unbuffered and with low volume requirement**

#### **Abstract**

Iron (Fe) concentrations and speciation in seawater can be investigated by adsorptive cathodic stripping voltammetry (ACSV) using an artificial ligand added to the sample. For Fe organic speciation, which is pH dependent, the pH flexibility of the ligand 1-nitroso-2-naphthol (NN) is of specific interest to investigate the impact of natural pH gradient and ocean acidification as opposed to other commonly used artificial ligands, only calibrated at a single pH value. However, the existing NN method, nitrogen purged and not catalysed, lacks sensitivity for such purpose. In this Chapter, the potential to enhance the ACSV reduction signal of Fe bound to NN ( $\text{FeNN}_3$ ) by dissolved oxygen ( $\text{O}_2$ ; NN-air method) has been explored. The NN-Air method has optimal sensitivity in unbuffered conditions, with an increase more than 10-fold the sensitivity experienced in deoxygenated conditions. The application of the method for the determination of dissolved iron (DFe) concentration and iron organic speciation was restricted by the presence of an interfering compound, identified as another NN-chelated trace metal, that is reduced at the same potential as Fe and undergoes the same catalytic process. Despite this limitation, all aspects for the application of the NN-Air method have been solved hereafter, as well as the procedure to verify the presence of such interference. If ensured as free of this interference, the high sensitivity of the NN-Air method could allow the investigation of iron organic speciation at natural seawater pH. Additionally, the determination of DFe in deoxygenated conditions suggested that Fe

organic speciation could be investigated in unbuffered conditions with NN. We also present further modifications to the original method allowing the measurement to be performed in volumes as low as 0.5 mL and present a novel way to calibrate NN solutions using its optical properties and to prepare them in Milli-Q water instead of methanol.

### 3.1. Introduction

The oceanic chemistry of trace metals have been thoroughly investigated in recent years because of their essential role in phytoplankton growth (de Baar et al., 2017; Morel and Price, 2003). Most attention has been given to iron (Fe), specifically to its dissolved fraction (DFe; practically defined by the porosity of the filters of 0.2 or 0.45  $\mu\text{m}$ ) because it limits phytoplankton growth across 40% of the global ocean (Moore et al., 2013), particularly in High Nutrient, Low Chlorophyll (HNLC) regions (e.g. Martin et al., 1990). DFe has also been shown to be responsible for taxonomic adaptation of living organisms such as prochlorococcus (Hogle et al., 2021). Fe limitation is notably due to its poor solubility in oxic seawater and, therefore, low DFe concentrations. DFe in seawater is mostly found under the ionic form  $\text{Fe}^{3+}$  and at much lower concentration  $\text{Fe}^{2+}$  (Liu and Millero, 2002). The poor solubility of Fe is compensated by its complexation by organic Fe-binding ligands. The organically-complexed Fe is thought to represent 99% of the DFe found in seawater (Gledhill and van den Berg, 1994; van den Berg, 1995). The critical role of Fe and other trace metals in phytoplankton development and carbon cycling have motivated their investigation worldwide notably through the program GEOTRACES ([www.geotraces.org](http://www.geotraces.org)). Such community efforts are key to constrain critical oceanic processes and future feedbacks of the global system in the context of ocean warming and acidification (Gattuso et al., 2015; Hoffmann et al., 2012; Hutchins and Boyd, 2016; Stockdale et al., 2016). Despite remarkable progress in reporting trace metal distribution and dynamics over the global ocean (e.g. Cloete et al., 2021; Ho et al., 2018; Roshan and DeVries, 2021), their organic speciation is still poorly resolved. In the case of Fe, 20,000 DFe data points were compiled by Tagliabue et al. (2016), while only 1,732 organic speciation data points could be compiled for the period 1995-2015 (Caprara et al., 2016) despite its major role in defining Fe solubility and bioavailability (Kuma et al., 1996). This difference is explained by the analytical difficulties met while measuring organic speciation.

Four main approaches are currently used to quantify DFe in seawater: inductively coupled plasma mass spectrometry (ICP-MS; Wu et al., 2007), spectrophotometry (Lohan et al., 2006), chemiluminescence (Obata et al., 1993), and voltammetry (Obata and van den Berg, 2001). The voltammetric methods developed to investigate Fe were reviewed by Laglera and Monticelli (2017). The most sensitive voltammetric methods are based on adsorptive cathodic stripping voltammetry (ACSV). The ACSV method relies on the complexation of labile DFe present in the sample by an added ligand (AL) forming an electroactive FeAL complex. Samples are classically acidified to release Fe from organic complexes. The FeAL complex is concentrated at the surface of a mercury drop electrode (MDE) by application of a potential near 0 V, and the reduction current (in nanoamperes, nA) of the complexed Fe<sup>3+</sup> into Fe<sup>2+</sup> is measured during the stripping step, where the potential is scanned cathodically, from positive to more negative potential. DFe concentration (in nmol.L<sup>-1</sup>) is retrieved by performing at least two known standard additions of DFe and by determining the intersection of the linear regression obtained. The ACSV method is not widely used despite its high sensitivity allowing the quantification of the sub-nanomolar DFe typically found in open ocean waters. The low number of application is notably explained by: 1- the use of mercury as a working electrode, rising environmental concerns; 2- by the difficulties met to release DFe from the organic matrix, leading to potential under-estimation DFe; 3- by the issues related to blank and contamination with the use of several chemicals, and 4- by the time involved to process the samples. The blank contamination is mostly due to the addition of a buffer the sample to reach the pH value of optimal sensitivity, and potentially by the acidification/alkalinisation step to release DFe from the organic matrix. The neutralisation of the organic matrix can also performed by UV-irradiation of the sample (Buck et al., 2007), which requires specific equipment and do not set free from the acidification of the sample, as DFe would otherwise precipitate (Liu and Millero, 2002). Despite progresses to overcome the limitations related to the blank offset, organic matrix, and analysis time recently developed for the AL dihydroxynaphthalene (DHN; Caprara et al., 2015; Laglera et al., 2016), the ACSV methods have rarely been used for the determination of DFe.

The limitations encountered for the determination of DFe by ACSV are also experienced while investigating Fe organic speciation. The most established approach to investigate Fe organic speciation

is the Competitive Ligand Equilibration followed by ACSV (CLE-ACSV). This method allows titration of the organic Fe-binding ligand in terms of concentration and binding strength of the detected ligand bulk conditional to the temperature, salinity and pH of the sample during analysis. The theory of this approach was detailed by van den Berg (1982) in the case of the titration of a natural organic copper complex against manganese oxides. More recently, instead of competition against manganese oxides, the addition of artificial ligands forming an electroactive complex with the metal of interest is preferred. The competition between the natural ligands and the added one is evaluated against a gradient of concentration of the metal of interest and requires the sample to be at chemical equilibrium, meaning that temperature and pH must be stable, and enough time allowed to the natural ligands and the AL to compete for the metal of interest, so as to reach thermodynamic equilibrium (Gerringa et al., 2014; Rue and Bruland, 1995; van den Berg, 1982; Wu and Luther, 1995). The ALs currently in use are the same as those used to determine DFe concentration. They are DHN (Caprara et al., 2015; Laglera et al., 2016; Sanvito and Monticelli, 2021, 2020; van den Berg, 2006), salicylaldehyde (SA; Abualhaija and van den Berg, 2014; Buck et al., 2007; Rue and Bruland, 1995), 2-(2-Thiazolylazo)-p-cresol (TAC; Croot and Johansson, 2000), and 1-nitroso-2-naphthol (NN; Aldrich and van den Berg, 1998; Gledhill and van den Berg, 1994; van den Berg, 1995). They all suffer from specific limitations reported in the references mentioned above and in Chapter 2.

The CLE-ACSV approach requires a chemical equilibrium in term of temperature and pH. To perform organic speciation titration at room temperature instead of in-situ is thought to have little impact on the titration results (Hiemstra and van Riemsdijk, 2006) or can be easily corrected (Hassler et al., 2013). On the other hand, the required pH buffering impacts Fe solubility (Bondietti et al., 1993; Liu and Millero, 2002) as well as natural ligand binding capacity (Avendaño et al., 2016; Gledhill et al., 2015; Zhu et al., 2021). To date, the impact of buffering the sample pH, irrespective of its original value, on Fe organic speciation is not clearly known (Avendaño et al., 2016; Gledhill et al., 2015) because the only ligand to be calibrated at different pH values, NN (Gledhill and van den Berg, 1994; van den Berg, 1995), shows limited sensitivity due to the absence of catalysis.

We present in this Chapter the exploratory work toward the use of NN under similar catalytic signal enhancement as SA and DHN using atmospheric oxygen (O<sub>2</sub>), and the reasons of why this NN-air method is not applicable for the determination of neither DFe nor Fe organic speciation in the actual state of the method development. Despite this unfortunate conclusion, we present our electrochemical apparatus inspired by Sanvito et al. (2019) and Sanvito and Monticelli (2020) suitable for the use of NN in volume as low as 0.5 mL, as well as the preparation and control of NN solution in Milli-Q water calibrated by spectrophotometry.

## 3.2. Method

### 3.2.1. Voltammetric apparatus and procedure

The voltammetric apparatus was composed of a 663 VA stand (Metrohm) installed in a laminar flow hood (Class 100) and equipped with a multi-mode electrode (MME, Metrohm) as MDE. The choice of the reference and auxiliary electrodes were investigated in this study to optimise sensitivity and volume requirement. The conditions used with the initial system (Figure 3.1a) and miniaturized system (Figure 3.1b) are compiled in Table 3.1. For both systems, a glassy carbon counter electrode was placed in a glass bridge filled with either UV-irradiated seawater or 3M KCl cleaned with manganese oxides. No difference on sensitivity and no Fe diffusion were observed with any of these 2 electrolyte solutions.

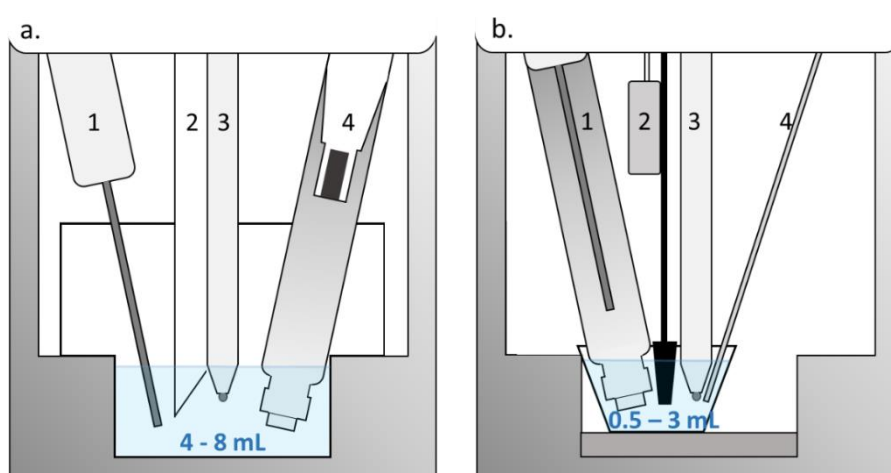


Figure 3.1. Electrode and cell as a) initially used and b) optimised in this study, with 1) the auxiliary electrode, 2a) Teflon stirrer, 2b) home-made stirrer with a vibrator, 3) SMDE, 4a) Ag/AgCl electrode in a glass bridge and 4b) silver wire. The numbers in blue represent the range of volume of sample for each set-up. The solid grey part represents the cell holder.

The three electrodes were controlled with a potentiostat/galvanostat Type III ( $\mu$ Autolab) controlled by the software NOVA 2.5 (Metrohm<sup>TM</sup>). MME and stirring device were controlled by an Autolab IME 663 (Metrohm<sup>TM</sup>) interface, whereas the mercury drop size and stirrer speed were selected on the 663 VA stand and optimized at the respective values of 1 and 6. The electric supply to the home-made stirrer was regulated with a 1.5 V control box plugged on the Autolab IME 663.

Table 3.1. Voltammetric set up and procedure of the classic NN method and proposed NN-Air approach to investigate Fe in seawater.

	Classic set up (Aldrich and van den Berg, 1998; Gledhill and van den Berg, 1994; van den Berg, 1995)	Compact set up (this study)
Sample volume	10 mL	0.5 – 3 mL
Stirring	Teflon stirrer (Metrohm <sup>TM</sup> )	Home-made stirrer with vibrator (3 V, 11500 $\pm$ 2000 rpm, JinLong Machinery <sup>TM</sup> )
Reference electrode	Silver - silver chloride electrode (Ag/AgCl ; Metrohm) with double bridge (3 mol.L <sup>-1</sup> KCl)	1.5 mm diameter silver wire (K.A. Rasmussen <sup>TM</sup> )
Catalysis	Hydrogen peroxide (1.7 mmol.L <sup>-1</sup> ) with 5 ppm SDS No catalysis for speciation	Atmospheric dissolved oxygen
pH (buffer)	6.9 (PIPES) 8.1 (Tris, HEPPS)	Unbuffered or 7.5 – 8.2 (POPSO, HEPPS, PIPES, borate)
Voltammetric method	Sampled-DC mode Adsorption potential: -0.05 V Scan rate: 50 mV/s Linear sweep wave Adsorption/step potential: -0.15 V/4 mV Scan rate: 40 mV/s	Square wave Adsorption/step potential: -0.3 V/5 mV Scan rate: 50 mV/s
Range of deposition time	300 s	60 s to 300 s (function of pH)
Interferences	HS or glutathione-like in Southern Ocean water?	HS or glutathione-like in Southern Ocean water? Other metal (unidentified)

### 3.2.2. Determination of DFe in test waters

In this study, the determination of DFe was attempted in Milli-Q water (Millipore, 18.2 M $\Omega$ ), in certified reference material (CRM; NASS-6 and NASS-7, National Research Council of Canada) diluted in Milli-Q, in natural seawater and in UV-irradiated seawater. The natural and UV-irradiated seawater were collected during the Southern Ocean Seasonal Experiment (<https://scale.org.za/>; 16/11/2019, 41°3S/09°4E, mix of waters sampled from 1300 to 2000 m). The test water was first sampled in an acid cleaned 50 L carboy (Nalgene) and subsampled in acid cleaned 500 mL HDPE bottles (Nalgene) and stored at room temperature. The water was UV-irradiated for 1 hour in quartz tubes in a home-made system made with 125W mercury light bulb placed in a PVC and Teflon™ structure ([http://pcwww.liv.ac.uk/~sn35/Site/UV\\_digestion\\_apparatus.html](http://pcwww.liv.ac.uk/~sn35/Site/UV_digestion_apparatus.html)). The seawater samples must be acidified to avoid DFe adsorption and flocculation while UV-irradiating for the elimination of the organic matrix. The pH was brought to a value < 2 with 25  $\mu$ L of a 50 % HCl solution (20 %, trace metal grade, Fisher Scientific) for 10 mL of sample. The pH was brought back to a value of around 8.1 by addition of 15  $\mu$ L of a 50 % ammonia (NH<sub>4</sub>OH; 29% Laporte™) for 10 mL of sample.

### 3.2.3. Reagents

Milli-Q water was supplied by a system combining an Elix 5 (Millipore™) linked to a 30 L polyethylene tank (Millipore) and a A10 Advantage Milli-Q (Millipore™) providing the reference conductance value of 18.2 M $\Omega$ . Polypropylene tubes (Fisher Scientific Sterilin™ 30 mL) used as reagent containers were cleaned by soaking in 0.6 M acid bath (HCl laboratory reagent grade 32 %, FisherScientific) for at least 2 weeks and thoroughly rinsed with Milli-Q 5 to 10 times. For laboratory use, LDPE and HDPE bottles of various volumes (Nalgene™) underwent a similar process but with a previous 1 week soaking in a detergent (Decon™) bath before first use. When required, contamination was checked against CRM NASS-6 and NASS-7 (National Research Council Canada) diluted 17 times in Milli-Q to simplify the pH adjustment, optimize the sensitivity, and check for contamination at the subnanomolar level. For sample collection, HDPE Nalgene™ bottles were cleaned following the classic process of 1 week in

detergent bath, 1 week in 1 M HCl bath, 1 week in 0.1 HCl bath with thorough Milli-Q rinsing at the end of each step.

NN (98 %, Acros Organics; 95 %, Sigma Aldrich) solutions were prepared in Milli-Q because of the unsatisfactory level of contamination of tested methanol (MeOH; Laboratory reagent grade, HPLC gradient grade, and Primar-Trace analysis grade, Fisher Scientific; Chromasol™ for HPLC  $\geq$  99.9 %, Sigma Aldrich). Further details, including verification of the NN concentration in Milli-Q, are provided in section 3.3.1. DFe solutions were prepared by dilution of a DFe standard ( $1\text{g.L}^{-1}$ , BDH™) and acidified to pH 2 (NBS scale) with 18  $\mu\text{L}$  of a 50 % HCl (20 %, trace metal grade, Fisher Scientific). The pH meter (827 pH Lab, Metrohm™) was calibrated with buffer solutions of pH 4.0, 7.0 and 9.18 (Specpure™ NIST traceable, Alfa Aesar).

To adjust the pH for buffers (Table 3.2) and seawater samples, HCl (20 %, trace metal grade, Fisher Scientific),  $\text{NH}_4\text{OH}$  (29% Laporte™) and  $1\text{ mol.L}^{-1}$  sodium hydroxide (NaOH; Analytical reagent grade, Fisher Scientific) were used. NaOH and buffers were cleaned twice by addition of  $100\text{ }\mu\text{mol.L}^{-1}$  manganese oxide, vigorously shaken, and left overnight before filtration through  $0.45\text{ }\mu\text{m}$  syringe filters (Millex HA, Millipore™) performed with a peristaltic pump (Rainin Dynamax RP-1). Filters and tubing (Teflon™ and Altec™ in PVC, respectively) were previously cleaned by passing 1 L of  $0.6\text{ mol.L}^{-1}$  HCl (laboratory reagent grade 32 %, FisherScientific) and 0.5 L of Milli-Q water and then kept clean by passing 200 mL of  $0.6\text{ mol.L}^{-1}$  HCl and Milli-Q water before use.

Table 3.2. Buffer used in this study.

Buffer name	CAS	Buffering range	$\text{pK}_a$ (25C)	Provider	Reference specificity
Boric acid	10043-35-3	8.2 - 10.1	9.2	Fisher Scientific	Analytical reagent grade
HEPPS / EPPS	16052-06-5	7.3 - 8.7	8.0	Merck	> 99%
PIPES	100037-69-2	6.1 - 7.5	6.8	Acros Organics	Sesquisodium salt, 97%
POPSO	68189-43-5	7.2 - 8.5	7.8	Sigma-Aldrich	$\geq$ 99%



The buffer tested (Table 3.2) in this study were prepared by dilution in Milli-Q to a final concentration of 1 mol.L<sup>-1</sup> except for POPSO (Sigma Aldrich) which was prepared at 0.25 mol.L<sup>-1</sup> in 0.40 mol.L<sup>-1</sup> NaOH to reach a pH value of 8.1 when diluted to 10 mmol.L<sup>-1</sup> in seawater. A pH value of 7.8 is reached if the POPSO solution is prepared in 0.35 M NaOH. The pH of the buffers was decreasing due to manganese oxide cleaning. The consumption of hydroxides ions by the formation of manganese and trace metals precipitate needed to be corrected with 1 nmol.L<sup>-1</sup> NaOH. The final concentration of any of the buffers added in the samples was 10 mmol.L<sup>-1</sup>. NN was added to always reach a concentration of 20 µmol.L<sup>-1</sup> (Aldrich and van den Berg, 1998).

### **3.3. Results and discussion**

#### **3.3.1. Spectrophotometric determination of the NN stock concentration**

NN is classically dissolved in MeOH because of the relation between solubility and solvent polarity observed for the naphthol group (Yun and Choi, 2000). Several high purity grades MeOH were purchased (see Section 3.2.3), but they were all contained unacceptable Fe concentrations (in the range of nmol.L<sup>-1</sup>) and so, were found unsuitable for Fe investigation. To avoid the issues related to MeOH contamination, NN solubilisation was attempted in Milli-Q water (NN-MQ). The spreadsheet developed to calibrate the concentration of NN-MQ solutions is freely available (Annex 1). The dissolved NN concentration in Milli-Q water is fixed by its (poor) solubility. NN is a coloured compound used for the detection of trace metals by spectrophotometry, notably Fe<sup>3+</sup>, Co<sup>2+</sup>, Ni<sup>2+</sup>, and Cu<sup>2+</sup> (detection limits of 430 nmol.L<sup>-1</sup> for Fe<sup>3+</sup>; Yun and Choi, 2000), however, at neutral pH, the absorbance signal is proportional to the free NN concentration (Yun and Choi, 2000). This means that the spectrophotometric calibration of NN partially dissolved in clean Milli-Q can be calibrated with NN fully dissolved in MeOH, even if the latter contains nanomolar traces of Fe. The Beer-Lambert's law relates the absorbance to a specific concentration through an extinction coefficient. To be able to calculate NN concentration in Milli-Q from the calibration obtained in MeOH, we had to check for changes in extinction coefficient in these solvents. To free the calibration from potential solvent effects,

the standard of known NN concentration prepared in MeOH (NN-MeOH references) where diluted from 10 to 1000-fold with Milli-Q in the spectrophotometric cell when analysed by spectrophotometry (DR 3900, Lange, HACH). For NN-MeOH references, the volume of the solution was calculated according to the dilution with Milli-Q and density of MeOH. The calibration curve was performed with two different standards measured over a period of 5 weeks (n = 34). The absence of drift from the spectrophotometer and stability of the NN-MeOH references in time are attested by the linearity of the calibration curve in time. To define the concentration of the NN solution diluted in Milli-Q, 0.5 mL of the NN solution are placed in the spectrophotometric cell and diluted with Milli-Q in 2 to 5 steps. As for the NN-MeOH references, the absorbance values are recorded for each dilution factor, and controlled by weighing. From the accurate weighing of the solution at the different levels of dilution for which the absorbance is measured (Figure 3.2), the concentration of the solution is recalculated. The calculation performed at each level of dilution are averaged to provide a final value for the day of the calibration, and the standard deviation calculated to provide an error on the determination of the concentration.

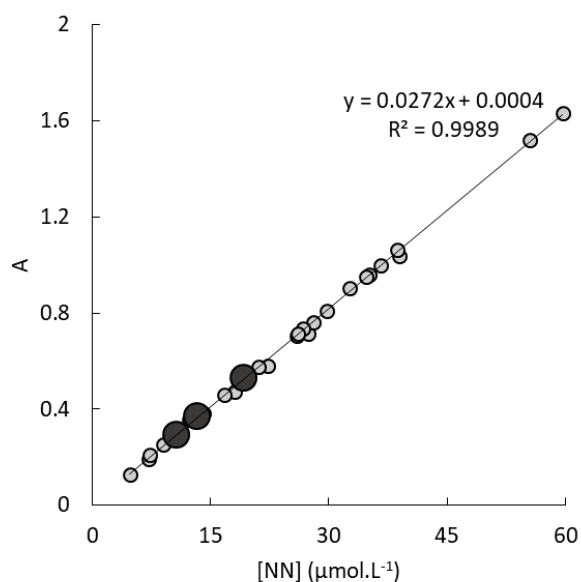


Figure 3.2. Calibration curve (black line) of the spectrophotometric determination from two diluted NN-MeOH standards over 5 weeks (light grey dots), and an example of the calibration of a NN-MQ solution with 3 dilutions (black dots).

The concentration of the NN-MQ solutions ranged from 0.3 to 0.5 mmol.L<sup>-1</sup> for a minimum of 4 mg of NN in 50 mL of Milli-Q. The relative variability on the determination of NN concentration, defined as the relative standard deviation of the concentrations calculated at the 3 different levels of dilution, was never higher than 5%. The relative error on the concentration of the ligand solution is comparable to the error on common preparation in MeOH, which is dependent on the accuracy of the weighing of the ligand, accuracy of successive dilutions, accuracy of the pipetting (limited for MeOH), and solvent evaporation in time. The advantage of the spectrophotometric calibration is that a daily control of the NN concentration can be performed within a few minutes. This approach is also much more accurate for the preparation of NN solution of low concentration. The initial method for the determination of Fe organic speciation using NN (Gledhill and van den Berg, 1994) used solutions at 10 and 20 mmol.L<sup>-1</sup>, for which it is complicated to pipette low volumes to reach low concentration in the sample. The high NN concentration in the samples have been shown to limit the detection of humic substances and thus underestimate the total ligand concentration (Laglera et al., 2011). This was attributed to the detection window (D), product of the side-reaction coefficient of the added ligand and of its concentration ( $D = [AL]^n * \beta_{FeAL}$ ), being too high and outcompeting part of the humic substances (Laglera et al., 2011). The use of a lower D is limited while diluting NN in MeOH because of the risk of propagating an error by successive dilutions, and because the addition of larger volume of MeOH could impact the sample. Our procedure to prepare NN-MQ solutions around 50-fold less concentrated than the classically used standards prepared in MeOH would be beneficial to explore the impact of lower D values on the detection of humic substances by CLE-ACSV.

### **3.3.2. O<sub>2</sub> catalysis and oxygenation of the sample**

The catalytic process of the reduction of Fe complexed with an added ligand in the presence of O<sub>2</sub> has been previously described for SA (Abualhaija and van den Berg, 2014) and the mechanism reinterpreted when applied to DHN (Laglera et al., 2016). When stripping the potential cathodically, O<sub>2</sub> is first reduced to H<sub>2</sub>O<sub>2</sub> and the Fe<sup>3+</sup> bound to the AL is reduced into Fe<sup>2+</sup> at the Hg surface. The newly formed H<sub>2</sub>O<sub>2</sub> oxidises Fe<sup>2+</sup> back into Fe<sup>3+</sup> which can be chelated again by the AL and immediately reduced to Fe<sup>2+</sup>, creating this catalytic effect. The dissociation of H<sub>2</sub>O<sub>2</sub> is common in biotic systems and known as

the Fenton reaction (Fenton, 1894). The regeneration and chelation process are much faster than the stripping and catalytically enhance the  $\text{Fe}^{3+}$  reduction signal, lowering the limit of detection.

To allow drop formation, the MME needs to be connected to a gas supply through the VA 663 Stand. The system is built so that the supplied gas is continuously flowing at the surface of the sample. This gas blanketing is useful to ensure good deoxygenation of the sample when required (e.g. Croot and Johansson, 2000; Gledhill and van den Berg, 1994; Pernet-Coudrier et al., 2013; Sukekava et al., 2018; van den Berg, 1995; Whitby and van den Berg, 2015), but is problematic if the voltammetric method requires the  $\text{O}_2$  naturally present in the sample as the catalyst (e.g. Abualhaija and van den Berg, 2014; Caprara et al., 2015; Laglera et al., 2016; Sanvito et al., 2019; Sanvito and Monticelli, 2021, 2020).

Table 3.3. Reproducibility of the mercury drop formation and oxygenation of the sample as shown by the stability of the  $\text{H}_2\text{O}_2$  reduction current peak.

Time (min)	2	4	6	8	10	12	14	16	18	Standard deviation	Average	Relative variability
$\text{H}_2\text{O}_2$ reduction current (nA)	133.7	133.2	133.1	132.5	133.0	133.1	132.4	133.8	133.5	0.5	133.2	0.4 %

The blanketing nitrogen flow can be stopped by tightening a screw located on the left side of the VA 663 Stand. However, the tightening of this screw was reported to disturb the mercury drop formation and the MME cartridge had to be connected on pressurised air (Abualhaija and van den Berg, 2014), leading to a high rate of mercury oxidation and electrochemical noise associated to mercury oxide compounds. In our case, the gas blanketing control by tightness of the screw did not impact the drop formation and drop size were found to be reproducible, as seen by the stability of the  $\text{H}_2\text{O}_2$  reduction signal (Table 3.3). The MME cartridge was thus connected to nitrogen, the left screw tightened to prevent any blanketing. To ensure constant  $\text{O}_2$  concentration, we used a small aquarium pump (HD-603, HDOM) placed in the laminar flow, as has been previously reported (Sanvito et al., 2019).

### 3.3.3. Voltammetric system adjustment for the NN-Air method

When measuring the  $\text{FeNN}_3$  reduction signal in the presence of air repetitively in the same solution, a decrease of the Fe signal was always observed, irrespective of the nature of the auxiliary electrodes

being used (platinum rod (Figure 3.3), glassy carbon rod or iridium wire). This interference was observed in Milli-Q, seawater and UV-irradiated seawater. However, when using a glass bridge with the platinum electrode, the signal was stable, and signal loss could be partly recovered (Figure 3.3), suggesting that the interfering compound(s) is/are produced at the auxiliary electrode and that they are kinetically unstable.

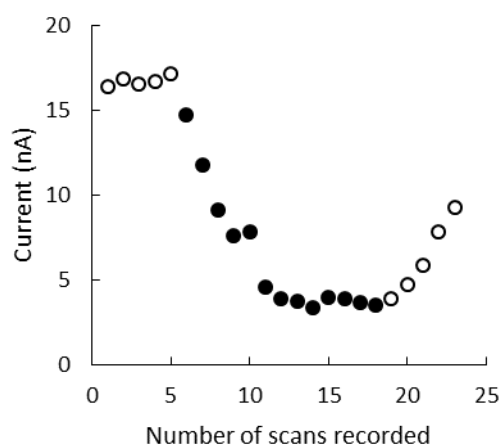


Figure 3.3. FeNN<sub>3</sub> reduction current with (open circle) and without (filled circle) glass bridge at the auxiliary platinum electrode in CRM NASS-6 diluted in Milli-Q, 2.5 min between each scan.

In the case of glassy carbon rod and iridium wire as auxiliary electrode, the initial peak is stable but the peak current does not increase with Fe additions (results not shown). We do not have an explanation for the latter. If an analysis was carried out in a fresh sample with the glass bridge at the auxiliary electrode but in the same cell just after experiencing the interference, the interference was persisting, suggesting strong adsorption of the interfering agent on cell walls and/or electrodes. Removal of the interference was only obtained by overnight 0.6 M HCl rinse. The fact that the glass bridge avoids such interferences attests to electrochemical production at the auxiliary electrode.

There are no interferences observed in the traditional NN method purged with N<sub>2</sub> in the presence of H<sub>2</sub>O<sub>2</sub> or KBrO<sub>3</sub> as oxidant with the auxiliary electrode in direct contact with the sample (Aldrich and van den Berg, 1998; Gledhill and van den Berg, 1994). This suggests implication of O<sub>2</sub> or a reduction by-product such as the superoxide anion (O<sub>2</sub><sup>•-</sup>) produced at the working electrode and having a short life-time in aqueous solutions (Hayyan et al., 2016). In our experiment, the species at the highest

concentrations are the AL, added buffer and carbonates, but interference was also observed in unbuffered solution. The implication of carbonates alone is excluded as this phenomenon is not observed with other organic ligands used in unpurged samples. We can conclude that the interference produced directly or indirectly at the auxiliary electrode is specific to the system NN/O<sub>2</sub>, with potential implication of carbonates from the dissolution of CO<sub>2</sub>. The implication of other trace metals complexed by NN is not excluded either (Yun and Choi, 2000). This interference is avoided by the isolation of the auxiliary electrode by a glass bridge, which was always used thereafter.

### **3.3.4. Comparison between oxygenated and deoxygenated sample**

Progressive deoxygenation and decarbonation by N<sub>2</sub> flow over an UV-irradiated and unbuffered seawater sample has been recorded (Figure 3.4) to show the impact of the presence of O<sub>2</sub> and carbonates on the voltammogram. The oxygenated sample shows O<sub>2</sub> reduction peak (0.00 V to -0.38 V), followed by the catalysed FeNN<sub>3</sub> reduction peak (-0.40 V to -0.60 V; centred at -0.52 V) which is located on the anodic side of a broad H<sub>2</sub>O<sub>2</sub> reduction peak (-0.38 V to -1.40 V; centred at -0.90 V). The reduction of vanadium bound to AL such as the DHN has also been identified at -0.90 V (Obata and van den Berg, 2001). It is known to be catalytically reduced following the same process as the FeNN<sub>3</sub> complex (Obata and van den Berg, 2001). It was also referenced at -0.90 V with the AL catechol (van den Berg and Huang, 1984). NN is known to bind with vanadium too (Yun and Choi, 2000), therefore, it is plausible that the vanadium-NN complex is reduced at -0.90 V, although this was not tested. The relatively high current centred at -0.90 V remaining after deoxygenation could also be partially explained by remaining O<sub>2</sub> traces in the sample, which was deoxygenated by nitrogen flow above the sample and not bubbled. The small bump located at -1.00 V was not identified (Figure 3.4). Sample deoxygenation reveals the free AL peak (here, NN) at -0.15 V, similar to methods with other ALs, notably DHN (Sanvito, 2021). In the absence (or close to absence) of O<sub>2</sub> and carbonates, the FeNN<sub>3</sub> reduction peak intensity is decreased by a factor of at least 10 and anodically shifted to -0.40 V.

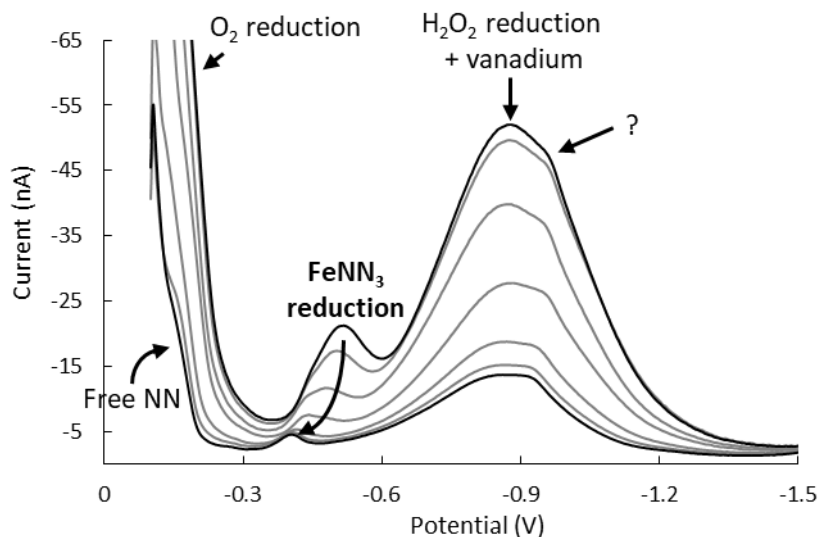


Figure 3.4. Selected voltammograms of deoxygenation experiment of a UV-irradiated seawater sample at natural pH and spiked with  $5 \text{ nmol.L}^{-1}$  of DFe for 30 s deposition. The highest and lowest voltammograms (black lines) correspond to the scan number 1 and 29 and higher and lower  $\text{O}_2$ , respectively. The deoxygenation steps (grey lines) correspond, from higher to lower, to the scans number 2, 5, 10, 15, and 21.

### 3.3.5. Comparison between compact and classic set up

In this section, the previously used cell for 5 mL of sample (Gourain, 2020) and the compact set up used with a volume as low as 0.5 mL were compared. The reduction of the sample volume using a silver wire as reference electrode (Figure 3.1; Sanvito et al., 2019; Sanvito and Monticelli, 2020) was attempted for the NN-Air method (Figure 3.5). The need of a glass bridge at the auxiliary electrode strongly limited the available volume for other electrodes and stirrer, and the Teflon stirrer used with our 5 mL cell (already slightly smaller diameter than classic Methrom<sup>TM</sup> stirrers; Gourain, 2020) did not fit, pressing for the development of a home-made stirrer. A direct comparison of the sensitivity obtained with our classic and miniaturised system (Table 3.1) has been performed simultaneously on 2 different systems (Figure 3.5) and confirmed on a single system (results not shown). Both set ups showed similar sensitivity in unbuffered UV-irradiated seawater (Figure 3.5). The sensitivity was as high as  $25 \text{ nA}/(\text{nmol.L}^{-1}.\text{min})$  in the CRM NASS-6 diluted in Milli-Q and  $20 \text{ }\mu\text{M}$  of NN added, attesting of the impact of the salinity on the sensitivity of the NN-Air method (result not shown). The sensitivity with the miniaturised system did not show significant variation in the range of 0.5 mL to 2.5 mL sample volume. The similar sensitivity values indicate optimal stirring from both set ups.

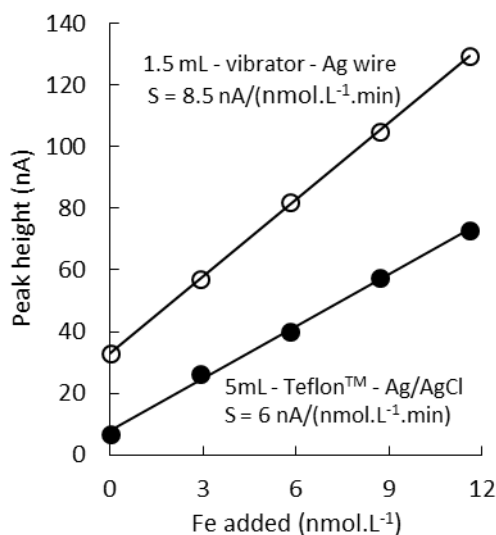


Figure 3.5. FeNN<sub>3</sub> reduction peak in unbuffered irradiated seawater with the compact (1.5 mL of sample, home-made stirrer with vibrator and a Ag wire as reference electrode; red) and classic (5mL of sample, a Teflon™ stirrer and a Ag/AgCl reference electrode; black) systems. The difference in sensitivity is explained by the cleanliness of the mercury.

Interestingly, both set ups have been found to be very sensitive to the presence of mercury oxides in the cartridge of the SMDE (result not shown). Optimal results were ensured by regular (every 10 days) filtration of the mercury by pipetting. Even if regular filtering of the mercury could be seen as tedious, a 5 min cleaning procedure of the MME during which the capillary is left untouched has been defined, ensuring maximum sensitivity and absence of impurity. The mercury was filtered after vigorous shaking of the MME to unstick mercury oxides from walls and connections. The needle was cleaned by simply screwing it off, wiping it gently, and screwing it back in with the exact same tightness. The absence of manipulation of the capillary is believed to increase the capillary lifetime.

### 3.3.6. Impact of buffers and pH on Fe-NN<sub>3</sub> signal in presence of O<sub>2</sub>

Buffered UV-seawater has been progressively alkalinised with NaOH (Analytical reagent grade, Fisher Scientific) cleaned with MnO<sub>2</sub>, or with NH<sub>4</sub>OH (29% Laporte™), and acidified with HCl (20 %, trace metal grade, Fisher Scientific) to quantify the pH impact on the catalysis of the FeNN<sub>3</sub> reduction peak (Figure 3.6a). pH was controlled by direct measurement through immersion of the pH sensor in the sample. Absence of contamination through the immersion of the pH sensor was checked by reversibility



of the acidification/alkalinisation, and by acquisition of voltammogram between pH control without acid/alkaline addition.

The deoxygenated UV-seawater buffered with POPSO (10 mmol.L<sup>-1</sup>) showed minimum value of 3 nA at pH 7.5 and maximum of 5 nA at pH 8.8 (Figure 3.6a), slightly decreasing at higher pH as shown for DHN by Laglera et al. (2016). Unlike these authors, we did not observe an increase in the half width of the peak proportional to the peak decrease (Laglera et al., 2016). From 7.7 to 8.2, the FeNN<sub>3</sub> peak was shouldered by the peak of the vanadium complexed by NN. Careful data treatment using ECDSOft (available online at <https://sites.google.com/site/daromasoft>) deconvolution tool attested that the FeNN<sub>3</sub> peak height was not impacted by the presence of the vanadium peak. The FeNN<sub>3</sub> peak potential (Figure 3.6b) varied from -0.44 V at pH 7.5 to -0.49 V at pH 9.0, with a slope of -33 mV/pH units. This linear shift in potential can be due to the variation of the protonation of NN.

The experiments performed in oxygenated conditions with either POPSO and PIPES as buffer (10 mmol.L<sup>-1</sup>) and alkalinised with either NaOH or NH<sub>3</sub> showed minimal peak height between pH 7.5 and 8.0 (Figure 3.6a). From pH 8, the sensitivity increased linearly with pH until reaching its maxima (around 70 nA) at pH 9.0. For pH above 9.0, the peak height decreases and the peak widened similarly to the FeDHN reduction peak (Laglera et al., 2016). The fact that this phenomenon is common to DHN and NN implies that the widening of the peak might be due to a variation in the catalytic process and is not specific to the AL used. FeNN<sub>3</sub> peak potential (Figure 3.6b) shows similar shift behaviour for all oxygenated experiment from around -0.50 V at pH 7.5 to around -0.62 V at pH 9.0, with an averaged slope of -90 mV/pH units. The factor 2 between the regression of oxygenated and deoxygenated samples attests to a change of the protonation of NN and to a change in the number of electrons involved in the reduction process, related to the catalytic loop involving O<sub>2</sub> (Walczak et al., 1997).

In contrast to the difference between oxygenated and deoxygenated samples, the potential shift observed as a function of the solution pH is very similar in oxygenated samples buffered with POPSO or PIPES. The pH difference between POPSO and PIPES at similar relative peak height is never more than 0.2. Although POPSO and PIPES do not buffer efficiently in the pH range 8 to 9 (Table 3.2), the natural

buffering capacity of the carbonate system acts a similar way in both solutions, probably explaining why the trends with pH in sensitivity and peak potentials are so similar between these two buffers.

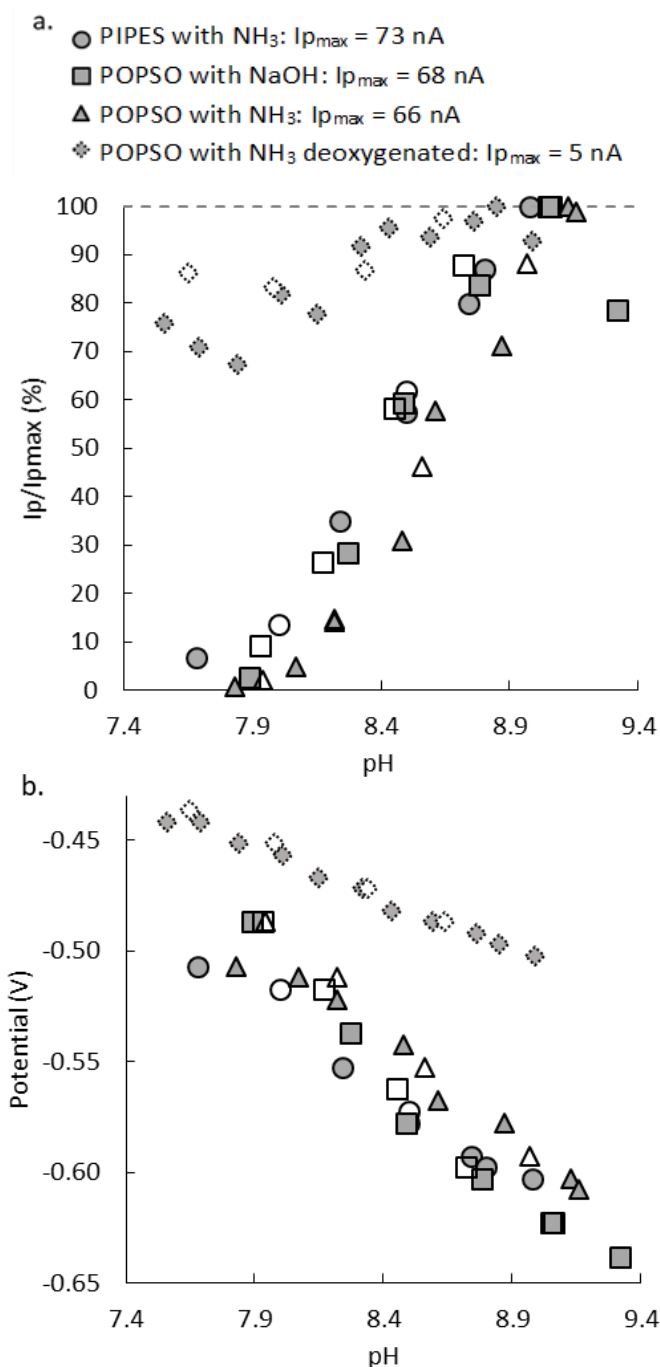


Figure 3.6. a) Relative peak height for each experiment and b) potential of the  $\text{FeNN}_3$  reduction peak in function of the pH successively alkalised (filled symbols) and acidified (empty symbols) in UV-irradiated seawater enriched with  $5 \text{ nmol.L}^{-1}$  Fe for 60 s deposition. The experiment was performed on samples oxygenated and alkalised with  $\text{NH}_3$  while buffered with PIPES (circles) and POPSO (triangles), with  $\text{NaOH}$  with POPSO (squares) and on deoxygenated sample with  $\text{NH}_3$  and POPSO (diamonds).

In the case of the NN-Air method, the Fenton reaction driving the catalytic reduction of  $\text{FeNN}_3$  complexes at the mercury drop surface is dependent on the pH, therefore, of the proton and hydroxide concentrations present in the diffusion layer. It has been previously shown that in unbuffered sample, the pH of the diffusion layer reaches a value near 9 (Laglera et al., 2016), corresponding to the optimal sensitivity of the NN-Air method. Therefore, the optimal application of the NN-Air method corresponds to unbuffered conditions, and which has been shown to be suitable for the investigation of Fe organic speciation using the artificial ligand DHN (Sanvito and Monticelli, 2020). As the pH of the sample is thought to not be impacted by the processes at play in the diffusion layer of the working electrode (Laglera et al., 2016; Sanvito and Monticelli, 2020), and that the NN-Air method in unbuffered conditions and oxygenated results in a more than 10-fold increase in sensitivity compared to the initial buffered and deoxygenated NN method, the NN-Air method seems suitable to investigate the impact of natural pH gradient and ocean acidification on Fe organic speciation.

### **3.3.7. The NN-Air limitation: peak height vs deposition time**

Standard additions of DFe were performed in oxygenated and deoxygenated UV-irradiated seawater containing  $20 \mu\text{mol.L}^{-1}$  of NN and unbuffered, and the  $\text{FeNN}_3$  peak height was measured in triplicate at different deposition times before each Fe addition (Figure 3.7). Two scans were recorded for each deposition time and each DFe addition. Linear regression was used to defined the initial DFe concentration (intersection of the horizontal axis) and the sensitivity (slope of the regression). For a peak corresponding to a single reduction process, the sensitivity is supposed to be proportional to the deposition time, and the DFe concentration should remain constant. In the deoxygenated sample (Figure 3.7a), the sensitivity was proportional to the deposition time, provided similar DFe concentration ranging from  $1.39 \text{ nmol.L}^{-1}$  to  $1.65 \text{ nmol.L}^{-1}$  (standard deviation ( $\sigma$ ) =  $0.13 \text{ nmol.L}^{-1}$ ,  $n = 4$ ) and similar normalised sensitivity ranging from  $0.40 \text{ nA}/(\text{nmol.L}^{-1}.\text{min})$  to  $0.51 \text{ nA}/(\text{nmol.L}^{-1}.\text{min})$  ( $\sigma = 0.05 \text{ nA}/(\text{nmol.L}^{-1}.\text{min})$ ,  $n = 4$ ). In the oxygenated samples, DFe increased with the deposition time applied, ranging from  $1.45 \text{ nmol.L}^{-1}$  with 30 s deposition to  $3.27 \text{ nmol.L}^{-1}$  with 180 s deposition. The sensitivity normalised to the deposition time was relatively stable, ranging from  $5.39 \text{ nA}/(\text{nmol.L}^{-1}.\text{min})$  to  $7.18 \text{ nA}/(\text{nmol.L}^{-1}.\text{min})$  ( $\sigma = 0.37 \text{ nA}/(\text{nmol.L}^{-1}.\text{min})$ ,  $n = 4$ ). The consistency of the sensitivity values attests

that the DFe overestimation was dependent of an issue with the initial peak not proportionally increasing with the deposition time.

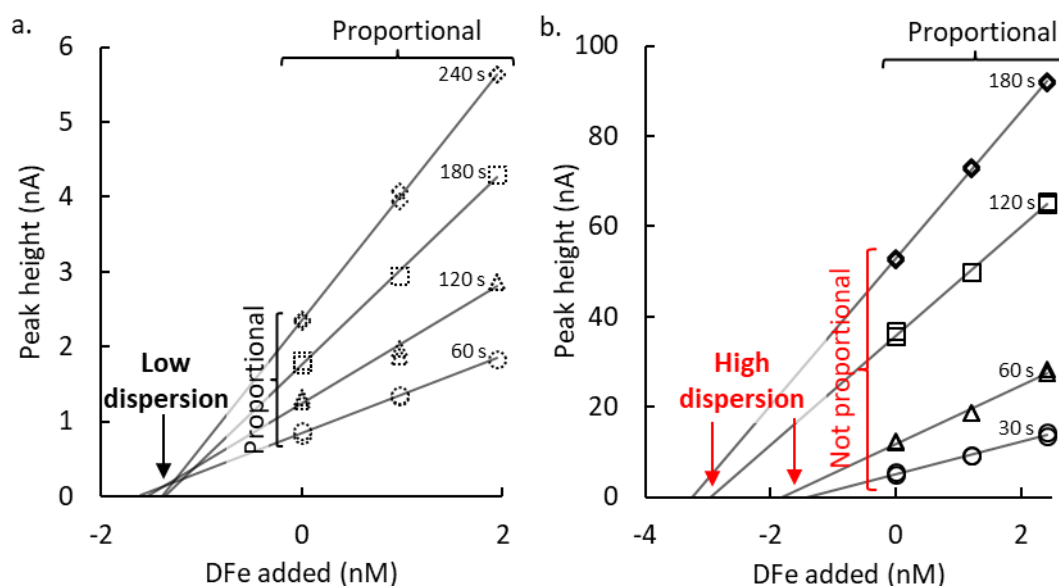


Figure 3.7. FeNN<sub>3</sub> reduction peak height in function of the DFe added in UV-irradiated seawater containing 20  $\mu\text{mol.L}^{-1}$  of NN and unbuffered to evaluate the proportionality of the reduction signal with the deposition time applied in a) a deoxygenated sample, and b) an oxygenated sample. Three scans were recorded for each deposition time and DFe addition, and the two closest retained.

Our results suggest that another element is being reduced at the same potential that the FeNN<sub>3</sub> complex. The seawater sample was UV-irradiated, meaning there was no dissolved organic matter in the sample (except for the added NN). The experiment has been reproduced in unbuffered UV-irradiated seawater, as well as in diluted CRM NASS-6 in Milli-Q, and with different NN available in the laboratory. All tests showed the same DFe overestimation with deposition time. The presence of an interfering organic compound as observed in natural seawater sampled in the Southern Ocean (Boye et al., 2001) or the specific implication of humic substances as suggested with other ALs (i.e. Buck et al., 2018; Laglera et al., 2011) was unlikely as it was observed in Milli-Q and UV-irradiated seawater. Moreover, such interfering organic compounds are usually observable on the voltammograms, while in our case the peak attributed to FeNN<sub>3</sub> was not showing any shouldering. Therefore, the overestimation of DFe with the deposition time in oxygenated samples was attributed to the catalytic enhancement of the reduction of another trace metal, which, unfortunately, could not be identified. However, the test presented here can be easily reproduced by other laboratories to verify the applicability of the methodology detailed in this work.

### **3.3.8. Suggestions for future work investigating the impact of pH on Fe organic speciation**

The need for quantifying the impact of ocean acidification on Fe organic speciation is indubitable to predict ocean primary production and carbon storage in the future. On the same level of interest, the influence of natural pH gradient is yet to be determined in deep waters and oxygen minimum zones at their *in-situ* pH values, lower than surface waters at which samples are classically buffered at. The use of NN in oxygenated conditions and not spiked with an added buffer is suggesting a way to answer these critical questions on Fe organic speciation. If the absence of overestimation of the initial peak in oxygenated conditions is confirmed by performing a similar experiment as in Section 3.3.7, the pH of the sample could be controlled by the CO<sub>2</sub> dissolved in the sample. This was already suggested for the AL DHN. However, specific care must be taken to ensure pH stability during the equilibration and analysis of the sample.

Regarding the analysis of the sample, previous works showed that the change of pH at the working electrode during the acquisition of the voltammogram (about 9; Laglera et al., 2016) is not impacting the result obtained on ligand titration using the AL DHN (Sanvito and Monticelli, 2021). This is because a limited amount of sample is concerned by the pH change happening in the diffusion layer of the working electrode (from a few  $\mu\text{m}$  to nm around the electrode; Laglera et al., 2016), and for a limited amount of time compared to the overnight equilibration of the sample (the time required to record the scan is around 20 s in our case). Despite the encouraging results obtained for DHN, the similarity of the values obtained by titration of the ligands with and without an added buffer must to be verified to validate the NN-Air method.

The regulation of the pH through the amount of CO<sub>2</sub> dissolved in the sample requires the control of the atmospheric CO<sub>2</sub> pressure (pCO<sub>2</sub>) during the equilibration of the sample. To do so, we suggest to isolate the aliquots in a chamber fed with compressed air and CO<sub>2</sub>. The pH should be checked before and after equilibration, and we suggest to place an extra aliquot of the sample in the chamber for this purpose, to not risk the contamination of an aliquot used for the CLE-ACSV titration. Preliminary work should

focus in comparing results obtained at pH values such as 7.0 in as a worst-case scenario of ocean acidification, 7.5 as in OMZ, 7.8 as in bottom waters, and 8.1 as in surface waters.

### **3.4. Conclusion**

In this study, several ways to improve the investigation of the DFe speciation by ACSV using the AL NN have been explored. We presented a novel way to calibrate the NN solution prepared in Milli-Q using its optical properties, and a voltammetric set up allowing the use of volumes of sample as low as 0.5 mL. Despite the limitation experienced in terms of overestimation of the DFe concentration with the deposition time, the catalytic enhancement of the FeNN<sub>3</sub> reduction current by the presence of O<sub>2</sub> in the sample has been shown as a potential way to enhance the sensitivity of the method by at least 10-fold. The NN-Air method may be of critical interest to investigate the impact of pH on the organic speciation of Fe, which so far suffered from the limited sensitivity of the method (Avendaño et al., 2016; Gledhill et al., 2015). This application could also ease the investigation of samples showing higher iron-binding ligand concentration than DFe concentrations requiring the use of reverse titration (Hawkes et al., 2013a). However, further work must focus on clarifying the issue related to the overestimation of the FeNN<sub>3</sub> reduction peak with the deposition time that has been attributed to the catalytic reduction of an interfering metal. The tests performed in this study can be easily reproduced in other work to attest of the validity of the application of the NN-Air method, potentially allowing to explore the impact of pH on organic speciation of Fe by controlling the pCO<sub>2</sub> pressure of the sample. The application of such methodology would provide results of better comparability to previous investigation of the impact of ocean acidification already performed under controlled pCO<sub>2</sub> (e.g. Hoffmann et al., 2013; Shi et al., 2010) and would help projecting the impact of ocean acidification on marine ecosystems (Hoffmann et al., 2012).

### 3.5. References

- Abualhaija, M.M., van den Berg, C.M.G., 2014. Chemical speciation of iron in seawater using catalytic cathodic stripping voltammetry with ligand competition against salicylaldehyde. *Mar. Chem.* 164, 60–74. <https://doi.org/10.1016/j.marchem.2014.06.005>
- Abualhaija, M.M., Whitby, H., van den Berg, C.M.G., 2015. Competition between copper and iron for humic ligands in estuarine waters. *Mar. Chem.* 172, 46–56. <https://doi.org/10.1016/j.marchem.2014.06.00510.1016/j.marchem.2015.03.010>
- Aldrich, A.P., van den Berg, C.M.G., 1998. Determination of Iron and Its Redox Speciation in Seawater Using Catalytic Cathodic Stripping Voltammetry. *Electroanalysis* 10, 369–373. [https://doi.org/10.1002/\(SICI\)1521-4109\(199805\)10:6<369::AID-ELAN369>3.0.CO;2-W](https://doi.org/10.1002/(SICI)1521-4109(199805)10:6<369::AID-ELAN369>3.0.CO;2-W)
- Altmann, R.S., Buffle, J., 1988. The use of differential equilibrium functions for interpretation of metal binding in complex ligand systems: Its relation to site occupation and site affinity distributions. *Geochim. Cosmochim. Acta* 52, 1505–1519. [https://doi.org/10.1016/0016-7037\(88\)90221-9](https://doi.org/10.1016/0016-7037(88)90221-9)
- Amin, S.A., Green, D.H., Gärdes, A., Romano, A., Trimble, L., Carrano, C.J., 2012. Siderophore-mediated iron uptake in two clades of *Marinobacter* spp. associated with phytoplankton: the role of light. *BioMetals* 25, 181–192. <https://doi.org/10.1007/s10534-011-9495-5>
- Amin, S.A., Green, D.H., Hart, M.C., Küpper, F.C., Sunda, W.G., Carrano, C.J., 2009. Photolysis of iron–siderophore chelates promotes bacterial–algal mutualism. *Proc. Natl. Acad. Sci.* 106, 17071–17076. <https://doi.org/10.1073/pnas.0905512106>
- Apte, S.C., Gardner, M.J., Ravenscroft, J.E., 1988. An evaluation of voltammetric titration procedures for the determination of trace metal complexation in natural waters by use of computers simulation. *Anal. Chim. Acta* 212, 1–21. [https://doi.org/10.1016/S0003-2670\(00\)84124-0](https://doi.org/10.1016/S0003-2670(00)84124-0)
- Ardiningsih, I., Zhu, K., Lodeiro, P., Gledhill, M., Reichart, G.-J., Achterberg, E.P., Middag, R., Gerringa, L.J.A., 2021. Iron Speciation in Fram Strait and Over the Northeast Greenland Shelf: An Inter-Comparison Study of Voltammetric Methods. *Front. Mar. Sci.* 7. <https://doi.org/10.3389/fmars.2020.609379>
- Avendaño, L., Gledhill, M., Achterberg, E.P., Rérolle, V.M.C., Schlosser, C., 2016. Influence of Ocean Acidification on the Organic Complexation of Iron and Copper in Northwest European Shelf Seas; a Combined Observational and Model Study. *Front. Mar. Sci.* 3. <https://doi.org/10.3389/fmars.2016.00058>
- Barbeau, K., Rue, E.L., Bruland, K.W., Butler, A., 2001. Photochemical cycling of iron in the surface ocean mediated by microbial iron(III)-binding ligands. *Nature* 413, 409–413. <https://doi.org/10.1038/35096545>
- Bar-On, Y.M., Phillips, R., Milo, R., 2018. The biomass distribution on Earth. *Proc. Natl. Acad. Sci.* 115, 6506–6511. <https://doi.org/10.1073/pnas.1711842115>
- Benner, R., Pakulski, J.D., Mccarthy, M., Hedges, J.I., Hatcher, P.G., 1992. Bulk Chemical Characteristics of Dissolved Organic Matter in the Ocean. *Science* 255, 1561–1564. <https://doi.org/10.1126/science.255.5051.1561>
- Bertrand, E.M., Saito, M.A., Rose, J.M., Riesselman, C.R., Lohan, M.C., Noble, A.E., Lee, P.A., DiTullio, G.R., 2007. Vitamin B12 and iron colimitation of phytoplankton growth in the Ross Sea. *Limnol. Oceanogr.* 52, 1079–1093. <https://doi.org/10.4319/lo.2007.52.3.1079>
- Blazevic, A., Orłowska, E., Kandioller, W., Jirsa, F., Keppler, B.K., Tafili-Kryeziu, M., Linert, W., Krachler, R.F., Krachler, R., Rompel, A., 2016. Photoreduction of Terrigenous Fe-Humic Substances Leads to Bioavailable Iron in Oceans. *Angew. Chem. Int. Ed.* 55, 6417–6422. <https://doi.org/10.1002/anie.201600852>
- Boiteau, R.M., Mende, D.R., Hawco, N.J., McIlvin, M.R., Fitzsimmons, J.N., Saito, M.A., Sedwick, P.N., DeLong, E.F., Repeta, D.J., 2016. Siderophore-based microbial adaptations to iron scarcity across the eastern Pacific Ocean. *Proc. Natl. Acad. Sci.* 113, 14237–14242. <https://doi.org/10/f9fvs4>

- Bondietti, G., Sinniger, J., Stumm, W., 1993. The reactivity of FE(III) (hydr)oxides: Effects of ligands in inhibiting the dissolution. *Colloids Surf. Physicochem. Eng. Asp.* 79, 157–167. [https://doi.org/10.1016/0927-7757\(93\)80171-A](https://doi.org/10.1016/0927-7757(93)80171-A)
- Boyd, P.W., Ibsanmi, E., Sander, S.G., Hunter, K.A., Jackson, G.A., 2010. Remineralization of upper ocean particles: Implications for iron biogeochemistry. *Limnol. Oceanogr.* 55, 1271–1288. <https://doi.org/10.4319/lo.2010.55.3.1271>
- Boye, M., van den Berg, C.M.G., de Jong, J.T.M., Leach, H., Croot, P., de Baar, H.J.W., 2001. Organic complexation of iron in the Southern Ocean. *Deep Sea Res. Part Oceanogr. Res. Pap.* 48, 1477–1497. [https://doi.org/10.1016/S0967-0637\(00\)00099-6](https://doi.org/10.1016/S0967-0637(00)00099-6)
- Browning, T.J., Achterberg, E.P., Engel, A., Mawji, E., 2021. Manganese co-limitation of phytoplankton growth and major nutrient drawdown in the Southern Ocean. *Nat. Commun.* 12, 884. <https://doi.org/10.1038/s41467-021-21122-6>
- Buck, K.N., Lohan, M.C., Berger, C.J.M., Bruland, K.W., 2007. Dissolved iron speciation in two distinct river plumes and an estuary: Implications for riverine iron supply. *Limnol. Oceanogr.* 52, 843–855. <https://doi.org/10.4319/lo.2007.52.2.0843>
- Buck, K.N., Moffett, J., Barbeau, K.A., Bundy, R.M., Kondo, Y., Wu, J., 2012. The organic complexation of iron and copper: an intercomparison of competitive ligand exchange-adsorptive cathodic stripping voltammetry (CLE-ACSV) techniques. *Limnol. Oceanogr. Methods* 10, 496–515. <https://doi.org/10.4319/lom.2012.10.496>
- Buck, K.N., Sedwick, P.N., Sohst, B., Carlson, C.A., 2018. Organic complexation of iron in the eastern tropical South Pacific: Results from US GEOTRACES Eastern Pacific Zonal Transect (GEOTRACES cruise GP16). *Mar. Chem., The U.S. GEOTRACES Eastern Tropical Pacific Transect (GP16)* 201, 229–241. <https://doi.org/10.1016/j.marchem.2017.11.007>
- Buck, K.N., Sohst, B., Sedwick, P.N., 2015. The organic complexation of dissolved iron along the U.S. GEOTRACES (GA03) North Atlantic Section. *Deep Sea Res. Part II Top. Stud. Oceanogr.* 116, 152–165. <https://doi.org/10.1016/j.dsr2.2014.11.016>
- Buma, A.G.J., de Baar, H.J.W., Nolting, R.F., van Bennekom, A.J., 1991. Metal enrichment experiments in the Weddell-Scotia Seas: Effects of iron and manganese on various plankton communities. *Limnol. Oceanogr.* 36, 1865–1878. <https://doi.org/10.4319/lo.1991.36.8.1865>
- Bundy, R.M., Biller, D.V., Buck, K.N., Bruland, K.W., Barbeau, K.A., 2014. Distinct pools of dissolved iron-binding ligands in the surface and benthic boundary layer of the California Current. *Limnol. Oceanogr.* 59, 769–787. <https://doi.org/10.4319/lo.2014.59.3.0769>
- Bundy, R.M., Boiteau, R.M., McLean, C., Turk-Kubo, K.A., McIlvin, M.R., Saito, M.A., Van Mooy, B.A.S., Repeta, D.J., 2018. Distinct Siderophores Contribute to Iron Cycling in the Mesopelagic at Station ALOHA. *Front. Mar. Sci.* 5. <https://doi.org/10.3389/fmars.2018.00061>
- Burgess, J., Twigg, M.V., 2006. Iron: Inorganic & Coordination Chemistry Based in part on the article Iron: Inorganic & Coordination Chemistry by Pelham N. Hawker & Martyn V. Twigg which appeared in the Encyclopedia of Inorganic Chemistry, First Edition., in: *Encyclopedia of Inorganic Chemistry*. John Wiley & Sons, Ltd. <https://doi.org/10.1002/0470862106.ia108>
- Caprara, S., Buck, K.N., Gerringa, L.J.A., Rijkenberg, M.J.A., Monticelli, D., 2016. A Compilation of Iron Speciation Data for Open Oceanic Waters. *Front. Mar. Sci.* 3. <https://doi.org/10.3389/fmars.2016.00221>
- Caprara, S., Laglera, L.M., Monticelli, D., 2015. Ultrasensitive and Fast Voltammetric Determination of Iron in Seawater by Atmospheric Oxygen Catalysis in 500  $\mu$ L Samples. *Anal. Chem.* 87, 6357–6363. <https://doi.org/10.1021/acs.analchem.5b01239>
- Cheize, M., Planquette, H.F., Fitzsimmons, J.N., Pelleter, E., Sherrell, R.M., Lambert, C., Bucciarelli, E., Sarthou, G., Le Goff, M., Liorzou, C., Chéron, S., Viollier, E., Gayet, N., 2019. Contribution of resuspended sedimentary particles to dissolved iron and manganese in the ocean: An experimental study. *Chem. Geol.* 511, 389–415. <https://doi.org/10.1016/j.chemgeo.2018.10.003>



- Cheize, M., Sarthou, G., Croot, P.L., Bucciarelli, E., Baudoux, A.-C., Baker, A.R., 2012. Iron organic speciation determination in rainwater using cathodic stripping voltammetry. *Anal. Chim. Acta* 736, 45–54. <https://doi.org/10.1016/j.aca.2012.05.011>
- Chen, M., Wang, W.-X., 2001. Bioavailability of natural colloid-bound iron to marine plankton: Influences of colloidal size and aging. *Limnol. Oceanogr.* 46, 1956–1967. <https://doi.org/10.4319/lo.2001.46.8.1956>
- Chisholm, S.W., Morel, F.M., 1991. *Limnology and Oceanography*, Volume 36, Number 8, December 1991. What Controls Phytoplankton Production in Nutrient-Rich Areas of the Open Sea?
- Cloete, R., Loock, J.C., van Horsten, N.R., Menzel Barraqueta, J.-L., Fietz, S., Mtshali, T.N., Planquette, H., García-Ibáñez, M.I., Roychoudhury, A.N., 2021. Winter dissolved and particulate zinc in the Indian Sector of the Southern Ocean: Distribution and relation to major nutrients (GEOTRACES G1pr07 transect). *Mar. Chem.* 236, 104031. <https://doi.org/10.1016/j.marchem.2021.104031>
- Coale, K., 1991. Effects of Iron, Manganese, Copper, and Zinc Enrichments on Productivity and Biomass in the Sub-Arctic Pacific. *Limnol. Oceanogr.* 36, 1851–1864. <https://doi.org/10.4319/lo.1991.36.8.1851>
- Cotton, S.A., 1972. Some aspects of the coordination chemistry of iron(III). *Coord. Chem. Rev.* 8, 185–223. [https://doi.org/10.1016/S0010-8545\(00\)80028-4](https://doi.org/10.1016/S0010-8545(00)80028-4)
- Croot, P.L., Andersson, K., Öztürk, M., Turner, D.R., 2004. The distribution and speciation of iron along 6°E in the Southern Ocean. *Deep Sea Res. Part II Top. Stud. Oceanogr., The SWEDARP 1997/98 Expedition 51*, 2857–2879. <https://doi.org/10.1016/j.dsr2.2003.10.012>
- Croot, P.L., Johansson, M., 2000. Determination of Iron Speciation by Cathodic Stripping Voltammetry in Seawater Using the Competing Ligand 2-(2-Thiazolylazo)-p-cresol (TAC). *Electroanalysis* 12, 565–576. [https://doi.org/10.1002/\(SICI\)1521-4109\(200005\)12:8<565::AID-ELAN565>3.0.CO;2-L](https://doi.org/10.1002/(SICI)1521-4109(200005)12:8<565::AID-ELAN565>3.0.CO;2-L)
- Dale, A.W., Nickelsen, L., Scholz, F., Hensen, C., Oschlies, A., Wallmann, K., 2015. A revised global estimate of dissolved iron fluxes from marine sediments. *Glob. Biogeochem. Cycles* 29, 691–707. <https://doi.org/10.1002/2014GB005017>
- de Baar, H.J.W., Boyd, P.W., Coale, K.H., Landry, M.R., Tsuda, A., Assmy, P., Bakker, D.C.E., Bozec, Y., Barber, R.T., Brzezinski, M.A., Buesseler, K.O., Boyé, M., Croot, P.L., Gervais, F., Gorbunov, M.Y., Harrison, P.J., Hiscock, W.T., Laan, P., Lancelot, C., Law, C.S., Levasseur, M., Marchetti, A., Millero, F.J., Nishioka, J., Nojiri, Y., van Oijen, T., Riebesell, U., Rijkenberg, M.J.A., Saito, H., Takeda, S., Timmermans, K.R., Veldhuis, M.J.W., Waite, A.M., Wong, C.-S., 2005. Synthesis of iron fertilization experiments: From the Iron Age in the Age of Enlightenment. *J. Geophys. Res. Oceans* 110. <https://doi.org/10.1029/2004JC002601>
- de Baar, H.J.W., Buma, A.G.J., Nolting, R.F., Cadée, G.C., Jacques, G., Tréguer, P.J., 1990. On iron limitation of the Southern Ocean: experimental observations in the Weddell and Scotia Seas. *Mar. Ecol. Prog. Ser.* 65, 105–122.
- de Baar, H.J.W., van Heuven, S.M.A.C., Abouchami, W., Xue, Z., Galer, S.J.G., Rehkämper, M., Middag, R., van Ooijen, J., 2017. Interactions of dissolved CO<sub>2</sub> with cadmium isotopes in the Southern Ocean. *Mar. Chem., SI: Honoring Frank Millero* 195, 105–121. <https://doi.org/10.1016/j.marchem.2017.06.010>
- Dittmar, T., Lennartz, S.T., Buck-Wiese, H., Hansell, D.A., Santinelli, C., Vanni, C., Blasius, B., Hehemann, J.-H., 2021. Enigmatic persistence of dissolved organic matter in the ocean. *Nat. Rev. Earth Environ.* 2, 570–583. <https://doi.org/10.1038/s43017-021-00183-7>
- Dulaquais, G., Waeles, M., Gerringa, L.J.A., Middag, R., Rijkenberg, M.J.A., Riso, R., 2018. The Biogeochemistry of Electroactive Humic Substances and Its Connection to Iron Chemistry in the North East Atlantic and the Western Mediterranean Sea. *J. Geophys. Res. Oceans* 123, 5481–5499. <https://doi.org/10/gd8db3>
- Fenton, H.J.H., 1894. LXXIII.—Oxidation of tartaric acid in presence of iron. *J. Chem. Soc. Trans.* 65, 899–910. <https://doi.org/10.1039/CT8946500899>

- Field, C.B., Behrenfeld, M.J., Randerson, J.T., Falkowski, P., 1998. Primary Production of the Biosphere: Integrating Terrestrial and Oceanic Components. *Science* 281, 237–240. <https://doi.org/10.1126/science.281.5374.237>
- Findlay, A.J., Estes, E.R., Gartman, A., Yücel, M., Kamyshny, A., Luther, G.W., 2019. Iron and sulfide nanoparticle formation and transport in nascent hydrothermal vent plumes. *Nat. Commun.* 10, 1–7. <https://doi.org/10.1038/s41467-019-09580-5>
- Fitzsimmons, J.N., Bundy, R.M., Al-Subiai, S.N., Barbeau, K.A., Boyle, E.A., 2015. The composition of dissolved iron in the dusty surface ocean: An exploration using size-fractionated iron-binding ligands. *Mar. Chem., SCOR WG 139: Organic Ligands – A Key Control on Trace Metal Biogeochemistry in the Ocean* 173, 125–135. <https://doi.org/10/f7fc99>
- Fourrier, P., Dulaquais, G., Guigue, C., Giamarchi, P., Sarthou, G., Whitby, H., Riso, R., 2022. Characterization of the vertical size distribution, composition and chemical properties of dissolved organic matter in the (ultra)oligotrophic Pacific Ocean through a multi-detection approach. *Mar. Chem.* 240, 104068. <https://doi.org/10.1016/j.marchem.2021.104068>
- Friedlingstein, P., Jones, M.W., O’Sullivan, M., Andrew, R.M., Hauck, J., Peters, G.P., Peters, W., Pongratz, J., Sitch, S., Quéré, C.L., Bakker, D.C.E., Canadell, J.G., Ciais, P., Jackson, R.B., Anthoni, P., Barbero, L., Bastos, A., Bastrikov, V., Becker, M., Bopp, L., Buitenhuis, E., Chandra, N., Chevallier, F., Chini, L.P., Currie, K.I., Feely, R.A., Gehlen, M., Gilfillan, D., Gkritzalis, T., Goll, D.S., Gruber, N., Gutekunst, S., Harris, I., Haverd, V., Houghton, R.A., Hurtt, G., Ilyina, T., Jain, A.K., Joetzjer, E., Kaplan, J.O., Kato, E., Klein Goldewijk, K., Korsbakken, J.I., Landschützer, P., Lauvset, S.K., Lefèvre, N., Lenton, A., Lienert, S., Lombardozzi, D., Marland, G., McGuire, P.C., Melton, J.R., Metzl, N., Munro, D.R., Nabel, J.E.M.S., Nakaoka, S.-I., Neill, C., Omar, A.M., Ono, T., Pregon, A., Pierrot, D., Poulter, B., Rehder, G., Resplandy, L., Robertson, E., Rödenbeck, C., Séférian, R., Schwinger, J., Smith, N., Tans, P.P., Tian, H., Tilbrook, B., Tubiello, F.N., Werf, G.R. van der, Wiltshire, A.J., Zaehle, S., 2019. Global Carbon Budget 2019. *Earth Syst. Sci. Data* 11, 1783–1838. <https://doi.org/10.5194/essd-11-1783-2019>
- Gattuso, J.-P., Magnan, A., Billé, R., Cheung, W.W.L., Howes, E.L., Joos, F., Allemand, D., Bopp, L., Cooley, S.R., Eakin, C.M., Hoegh-Guldberg, O., Kelly, R.P., Pörtner, H.-O., Rogers, A.D., Baxter, J.M., Laffoley, D., Osborn, D., Rankovic, A., Rochette, J., Sumaila, U.R., Treyer, S., Turley, C., 2015. Contrasting futures for ocean and society from different anthropogenic CO<sub>2</sub> emissions scenarios. *Science* 349. <https://doi.org/10.1126/science.aac4722>
- Genovese, C., Grotti, M., Ardini, F., Wuttig, K., Vivado, D., Cabanes, D., Townsend, A., Hassler, C., Lannuzel, D., 2022. Effect of salinity and temperature on the determination of dissolved iron-binding organic ligands in the polar marine environment. *Mar. Chem.* 238, 104051. <https://doi.org/10.1016/j.marchem.2021.104051>
- Genovese, C., Grotti, M., Pittaluga, J., Ardini, F., Janssens, J., Wuttig, K., Moreau, S., Lannuzel, D., 2018. Influence of organic complexation on dissolved iron distribution in East Antarctic pack ice. *Mar. Chem.* 203, 28–37. <https://doi.org/10.1016/j.marchem.2018.04.005>
- Gerringa, L.J.A., Gledhill, M., Ardiningsih, I., Muntjewerf, N., Laglera, L.M., 2021. Comparing CLE-AdCSV applications using SA and TAC to determine the Fe-binding characteristics of model ligands in seawater. *Biogeosciences* 18, 5265–5289. <https://doi.org/10.5194/bg-18-5265-2021>
- Gerringa, L.J.A., Herman, P.M.J., Poortvliet, T.C.W., 1995. Comparison of the linear Van den Berg/Ružić transformation and a non-linear fit of the Langmuir isotherm applied to Cu speciation data in the estuarine environment. *Mar. Chem.* 48, 131–142. [https://doi.org/10.1016/0304-4203\(94\)00041-B](https://doi.org/10.1016/0304-4203(94)00041-B)
- Gerringa, L.J.A., Rijkenberg, M.J.A., Schoemann, V., Laan, P., de Baar, H.J.W., 2015. Organic complexation of iron in the West Atlantic Ocean. *Mar. Chem., Cycles of metals and carbon in the oceans - A tribute to the work stimulated by Hein de Baar* 177, 434–446. <https://doi.org/10.1016/j.marchem.2015.04.007>

- Gerringa, L.J.A., Rijkenberg, M.J.A., Thuróczy, C.-E., Maas, L.R.M., 2014. A critical look at the calculation of the binding characteristics and concentration of iron complexing ligands in seawater with suggested improvements. *Environ. Chem.* 11, 114–136. <https://doi.org/10/f52sbv>
- Gledhill, M., Achterberg, E.P., Li, K., Mohamed, K.N., Rijkenberg, M.J.A., 2015. Influence of ocean acidification on the complexation of iron and copper by organic ligands in estuarine waters. *Mar. Chem., Cycles of metals and carbon in the oceans - A tribute to the work stimulated by Hein de Baar* 177, 421–433. <https://doi.org/10.1016/j.marchem.2015.03.016>
- Gledhill, M., Buck, K.N., 2012. The Organic Complexation of Iron in the Marine Environment: A Review. *Front. Microbiol.* 3. <https://doi.org/10.3389/fmicb.2012.00069>
- Gledhill, M., van den Berg, C.M.G., 1994. Determination of complexation of iron(III) with natural organic complexing ligands in seawater using cathodic stripping voltammetry. *Mar. Chem.* 47, 41–54. [https://doi.org/10.1016/0304-4203\(94\)90012-4](https://doi.org/10.1016/0304-4203(94)90012-4)
- Gupta, B.S., Taha, M., Lee, M.-J., 2013. Stability Constants for the Equilibrium Models of Iron(III) with Several Biological Buffers in Aqueous Solutions. *J. Solut. Chem.* 42, 2296–2309. <https://doi.org/10.1007/s10953-013-0107-6>
- Hassler, C., Cabanes, D., Blanco-Ameijeiras, S., Sander, S.G., Benner, R., Hassler, C., Cabanes, D., Blanco-Ameijeiras, S., Sander, S.G., Benner, R., 2019. Importance of refractory ligands and their photodegradation for iron oceanic inventories and cycling. *Mar. Freshw. Res.* 71, 311–320. <https://doi.org/10.1071/MF19213>
- Hassler, C.S., Berg, V.D., G, C.M., Boyd, P.W., 2017. Toward a Regional Classification to Provide a More Inclusive Examination of the Ocean Biogeochemistry of Iron-Binding Ligands. *Front. Mar. Sci.* 4. <https://doi.org/10.3389/fmars.2017.00019>
- Hassler, C.S., Legiret, F.-E., Butler, E.C.V., 2013. Measurement of iron chemical speciation in seawater at 4°C: The use of competitive ligand exchange–adsorptive cathodic stripping voltammetry. *Mar. Chem.* 149, 63–73. <https://doi.org/10.1016/j.marchem.2012.12.007>
- Hassler, C.S., Norman, L., Mancuso Nichols, C.A., Clementson, L.A., Robinson, C., Schoemann, V., Watson, R.J., Doblin, M.A., 2015. Iron associated with exopolymeric substances is highly bioavailable to oceanic phytoplankton. *Mar. Chem., SCOR WG 139: Organic Ligands – A Key Control on Trace Metal Biogeochemistry in the Ocean* 173, 136–147. <https://doi.org/10.1016/j.marchem.2014.10.002>
- Hawkes, J. A., Connelly, D.P., Gledhill, M., Achterberg, E.P., 2013. The stabilisation and transportation of dissolved iron from high temperature hydrothermal vent systems. *Earth Planet. Sci. Lett.* 375, 280–290. <https://doi.org/10.1016/j.epsl.2013.05.047>
- Hawkes, Jeffrey A., Gledhill, M., Connelly, D.P., Achterberg, E.P., 2013. Characterisation of iron binding ligands in seawater by reverse titration. *Anal. Chim. Acta* 766, 53–60. <https://doi.org/10.1016/j.aca.2012.12.048>
- Hayyan, M., Hashim, M.A., AlNashef, I.M., 2016. Superoxide Ion: Generation and Chemical Implications. *Chem. Rev.* 116, 3029–3085. <https://doi.org/10.1021/acs.chemrev.5b00407>
- Hiemstra, T., van Riemsdijk, W.H., 2006. Biogeochemical speciation of Fe in ocean water. *Mar. Chem.* 102, 181–197. <https://doi.org/10.1016/j.marchem.2006.03.008>
- Ho, P., Lee, J.-M., Heller, M.I., Lam, P.J., Shiller, A.M., 2018. The distribution of dissolved and particulate Mo and V along the U.S. GEOTRACES East Pacific Zonal Transect (GP16): The roles of oxides and biogenic particles in their distributions in the oxygen deficient zone and the hydrothermal plume. *Mar. Chem., The U.S. GEOTRACES Eastern Tropical Pacific Transect (GP16)* 201, 242–255. <https://doi.org/10.1016/j.marchem.2017.12.003>
- Hoffmann, L.J., Breitbarth, E., Boyd, P.W., Hunter, K.A., 2012. Influence of ocean warming and acidification on trace metal biogeochemistry. *Mar. Ecol. Prog. Ser.* 470, 191–205. <https://doi.org/10.3354/meps10082>
- Hogle, S.L., Hackl, T., Bundy, R.M., Park, J., Satinsky, B., Satinsky, B., Hiltunen, T., Biller, S., Berube, P.M., Chisholm, S.W., 2021. Siderophores as an iron source for *Prochlorococcus* in deep

- chlorophyll maximum layers of the oligotrophic ocean.  
<https://doi.org/10.1101/2021.11.13.468467>
- Hopkinson, B.M., Morel, F.M.M., 2009. The role of siderophores in iron acquisition by photosynthetic marine microorganisms. *BioMetals* 22, 659–669. <https://doi.org/10.1007/s10534-009-9235-2>
- Hoppe, C.J.M., Hassler, C.S., Payne, C.D., Tortell, P.D., Rost, B., Trimborn, S., 2013. Iron Limitation Modulates Ocean Acidification Effects on Southern Ocean Phytoplankton Communities. *PLoS ONE* 8. <https://doi.org/10.1371/journal.pone.0079890>
- Hopwood, M.J., Carroll, D., Höfer, J., Achterberg, E.P., Meire, L., Le Moigne, F.A.C., Bach, L.T., Eich, C., Sutherland, D.A., González, H.E., 2019. Highly variable iron content modulates iceberg-ocean fertilisation and potential carbon export. *Nat. Commun.* 10, 1–10. <https://doi.org/10.1038/s41467-019-13231-0>
- Hunter, K.A., 2005. Comment on ‘Measuring Marine Iron(III) Complexes by CLE-AdSV.’ *Environ. Chem.* 2, 85–87. <https://doi.org/10.1071/EN05030>
- Hutchins, D.A., Boyd, P.W., 2016. Marine phytoplankton and the changing ocean iron cycle. *Nat. Clim. Change* 6, 1072–1079. <https://doi.org/10.1038/nclimate3147>
- Ingall, E.D., Diaz, J.M., Longo, A.F., Oakes, M., Finney, L., Vogt, S., Lai, B., Yager, P.L., Twining, B.S., Brandes, J.A., 2013. Role of biogenic silica in the removal of iron from the Antarctic seas. *Nat. Commun.* 4, 1981. <https://doi.org/10.1038/ncomms2981>
- Janssens, J., Meiners, K.M., Townsend, A.T., Lannuzel, D., 2018. Organic Matter Controls of Iron Incorporation in Growing Sea Ice. *Front. Earth Sci.* 6.
- Johnson, K.S., Gordon, R.M., Coale, K.H., 1997. What controls dissolved iron concentrations in the world ocean? *Mar. Chem.* 57, 137–161. [https://doi.org/10.1016/S0304-4203\(97\)00043-1](https://doi.org/10.1016/S0304-4203(97)00043-1)
- Kleint, C., Hawkes, J.A., Sander, S.G., Koschinsky, A., 2016. Voltammetric Investigation of Hydrothermal Iron Speciation. *Front. Mar. Sci.* 3, UNSP 75. <https://doi.org/10.3389/fmars.2016.00075>
- Krachler, R., Krachler, R.F., Wallner, G., Hann, S., Laux, M., Cervantes Recalde, M.F., Jirsa, F., Neubauer, E., von der Kammer, F., Hofmann, T., Keppler, B.K., 2015. River-derived humic substances as iron chelators in seawater. *Mar. Chem.* 174, 85–93. <https://doi.org/10.1016/j.marchem.2015.05.009>
- Kuma, K., Nishioka, J., Matsunaga, K., 1996. Controls on iron(III) hydroxide solubility in seawater: The influence of pH and natural organic chelators. *Limnol. Oceanogr.* 41, 396–407. <https://doi.org/10.4319/lo.1996.41.3.0396>
- Laglera, L.M., Battaglia, G., van den Berg, C.M.G., 2011. Effect of humic substances on the iron speciation in natural waters by CLE/CSV. *Mar. Chem.* 127, 134–143. <https://doi.org/10.1016/j.marchem.2011.09.003>
- Laglera, L.M., Battaglia, G., van den Berg, C.M.G., 2007. Determination of humic substances in natural waters by cathodic stripping voltammetry of their complexes with iron. *Anal. Chim. Acta* 599, 58–66. <https://doi.org/10.1016/j.aca.2007.07.059>
- Laglera, L.M., Caprara, S., Monticelli, D., 2016. Towards a zero-blank, preconcentration-free voltammetric method for iron analysis at picomolar concentrations in unbuffered seawater. *Talanta* 150, 449–454. <https://doi.org/10.1016/j.talanta.2015.12.060>
- Laglera, L.M., Monticelli, D., 2017. Iron detection and speciation in natural waters by electrochemical techniques: A critical review. *Curr. Opin. Electrochem.* 3, 123–129. <https://doi.org/10.1016/j.coelec.2017.07.007>
- Laglera, L.M., Tovar-Sanchez, A., Sukekava, C.F., Naik, H., Naqvi, S.W.A., Wolf-Gladrow, D.A., 2019. Iron organic speciation during the LOHAFEX experiment: Iron ligands release under biomass control by copepod grazing. *J. Mar. Syst.* 103151. <https://doi.org/10.1016/j.jmarsys.2019.02.002>
- Langmuir, I., 1916. THE CONSTITUTION AND FUNDAMENTAL PROPERTIES OF SOLIDS AND LIQUIDS. PART I. SOLIDS. *J. Am. Chem. Soc.* 38, 2221–2295. <https://doi.org/10.1021/ja02268a002>

- Lannuzel, D., Vancoppenolle, M., van der Merwe, P., de Jong, J., Meiners, K.M., Grotti, M., Nishioka, J., Schoemann, V., 2016. Iron in sea ice: Review and new insights. *Elem. Sci. Anthr.* 4, 000130. <https://doi.org/10.12952/journal.elementa.000130>
- Lis, H., Shaked, Y., Kranzler, C., Keren, N., Morel, F.M.M., 2015. Iron bioavailability to phytoplankton: an empirical approach. *ISME J.* 9, 1003–1013. <https://doi.org/10.1038/ismej.2014.199>
- Liu, X., Millero, F.J., 2002. The solubility of iron in seawater. *Mar. Chem.* 77, 43–54. [https://doi.org/10.1016/S0304-4203\(01\)00074-3](https://doi.org/10.1016/S0304-4203(01)00074-3)
- Lodeiro, P., Rey-Castro, C., David, C., Achterberg, E.P., Puy, J., Gledhill, M., 2020. Acid-base properties of dissolved organic matter extracted from the marine environment. *Sci. Total Environ.* 729, 138437. <https://doi.org/10.1016/j.scitotenv.2020.138437>
- Lohan, M.C., Aguilar-Islas, A.M., Bruland, K.W., 2006. Direct determination of iron in acidified (pH 1.7) seawater samples by flow injection analysis with catalytic spectrophotometric detection: Application and intercomparison. *Limnol. Oceanogr. Methods* 4, 164–171. <https://doi.org/10.4319/lom.2006.4.164>
- Longhini, C.M., Mahieu, L., Sá, F., van den Berg, C.M.G., Salaün, P., Neto, R.R., 2021. Coastal waters contamination by mining tailings: What triggers the stability of iron in the dissolved and soluble fractions? *Limnol. Oceanogr.* 66, 171–187. <https://doi.org/10.1002/lno.11595>
- Louis, Y., Garnier, C., Lenoble, V., Omanović, D., Mounier, S., Pižeta, I., 2009. Characterisation and modelling of marine dissolved organic matter interactions with major and trace cations. *Mar. Environ. Res.* 67, 100–107. <https://doi.org/10.1016/j.marenvres.2008.12.002>
- Mahmood, A., Abualhaija, M.M., van den Berg, C.M.G., Sander, S.G., 2015. Organic speciation of dissolved iron in estuarine and coastal waters at multiple analytical windows. *Mar. Chem.* 177, 706–719. <https://doi.org/10.1016/j.marchem.2015.11.001>
- Mahowald, N., Engelstaedter, S., Luo, C., Sealy, A., Artaxo, P., Benitez-Nelson, C., Bonnet, S., Chen, Y., Chuang, P., Cohen, D., Dulac, F., Herut, B., Johansen, A., Kubilay, N., Losno, R., Maenhaut, W., Paytan, A., Prospero, J., Shank, L., Siefert, R., 2009. Atmospheric Iron Deposition: Global Distribution, Variability, and Human Perturbations. *Annu. Rev. Mar. Sci.* 1. <https://doi.org/10.1146/annurev.marine.010908.163727>
- Martin, J.H., Fitzwater, S.E., 1988. Iron deficiency limits phytoplankton growth in the north-east Pacific subarctic. *Nature* 331, 341–343. <https://doi.org/10.1038/331341a0>
- Martin, J.H., Fitzwater, S.E., Gordon, R.M., 1990. Iron deficiency limits phytoplankton growth in Antarctic waters. *Glob. Biogeochem. Cycles* 4, 5–12. <https://doi.org/10.1029/GB004i001p00005>
- Martin, J.H., Gordon, R.M., Fitzwater, S., Broenkow, W.W., 1989. Vertex: phytoplankton/iron studies in the Gulf of Alaska. *Deep Sea Res. Part Oceanogr. Res. Pap.* 36, 649–680. [https://doi.org/10.1016/0198-0149\(89\)90144-1](https://doi.org/10.1016/0198-0149(89)90144-1)
- McQuaid, J.B., Kustka, A.B., Oborník, M., Horák, A., McCrow, J.P., Karas, B.J., Zheng, H., Kindeberg, T., Andersson, A.J., Barbeau, K.A., Allen, A.E., 2018. Carbonate-sensitive phytotransferrin controls high-affinity iron uptake in diatoms. *Nature* 555, 534–537. <https://doi.org/10.1038/nature25982>
- Mentges, A., Feenders, C., Seibt, M., Blasius, B., Dittmar, T., 2017. Functional Molecular Diversity of Marine Dissolved Organic Matter Is Reduced during Degradation. *Front. Mar. Sci.* 4. <https://doi.org/10.3389/fmars.2017.00194>
- Millero, F., 2001. Speciation of metals in natural waters. *Geochem. Trans.* 2, 56–64. <https://doi.org/10.1039/B104809K>
- Millero, F.J., Woosley, R., Ditrolio, B., Waters, J., 2009. Effect of Ocean Acidification on the Speciation of Metals in Seawater. *Oceanography* 22, 72–85. <https://doi.org/10.5670/oceanog.2009.98>

- Mills, M.M., Ridame, C., Davey, M., La Roche, J., Geider, R.J., 2004. Iron and phosphorus co-limit nitrogen fixation in the eastern tropical North Atlantic. *Nature* 429, 292–294. <https://doi.org/10.1038/nature02550>
- Mohamed, K.N., Steigenberger, S., Nielsdottir, M.C., Gledhill, M., Achterberg, E.P., 2011. Dissolved iron(III) speciation in the high latitude North Atlantic Ocean. *Deep Sea Res. Part Oceanogr. Res. Pap.* 58, 1049–1059. <https://doi.org/10.1016/j.dsr.2011.08.011>
- Moore, C.M., Mills, M.M., Arrigo, K.R., Berman-Frank, I., Bopp, L., Boyd, P.W., Galbraith, E.D., Geider, R.J., Guieu, C., Jaccard, S.L., Jickells, T.D., La Roche, J., Lenton, T.M., Mahowald, N.M., Marañón, E., Marinov, I., Moore, J.K., Nakatsuka, T., Oschlies, A., Saito, M.A., Thingstad, T.F., Tsuda, A., Ulloa, O., 2013. Processes and patterns of oceanic nutrient limitation. *Nat. Geosci.* 6, 701–710. <https://www.nature.com/articles/ngeo1765>
- Morel, F.M.M., Kustka, A.B., Shaked, Y., 2008. The role of unchelated Fe in the iron nutrition of phytoplankton. *Limnol. Oceanogr.* 53, 400–404. <https://doi.org/10.4319/lo.2008.53.1.0400>
- Morel, F.M.M., Price, N.M., 2003. The Biogeochemical Cycles of Trace Metals in the Oceans. *Science* 300, 944–947. <https://doi.org/10.1126/science.1083545>
- Nagai, T., Imai, A., Matsushige, K., Yokoi, K., Fukushima, T., 2004. Voltammetric determination of dissolved iron and its speciation in freshwater. *Limnology* 5, 87–94. <https://doi.org/10.1007/s10201-004-0121-x>
- Nichols, C.M., Lardière, S.G., Bowman, J.P., Nichols, P.D., A E Gibson, J., Guézennec, J., 2005. Chemical characterization of exopolysaccharides from Antarctic marine bacteria. *Microb. Ecol.* 49, 578–589. <https://doi.org/10.1007/s00248-004-0093-8>
- Nolting, R.F., Gerringa, L.J.A., Swagerman, M.J.W., Timmermans, K.R., de Baar, H.J.W., 1998. Fe (III) speciation in the high nutrient, low chlorophyll Pacific region of the Southern Ocean. *Mar. Chem.* 62, 335–352. [https://doi.org/10.1016/S0304-4203\(98\)00046-2](https://doi.org/10.1016/S0304-4203(98)00046-2)
- Norman, L., Worms, I.A.M., Angles, E., Bowie, A.R., Nichols, C.M., Ninh Pham, A., Slaveykova, V.I., Townsend, A.T., David Waite, T., Hassler, C.S., 2015. The role of bacterial and algal exopolymeric substances in iron chemistry. *Mar. Chem., SCOR WG 139: Organic Ligands – A Key Control on Trace Metal Biogeochemistry in the Ocean* 173, 148–161. <https://doi.org/10.1016/j.marchem.2015.03.015>
- Obata, H., van den Berg, C.M.G., 2001. Determination of Picomolar Levels of Iron in Seawater Using Catalytic Cathodic Stripping Voltammetry. *Anal. Chem.* 73, 2522–2528. <https://doi.org/10.1021/ac001495d>
- Obata, Hajime., Karatani, Hajime., Nakayama, Eiichiro., 1993. Automated determination of iron in seawater by chelating resin concentration and chemiluminescence detection. *Anal. Chem.* 65, 1524–1528. <https://doi.org/10.1021/ac00059a007>
- Omanović, D., Garnier, C., Pižeta, I., 2015. ProMCC: An all-in-one tool for trace metal complexation studies. *Mar. Chem., SCOR WG 139: Organic Ligands – A Key Control on Trace Metal Biogeochemistry in the Ocean* 173, 25–39. <https://doi.org/10.1016/j.marchem.2014.10.011>
- Pernet-Coudrier, B., Waeles, M., Filella, M., Quentel, F., Riso, R.D., 2013. Simple and simultaneous determination of glutathione, thioacetamide and refractory organic matter in natural waters by DP-CSV. *Sci. Total Environ.* 463–464, 997–1005. <https://doi.org/10.1016/j.scitotenv.2013.06.053>
- Pižeta, I., Sander, S.G., Hudson, R.J.M., Omanović, D., Baars, O., Barbeau, K.A., Buck, K.N., Bundy, R.M., Carrasco, G., Croot, P.L., Garnier, C., Gerringa, L.J.A., Gledhill, M., Hirose, K., Kondo, Y., Laglera, L.M., Nuester, J., Rijkenberg, M.J.A., Takeda, S., Twining, B.S., Wells, M., 2015. Interpretation of complexometric titration data: An intercomparison of methods for estimating models of trace metal complexation by natural organic ligands. *Mar. Chem., SCOR WG 139: Organic Ligands – A Key Control on Trace Metal Biogeochemistry in the Ocean* 173, 3–24. <https://doi.org/10.1016/j.marchem.2015.03.006>

- Poulton, S.W., Raiswell, R., 2002. The low-temperature geochemical cycle of iron: From continental fluxes to marine sediment deposition. *Am. J. Sci.* 302, 774–805. <https://doi.org/10.2475/ajs.302.9.774>
- Quentel, F., Madec, C., Courtot-coupez, J., 1987. Determination of Humic Substances in Seawater by Electrochemistry (Mechanisms). *Anal. Lett.* 20, 47–62. <https://doi.org/10.1080/00032718708082236>
- Raspor, B., Nürnberg, H.W., Valenta, P., Branica, M., 1980. Kinetics and mechanism of trace metal chelation in sea water. *J. Electroanal. Chem. Interfacial Electrochem.* 115, 293–308. [https://doi.org/10.1016/S0022-0728\(80\)80333-0](https://doi.org/10.1016/S0022-0728(80)80333-0)
- Raymond, K.N., Allred, B.E., Sia, A.K., 2015. Coordination Chemistry of Microbial Iron Transport. *Acc. Chem. Res.* 48, 2496–2505. <https://doi.org/10.1021/acs.accounts.5b00301>
- Rickard, D., Luther, G.W., 2007. Chemistry of Iron Sulfides. *Chem. Rev.* 107, 514–562. <https://doi.org/10.1021/cr0503658>
- Roshan, S., DeVries, T., 2021. Global Contrasts Between Oceanic Cycling of Cadmium and Phosphate. *Glob. Biogeochem. Cycles* 35, e2021GB006952. <https://doi.org/10.1029/2021GB006952>
- Rue, E.L., Bruland, K.W., 1997. The role of organic complexation on ambient iron chemistry in the equatorial Pacific Ocean and the response of a mesoscale iron addition experiment. *Limnol. Oceanogr.* 42, 901–910. <https://doi.org/10.4319/lo.1997.42.5.0901>
- Rue, E.L., Bruland, K.W., 1995. Complexation of iron(III) by natural organic ligands in the Central North Pacific as determined by a new competitive ligand equilibration/adsorptive cathodic stripping voltammetric method. *Mar. Chem., The Chemistry of Iron in Seawater and its Interaction with Phytoplankton* 50, 117–138. [https://doi.org/10.1016/0304-4203\(95\)00031-L](https://doi.org/10.1016/0304-4203(95)00031-L)
- Ružić, I., 1982. Theoretical aspects of the direct titration of natural waters and its information yield for trace metal speciation. *Anal. Chim. Acta* 140, 99–113. [https://doi.org/10.1016/S0003-2670\(01\)95456-X](https://doi.org/10.1016/S0003-2670(01)95456-X)
- Sanvito, F., Monticelli, D., 2021. Exploring bufferless iron speciation in seawater by Competitive Ligand Equilibration-Cathodic Stripping Voltammetry: Does pH control really matter? *Talanta* 229, 122300. <https://doi.org/10.1016/j.talanta.2021.122300>
- Sanvito, F., Monticelli, D., 2020. Fast iron speciation in seawater by catalytic Competitive Ligand Equilibration-Cathodic Stripping Voltammetry with tenfold sample size reduction. *Anal. Chim. Acta* 1113, 9–17. <https://doi.org/10.1016/j.aca.2020.04.002>
- Sanvito, F., Pacileo, L., Monticelli, D., 2019. Fostering and Understanding Iron Detection at the Ultratrace Level by Adsorptive Stripping Voltammetry with Catalytic Enhancement. *Electroanalysis* 31, 212–216. <https://doi.org/10.1002/elan.201800675>
- Scatchard, G., 1949. The Attractions of Proteins for Small Molecules and Ions. *Ann. N. Y. Acad. Sci.* 51, 660–672. <https://doi.org/10.1111/j.1749-6632.1949.tb27297.x>
- Schoffman, H., Lis, H., Shaked, Y., Keren, N., 2016. Iron–Nutrient Interactions within Phytoplankton. *Front. Plant Sci.* 7.
- Schuback, N., Schallenberg, C., Duckham, C., Maldonado, M.T., Tortell, P.D., 2015. Interacting Effects of Light and Iron Availability on the Coupling of Photosynthetic Electron Transport and CO<sub>2</sub>-Assimilation in Marine Phytoplankton. *PLOS ONE* 10, e0133235. <https://doi.org/10.1371/journal.pone.0133235>
- Shaked, Y., Buck, K.N., Mellett, T., Maldonado, M.T., 2020. Insights into the bioavailability of oceanic dissolved Fe from phytoplankton uptake kinetics. *ISME J.* 14, 1182–1193. <https://doi.org/10.3389/fmicb.2020.00204>
- Shi, D., Xu, Y., Hopkinson, B.M., Morel, F.M.M., 2010. Effect of Ocean Acidification on Iron Availability to Marine Phytoplankton. *Science* 327, 676–679. <https://doi.org/10.1126/science.1183517>
- Slagter, H.A., Reader, H.E., Rijkenberg, M.J.A., Rutgers van der Loeff, M., de Baar, H.J.W., Gerringa, L.J.A., 2017. Organic Fe speciation in the Eurasian Basins of the Arctic Ocean and its relation to terrestrial DOM. *Mar. Chem.* 197, 11–25. <https://doi.org/10.1016/j.marchem.2017.10.005>

- Stockdale, A., Tipping, E., Lofts, S., Mortimer, R.J.G., 2016. Effect of Ocean Acidification on Organic and Inorganic Speciation of Trace Metals. *Environ. Sci. Technol.* 50, 1906–1913. <https://doi.org/10.1021/acs.est.5b05624>
- Su, H., Yang, R., Pižeta, I., Omanović, D., Wang, S., Li, Y., 2016. Distribution and Speciation of Dissolved Iron in Jiaozhou Bay (Yellow Sea, China). *Front. Mar. Sci.* 3. <https://doi.org/10.3389/fmars.2016.00099>
- Sukekava, C., Downes, J., Slagter, H.A., Gerringa, L.J.A., Laglera, L.M., 2018. Determination of the contribution of humic substances to iron complexation in seawater by catalytic cathodic stripping voltammetry. *Talanta* 189, 359–364. <https://doi.org/10.1016/j.talanta.2018.07.021>
- Sunda, W.G., 2012. Feedback Interactions between Trace Metal Nutrients and Phytoplankton in the Ocean. *Front. Microbiol.* 3. <https://doi.org/10.3389/fmicb.2012.00204>
- Tagliabue, A., 2014. More to hydrothermal iron input than meets the eye. *Proc. Natl. Acad. Sci.* 111, 16641–16642. <https://doi.org/10.1073/pnas.1419829111>
- Tagliabue, A., Aumont, O., Bopp, L., 2014a. The impact of different external sources of iron on the global carbon cycle. *Geophys. Res. Lett.* 41, 920–926. <https://doi.org/10.1002/2013GL059059>
- Tagliabue, A., Aumont, O., DeAth, R., Dunne, J.P., Dutkiewicz, S., Galbraith, E., Misumi, K., Moore, J.K., Ridgwell, A., Sherman, E., Stock, C., Vichi, M., Völker, C., Yool, A., 2016. How well do global ocean biogeochemistry models simulate dissolved iron distributions?: GLOBAL IRON MODELS. *Glob. Biogeochem. Cycles* 30, 149–174. <https://doi.org/10.1002/2015GB005289>
- Tagliabue, A., Bopp, L., Dutay, J.-C., Bowie, A.R., Chever, F., Jean-Baptiste, P., Bucciarelli, E., Lannuzel, D., Remenyi, T., Sarthou, G., Aumont, O., Gehlen, M., Jeandel, C., 2010. Hydrothermal contribution to the oceanic dissolved iron inventory. *Nat. Geosci.* 3, 252–256. <https://doi.org/10.1038/ngeo818>
- Tagliabue, A., Mtshali, T., Aumont, O., Bowie, A.R., Klunder, M.B., Roychoudhury, A.N., Swart, S., 2012. A global compilation of dissolved iron measurements: focus on distributions and processes in the Southern Ocean 17. <https://doi.org/10.5194/bg-9-2333-2012>
- Tagliabue, A., Resing, J., 2016. Impact of hydrothermalism on the ocean iron cycle. *Philos. Trans. R. Soc. Math. Phys. Eng. Sci.* 374, 20150291. <https://doi.org/10.1098/rsta.2015.0291>
- Tagliabue, A., Sallée, J.-B., Bowie, A.R., Lévy, M., Swart, S., Boyd, P.W., 2014b. Surface-water iron supplies in the Southern Ocean sustained by deep winter mixing. *Nat. Geosci.* 7, 314–320. <https://doi.org/10.1038/ngeo2101>
- Taylor, S.R., 1964. Abundance of chemical elements in the continental crust: a new table. *Geochim. Cosmochim. Acta* 28, 1273–1285. [https://doi.org/10.1016/0016-7037\(64\)90129-2](https://doi.org/10.1016/0016-7037(64)90129-2)
- Tortell, P.D., Maldonado, M.T., Granger, J., Price, N.M., 1999. Marine bacteria and biogeochemical cycling of iron in the oceans. *FEMS Microbiol. Ecol.* 29, 1–11. <https://doi.org/10.1111/j.1574-6941.1999.tb00593.x>
- Tortell, P.D., Maldonado, M.T., Price, N.M., 1996. The role of heterotrophic bacteria in iron-limited ocean ecosystems. *Nature* 383, 330–332. <https://doi.org/10.1038/383330a0>
- Town, R.M., van Leeuwen, H.P., 2005. Measuring Marine Iron(III) Complexes by CLE-AdSV. *Environ. Chem.* 2, 80–84. <https://doi.org/10.1071/EN05021>
- Twining, B.S., Baines, S.B., 2013. The Trace Metal Composition of Marine Phytoplankton. *Annu. Rev. Mar. Sci.* 5, 191–215. <https://doi.org/10.1146/annurev-marine-121211-172322>
- van den Berg, C.M.G., 2006. Chemical Speciation of Iron in Seawater by Cathodic Stripping Voltammetry with Dihydroxynaphthalene. *Anal. Chem.* 78, 156–163. <https://doi.org/10.1021/ac051441+>
- van den Berg, C.M.G., 2005. Organic Iron Complexation Is Real, The Theory Is Used Incorrectly. Comment on “Measuring Marine Iron(III) Complexes by CLE-AdSV.” *Environ. Chem.* 2, 88. <https://doi.org/10.1071/EN05029>



- van den Berg, C.M.G., 1995. Evidence for organic complexation of iron in seawater. *Mar. Chem., The Chemistry of Iron in Seawater and its Interaction with Phytoplankton* 50, 139–157. [https://doi.org/10.1016/0304-4203\(95\)00032-M](https://doi.org/10.1016/0304-4203(95)00032-M)
- van den Berg, C.M.G., 1982. Determination of copper complexation with natural organic ligands in seawater by equilibration with MnO<sub>2</sub> II. Experimental procedures and application to surface seawater. *Mar. Chem.* 11, 323–342. [https://doi.org/10.1016/0304-4203\(82\)90029-9](https://doi.org/10.1016/0304-4203(82)90029-9)
- Van den Berg, C.M.G., Huang, Z.Qiang., 1984. Direct electrochemical determination of dissolved vanadium in seawater by cathodic stripping voltammetry with the hanging mercury drop electrode. *Anal. Chem.* 56, 2383–2386. <https://doi.org/10.1021/ac00277a028>
- van den Berg, C.M.G., Nimmo, M., Daly, P., Turner, D.R., 1990. Effects of the detection window on the determination of organic copper speciation in estuarine waters. *Anal. Chim. Acta* 232, 149–159. [https://doi.org/10.1016/S0003-2670\(00\)81231-3](https://doi.org/10.1016/S0003-2670(00)81231-3)
- Velasquez, I.B., Ibisani, E., Maas, E.W., Boyd, P.W., Nodder, S., Sander, S.G., 2016. Ferrioxamine Siderophores Detected amongst Iron Binding Ligands Produced during the Remineralization of Marine Particles. *Front. Mar. Sci.* 3. <https://doi.org/10.3389/fmars.2016.00172>
- Walczak, M.M., Dryer, D.A., Jacobson, D.D., Foss, M.G., Flynn, N.T., 1997. pH Dependent Redox Couple: An Illustration of the Nernst Equation. *J. Chem. Educ.* 74, 1195. <https://doi.org/10.1021/ed074p1195>
- Wang, H., Wang, W., Liu, M., Zhou, H., Ellwood, M.J., Butterfield, D.A., Buck, N.J., Resing, J.A., 2022. Iron ligands and isotopes in hydrothermal plumes over backarc volcanoes in the Northeast Lau Basin, Southwest Pacific Ocean. *Geochim. Cosmochim. Acta* 336, 341–352. <https://doi.org/10.1016/j.gca.2022.09.026>
- Wang, P., Ding, Y., Liang, Y., Liu, M., Lin, X., Ye, Q., Shi, Z., 2021. Linking molecular composition to proton and copper binding ability of fulvic acid: A theoretical modeling approach based on FT-ICR-MS analysis. *Geochim. Cosmochim. Acta* 312, 279–298. <https://doi.org/10.1016/j.gca.2021.07.019>
- Welch, K.D., Davis, T.Z., Aust, S.D., 2002. Iron Autoxidation and Free Radical Generation: Effects of Buffers, Ligands, and Chelators. *Arch. Biochem. Biophys.* 397, 360–369. <https://doi.org/10.1006/abbi.2001.2694>
- Wells, M., Buck, K.N., Sander, S.G., 2013. New approach to analysis of voltammetric ligand titration data improves understanding of metal speciation in natural waters. *Limnol. Oceanogr. Methods* 11, 450–465. <https://doi.org/10.4319/lom.2013.11.450>
- Whitby, H., Planquette, H., Cassar, N., Bucciarelli, E., Osburn, C.L., Janssen, D.J., Cullen, J.T., González, A.G., Völker, C., Sarthou, G., 2020. A call for refining the role of humic-like substances in the oceanic iron cycle. *Sci. Rep.* 10, 1–12. <https://doi.org/10.1038/s41598-020-62266-7>
- Whitby, H., van den Berg, C.M.G., 2015. Evidence for copper-binding humic substances in seawater. *Mar. Chem., SCOR WG 139: Organic Ligands – A Key Control on Trace Metal Biogeochemistry in the Ocean* 173, 282–290. <https://doi.org/10.1016/j.marchem.2014.09.011>
- Williford, T., Amon, R.M.W., Benner, R., Kaiser, K., Bauch, D., Stedmon, C., Yan, G., Walker, S.A., van der Loeff, M.R., Klunder, M.B., 2021. Insights into the origins, molecular characteristics and distribution of iron-binding ligands in the Arctic Ocean. *Mar. Chem.* 231, 103936. <https://doi.org/10.1016/j.marchem.2021.103936>
- Worsfold, P.J., Lohan, M.C., Ussher, S.J., Bowie, A.R., 2014. Determination of dissolved iron in seawater: A historical review. *Mar. Chem.* 166, 25–35. <https://doi.org/10.1016/j.marchem.2014.08.009>
- Wu, J., Luther, G.W., 1995. Complexation of Fe(III) by natural organic ligands in the Northwest Atlantic Ocean by a competitive ligand equilibration method and a kinetic approach. *Mar. Chem., The Chemistry of Iron in Seawater and its Interaction with Phytoplankton* 50, 159–177. [https://doi.org/10.1016/0304-4203\(95\)00033-N](https://doi.org/10.1016/0304-4203(95)00033-N)

- Wu, S., He, M., Hu, B., Jiang, Z., 2007. Determination of trace rare earth elements in natural water by electrothermal vaporization ICP-MS with pivaloyltrifluoroacetone as chemical modifier. *Microchim. Acta* 159, 269–275. <https://doi.org/10.1007/s00604-007-0764-5>
- Yun, J., Choi, H., 2000. Micellar colorimetric determination of iron, cobalt, nickel and copper using 1-nitroso-2-naphthol. *Talanta* 52, 893–902. <https://doi.org/10/fnrgrn7>
- Zhu, K., Hopwood, M.J., Groenenberg, J.E., Engel, A., Achterberg, E.P., Gledhill, M., 2021. Influence of pH and Dissolved Organic Matter on Iron Speciation and Apparent Iron Solubility in the Peruvian Shelf and Slope Region. *Environ. Sci. Technol.* 55, 9372–9383. <https://doi.org/10.1021/acs.est.1c02477>
- Zigah, P.K., McNichol, A.P., Xu, L., Johnson, C., Santinelli, C., Karl, D.M., Repeta, D.J., 2017. Allochthonous sources and dynamic cycling of ocean dissolved organic carbon revealed by carbon isotopes. *Geophys. Res. Lett.* 44, 2407–2415. <https://doi.org/10.1002/2016GL071348>



## Note for the reader

The following Chapter is in final stage of preparation for publication and is nearly ready for submission to the journal *Frontiers in Marine Sciences*. This might explain repetitions regarding the description of the methodological context and of the scientific background. This paper is co-authored by D. Omanović, and the supervisory team of this Thesis.

To be submitted as: **Mahieu, L.**, Whitby, H., Omanović, D., Salaün, P.: Conditioning, equilibration, voltammetric, and data treatment procedures for iron speciation in seawater using salicylaldoxime by cathodic stripping voltammetry.

## **Chapter 4**

### **4. Conditioning, equilibration, voltammetric, and data treatment procedures for iron speciation in seawater using salicylaldoxime by cathodic stripping voltammetry**

#### **Abstract**

The method of competitive ligand exchange followed by adsorptive cathodic stripping voltammetry (CLE-ACSV) for the determination of dissolved iron (DFe) organic speciation parameters (conditional total ligand concentration ([L]) and conditional stability constant ( $\log K_{\text{FeL,Fe}}^{\text{cond}}$ )) in seawater is currently only used by a few laboratories. One likely explanation is the set of experimental challenges that a new analyst must face, from conditioning of the tubes, stability of the voltammetric signal or fitting of the titration to name a few. Here, we present a set of observations and recommendations with the aim to facilitate the implementation of such methodology. Firstly, we detail our optimised conditioning procedures for the voltammetric cell and for titration tubes that ensure a stable ACSV signal when using the added ligand salicylaldoxime (SA); we also present a set of experimental development procedures that significantly decrease the analytical time of the voltammetric analysis. Secondly, we propose a step-by-step procedure for the fitting of titration data. It aims to limit user subjectivity on the titration results, and relies in the combined use of the software ProMCC and of a spreadsheet specifically developed for independent statistically-driven selection of the titration data and determination of the quality flag of the titration. The reproducibility of the proposed methodology has been evaluated on 20 duplicates (39 titrations). The accuracy of our CLE-ACSV application was estimated at 20% of the mean [L] (in our case,  $\pm 0.5 \text{ nmoleq. Fe}^{-1}$ ) and at  $\pm 0.2$  in term of  $\log K_{\text{FeL,Fe}}^{\text{cond}}$ , corresponding to 20% of

the estimated range cover by a single detection window. Finally, the sequential addition of DFe and SA followed by a short equilibration time was compared with overnight equilibration after simultaneous addition of DFe and SA on 24 samples (48 titrations). Contrary to previous assumptions, we did not observe systematic overestimation of [L] and  $\log K_{\text{FeL}}^{\text{cond}}$  of the sequential procedure. Instead, a rather large range of differences was observed across samples for  $\Delta[\text{L}]$  (from -2.3 to 3.1 nmoleqFe.L<sup>-1</sup>, mean of  $0.6 \pm 1.5$  nmoleqFe.L<sup>-1</sup>) and  $\Delta\log K_{\text{FeL,Fe}'}^{\text{cond}}$  (from -0.7 to 0.6, mean of  $-0.2 \pm 0.4$ ). This is calling for further investigation of the equilibration time procedure on the CLE-ACSV results obtained.

## 4.1. Introduction

A fraction of the dissolved organic matter (DOM) is able to bind iron (Fe) and enhance its dissolution in seawater above the theoretical solubility limit (Liu and Millero, 2002). This complexation maintains Fe in the dissolved phase (DFe, defined by the porosity of the filter used of 0.2 or 0.45  $\mu\text{m}$ ), increasing its residence time in the water column and thus potential bioavailability. It is thought that more than 99% of DFe is found bound to the fraction of the DOM called Fe-binding ligands (FeL; Gledhill and van den Berg, 1994), however, there is still much to learn about their composition and biogeochemical cycling (Gledhill and Buck, 2012; Hassler et al., 2017). Multiple studies have focused on some aspects of the organic iron ligand pool, from acid-base properties (Lodeiro et al., 2020; Wang et al., 2021) to photodegradation (Barbeau et al., 2001; Hassler et al., 2019), or transformation through remineralisation (Bressac et al., 2019; Whitby et al., 2020a). A considerable number of methods based on electrochemistry have been developed to investigate and identify FeL groups. So far, studies helped to define the ability of exopolymeric substances to bind Fe (Hassler et al., 2015, 2011; Norman et al., 2015), and to identify the essential role of the electroactive fraction of humic-like substances (eHS), thought to control DFe distribution in open-ocean deep waters (Whitby et al., 2020b). Despite progresses in the characterisation of DOM and specific FeL, the links between DOM, FeL and DFe distribution are not fully resolved (e.g. Fourier et al., 2022).

#### 4.1.1. The CLE-ACSV approach

The competitive ligand exchange followed by adsorptive cathodic stripping voltammetry (CLE-ACSV) is classically used to investigate the complexing parameters of the FeL fraction. Namely, it allows the determination of the conditional total ligand concentration ( $[L]$ ) and the conditional stability constant (expressed as a logarithmic value,  $\log K_{\text{FeL}}^{\text{cond}}$ ). The CLE-ACSV approach has been thoroughly explained previously (e.g. Abualhaija and van den Berg, 2014; Gerringa et al., 2014; Gledhill and van den Berg, 1994; Pižeta et al., 2015; Rue and Bruland, 1995; Chapter 2). Briefly, its principle is based on the competition for Fe complexation between the natural FeL and an added ligand (AL) of well-characterised ability to bind Fe. This competition is carried out in several aliquots of the sample at increasing DFe concentration for a certain amount of time, ideally until a chemical equilibrium is reached between AL, FeL and DFe. Then, for each aliquot, the FeAL complex is quantified by ACSV on a mercury drop electrode (MDE). The measurement consists of an accumulation step, where FeAL adsorbs on the mercury surface, before a stripping step, where adsorbed and bound  $\text{Fe}^{3+}$  is reduced to  $\text{Fe}^{2+}$ . By plotting the intensity of the FeAL reduction peak against total DFe, a titration curve is obtained (total DFe being the sum of naturally present and added DFe). At high DFe, natural FeL are saturated and the FeAL signal is linear and proportional to DFe additions while at low DFe, FeL and AL are competing for DFe. There are several methods that can be used to obtain  $[L]$  and  $\log K_{\text{FeL}}^{\text{cond}}$  from the titration curve (Pižeta et al., 2015), but those based on the Langmuir isotherm are the most commonly used, greatly facilitated by user-friendly software such as ProMCC (Omanović et al., 2015). This software treats the titration curve simultaneously by the Scatchard transformation (Scatchard, 1949), the Ružić/van den Berg linearization (Ružić, 1982; van den Berg, 1982), and the Langmuir/Gerringa transformation (Gerringa et al., 2014, 1995) and provides the user with the accuracy of the fitting for each datapoint. There is currently no consensus on an optimised procedure to be used for the estimation of titration accuracy despite the common use of the software ProMCC.

#### 4.1.2. Added ligand and detection window

There are currently four AL in use to study DFe organic speciation in marine systems: 1-nitroso-2-naphthol (NN; Gledhill and van den Berg, 1994; van den Berg, 1995), 2-(2-thiazolylazo)-p-cresol (TAC; Croot and Johansson, 2000), dihydroxynaphthalene (DHN; Sanvito and Monticelli, 2020; van den Berg, 2006), and salicylaldehyde (SA; Abualhaija and van den Berg, 2014; Buck et al., 2007; Rue and Bruland, 1995). They all suffer from specific limitations. NN can be used at different pH but suffers from sensitivity issues limiting its use (Avendaño et al., 2016; Gledhill et al., 2015), despite potential for catalytic enhancement of its sensitivity in the presence of oxygen (Chapter 3). It also does not compete with part of the HS, resulting in underestimation of [L] (Ardiningsih et al., 2021; Laglera et al., 2011) similarly to the added ligand TAC (Laglera et al., 2011), while previous studies suggested an overestimation of [L] with SA (Gerringa et al., 2021; Slagter et al., 2019). DHN is not as widely used because of its relatively quick oxidation by oxygen which occurs within the time scale of the equilibration step (Sanvito and Monticelli, 2020).

SA has been used at the basin scale (Buck et al., 2018, 2015), in hydrothermal systems (Kleint et al., 2016), and seems to not suffer from interference with HS (Abualhaija and van den Berg, 2014). There are, however, doubts regarding its chemistry and the optimum experimental conditions for use. Abualhaija and van den Berg (2014) suggested that a non-electroactive  $\text{FeSA}_2$  complex slowly formed during the overnight equilibration step when using SA concentrations in the range of  $25 \mu\text{mol.L}^{-1}$ ; they thus advised to use a low SA concentration ( $5 \mu\text{mol.L}^{-1}$ ). Their equilibration procedure consisted of first adding DFe to the aliquot and left to equilibrate with the natural ligands for at least 10 min and not more than 2 hours, followed by addition of  $5 \mu\text{mol.L}^{-1}$  SA and an overnight equilibration time (i.e. from 6h to 16h). On the other hand, Rue and Bruland (1995) and Buck et al. (2007) reported a shorter sequential equilibration procedure: DFe was first added and left to equilibrate with natural ligands for a minimum of 2 h; a relatively high SA concentration ( $27.5 \mu\text{mol.L}^{-1}$  or  $25 \mu\text{mol.L}^{-1}$ ) was then added and left to equilibrate for a minimum of 15 min before voltammetric analysis was made. It is currently unclear what the differences of these 2 equilibration procedures may have on [L] and  $\log K_{\text{FeL,Fe}}^{\text{cond}}$  (Gerringa et al., 2021).



Another potential source of divergence between methods is related to the complexing ability of the AL. The AL concentration ( $[AL]$ ) and its conditional stability constant ( $K_{FeAL,Fe}^{cond}$  or  $\beta_{FeAL,Fe}^{cond}$ ) defines the detection window of the titration ( $D = [AL]^{n*}\beta_{FeAL,Fe}^{cond}$ ), often expressed as a logarithmic value ( $\log D$ ; Table 1). The range of  $D$  for which an AL is able to compete with FeL has been estimated to range between 1 to 2 orders of magnitude above and below  $D$  (Apte et al., 1988; Laglera et al., 2013; Laglera and Filella, 2015; Miller and Bruland, 1997; van den Berg and Donat, 1992). In the case of SA, higher  $[L]$  than those obtained with TAC or NN are systematically observed (Ardiningsih et al., 2021; Buck et al., 2016; Slagter et al., 2019), possibly due to those latter ligands being insensitive to a fraction of weaker complexing HS (Ardiningsih et al., 2021; Boye et al., 2001; Gerringa et al., 2021; Laglera et al., 2011; van den Berg, 2006), in agreement with their higher detection window.

Table 4.1. Typical AL concentrations and corresponding detection windows ( $\log D$ ) for the different ALs in use to investigate FeL by CLE-ACSV.  $n$ ,  $K_{FeAL,Fe}^{cond}$  or  $\beta_{FeAL,Fe}^{cond}$  used for the calculation of  $D$  were taken in the references.

AL	Concentration ( $\mu\text{mol.L}^{-1}$ )	D	Reference
NN	2	2.4	van den Berg (1995)
	7	4	
	8.7	4.3	
	15	5	
TAC	10	2.4	Croot and Johansson (2000)
SA	5	1.2	Abualhaija and van den Berg (2014)
	25	1.9	Buck et al. (2007)
DHN	0.5	2.7	Sanvito and Monticelli (2020)
	1	3.2	
	5	4	
	10	4.2	

Although the FeSA signal has been reported to be stable in the presence of oxygen (Abualhaija and van den Berg, 2014), a decreasing signal has been reported by several authors (Gerringa et al., 2021; Ardiningsih et al., 2021; Buck et al., 2007; Rue and Bruland, 1995). This instability may have various

causes, ranging from progressive deoxygenation of the sample, adsorption onto the voltammetric cell or kinetically slow formation of electro-inactive FeSA<sub>2</sub> complexes (Abualhaija and van den Berg, 2014). The need for specific conditioning of the voltammetric cells and sample vessels prior to the use of SA has recently been put forward (Gerringa et al., 2021 and associated community comment), and is yet to be addressed.

#### 4.1.3. Sample preparation and technical limitations

The quality and reliability of ligand titration results is also dependent on the preparation of the analysis. It is recommended to titrate ligands with two aliquots of the natural sample (without any metal added) and at least 8 aliquots with metal addition of the metal (Garnier et al., 2004; Gledhill and Buck, 2012; Omanović et al., 2015; Sander et al., 2011). Analysing two aliquots without added metal helps ensuring the validity of the initial point by conditioning the voltammetric cell and resolving any carried-over from previous measurement. The concentration range for DFe additions is typically dictated by the amount of DFe in the sample or adjusted to the amount of FeL detected (Gledhill and Buck, 2012). The fitting of the titration heavily depends on the sensitivity of the method in that considered sample. It is given by the slope of the peak intensity *versus* added DFe when all natural FeL are saturated by DFe. In ProMCC, the sensitivity can be defined by considering the slope drawn by the last aliquots of the titration (i.e. assuming that all natural ligands are saturated; Omanović et al., 2015). In that case, it is recommended to use at least the 3 last aliquots with an optimum of 5 (Omanović et al., 2015; Pižeta et al., 2015). Alternatively, the sensitivity can also be fitted, meaning that instead of assuming FeL saturation in the last aliquots, the sensitivity is optimised by iteration to limit the fitting error on the whole titration (Omanović et al., 2015). Accurate determination of the sensitivity is still a challenge of the CLE-ACSV approach (Gerringa et al., 2014, 1995; Omanović et al., 2015; Pižeta et al., 2015). So far, there is no common best practice for its definition, and it is recommended to verify the robustness of the different approaches applicable for each CLE-ACSV application. The fitting of the data is more challenging when more than one class of FeL is detected. In some cases, and mostly with the AL SA, the shape of the titration suggests the presence of two distinct classes of FeL, whose complexing parameters can be quantified (Buck et al., 2015; Gledhill and Buck, 2012; Ibisani et al., 2011). The

main issue regarding the fitting of the titration data for more than one class of FeL is the accuracy on each class detected, which depends on the number of aliquots prepared. Common practice consists of limiting the number of aliquots to optimise the experimental time, impacting the resolution of the titration and potentially the number of FeL classes detected (Buck et al., 2012). The results can also be impacted by subjectivity of the analyst while interpreting the titration data. Comparison effort on the interpretation of CLE-ACSV titrations revealed discrepancies that were explained by the choices of the analyst on the selection of the titration datapoints (Pižeta et al., 2015), justifying the development of systematic approach for analysing titration data, which should result in better reproducibility between laboratories.

In this work, we revisit some of the limiting factors that prevent a wider use and comparability of the SA method for DFe organic speciation. We propose an optimised methodology that spans the conditioning of the aliquot tubes (Metal Free, Labcon™), the optimisation of voltammetric parameters for the detection of the electroactive FeSA complex, and recommendations for data treatment for voltammograms and FeL titrations. We present a procedure for an easy, quick and reliable measurement of the peak-height using the freely available software ECDSOft (available online at <https://sites.google.com/site/daromasoft>). We also developed a procedure aiming to offer a more systematic approach for the treatment of titration data to limit the impact of the analyst's subjectivity. Based on the use of the software ProMCC (available online at <https://sites.google.com/site/daromasoft>) with a home-made spreadsheet, the procedure uses a statistical selection of titration datapoints, and automatically produces quality flags for the titration data. Finally, we estimated the reproducibility of the sequential addition of Fe and SA applied for short equilibration time (Buck et al., 2007; Rue and Bruland, 1995), and present here a comparison of the speciation parameters ( $[L]$  and  $\log K_{\text{FeL,Fe}}^{\text{cond}}$ ) obtained by sequential and short equilibration with overnight equilibration, for which Fe and SA are added simultaneously (Abualhaija and van den Berg, 2014).

## 4.2. Method

This work is focusing on technical specificities related to the application of the CLE-ACSV method using SA. For the theoretical aspect of the method, please refer to previous work (e.g. Abualhaija and van den Berg, 2014; Gerringa et al., 2014; Gledhill and van den Berg, 1994; Pižeta et al., 2015; Rue and Bruland, 1995; Chapter 2).

### 4.2.1. Apparatus

The apparatus used in this study is the same as in Chapter 3. Two voltammetric systems were each composed of a 663 VA stand (Metrohm™) installed in a laminar flow hood (class-100), supplied with nitrogen and equipped with a multi-mode electrode (MME, Metrohm™) used as mercury drop electrode (MDE), a glassy carbon counter electrode and a silver/silver chloride reference electrode. For each system, a potentiostat/galvanostat  $\mu$ Autolab III and an IME663 were controlled by the software NOVA 2.5 (Metrohm™), allowing automatic formation of the drop (size 3) and stirring of the solution through home-made vibrating devices. The home-made stirring device consisted of a small (6 mm diameter, 12 mm long) vibration motor (1.5 V, 10200 rpm, JinLong Machinery, China) connected to a melted pipette with the flat-tip penetrating the solution. This vibrating device optimises the sensitivity and reproducibility of the analysis (Chapter 2), in a similar way as when directly connected to the working electrode (Chapman and van den Berg, 2007).

Voltammetric measurements were carried out in oxygenated solution in custom made Teflon™ cells allowing the user to perform analyses in 5 mL of samples (Gourain, 2020; Chapter 2). Working at low volumes and under oxygenated conditions (as opposed to under a nitrogen blanket) required adjustments to the typical set up, which are detailed in Chapter 2. Both the counter and reference electrodes were placed in glass bridges filled with 3M KCl solution previously cleaned of organics (through UV radiation in quartz tube for 6h) and cleaned of metals with overnight equilibration with manganese oxides (Yokoi and van den Berg, 1998). To avoid progressive deoxygenation of the sample, the nitrogen blanket gas flow was stopped by tightening the screw on the left side of the 663 VA stand and a small aquarium pump (HD-603, HDOM™), placed inside the laminar flow hood, was used to

blow a small stream of air above the water sample, ensuring constant dissolved oxygen concentration (Sanvito et al., 2019; Sanvito et al., 2020; Chapter 2).

Working under oxygenated conditions can increase the speed at which the mercury is oxidised. Oxidation can cause increased noise in the voltammetric scans obtained, affecting titration data. To mitigate this, the needle was cleaned daily by simply screwing it off, wiping it gently, and screwing it back in with the exact same tightness. The mercury was filtered weekly after vigorous shaking of the MDE cartridge to unstick mercury oxides from the walls and connections, without touching the fitting of the capillary. More regular cleaning was preferred and were observed to be easier, faster and overall better for the capillary rather than a less frequent cleaning, which often required complete dismantling of the cartridge to remove the higher mercury oxide content.

#### **4.2.2. Voltammetric procedure**

The procedure is adjusted from (Abualhaija and van den Berg, 2014) and (Buck et al., 2007) using the software NOVA 2.5 (Metrohm™). Three new drops were formed prior to the analysis by DP-ACSV (Differential Pulse Adsorptive Cathodic Stripping Voltammetry) using the following parameters: deposition at -0.05 V (optimisation presented hereafter) for 30 s to 3 min (depending on the sampling depth of the sample), 3 s of equilibration (no stirring), stripping from -0.25 to -0.6 V with a 6 mV step, 50 mV amplitude, 35 ms pulse time and 200 ms interval time. The solution was vibrated during the deposition time and stagnant during the stripping step.

#### **4.2.3. Reagent preparation**

The preparation of the SA solution is adjusted from Abualhaija and van den Berg (2014). SA (SA; 98% Acros Organics™) stock solution of 20 mL at 0.1 mol.L<sup>-1</sup> was prepared in Milli-Q water (Millipore, 18.2 MΩ) only once and stored in the fridge at pH < 1 (adjusted with 260 µL of 20 % of Trace Metal Grade HCl, FisherScientific™; Abualhaija and van den Berg, 2014). From this stock solution, a solution of 20 mL at 5 mmol.L<sup>-1</sup> was prepared when necessary (around once a month) by dilution of 1 mL of the stock solution with Milli-Q and kept refrigerated at pH 2. Gentle heating of the stock solution (between 30 and 35 °C) was necessary to prevent the presence of a secondary phase before the

preparation of the SA solution at  $5 \text{ mmol.L}^{-1}$ , which was prepared 24 hrs prior to use to ensure stability and homogeneity. A batch of 250 mL of a  $1 \text{ mol.L}^{-1}$  borate buffer (boric acid, analytical reagent grade, Fisher Scientific<sup>TM</sup>) in  $0.4 \text{ mol.L}^{-1}$  ammonia ( $\text{NH}_4\text{OH}$ ; 29% Laporte<sup>TM</sup>) was prepared as necessary and left to equilibrate for three days prior to use. After three days, the pH obtained in seawater samples spiked with  $25 \text{ }\mu\text{mol.L}^{-1}$  of SA and  $10 \text{ mmol.L}^{-1}$  of the buffer was  $8.18 \pm 0.03$ .

Two Fe standards at pH 2 were prepared weekly and one monthly from a Fe stock solution at 1000 ppm ( $17.9 \text{ mmol.L}^{-1}$ ; BDH<sup>TM</sup>). 10 mL of the monthly standard at  $50 \text{ }\mu\text{mol.L}^{-1}$  Fe were prepared by weighing 10 g of Milli-Q and spiking it with 15  $\mu\text{L}$  of Trace Metal Grade HCl and 28  $\mu\text{L}$  of Fe at 1000 ppm. The first weekly standard was prepared by weighing 10 g of Milli-Q spiked with 15  $\mu\text{L}$  of Trace Metal Grade HCl and 5.6  $\mu\text{L}$  of Fe at 1000 ppm for a final Fe concentration of  $10 \text{ }\mu\text{mol.L}^{-1}$ . 20 mL of the second weekly standard at  $2 \text{ }\mu\text{mol.L}^{-1}$  Fe was prepared by weighing 16 mL of Milli-Q, spiked with 10  $\mu\text{L}$  of Trace Metal Grade HCl and 4 mL of the standard at  $10 \text{ }\mu\text{mol.L}^{-1}$ . This latter standard was used to prepare the titrations.

#### **4.2.4. Sample preparation**

Most FeL titrations were obtained using the sequential equilibration procedure (Buck et al., 2018, 2015, 2007; Rue and Bruland, 1995), but an overnight equilibration procedure using the same SA concentration was also used for comparison purposes. The sequential equilibration consists of spiking seawater aliquots with  $10 \text{ mmol.L}^{-1}$  of borate buffer and Fe, leaving to equilibrate for at least 2 h, add  $25 \text{ }\mu\text{mol.L}^{-1}$  of SA ( $D = 79$ ;  $\log D = 1.9$ ; Buck et al., 2007) and wait a minimum of 15 min prior to the start of the analysis. The overnight equilibration procedure here consists of adding borate, Fe and SA successively and leaving the mixture to equilibrate overnight (minimum of 8 h). A specific set of tubes were prepared for each equilibration procedure. The sets were composed of 16 tubes with DFe additions ranging from 0 to  $15 \text{ nmol.L}^{-1}$  (Table 1). Prior to preparation, samples were left to thaw overnight in the dark at room temperature. If duplicates were analysed within a few days, they were kept in the fridge. If more time was needed before the second analysis, they were frozen back at  $-20 \text{ }^\circ\text{C}$ . The samples analysed in this study were sampled in the Western Tropical South Pacific in 2019 during the

cruise GPpr14 (TONGA cruise; Guieu and Bonnet, 2019). For complementary information regarding DFe and FeL sampling and results please refer to Tilliette et al. (2022) and Chapter 5.

#### **4.2.5. Peak height extraction from voltammetric measurements**

The treatment applied for the data presented in this work consisted of the conversion of the initial voltammograms into second derivative scans, prior to automated peak height determination, completed by manual peak determination when necessary. This treatment was performed using the freely available ECDSOft (available online at <https://sites.google.com/site/daromasoft>) following a procedure detailed in Annex 2. The use of the peak height of the second derivative peak instead of the peak height or peak area of the raw scan is favoured in case of curvature of the baseline under the peak (Cobelo-García et al., 2014; Salaün et al., 2007). For example, if the baseline is approximated by a 3<sup>rd</sup> polynomial, the 2<sup>nd</sup> derivative will transform it to a linear one, avoiding manual and user dependent choice of the baseline (Omanovic et al., 2010). However, it is crucial that the half-width of the second derivative peak is unchanged for the treated dataset (e.g. complexometric titration). In our case, the half-width of the FeSA peak was not changing with the addition of Fe, suggesting that the second derivative can be used for quantification purposes. Before the conversion of the scans into second derivative using the Savitzky-Golay method, the number of data points was increased by a factor of 3 by simple linear interpolation between two adjacent points and the scan was smoothed using a factor 10 for the Savitzky-Golay method. The increase of data points is beneficial when the number of points defining the peak is relatively low (due to larger voltage scan step, 6 mV in our case). These steps are performed using the tab 'Process' in ECDSOft. The smoothing and data point increase did not impact the peak height values compared to their determination on initial voltammograms (results not shown), but eased the automated voltammogram handling by the software, which experienced less peak height determination failure.

### **4.3. Result and discussion**

#### **4.3.1. Conditioning procedure for cell and tubes**

In the case of SA, a systematic decrease of the FeSA reduction peak was recently highlighted despite overnight conditioning of the cell with UV-irradiated seawater spiked with SA repeated five

consecutive times before analysis (Gerringa et al., 2021). We also observed a strong decrease of the signal with time in the voltammetric cell in the absence of conditioning (Figure 1b). We hypothesised that, in the case of the AL SA, either Fe, SA or FeSA<sub>x</sub> complexes can be scavenged from the solution by adsorption onto cell walls and electrodes. To minimise such adsorption, we developed a procedure to saturate the adsorption sites with a high amount of Fe (based on Gerringa et al., 2021 and associated discussions within the community). Figure 1 presents the difference in stability of the signal in a voltammetric cell with (Figure 4.1a) and without (Figure 4.1b) conditioning. The conditioning procedure consisted of leaving overnight (at least 8 h) a buffered seawater sample spiked with 25  $\mu\text{mol.L}^{-1}$  of SA and 100  $\text{nmol.L}^{-1}$  Fe in the cell. The cell was then rinsed three times with Milli-Q water before measuring in a new buffered seawater sample containing 25  $\mu\text{mol.L}^{-1}$  of SA but no added Fe (Figure 4.1a). A high initial FeSA peak was observed, suggesting that the three Milli-Q rinses did not efficiently remove precipitated excess Fe. The initial signal was stable over 5 scans, and DFe additions of 4  $\text{nmol.L}^{-1}$  performed in the same sample showed a stable signal. A lack of linearity was observed between the peak heights of with the DFe additions. This can be explained by the presence of natural organic ligands in the sample, which will impact the total Fe concentration calculated, and thus impede efforts to determine whether the conditioning step results in overall contamination of sample. Following the three Milli-Q rinses and the analysis of a buffered seawater sample containing 25  $\mu\text{mol.L}^{-1}$  SA, the next sample was not contaminated (Figure 4.2). The stability of the FeSA peak in subsequent scans was similar if the conditioning solution was spiked or not with 25  $\mu\text{mol.L}^{-1}$  of SA, suggesting that the conditioning was only dependent on the saturation of the binding sites for Fe in the PTFE voltammetric cell.

The optimal conditioning procedure for the PTFE voltammetric cell consisted of leaving overnight a seawater sample spiked with 10  $\text{mmol.L}^{-1}$  of borate buffer and 100 to 300  $\text{nmol.L}^{-1}$  of Fe, to clean the cell from potential carried-over DFe with a seawater sample containing 10  $\text{mmol.L}^{-1}$  of borate buffer and 25  $\mu\text{mol.L}^{-1}$  of SA for 10 min, and, finally, to rinse it 3 times with Milli-Q. Following this procedure, the signal was stable over weeks of analysis if the cell is only rinsed with Milli-Q or seawater sample



(Figure 4.1a) and not with acid (Figure 4.1b). During the analysis of a sample, the cell is not rinsed between the aliquots. When not used, the cell is kept filled with Milli-Q.

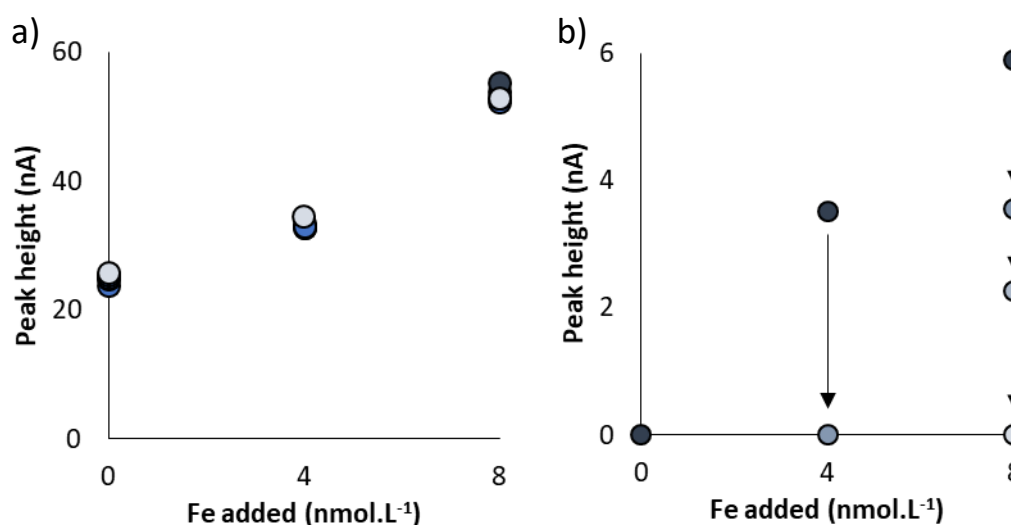


Figure 4.1. Stability of the FeSA reduction signal in a buffered open-ocean seawater sample containing  $25 \mu\text{mol.L}^{-1}$  after a) overnight conditioning with  $100 \text{ nmol.L}^{-1}$  of and b) deconditioning of the cell by 15 min rinse with  $0.5 \text{ mol.L}^{-1}$  HCl. 5 scans were recorded if the peak was stable, or until the signal reached 0 nA if unstable. For each DFe addition, the first voltammogram recorded are darkest and become paler with time (90 s between voltammograms with 60 s deposition time).

Similar to the voltammetric cell, a specific methodology was empirically developed to condition the tubes (Metal Free, Labcon<sup>TM</sup>) used to prepare the aliquots of the samples. The best results in terms of reproducibility of the titrations and absence of outlier aliquots were obtained with a two-step procedure. Firstly, the tubes are left for one week with a buffered seawater sample spiked with  $25 \mu\text{mol.L}^{-1}$  of SA, and DFe concentration ranging from  $50 \text{ nmol.L}^{-1}$  to 10-fold the DFe that was used to titrate the ligands (e.g. step 1 in Table 4.1). Secondly, after rinsing each tube 3 times with Milli-Q, they were left with a buffered seawater sample with  $25 \mu\text{mol.L}^{-1}$  of SA and with the corresponding DFe additions chosen for the titration (e.g. step 2 in Table 4.1). This second equilibration step lasted for at least two days. Then, titrations can be prepared and left to equilibrate following the chosen procedure (e.g. sequential or overnight). For most set of tubes, several titrations were needed to obtain reproducible results. The tubes were rinsed three time with Milli-Q water between each sample, or filled with Milli-Q and stored at room temperature in the dark when not in use. Attempts to condition the tubes with lower DFe concentrations resulted in the lower FeSA signal in our reference seawater, and the curvature shown in Figure 4.2 was missed due to the emergence of a quantifiable peak at too high DFe additions. Because

using a longer deposition time did not resolve the issue, we concluded that the loss of signal was not explained by lower sensitivity but by adsorption onto the tube walls. Faster conditioning of the tubes was also attempted in the absence of SA, but resulted in persistent Fe release from the tube evidenced by a strong FeSA signal in aliquots of low DFe addition and linearity of the titration, suggesting a lack of stability of the conditioning. We recommend using bulk open ocean seawater available at a sufficient volume both to condition all set of tubes and the cell, and also as a reference seawater to check the conditioning. Ideally, the type of water used for conditioning and as a reference is collected in the same area that the samples, to have similar DFe and FeL concentrations.

Table 4.2. DFe concentrations in  $\text{nmol.L}^{-1}$  to be added in 5 mL of seawater sample with 25  $\mu\text{M}$  of SA and 10 mM of borate buffer for conditioning of Metal Free (Labcon<sup>TM</sup>) tubes and ligand titration as used in this study. Note that recommendations are different for voltammetric cells.

DFe to be used in the tube	0	0	0.8	1.6	2.5	3	3.5	4	4.5	5	6	7	8	10	12	15
DFe for step 1	50	50	50	50	50	50	50	50	50	50	60	70	80	100	120	150
DFe for step 2	0	0	0.8	1.6	2.5	3	3.5	4	4.5	5	6	7	8	10	12	15

The difference in the conditioning process between the PTFE voltammetric cell and the Metal Free Labcon<sup>TM</sup> tubes is possibly explained by the different material used, each material having specific adsorption properties (Gerringa et al., 2021). The strength of the adsorption could vary from one material to another, and therefore, the adsorbed compounds could be more or less labile. But this is not enough to explain fully our results. Previous authors experienced strong signal decrease with the use of SA, but not with TAC, although similar materials were used (Gerringa et al., 2021). This implies that the conditioning process is specific to SA. The processes at play are unclear but our observations suggest the saturation of adsorption sites for DFe for the PTFE cell, and the formation of inert  $\text{FeSA}_x$  species that saturate active adsorption sites of the tubes, preventing further adsorption of Fe while being sufficiently inert to not be redissolved into the low Fe sample solutions. The application of the conditioning procedures established above for the voltammetric cell and the tubes leads to very

reproducible scans in the same open ocean water as used for the conditioning (Figure 4.2). The high FeSA peak height measured for the first aliquot analysed, one of the two without DFe added, is explained by the carried-over DFe of the last aliquot of a previous sample. It suggested that in case of quick emergence of the FeSA reduction current peak, a third initial point should be implemented to ensure the good quality of the initial duplicate measured. In our application, most titrations show the emergence of the FeSA signal from 2 nmol.L<sup>-1</sup> to 5 nmol.L<sup>-1</sup> of DFe added, meaning that the multiple analysis of an aliquot giving no signal is not necessary.

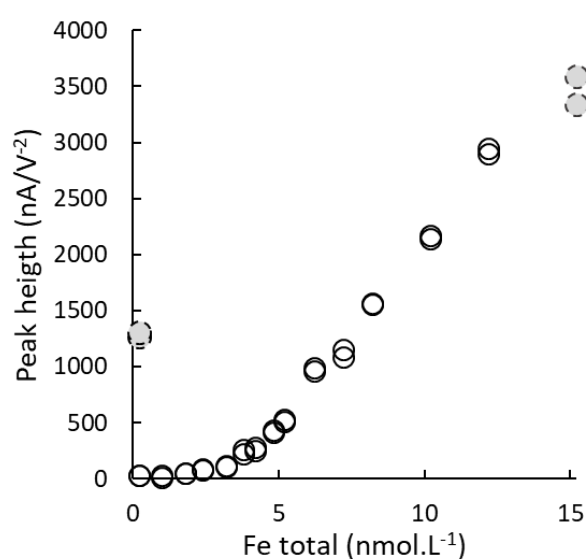


Figure 4.2. Titration of the open ocean seawater used for voltammetric cell and tubes conditioning with 25  $\mu\text{mol.L}^{-1}$  of SA and buffered at 8.18 with 10  $\text{mmol.L}^{-1}$  of borate. Duplicates were recorded with a deposition time and potential of 60 s and 0.05 V, respectively. The sample was equilibrated following the sequential procedure equilibration. The black empty dots represent the data selected to determine [L] and  $\log K_{\text{FeL,Fe}}^{\text{cond}}$  (procedure detailed hereafter). Grey dashed dots represent the discarded data, corresponding to carry-over Fe in the cell from previous analysis at the start of the titration, and saturation of the working electrode with the last aliquot.

#### 4.3.2. Effect of the deposition potential

The impact of the deposition potential on the FeSA reduction current was investigated in a buffered seawater sample containing 25  $\mu\text{mol.L}^{-1}$  of SA (Figure 4.3). The experiment was performed several times, twice starting at -0.10 V up to +0.06 V, and twice starting at +0.06 V down to -0.10 V. Increments were of 0.02 V. By applying a deposition potential of 0.05 V, the sensitivity of the method is increased

by around 3-fold and 1.8-fold compared to the previously applied values of -0.05 V (Rue and Bruland, 1995) and 0 V used by (Abualhaija and van den Berg, 2014; Buck et al., 2007). A deposition potential above 0 V was previously attempted (Buck et al., 2007) but resulted in a progressive decrease of the signal. In our case, the signal is stable and we attribute this stability to the use of a glass bridge that might prevent any reductive side-reactions at the counter electrode (Chapter 3), although the hypothesis was not tested. The sensitivity of the SA method is known to decrease with the sample's depth (Buck et al., 2018, 2015, 2007; Rue and Bruland, 1995). These authors observed an overall lower sensitivity in deep samples collected in the Pacific compared to the Atlantic, and attributed this change to the composition or structure of the DOM with the aging of water masses (Buck et al., 2018). The sensitivity loss is generally compensated by the deposition time used, ranging from 90 s to 600 s in Pacific Ocean samples (Buck et al., 2018). The deposition time required in our study with a deposition potential of 0.05 V ranged from 45 s in surface samples to 120 s in deep samples collected in the Western Tropical South Pacific. It is well known that the adsorption of organic compounds can lower the sensitivity of the ACSV method of Fe detection (e.g. Yokoi and van den Berg, 1992). Our results suggest that a higher deposition potential limits the adsorption of negatively charged refractory DOM at the mercury electrode. Higher deposition potentials than +0.07 V were not tested to avoid extensive oxidation of the mercury electrode and a deposition potential of +0.05 V was chosen, which allowed analysis of a complete titration of 16 aliquots with triplicate voltammograms in less than 1 h even for deep samples showing lower sensitivity (e.g. Buck et al., 2018, 2007; Cabanes et al., 2020).

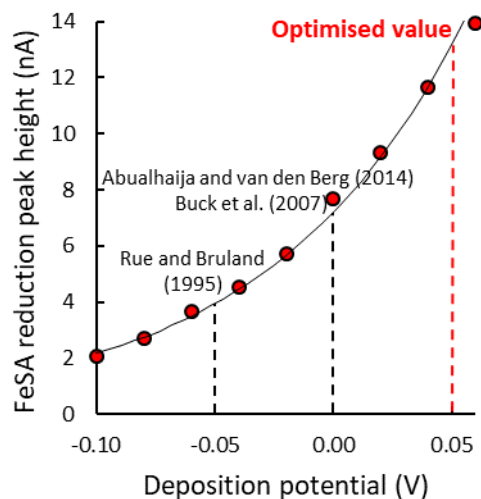


Figure 4.3. Reduction current of the FeSA peak after 45 s deposition as a function of the deposition potential applied in a seawater sample buffered to pH 8.18 containing  $25\mu\text{mol.L}^{-1}$  of SA. Previously published values (-0.05 V and 0.00 V) and the one selected in this study (0.05 V) are noted.

#### 4.3.3. Procedure for the interpretation of ligand titrations

Despite the development of software to ease and facilitate the interpretation of ligand titrations (e.g. Omanović et al., 2015), the impact of choices made by the analyst during the interpretation can impact the results and limit the comparability of datasets (Pižeta et al., 2015). The result is notably impacted by the choice of the mathematical treatment used to retrieve the  $\log K_{\text{FeL,Fe}}^{\text{cond}}$  of the natural ligand, by the definition of the sensitivity of the method (e.g. Omanović et al., 2015) and by the data selection of the analyst (Buck et al., 2012). We propose a procedure to treat titration data in a systematic way to statistically and automatically exclude potential outliers without bias or subjectivity, and to model ligand characteristics using simultaneously the most common fittings currently in use (Gerringa et al., 2014; Ružić, 1982; Scatchard, 1949; van den Berg, 1982).

The first step was to assess how to best define the sensitivity of the measurement. The optimisation of the definition of the sensitivity should be tested for every dataset. We suggest to perform duplicate analyses of several samples and to compare them as in Table 4.3. In this work, we compared the use of the peak heights from the three last linear aliquots with the mathematical fit proposed in ProMCC. To do so, replicate titrations were fitted using both definitions, the differences between duplicates in [L]

( $\Delta[L]$ ) and in  $\log K_{\text{FeL,Fe}'}^{\text{cond}}$  ( $\Delta\log K_{\text{FeL,Fe}'}^{\text{cond}}$ ) were determined, and the standard deviations of the  $\Delta[L]$  and  $\Delta\log K_{\text{FeL,Fe}'}^{\text{cond}}$  obtained with each mode compared. Then, the dispersion was calculated, relative to the mean value. For  $[L]$ , the standard deviation was divided by the mean  $[L]$  of the titrations, while for  $\log K_{\text{FeL,Fe}'}^{\text{cond}}$ , the standard deviation was divided by the acknowledged range of values covered by a single detection window (2; Apte et al., 1988; Gerringa et al., 2014). The most consistent results were obtained by defining the sensitivity with the 3 last aliquots of the titration, with 22% of dispersion for  $\Delta[L]$ , against 46% for the mathematical fitting. Differences for  $\Delta\log K_{\text{FeL,Fe}'}^{\text{cond}}$  were in comparison negligible. The definition of the sensitivity with the 3 last aliquots has been implemented in our procedure. Despite recommendations from Gerringa et al. (2014) to use 4 aliquots, our results showed that in our case the accuracy was not impacted by the use of 3 or 4 aliquots (results not shown). The options offered by the software ProMCC of linear or logarithmic fitting of the sensitivity did not limit the dispersion of the calculated  $[L]$  (results not shown).

Table 4.3. Differences in  $[L]$  and  $\log K_{\text{FeL,Fe}'}^{\text{cond}}$  on duplicate analyses due to the definition of the sensitivity during titration data fitting. The dispersion corresponds to the standard deviation divided by the mean  $[L]$  for  $\Delta[L]$ , and by the acknowledged range covered by a single detection window for  $\Delta\log K_{\text{FeL,Fe}'}^{\text{cond}}$  (2; Apte et al., 1988; Gerringa et al., 2014).

Definition of the sensitivity	With the 3 last aliquots		Fitted by ProMCC	
Sample label	$\Delta[L]$ (nmoleqFe.L <sup>-1</sup> )	$\Delta\log K_{\text{FeL,Fe}'}^{\text{cond}}$	$\Delta[L]$ (nmoleqFe.L <sup>-1</sup> )	$\Delta\log K_{\text{FeL,Fe}'}^{\text{cond}}$
ST6-21	0.0	0.3	-0.7	0.1
ST6-20	3.0	-0.5	8.1	-0.3
ST6-11	0.5	0.0	0.6	0.0
ST6-7	-0.6	-0.5	3.6	-0.6
ST6-5	0.5	-0.3	2.4	-0.3
ST6-3	-1.7	0.0	-2.2	-0.1
ST2-7	0.0	-0.2	3.2	-0.3
ST7-17	0.0	0.1	0.7	0.0
ST7-17_2	-0.8	-0.1	-1.5	0.0
Standard deviation	1.3	0.3	3.2	0.2
<b>Dispersion</b>	<b>22%</b>	<b>14%</b>	<b>46%</b>	<b>11%</b>

The procedure developed for the interpretation of ligand titration relies on the combined use of ProMCC and of the spreadsheet specifically prepared to keep track of the fitting performed and define the quality flag of the titration (Figure 4; Annex 3 and 4). A step-by-step description of the procedure is detailed in Annex 3 and included within the spreadsheet (Annex 4).

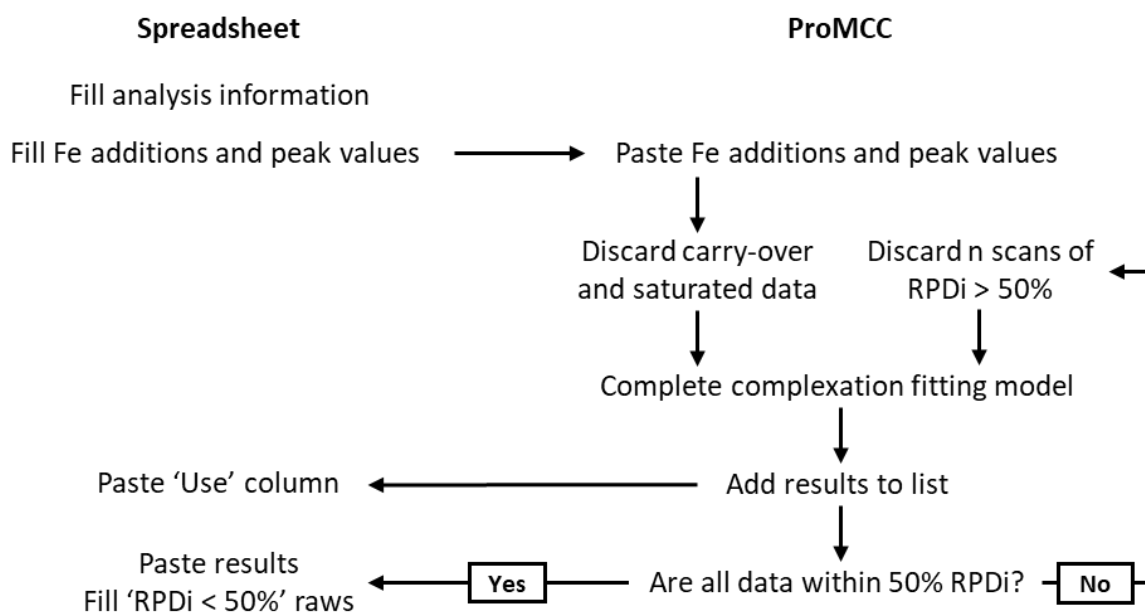


Figure 4.4. Diagram describing the procedure developed for the interpretation of ligand titration data, with n corresponding to the number of voltammograms recorded for each aliquot. RPDi is the Relative Percentage Difference.

Briefly, the user first needs to enter analysis information as requested and add the titration data to both the spreadsheet and ProMCC. From ProMCC, a pre-selection is made, based on the visual presence of carry-over Fe (high values for the first aliquot) or saturation at the end of the titration (flattening of the curve; Figure 4.2). A first fitting is then performed, with the result being added to the results list and the titration data saved in the spreadsheet. Following this, the graphical error of the titration presented as relative percentage difference (RPDi) calculated in ProMCC is used: data points with an RPDi higher than 50% are discarded, in order of decreasing RPDi values. The RPDi values for all data from all aliquots are considered, because this step aims to discard voltammograms of poor quality, not to evaluate the validity of an aliquot. Following this process, if all voltammograms of an aliquot have an issue (e.g. due to contamination or problem during the preparation), they will be discarded anyway. Following each data deletion step, the 'Complete Complexation Fitting Model' fit is applied in

ProMCC. The number of data points to be discarded for each fitting corresponds to the number of voltammogram recorded per aliquot (e.g. 3 points can be discarded if triplicates were recorded, 2 points if duplicates, etc...). The data deletion and fitting steps are reproduced until all data show an RPDi < 50%. The result of each fitting and the used data must be saved in the spreadsheet for traceability of the treatment process. The RPDi used to define the validity of the data is automatically calculated in ProMCC, and, therefore, the data selection is not impacted by the analyst.

#### 4.3.4. Automated determination of the quality flag within the spreadsheet

A quality flag (QF) system was implemented to rapidly visualise the confidence in the results with values ranging from 1 to 4, 1 being highly confident. The motive for such QF are that the values of [L] and  $\log K_{\text{FeL,Fe}'}^{\text{cond}}$  obtained through the data fitting is dependent on the quality of the titration data, which is not always clearly stated by authors. Additionally, to our knowledge, there is no open access tools to keep track of the choices made when fitting titration data (e.g. how many data points were discarded, which ones, how was the sensitivity defined, etc...). This motivated the development of a spreadsheet combining the record of the metadata of the analysis, the record of the titration data, and the visualisation of the whole and selected complexometric data. The spreadsheet is meant to be used in tandem with ProMCC. This spreadsheet (Annex 4) is perfectible and is open to user's suggestions.

The QF value is based on three aspects. The first relates to the number of fittings performed during the data selection procedure to reach a RPDi below 50% for all data points, with the QF being equal to the number of fittings performed. The second, automated, relies on the errors on [L] and  $\log K_{\text{FeL,Fe}'}^{\text{cond}}$ , and the averaged error given by ProMCC. For [L], an error of  $\pm 0.5 \text{ nmoleqFe.L}^{-1}$  is accepted. This value corresponds to  $\pm 10\%$  of the averaged [L] observed in our analyses. It should be systematically determined for each individual dataset. For  $\log K_{\text{FeL,Fe}'}^{\text{cond}}$ , an error of  $\pm 0.2$  is accepted, corresponding to  $\pm 10\%$  of the range of 2 unit of  $\log K_{\text{FeL,Fe}'}^{\text{cond}}$  covered by an analytical window (Apte et al., 1988; Gerringa et al., 2014). Therefore, the limit of the criteria on the average error calculated by ProMCC as root-mean-square error (RMSE) is 20% (to correspond to  $\pm 10\%$ ). If two of the tests performed on [L],  $\log$



$K_{\text{FeL,Fe}'}^{\text{cond}}$  and average error are successful, the QF value previously defined by the number of fittings performed to reach  $\text{RPDi} < 50\%$  is lowered by one (meaning the confidence is increased).

The third aspect defining the QF relies on the convergence of the fittings. Indeed, successive fittings can lower the error on the parameters, but the parameter can show similar results in terms of [L] and  $\log K_{\text{FeL,Fe}'}^{\text{cond}}$  despite data points having been discarded. Therefore, the appropriate QF to be retained for the titration should correspond to the first fitting reaching the value that will be saved for the titration. An automated verification was implemented to check the convergence of [L] and  $\log K_{\text{FeL,Fe}'}^{\text{cond}}$  along successive fittings and data selection. The QF is lowered by one if the values change by less than 20% of the method accuracy, so by  $0.1 \text{ nmoleqFe.L}^{-1}$  for [L] and by 0.04 for  $\log K_{\text{FeL,Fe}'}^{\text{cond}}$ . The rules to define the QF based on the error and on the convergence of the fittings are not cumulative, meaning that the QF cannot be lowered by more than one level.

#### 4.3.5. Reproducibility of ligand titrations

The reproducibility of ligand titration and data treatment using  $25 \mu\text{mol.L}^{-1}$  of SA and a sequential equilibration procedure was compared on 39 samples run in duplicate. Results are presented in Table 4.4 and ordered along their sampling depth, from shallowest to deepest. The samples were randomly chosen within a set collected in the Western South Tropical Pacific in 2019 (Guieu and Bonnet, 2019) to cover a large range of biogeochemical conditions (e.g. DFe from  $0.18 \text{ nmol.L}^{-1}$  to  $1.09 \text{ nmol.L}^{-1}$ ; Tillette et al., 2022; Chapter 5). Therefore, the evaluation of the titration uncertainty on [L] and  $\log K_{\text{FeL,Fe}'}^{\text{cond}}$  can be used as reference boundaries for other open ocean studies considering a single class of ligand and using a similar procedure as ours.

The average uncertainty of [L] determination was  $\pm 0.6 \text{ nmoleqFe.L}^{-1}$ , roughly corresponding to  $\pm 10\%$  of the average [L] value of  $5.1 \text{ nmoleqFe.L}^{-1}$ . The average uncertainty in  $\Delta \log K_{\text{FeL,Fe}'}^{\text{cond}}$  was of  $\pm 0.2$ , corresponding to  $\pm 10\%$  of the lower range of 2 units of  $\log K_{\text{FeL,Fe}'}^{\text{cond}}$  covered by a single detection window (Apte et al., 1988; Gerringa et al., 2014). The duplicate analyses presented above have shown  $\Delta[\text{L}]$  ranging from 0.0 to  $3.0 \text{ nmoleqFe.L}^{-1}$  and  $\Delta \log K_{\text{FeL,Fe}'}^{\text{cond}}$  ranging from 0.0 to 0.9. There was no

correlation for  $\Delta[L]$  and  $\Delta\log K_{\text{FeL,Fe}'}^{\text{cond}}$  with either the QF, DFe concentration, depth, location, or time between replicates (ranging from a few hours up to three weeks). Overall, the standard deviation of  $\Delta[L]$  and  $\Delta\log K_{\text{FeL,Fe}'}^{\text{cond}}$  values was of 1.1 (i.e.  $\pm 0.6$ ) nmoleqFe.L<sup>-1</sup> and 0.4 (e.g.  $\pm 0.2$ ), respectively, meaning that the difference between the replicates is statistically within the uncertainty of the parameter determination for [L] of 0.6 nmoleqFe.L<sup>-1</sup> and for  $\log K_{\text{FeL,Fe}'}^{\text{cond}}$  of 0.2, respectively. The difference between replicates, or the difference between the titrations, can originate from technical issues from the voltammetric systems, sample preparation and/or sample thawing as well as other unidentified sources of uncertainty.

Table 4.4. FeL characteristics of duplicate samples from the Western South Tropical Pacific prepared following the sequential equilibration procedure. The QF is defined as in Section 4.3.4.

Sample label	Depth (m)	[L] (nmoleqFe.L <sup>-1</sup> )	$\log K_{\text{FeL,Fe}'}^{\text{cond}}$	QF	$\Delta[L]$ (nmoleqFe.L <sup>-1</sup> )	$\Delta\log K_{\text{FeL,Fe}'}^{\text{cond}}$
ST6-23	25	4.8 ± 0.5	11.8 ± 0.4	1	0.2	-0.1
		4.7 ± 0.4	11.9 ± 0.2	2		
ST4-23	39	4.5 ± 0.7	11.4 ± 0.2	2	-0.3	0.1
		4.8 ± 0.5	11.3 ± 0.2	1		
ST7-23	40	5.2 ± 0.4	12.0 ± 0.1	1	0.4	0.5
		4.8 ± 0.6	11.5 ± 0.2	3		
ST6-21	55	5.2 ± 0.5	11.9 ± 0.2	1	0.0	0.3
		5.3 ± 0.9	11.6 ± 0.2	3		
ST6-20	62	7.6 ± 1.6	11.3 ± 0.3	1	3.0	-0.5
		4.7 ± 0.6	11.8 ± 0.2	2		
ST4-20	102	6.2 ± 0.9	11.5 ± 0.2	2	1.3	-0.4
		4.9 ± 0.4	11.9 ± 0.2	3		
ST4-19	120	5.7 ± 0.7	11.7 ± 0.2	1	2.0	-0.2
		3.7 ± 0.6	11.9 ± 1.0	1		
ST4-17	200	5.1 ± 0.5	11.9 ± 0.2	3	-0.6	0.1
		5.7 ± 0.6	11.8 ± 0.2	3		
ST7-19	200	4.7 ± 0.8	11.3 ± 0.2	3	-0.3	-0.9
		5.0 ± 0.4	12.2 ± 0.2	1		
ST6-11	300	4.9 ± 0.6	11.8 ± 0.2	3	0.5	0.0
		4.4 ± 0.4	11.8 ± 0.2	2		

ST7-17	350	4.0 ± 0.8	11.4 ± 0.3	3	0.0	0.1
		4.0 ± 0.6	11.3 ± 0.2	2		
ST7-17	350	4.0 ± 0.8	11.4 ± 0.3	3	-0.8	-0.1
		4.8 ± 0.6	11.5 ± 0.2	2		
ST6-7	490	6.2 ± 1.3	11.1 ± 0.3	4	-0.6	-0.5
		6.8 ± 0.7	11.7 ± 0.1	2		
ST6-5	640	5.7 ± 0.5	11.7 ± 0.1	2	0.5	-0.3
		5.2 ± 0.5	12.0 ± 0.2	3		
ST10-T3-7	647	5.8 ± 0.7	10.7 ± 0.1	1	0.3	-0.9
		5.5 ± 0.6	11.6 ± 0.2	1		
ST7-15	670	4.8 ± 0.6	11.7 ± 0.2	2	1.9	-0.4
		2.9 ± 0.4	12.1 ± 0.5	3		
ST6-3	800	4.6 ± 0.6	11.3 ± 0.2	1	-1.7	0.0
		6.3 ± 1.1	11.3 ± 0.2	2		
ST7-13	1050	3.8 ± 0.5	11.8 ± 0.3	2	0.7	0.1
		3.1 ± 0.4	11.8 ± 0.3	2		
ST7-13	1050	3.8 ± 0.5	11.8 ± 0.3	2	0.6	0.4
		3.2 ± 0.5	11.5 ± 0.3	1		
ST2-7	1800	9.3 ± 1.0	11.5 ± 0.2	1	0.0	-0.2
		9.3 ± 0.9	11.7 ± 0.2	3		
<b>Mean ± standard deviation:</b>					<b>-0.2 ± 0.4</b>	<b>0.2 ± 0.1</b>

The  $\Delta[L]$  of 80% of the data are within  $\pm 10\%$  of the mean  $[L]$  value (e.g.  $\pm 0.5$  nmoleqFe.L<sup>-1</sup> here), and 75% of the  $\Delta \log K_{\text{FeL,Fe}'}^{\text{cond}}$  are within  $\pm 10\%$  of the 2 units range of  $\log K_{\text{FeL,Fe}'}^{\text{cond}}$  covered by a single detection window (e.g.  $\pm 0.2$ ). We conclude that the ligand titrations are accurate at  $\pm 10\%$  for  $[L]$  and at  $\pm 0.2$  for  $\log K_{\text{FeL,Fe}'}^{\text{cond}}$ . These intervals can be used to detect outliers in datasets, considering the relative homogeneity of water masses in the open ocean. Specific care must be taken when considering samples suspected to be biologically dynamic such as surface, coastal, or incubation samples, as our study might not cover the entirety of the biogeochemical conditions that can be encountered in marine systems. We suggest to perform the analysis of multiple replicates within the acquisition of a dataset to

constrain the uncertainty of the values obtained and ease the comparison of such datasets. Currently, replicates of titrations and determination of these uncertainties are seldomly reported.

#### 4.3.6. Comparison of equilibration procedure

Sequential and overnight equilibration procedures were compared on 24 samples (Table 4.5) collected in the Western South Tropical Pacific in 2019 (Guieu and Bonnet, 2019), different that the one used for duplicate analyses (Table 4.4) because of the volume of sample available. The samples are listed along the sampling depth (Table 4.5) and it is apparent that a higher deposition time had to be used for deeper samples, in line with previous studies (e.g. Buck et al., 2018). The deposition time requirement is also on average 1.6-fold lower with the sequential equilibration than with the overnight equilibration. This could be related to the slow formation kinetic of the electro-inactive  $\text{FeSA}_2$  complex (Abualhaija and van den Berg, 2014), and therefore decrease in the detectable  $\text{FeSA}$  concentration in the sample with time. If this is the case, the calibration of the overnight procedure with 25  $\mu\text{M}$  SA should be carried out rather than using the stability constant determined through the sequential procedure. However, the  $\beta_{\text{FeSA}}$  calibrated by Abualhaija and van den Berg (2014) and the  $\beta_{\text{FeSA}_2}$  calibrated by Buck et al. (2007) result in  $\alpha_{\text{FeSA}}$  of 123 and in  $\alpha_{\text{FeSA}_2}$  of 79 for 25  $\mu\text{mol.L}^{-1}$  of SA. This leads to a shift of 0.2 in  $\log K_{\text{FeL,Fe}'}^{\text{cond}}$ , which is still within the uncertainty of the analysis (Section 4.3.5). The slow formation of an electro-inactive  $\text{FeSA}_2$  complex is a problem that can be avoided by using a lower SA concentration (e.g. 5  $\mu\text{mol.L}^{-1}$ ) while still keeping a long equilibration time, as recommended previously (Abualhaija and van den Berg, 2014; Gerringa et al., 2021).

Table 4.5. Comparison of the sequential and overnight equilibration procedure on FeL characteristics. The determination of the QF is detailed in Section 4.3.4.

Sample label	Depth (m)	Equilibration	[L] (nmoleqFe <sup>-1</sup> )	log K <sub>FeL,Fe'</sub> <sup>cond</sup>	QF	Deposition time (s)	Δ[L] (nmoleqFe.L <sup>-1</sup> )	Δlog K <sub>FeL,Fe'</sub> <sup>cond</sup>	Deposition time ratio
ST10-T3-23	15	Sequential	8.8 ± 0.7	11.9 ± 0.2	1	20	-0.1	-0.3	1.5
		Overnight	8.7 ± 0.6	11.6 ± 0.1	1	30			
ST10-T3-21	35	Sequential	5.2 ± 0.3	12.0 ± 0.2	1	20	0.2	0.0	1.5
		Overnight	5.4 ± 0.4	12.0 ± 0.2	1	30			
ST2-23	35	Sequential	3.1 ± 0.4	11.3 ± 0.2	1	45	3.1	0.1	2
		Overnight	6.2 ± 0.8	11.4 ± 0.2	2	90			
ST4-23	39	Sequential	4.5 ± 0.7	11.4 ± 0.2	2	45	0.2	-0.1	2
		Overnight	4.7 ± 0.6	11.3 ± 0.2	3	90			
ST2-21	73	Sequential	2.8 ± 0.4	11.3 ± 0.2	1	45	0.8	0.1	2
		Overnight	3.6 ± 0.7	11.4 ± 0.3	1	90			
ST10-T3-17	75	Sequential	5.8 ± 0.5	11.7 ± 0.2	1	30	2.6	-0.2	1
		Overnight	8.4 ± 0.7	11.5 ± 0.1	2	30			
ST4-20	102	Sequential	4.9 ± 0.4	11.9 ± 0.2	2	45	-2.2	0.3	2
		Overnight	2.7 ± 0.5	12.2 ± 0.5	3	90			
ST2-19	105	Sequential	5.0 ± 1.1	11.1 ± 0.3	2	45	1.2	0.2	1.3
		Overnight	6.2 ± 1.0	11.3 ± 0.2	2	60			
ST2-17	151	Sequential	3.7 ± 0.4	11.9 ± 0.2	3	35	3.1	-0.4	1.7
		Overnight	6.8 ± 1.2	11.5 ± 0.2	2	60			
ST10-T3-12	187	Sequential	3.9 ± 0.4	11.9 ± 0.2	1	30	2.3	-0.3	1
		Overnight	6.2 ± 0.7	11.6 ± 0.2	1	30			
ST2-15	303	Sequential	5.4 ± 0.8	11.5 ± 0.2	1	45	0.5	-0.6	2
		Overnight	5.9 ± 2.0	10.9 ± 0.3	4	90			
ST10-T3-9	389	Sequential	5.7 ± 0.9	11.4 ± 0.2	3	25	0.3	-0.2	1.6
		Overnight	6.0 ± 0.9	11.2 ± 0.2	1	40			

ST10-T3-8	510	Sequential	5.3 ± 0.6	11.8 ± 0.2	1	25	0.0	-0.5	1.6
		Overnight	5.3 ± 0.8	11.3 ± 0.2	1	40			
ST2-13	550	Sequential	6.9 ± 2.2	10.5 ± 0.2	3	35	0.3	0.6	1.7
		Overnight	7.2 ± 1.1	11.1 ± 0.2	1	60			
ST10-T3-7	647	Sequential	5.8 ± 0.7	10.7 ± 0.1	1	30	-0.1	0.4	1.7
		Overnight	5.7 ± 0.9	11.1 ± 0.2	2	50			
ST10-T3-1	701	Sequential	5.3 ± 0.5	12.0 ± 0.2	1	30	0.6	-0.7	1.7
		Overnight	5.9 ± 0.9	11.3 ± 0.2	3	50			
ST2-11	797	Sequential	5.2 ± 0.6	11.7 ± 0.2	2	45	2.2	-0.5	1.3
		Overnight	7.4 ± 1.4	11.2 ± 0.3	2	60			
ST8-15	800	Sequential	4.2 ± 0.8	11.4 ± 0.4	2	45	0.6	-0.7	2
		Overnight	4.8 ± 1.5	10.7 ± 0.3	2	90			
ST8-13	1089	Sequential	3.7 ± 0.4	11.8 ± 0.2	1	45	2.5	-0.7	2
		Overnight	6.2 ± 1.2	11.1 ± 0.3	1	90			
ST2-9	1200	Sequential	8.1 ± 0.9	11.2 ± 0.2	1	45	-2.2	0.3	1.3
		Overnight	5.9 ± 0.6	11.5 ± 0.2	1	60			
ST2-7	1800	Sequential	9.3 ± 1.0	11.5 ± 0.2	3	80	-2.3	0.5	1.5
		Overnight	7.0 ± 1.9	11.0 ± 0.2	1	120			
ST8-11	1899	Sequential	5.3 ± 0.6	11.5 ± 0.2	2	60	0.5	0.0	1
		Overnight	5.8 ± 0.6	11.5 ± 0.2	1	60			
ST8-10	2400	Sequential	5.7 ± 0.5	11.3 ± 0.1	1	45	-0.2	0.0	1.3
		Overnight	5.5 ± 0.8	11.3 ± 0.2	2	60			
ST2-1	3446	Sequential	5.2 ± 0.6	11.7 ± 0.2	2	120	-0.6	-0.4	1.3
		Overnight	4.6 ± 0.7	11.3 ± 0.3	1	150			
<b>Mean ± standard deviation:</b>							<b>0.6 ± 1.5</b>	<b>-0.2 ± 0.4</b>	<b>1.6 ± 0.3</b>

It has been suggested that a shorter equilibration time could overestimate  $[L]$  and  $\log K_{FeL,Fe}^{cond}$ , as some dissociation kinetic of complexes of Fe and natural ligands could be too slow (Gerringa et al., 2021, 2014). Here, it was decided to use the same SA concentration of  $25 \mu\text{mol.L}^{-1}$  for sequential and overnight equilibration to state the impact of the equilibration time on derived complexation parameters. The samples have been randomly selected across a wide range of depth and trophic regimes to verify if the two equilibration procedures are converging or not, depending on the biogeochemical conditions and, potentially, on the ligand pool composition. ST8 was sampled in the oligotrophic South Pacific Gyre, ST10-T3 and ST4 in the Lau Basin, hotspot of diazotrophic activity (Bonnet et al., 2017), with ST10-T3 in the Eastern Lau Basin and subject to surface and bottom DFe enrichment (Tilliette et al., 2022). ST2 was sampled in the Melanesian Basin in which strong thiol concentrations have been measured at several depths (Portlock et al., in prep.). In this dataset, 13 comparisons out of 24 are showing a  $\Delta[L]$  within  $\pm 10\%$  of the mean value, and 9 out of 24 comparisons show a  $\Delta\log K_{FeL,Fe}^{cond}$  within  $\pm 0.2$  (54% and 38% of the 24 comparisons performed, respectively). None of the comparison performed at ST2 show converging values of both  $\Delta[L]$  and  $\Delta\log K_{FeL,Fe}^{cond}$ , which could be related to specificities of the DOM. It does strongly suggest that the composition of the DOM can impact the equilibration kinetics of the sample.

The absence of pattern for the increase or decrease of  $[L]$  and  $\log K_{FeL,Fe}^{cond}$ , between the two equilibration procedures questions the establishment of the steady-state equilibrium of the partitioning of Fe between natural and added ligands in some samples. In view of our results, it is not possible to recommend one of the procedures over the other, even if the sequential procedure requires lower deposition time and, therefore, requires less time for the analysis of the samples. It is, as well, the one minimising the formation of  $\text{FeSA}_2$ , which is thought to be a limiting factor of the method at higher equilibration time (Gerringa et al., 2021). With this comparison, we also state that differences with other methods using overnight equilibration cannot be attributed only to the lack of equilibrium using sequential equilibration as stated in latest comparison studies (e.g. with TAC; Ardiningsih et al., 2021; Gerringa et al., 2021). However, our results suggest further investigation of the impact of the equilibration procedure on the results obtained by CLE-ACSV using SA.

## 4.4. Conclusion

We present in this paper a suite of recommendations that will hopefully improve and ease the use of SA as an artificial ligand to investigate DFe speciation by CLE-ACSV. The conditioning, voltammetric and voltammogram treatment procedures should help users to apply the SA method, while the titration fitting procedure should improve comparison of results between laboratories. The titration fitting spreadsheet and procedure are, however, perfectible in ways that will only be revealed by more comparative studies and collaborative work. The automated definition of the QF implemented in this work could have a limited applicability with regards to the reproducibility and accuracy of other methods. However, this can be easily overcome and adjusted. We believe that the use of such tools and procedures is a necessity to reach better data quality, reduce subjective bias, and improve data comparison between laboratories, ultimately improving our understanding of the organic speciation of trace metals in the ocean. The interpretation procedure developed to lower the impact of the subjectivity of the analyst can be used for the interpretation of organic speciation data regarding any metal and application specificities such as number of aliquots and voltammogram recorded, as long as care is taken to prove the validity of the application as presented here. Essential aspects for the validation of the procedure include tests on the definition of the sensitivity, and estimation of the application uncertainty by estimation of the reproducibility. Our comparison of equilibration procedures (sequential *versus* overnight) did not show a systematic shift in [L] and  $\log K_{\text{FeL,Fe}}^{\text{cond}}$ , but a rather spread range of differences across samples. The impact of the equilibration time on the CLE-ACSV results obtained should be explored further in future studies, notably on reference compounds such as siderophores and humic-like material to better constrain the limits of the two equilibration methods currently in use and the exchange kinetic between the natural binding ligands and the added SA. The equilibration kinetic for DFe against SA could be a way to discriminate different kind of ligands or binding-sites in natural samples. Such experiment has already been tested but on the time scale of hours to days (Croot and Heller, 2012; Witter and Luther, 1998; Wu and Luther, 1995), notably limited regarding the analysis time. Our optimised SA method with lower analysis time could allow the investigation of the equilibration kinetic in the time scale minutes to hours, opening a way to further explore this field.



## 4.5. References

- Abualhaija, M.M., van den Berg, C.M.G., 2014. Chemical speciation of iron in seawater using catalytic cathodic stripping voltammetry with ligand competition against salicylaldoxime. *Marine Chemistry* 164, 60–74. <https://doi.org/10.1016/j.marchem.2014.06.005>
- Apte, S.C., Gardner, M.J., Ravenscroft, J.E., 1988. An evaluation of voltammetric titration procedures for the determination of trace metal complexation in natural waters by use of computers simulation. *Analytica Chimica Acta* 212, 1–21. [https://doi.org/10.1016/S0003-2670\(00\)84124-0](https://doi.org/10.1016/S0003-2670(00)84124-0)
- Ardiningsih, I., Zhu, K., Lodeiro, P., Gledhill, M., Reichart, G.-J., Achterberg, E.P., Middag, R., Gerringa, L.J.A., 2021. Iron Speciation in Fram Strait and Over the Northeast Greenland Shelf: An Inter-Comparison Study of Voltammetric Methods. *Front. Mar. Sci.* 7. <https://doi.org/10.3389/fmars.2020.609379>
- Avendaño, L., Gledhill, M., Achterberg, E.P., Rérolle, V.M.C., Schlosser, C., 2016. Influence of Ocean Acidification on the Organic Complexation of Iron and Copper in Northwest European Shelf Seas; a Combined Observational and Model Study. *Front. Mar. Sci.* 3. <https://doi.org/10.3389/fmars.2016.00058>
- Barbeau, K., Rue, E.L., Bruland, K.W., Butler, A., 2001. Photochemical cycling of iron in the surface ocean mediated by microbial iron( iii )-binding ligands. *Nature* 413, 409–413. <https://doi.org/10.1038/35096545>
- Bonnet, S., Caffin, M., Berthelot, H., Moutin, T., 2017. Hot spot of N<sub>2</sub> fixation in the western tropical South Pacific pleads for a spatial decoupling between N<sub>2</sub> fixation and denitrification. *Proceedings of the National Academy of Sciences* 114, E2800–E2801. <https://doi.org/10.1073/pnas.1619514114>
- Boye, M., van den Berg, C.M.G., de Jong, J.T.M., Leach, H., Croot, P., de Baar, H.J.W., 2001. Organic complexation of iron in the Southern Ocean. *Deep Sea Research Part I: Oceanographic Research Papers* 48, 1477–1497. [https://doi.org/10.1016/S0967-0637\(00\)00099-6](https://doi.org/10.1016/S0967-0637(00)00099-6)
- Bressac, M., Guieu, C., Ellwood, M.J., Tagliabue, A., Wagener, T., Laurenceau-Cornec, E.C., Whitby, H., Sarthou, G., Boyd, P.W., 2019. Resupply of mesopelagic dissolved iron controlled by particulate iron composition. *Nature Geoscience* 12, 995–1000. <https://doi.org/10.1038/s41561-019-0476-6>
- Buck, K.N., Gerringa, L.J.A., Rijkenberg, M.J.A., 2016. An Intercomparison of Dissolved Iron Speciation at the Bermuda Atlantic Time-series Study (BATS) Site: Results from GEOTRACES Crossover Station A. *Front. Mar. Sci.* 3, UNSP 262. <https://doi.org/10.3389/fmars.2016.00262>
- Buck, K.N., Lohan, M.C., Berger, C.J.M., Bruland, K.W., 2007. Dissolved iron speciation in two distinct river plumes and an estuary: Implications for riverine iron supply. *Limnology and Oceanography* 52, 843–855. <https://doi.org/10.4319/lo.2007.52.2.0843>
- Buck, K.N., Moffett, J., Barbeau, K.A., Bundy, R.M., Kondo, Y., Wu, J., 2012. The organic complexation of iron and copper: an intercomparison of competitive ligand exchange-adsorptive cathodic stripping voltammetry (CLE-ACSV) techniques. *Limnology and Oceanography: Methods* 10, 496–515. <https://doi.org/10.4319/lom.2012.10.496>
- Buck, K.N., Sedwick, P.N., Sohst, B., Carlson, C.A., 2018. Organic complexation of iron in the eastern tropical South Pacific: Results from US GEOTRACES Eastern Pacific Zonal Transect (GEOTRACES cruise GP16). *Marine Chemistry, The U.S. GEOTRACES Eastern Tropical Pacific Transect (GP16)* 201, 229–241. <https://doi.org/10.1016/j.marchem.2017.11.007>
- Buck, K.N., Sohst, B., Sedwick, P.N., 2015. The organic complexation of dissolved iron along the U.S. GEOTRACES (GA03) North Atlantic Section. *Deep Sea Research Part II: Topical Studies in Oceanography* 116, 152–165. <https://doi.org/10.1016/j.dsr2.2014.11.016>

- Cabanes, D.J.E., Norman, L., Bowie, A.R., Strmečki, S., Hassler, C.S., 2020. Electrochemical evaluation of iron-binding ligands along the Australian GEOTRACES southwestern Pacific section (GP13). *Marine Chemistry* 219, 103736. <https://doi.org/10.1016/j.marchem.2019.103736>
- Chapman, C.S., van den Berg, C.M.G., 2007. Anodic Stripping Voltammetry Using a Vibrating Electrode. *Electroanalysis* 19, 1347–1355. <https://doi.org/10.1002/elan.200703873>
- Croot, P.L., Heller, M.I., 2012. The Importance of Kinetics and Redox in the Biogeochemical Cycling of Iron in the Surface Ocean. *Front. Microbiol.* 3. <https://doi.org/10/ggr9x2>
- Cobelo-García, A., Santos-Echeandía, J., López-Sánchez, D.E., Almécija, C., Omanović, D., 2014. Improving the Voltammetric Quantification of Ill-Defined Peaks Using Second Derivative Signal Transformation: Example of the Determination of Platinum in Water and Sediments. *Anal. Chem.* 86, 2308–2313. <https://doi.org/10.1021/ac403558y>
- Croot, P.L., Johansson, M., 2000. Determination of Iron Speciation by Cathodic Stripping Voltammetry in Seawater Using the Competing Ligand 2-(2-Thiazolylazo)-p-cresol (TAC). *Electroanalysis* 12, 565–576. [https://doi.org/10.1002/\(SICI\)1521-4109\(200005\)12:8<565::AID-ELAN565>3.0.CO;2-L](https://doi.org/10.1002/(SICI)1521-4109(200005)12:8<565::AID-ELAN565>3.0.CO;2-L)
- Fourrier, P., Dulaquais, G., Guigue, C., Giamarchi, P., Sarthou, G., Whitby, H., Riso, R., 2022. Characterization of the vertical size distribution, composition and chemical properties of dissolved organic matter in the (ultra)oligotrophic Pacific Ocean through a multi-detection approach. *Marine Chemistry* 240, 104068. <https://doi.org/10.1016/j.marchem.2021.104068>
- Garnier, C., Pižeta, I., Mounier, S., Benaïm, J.Y., Branica, M., 2004. Influence of the type of titration and of data treatment methods on metal complexing parameters determination of single and multi-ligand systems measured by stripping voltammetry. *Analytica Chimica Acta* 505, 263–275. <https://doi.org/10.1016/j.aca.2003.10.066>
- Gerringa, L.J.A., Gledhill, M., Ardiningsih, I., Muntjewerf, N., Laglera, L.M., 2021. Comparing CLE-AdCSV applications using SA and TAC to determine the Fe-binding characteristics of model ligands in seawater. *Biogeosciences* 18, 5265–5289. <https://doi.org/10.5194/bg-18-5265-2021>
- Gerringa, L.J.A., Herman, P.M.J., Poortvliet, T.C.W., 1995. Comparison of the linear Van den Berg/Ružić transformation and a non-linear fit of the Langmuir isotherm applied to Cu speciation data in the estuarine environment. *Marine Chemistry* 48, 131–142. [https://doi.org/10.1016/0304-4203\(94\)00041-B](https://doi.org/10.1016/0304-4203(94)00041-B)
- Gerringa, L.J.A., Rijkenberg, M.J.A., Thuróczy, C.-E., Maas, L.R.M., 2014. A critical look at the calculation of the binding characteristics and concentration of iron complexing ligands in seawater with suggested improvements. *Environ. Chem.* 11, 114–136. <https://doi.org/10.1071/EN13072>
- Gledhill, M., Achterberg, E.P., Li, K., Mohamed, K.N., Rijkenberg, M.J.A., 2015. Influence of ocean acidification on the complexation of iron and copper by organic ligands in estuarine waters. *Marine Chemistry, Cycles of metals and carbon in the oceans - A tribute to the work stimulated by Hein de Baar* 177, 421–433. <https://doi.org/10.1016/j.marchem.2015.03.016>
- Gledhill, M., Buck, K.N., 2012. The Organic Complexation of Iron in the Marine Environment: A Review. *Front. Microbiol.* 3. <https://doi.org/10.3389/fmicb.2012.00069>
- Gledhill, M., van den Berg, C.M.G., 1994. Determination of complexation of iron(III) with natural organic complexing ligands in seawater using cathodic stripping voltammetry. *Marine Chemistry* 47, 41–54. [https://doi.org/10.1016/0304-4203\(94\)90012-4](https://doi.org/10.1016/0304-4203(94)90012-4)
- Guieu, C., Bonnet, S., 2019. TONGA 2019 cruise, L'Atalante R/V. <https://doi.org/10.17600/18000884>
- Hassler, C., Cabanes, D., Blanco-Ameijeiras, S., Sander, S.G., Benner, R., Hassler, C., Cabanes, D., Blanco-Ameijeiras, S., Sander, S.G., Benner, R., 2019. Importance of refractory ligands and their photodegradation for iron oceanic inventories and cycling. *Mar. Freshwater Res.* 71, 311–320. <https://doi.org/10.1071/MF19213>

- Hassler, C.S., Berg, V.D., G, C.M., Boyd, P.W., 2017. Toward a Regional Classification to Provide a More Inclusive Examination of the Ocean Biogeochemistry of Iron-Binding Ligands. *Front. Mar. Sci.* 4. <https://doi.org/10.3389/fmars.2017.00019>
- Hassler, C.S., Norman, L., Mancuso Nichols, C.A., Clementson, L.A., Robinson, C., Schoemann, V., Watson, R.J., Doblin, M.A., 2015. Iron associated with exopolymeric substances is highly bioavailable to oceanic phytoplankton. *Marine Chemistry, SCOR WG 139: Organic Ligands – A Key Control on Trace Metal Biogeochemistry in the Ocean* 173, 136–147. <https://doi.org/10.1016/j.marchem.2014.10.002>
- Hassler, C.S., Schoemann, V., Nichols, C.M., Butler, E.C.V., Boyd, P.W., 2011. Saccharides enhance iron bioavailability to Southern Ocean phytoplankton. *Proceedings of the National Academy of Sciences* 108, 1076–1081. <https://doi.org/10.1073/pnas.1010963108>
- Ibisanmi, E., Sander, S.G., Boyd, P.W., Bowie, A.R., Hunter, K.A., 2011. Vertical distributions of iron-(III) complexing ligands in the Southern Ocean. *Deep Sea Research Part II: Topical Studies in Oceanography, Biogeochemistry of the Australian Sector of the Southern Ocean* 58, 2113–2125. <https://doi.org/10.1016/j.dsr2.2011.05.028>
- Kleint, C., Hawkes, J.A., Sander, S.G., Koschinsky, A., 2016. Voltammetric Investigation of Hydrothermal Iron Speciation. *Front. Mar. Sci.* 3, UNSP 75.
- Laglera, L.M., Battaglia, G., van den Berg, C.M.G., 2011. Effect of humic substances on the iron speciation in natural waters by CLE/CSV. *Marine Chemistry* 127, 134–143. <https://doi.org/10.1016/j.marchem.2011.09.003>
- Laglera, L.M., Downes, J., Santos-Echeandía, J., 2013. Comparison and combined use of linear and non-linear fitting for the estimation of complexing parameters from metal titrations of estuarine samples by CLE/AdCSV. *Marine Chemistry* 155, 102–112. <https://doi.org/10.1016/j.marchem.2013.06.005>
- Laglera, L.M., Filella, M., 2015. The relevance of ligand exchange kinetics in the measurement of iron speciation by CLE–AdCSV in seawater. *Marine Chemistry, SCOR WG 139: Organic Ligands – A Key Control on Trace Metal Biogeochemistry in the Ocean* 173, 100–113. <https://doi.org/10.1016/j.marchem.2014.09.005>
- Liu, X., Millero, F.J., 2002. The solubility of iron in seawater. *Marine Chemistry* 77, 43–54. [https://doi.org/10.1016/S0304-4203\(01\)00074-3](https://doi.org/10.1016/S0304-4203(01)00074-3)
- Lodeiro, P., Rey-Castro, C., David, C., Achterberg, E.P., Puy, J., Gledhill, M., 2020. Acid-base properties of dissolved organic matter extracted from the marine environment. *Science of The Total Environment* 729, 138437. <https://doi.org/10.1016/j.scitotenv.2020.138437>
- Miller, L.A., Bruland, K.W., 1997. Competitive equilibration techniques for determining transition metal speciation in natural waters: Evaluation using model data. *Analytica Chimica Acta* 343, 161–181. [https://doi.org/10.1016/S0003-2670\(96\)00565-X](https://doi.org/10.1016/S0003-2670(96)00565-X)
- Norman, L., Worms, I.A.M., Angles, E., Bowie, A.R., Nichols, C.M., Ninh Pham, A., Slaveykova, V.I., Townsend, A.T., David Waite, T., Hassler, C.S., 2015. The role of bacterial and algal exopolymeric substances in iron chemistry. *Marine Chemistry, SCOR WG 139: Organic Ligands – A Key Control on Trace Metal Biogeochemistry in the Ocean* 173, 148–161. <https://doi.org/10.1016/j.marchem.2015.03.015>
- Omanović, D., Garnier, C., Pižeta, I., 2015. ProMCC: An all-in-one tool for trace metal complexation studies. *Marine Chemistry, SCOR WG 139: Organic Ligands – A Key Control on Trace Metal Biogeochemistry in the Ocean* 173, 25–39. <https://doi.org/10.1016/j.marchem.2014.10.011>
- Pižeta, I., Sander, S.G., Hudson, R.J.M., Omanović, D., Baars, O., Barbeau, K.A., Buck, K.N., Bundy, R.M., Carrasco, G., Croot, P.L., Garnier, C., Gerringa, L.J.A., Gledhill, M., Hirose, K., Kondo, Y., Laglera, L.M., Nueter, J., Rijkenberg, M.J.A., Takeda, S., Twining, B.S., Wells, M., 2015. Interpretation of complexometric titration data: An intercomparison of methods for estimating models of trace metal complexation by natural organic ligands. *Marine Chemistry, SCOR WG 139: Organic Ligands – A Key Control on Trace Metal Biogeochemistry in the Ocean* 173, 3–24. <https://doi.org/10.1016/j.marchem.2015.03.006>

- Rue, E.L., Bruland, K.W., 1995. Complexation of iron(III) by natural organic ligands in the Central North Pacific as determined by a new competitive ligand equilibration/adsorptive cathodic stripping voltammetric method. *Marine Chemistry, The Chemistry of Iron in Seawater and its Interaction with Phytoplankton* 50, 117–138. [https://doi.org/10.1016/0304-4203\(95\)00031-L](https://doi.org/10.1016/0304-4203(95)00031-L)
- Ružić, I., 1982. Theoretical aspects of the direct titration of natural waters and its information yield for trace metal speciation. *Analytica Chimica Acta* 140, 99–113. [https://doi.org/10.1016/S0003-2670\(01\)95456-X](https://doi.org/10.1016/S0003-2670(01)95456-X)
- Salaün, P., Planer-Friedrich, B., van den Berg, C.M.G., 2007. Inorganic arsenic speciation in water and seawater by anodic stripping voltammetry with a gold microelectrode. *Analytica Chimica Acta* 585, 312–322. <https://doi.org/10.1016/j.aca.2006.12.048>
- Sander, S.G., Hunter, K.A., Harms, H., Wells, M., 2011. Numerical Approach to Speciation and Estimation of Parameters Used in Modeling Trace Metal Bioavailability. *Environ. Sci. Technol.* 45, 6388–6395. <https://doi.org/10.1021/es200113v>
- Sanvito, F., Monticelli, D., 2020. Fast iron speciation in seawater by catalytic Competitive Ligand Equilibration-Cathodic Stripping Voltammetry with tenfold sample size reduction. *Analytica Chimica Acta* 1113, 9–17. <https://doi.org/10.1016/j.aca.2020.04.002>
- Scatchard, G., 1949. The Attractions of Proteins for Small Molecules and Ions. *Annals of the New York Academy of Sciences* 51, 660–672. <https://doi.org/10.1111/j.1749-6632.1949.tb27297.x>
- Slagter, H.A., Laglera, L.M., Sukekava, C., Gerringa, L.J.A., 2019. Fe-Binding Organic Ligands in the Humic-Rich TransPolar Drift in the Surface Arctic Ocean Using Multiple Voltammetric Methods. *Journal of Geophysical Research: Oceans* 124, 1491–1508. <https://doi.org/10.1029/2018JC014576>
- Tilliette, C., Taillandier, V., Bouruet-Aubertot, P., Grima, N., Maes, C., Montanes, M., Sarthou, G., Vorrath, M.-E., Arnone, V., Bressac, M., González-Santana, D., Gazeau, F., Guieu, C., 2022. Dissolved Iron Patterns Impacted by Shallow Hydrothermal Sources Along a Transect Through the Tonga-Kermadec Arc. *Global Biogeochemical Cycles* 36, e2022GB007363. <https://doi.org/10.1029/2022GB007363>
- van den Berg, C.M.G., 2006. Chemical Speciation of Iron in Seawater by Cathodic Stripping Voltammetry with Dihydroxynaphthalene. *Anal. Chem.* 78, 156–163. <https://doi.org/10.1021/ac051441+>
- van den Berg, C.M.G., 1995. Evidence for organic complexation of iron in seawater. *Marine Chemistry, The Chemistry of Iron in Seawater and its Interaction with Phytoplankton* 50, 139–157. [https://doi.org/10.1016/0304-4203\(95\)00032-M](https://doi.org/10.1016/0304-4203(95)00032-M)
- van den Berg, C.M.G., 1982. Determination of copper complexation with natural organic ligands in seawater by equilibration with MnO<sub>2</sub> II. Experimental procedures and application to surface seawater. *Marine Chemistry* 11, 323–342. [https://doi.org/10.1016/0304-4203\(82\)90029-9](https://doi.org/10.1016/0304-4203(82)90029-9)
- van den Berg, C.M.G., Donat, J.R., 1992. Determination and data evaluation of copper complexation by organic ligands in sea water using cathodic stripping voltammetry at varying detection windows. *Analytica Chimica Acta* 257, 281–291. [https://doi.org/10.1016/0003-2670\(92\)85181-5](https://doi.org/10.1016/0003-2670(92)85181-5)
- Wang, P., Ding, Y., Liang, Y., Liu, M., Lin, X., Ye, Q., Shi, Z., 2021. Linking molecular composition to proton and copper binding ability of fulvic acid: A theoretical modeling approach based on FT-ICR-MS analysis. *Geochimica et Cosmochimica Acta* 312, 279–298. <https://doi.org/10.1016/j.gca.2021.07.019>
- Whitby, H., Bressac, M., Sarthou, G., Ellwood, M.J., Guieu, C., Boyd, P.W., 2020a. Contribution of Electroactive Humic Substances to the Iron-Binding Ligands Released During Microbial Remineralization of Sinking Particles. *Geophysical Research Letters* 47, e2019GL086685. <https://doi.org/10.1029/2019GL086685>
- Whitby, H., Planquette, H., Cassar, N., Bucciarelli, E., Osburn, C.L., Janssen, D.J., Cullen, J.T., González, A.G., Völker, C., Sarthou, G., 2020b. A call for refining the role of humic-like

- substances in the oceanic iron cycle. *Scientific Reports* 10, 1–12. <https://doi.org/10.1038/s41598-020-62266-7>
- Witter, A.E., Luther, G.W., 1998. Variation in Fe-organic complexation with depth in the Northwestern Atlantic Ocean as determined using a kinetic approach. *Marine Chemistry* 62, 241–258. [https://doi.org/10.1016/S0304-4203\(98\)00044-9](https://doi.org/10.1016/S0304-4203(98)00044-9)
- Wu, J., Luther, G.W., 1995. Complexation of Fe(III) by natural organic ligands in the Northwest Atlantic Ocean by a competitive ligand equilibration method and a kinetic approach. *Marine Chemistry, The Chemistry of Iron in Seawater and its Interaction with Phytoplankton* 50, 159–177. [https://doi.org/10.1016/0304-4203\(95\)00033-N](https://doi.org/10.1016/0304-4203(95)00033-N)
- Yokoi, K., van den Berg, C.M.G., 1992. The determination of iron in seawater using catalytic cathodic stripping voltammetry. *Electroanalysis* 4, 65–69. <https://doi.org/10.1002/elan.1140040113>



## **Note for the reader**

The following Chapter is in final stage of preparation for publication and is nearly ready for submission to the journal *Frontiers in the Research Topic 'Hydrothermal and submarine volcanic activity: Impacts on ocean chemistry and plankton dynamics'*. This might explain repetitions regarding the description of the methodological context and of the scientific background.

To be submitted as: **Mahieu, L.**, Whitby, H., Dulaquais, G., Tilliette, C., Guigue, C., Tedetti, M., Lefevre, D., Fourrier, Bressac, M., P., Sarthou, G., Bonnet, S., Guieu, C., Salaün, P.: Iron-binding by dissolved organic matter in the Western Tropical South Pacific (GEOTRACES cruise GPpr14).

## **Chapter 5**

### **5. Iron-binding by dissolved organic matter in the Western Tropical South Pacific (GEOTRACES cruise GPpr14)**

#### **Abstract**

Iron (Fe) is essential for phytoplankton growth, but its scarcity in seawater limits primary production. The solubility enhancement of dissolved Fe (DFe) by complexation with a specific fraction of the dissolved organic matter (DOM) called Fe-binding ligands partly sustains primary production, but the Fe-binding ligands composition is poorly constrained. This is due to the DOM diversity, heterogeneity in Fe-binding ligand composition and distribution, and limited number of available data, hampering our understanding of the Fe cycling and subsequently on nitrogen and carbon cycling. Here, we present the conditional concentrations ( $[L]$ ) and binding-strengths ( $\log K_{\text{FeL,Fe}'}^{\text{cond}}$ ) of Fe-binding ligands on 103 samples collected in the Western Tropical South Pacific Ocean (WTSP) during the GEOTRACES TONGA cruise (GPpr14), area subject to intense Fe inputs from hydrothermal activity, fueling one of the most intense diazotrophic activity worldwide. Ligands were analyzed by competitive ligand exchange followed by adsorptive cathodic stripping voltammetry (CLE-ACSV) using salicylaldoxime at  $25 \mu\text{mol.L}^{-1}$ . We found a mean  $[L]$  of  $5.2 \pm 1.2 \text{ nmoleqFe.L}^{-1}$  ( $n = 103$ ), in large excess compared to DFe ( $[L]_{\text{ex}} = 4.6 \pm 1.1 \text{ nmoleqFe.L}^{-1}$ ). The large unsaturation of the Fe-binding ligands suggested the predominance of precipitation processes of the hydrothermally sourced DFe over stabilization by Fe-binding ligands. Nevertheless,  $[L]$  and DFe were positively correlated, meaning the  $[L]$  partly explained DFe distribution. 84% of the samples were falling in the class of intermediate strength  $L_2$  class (mean  $\log K_{\text{FeL,Fe}'}^{\text{cond}}$  of  $11.6 \pm 0.4$ ,  $n = 103$ ). As the  $L_2$  class is often considered as mostly composed of humic-like substances (HS-like), our Fe-binding ligands data were compared to electrochemical and



fluorescent determination of HS-like. The electroactive fraction of HS-like (eHS) explained 20 to 40% of the [L] in surface waters, and 8 to 18% in deep waters. eHS was not positively correlated to DFe, contrasting with other oceanic regions. The Fe-binding ability of the HS-like fluorescent DOM (FDOM) could not be estimated, but the latter showed positive correlation with DFe and with the apparent oxygen use (AOU), proxy of the microbial mineralization of the DOM. Enhanced HS-like FDOM content in deep waters suggested hydrothermal influence on this fraction in the WTSP. Unusual relationship between tryptophan-like FDOM and [L] was also suggesting variability in the biological defense mechanisms developed to neutralize hydrothermally sourced toxic metals. Our study highlighted the interest to further compare electrochemical and fluorescence analyses of the Fe-binding ability of the DOM to constrain DFe distribution, biological processes and Fe-binding ligands composition.

## **5.1. Introduction**

Iron (Fe) is an essential element for phytoplankton because of its role in multiple metabolic processes (Twining and Baines, 2013). It is in such a high demand that its availability limits primary production across around 40% of the ocean (Moore et al., 2013). Fe scarcity is also explained by its very low solubility in seawater (Liu and Millero, 2002). Fe is quickly hydrolysed and exported as oxyhydroxide aggregates in oxygenated conditions (Liu and Millero, 2002), and as Fe-sulphide (mostly pyrite) in more anoxic environments such as hydrothermal vents (Rickard and Luther, 2007). However, despite its low solubility and inorganic scavenging, the Fe concentration found in the dissolved fraction (DFe; defined by the filter of 0.2  $\mu\text{m}$  or 0.45  $\mu\text{m}$  pore size) is higher than what is expected from its inorganic speciation (Liu and Millero, 2002). This is partly explained by extensive complexation of DFe by a fraction of the dissolved organic matter (DOM), known as Fe-binding ligands, enhancing Fe solubility, and increasing its residence time in surface waters and bioavailability to phytoplankton. It is generally accepted that most DFe (> 99%) is complexed to organic ligands (Gledhill and Buck, 2012). Knowledge of the nature and cycling of these ligands is required to understand and predict Fe distributions and bioavailability, but obtaining this information is challenging. Characterisation of the Fe complexing fraction is difficult because of the sheer diversity of DOM (Dittmar et al., 2021; Mentges et al., 2017) and the relatively low abundance of Fe-binding compounds. The bioavailability of DFe complexed by

the wide variety of Fe-binding ligands present in seawater is also difficult to evaluate (Shaked et al., 2020; Shi et al., 2010). Various methods enable measurement of the major individual Fe-binding ligand groups, namely siderophores (Boiteau and Repeta, 2022; Bundy et al., 2018), humic-like substances (HS; Laglera et al., 2007; Pernet-Coudrier et al., 2013; Sukekava et al., 2018; Whitby and van den Berg, 2015), and exopolymeric substances (EPS; Hassler et al., 2015, 2011; Norman et al., 2015). Those methods, however, have a limited resolution because of the diversity encountered within each group.

The identification issue posed by the DOM diversity and by the specific complexing ability of each compound is partly overcome by the Competitive Ligand Exchange (CLE) approach, based on the competition between the natural Fe-binding ligands and an added competitive ligand at increasing DFe concentrations. The titration of the natural Fe-binding ligands is indirectly followed by the quantification of the electroactive complex formed by the competitive ligand and DFe, by adsorptive cathodic stripping voltammetry (ACSV). This approach allows the determination of the maximum amount of DFe that can be complexed by the natural DOM present within a sample, defined as the Fe-binding ligand concentration ( $[L]$ ), and the averaged conditional stability constant ( $\log K_{\text{FeL,Fe}'}^{\text{cond}}$ ) of the Fe-binding complexes within the detection window. The  $\log K_{\text{FeL,Fe}'}^{\text{cond}}$  values obtained by CLE-ACSV are commonly divided into classes, with  $L_1$  corresponding to stronger ligands ( $\log K_{\text{FeL,Fe}'}^{\text{cond}} > 12$ ),  $L_2$  to intermediate ligands ( $>10 \log K_{\text{FeL,Fe}'}^{\text{cond}} < 12$ ) and  $L_3$  to weaker ligands ( $\log K_{\text{FeL,Fe}'}^{\text{cond}} < 10$ ; Gledhill and Buck, 2012). These classes roughly correspond to the three major types of ligand identified in the environment, with siderophores falling into the  $L_1$  class, HS falling into  $L_2$ , and EPS into  $L_3$  (Hassler et al., 2017), although classes can overlap and remain a simplistic view of the Fe organic speciation. The binding ability of the DOM is rather a continuum of  $\log K_{\text{FeL,Fe}'}^{\text{cond}}$  values that a specific value as determined by CLE-ACSV (Gledhill and Buck, 2012). The  $\log K_{\text{FeL,Fe}'}^{\text{cond}}$  determined by CLE-ACSV is an average value of all the titrated ligands, and it is not well understood how the  $\log K_{\text{FeL,Fe}'}^{\text{cond}}$  of each compound is weighted during the titration of the Fe-binding ligands mixture. This has been shown to be of importance notably with the  $L_1$  class, as a  $\log K_{\text{FeL,Fe}'}^{\text{cond}} > 12$  could be over-interpreted as corresponding to siderophore compounds, when siderophore concentrations (e.g. Bundy et al., 2018;

Mawji et al., 2008) are generally orders of magnitude lower than the L<sub>1</sub> class detected by CLE-ACSV (e.g. Buck et al., 2018). Whilst being mindful of limitations, this classification remains a helpful way to interpret Fe-binding ligand data and to compare studies.

The classification of binding strength presented by Gledhill and Buck (2012) has been used to compare the first basin scale datasets on Fe-binding ligand characteristic from samples collected in the West Atlantic (Gerringa et al., 2015), in the North Atlantic (Buck et al., 2015) and in the Tropical Pacific (Buck et al., 2018). Despite a general trend of decreasing  $\log K_{\text{FeL,Fe}'}^{\text{cond}}$  and increasing [L] with depth and water mass aging (Buck et al., 2018, 2015; Gerringa et al., 2015), L<sub>1</sub> has been shown to correlate with increasing DFe concentration at hydrothermal vents (Buck et al., 2018, 2015). L<sub>1</sub> ligands were also observed in hydrothermal fluid samples collected at the New Hebrides Island arc in the Western Tropical South Pacific (WTSP) with concentrations reaching the micromolar range for [L] and DFe (Kleint et al., 2016). These authors also detected weaker L<sub>3</sub> ligands in several WTSP hydrothermal samples (Kleint et al., 2016), while intermediate L<sub>2</sub> ligands have been observed in hydrothermal plumes in the Southern Ocean (Hawkes et al., 2013). In hydrothermal fluids, concentrations of DFe and [L] can vary from the nanomolar (e.g. Hawkes et al., 2013; Resing et al., 2015; Tilliette et al., 2022) to micromolar range (e.g. Kleint et al., 2016) depending on the initial fluid chemistry, which is geographically diverse and variable over time (Kleint et al., 2019). The free ionic Fe<sup>2+</sup> initially found in hot and acidic hydrothermal fluid (Kleint et al., 2017) is quickly oxidised and scavenged during mixing with seawater by the formation of Fe-sulphides and Fe-oxyhydroxide minerals (Millero et al., 1987), but it can also be adsorbed on organic matrixes (Toner et al., 2009) or stabilised by Fe-binding ligands (Kleint et al., 2017; Sander and Koschinsky, 2011; Santana-Casiano et al., 2022). The inorganic transport of DFe as Fe-sulphide nanoparticles and colloidal Fe-oxyhydroxide has also been observed (Yücel et al., 2021, 2011), and the accessibility of these fractions by Fe-binding ligands, even if strongly suggested in recent studies (e.g. Kleint et al., 2016), is yet to be attested. The variable interplay between the inorganic and organic processes impacting the amount of DFe sourced by hydrothermal activity is an essential aspect to constrain the global DFe distribution as it could account for an estimated 9% of the deep-ocean DFe budget (Sander and Koschinsky, 2011).

At the Tonga volcanic arc in the WTSP, the subduction of the Pacific Plate under the Australian Plate is responsible for intense volcanic activity and high density of submarine volcanoes (German et al., 2006). This submarine hydrothermal activity has been shown to fuel the area with DFe, with up to 70 nmol.L<sup>-1</sup> of DFe measured within the photic layer (Guieu et al., 2018). In addition, the highest rates of nitrogen fixation ever observed have been measured in the Lau Basin, potentially making it one of the main sources of nitrogen for the global ocean (Bonnet et al., 2018, 2017). The co-occurrence of aeolian and submarine volcanism with intense diazotrophic activity motivated the GEOTRACES process cruise GPpr14 (TONGA cruise; Guieu and Bonnet, 2019), which crossed the Melanesian basin, the Lau basin, and the western part of the South Pacific gyre (Figure 5.1) between October 31<sup>st</sup> and December 5<sup>th</sup> 2019. The cruise immediately followed a strong volcanic eruption which occurred in October 2019 and resulted in the emergence of a new island called Late'iki in the Lau basin (Plank et al., 2020). The particularity of the Late'iki island is that due its weak geological structure, oceanic erosion made it disappear less than two months after it emerged (Yeo et al., 2022), within the timeframe of the TONGA cruise, potentially impacting the biological activity and DFe cycling in the area.

The TONGA transect was the opportunity to quantify for the first time [L] and  $\log K_{\text{FeL,Fe}'}^{\text{cond}}$  at the basin scale to explore the relation between Fe-binding ligands and DFe distributions in the area. In addition to our Fe-binding ligands characterization, several complementary analyses targeting specific fraction of the DOM were conducted notably regarding HS-like material. They are of specific interest as they have been estimated to represent around 50% of the DOM (Zigah et al., 2017) and partially able to bind with Fe. The diversity of the HS-like material is responsible for various properties, notably in term of electroactivity and photoreactivity, the latter in terms of absorbance and fluorescence. It has been shown that electroactive HS (eHS) are able to control Fe solubility in various natural waters (e.g. Dulaquais et al., 2018; Fourrier et al., 2022; Laglera et al., 2019; Sukekava et al., 2018; Whitby et al., 2020). Similarly, the HS-like fluorescent component of the DOM (FDOM) is suspected to play a role on DFe distributions as shown by its distribution and quenching experiments (Hioki et al., 2014; Jia et al., 2021; Ohno et al., 2008; Tani et al., 2003). The complementarity and/or overlapping of these two different

operationally-defined fractions of HS is, however, not well constrained as few comparisons have been made between eHS and HS-like FDOM.

We present here the results obtained for Fe-binding ligand characteristics during this transect using the same competitive ligand method that was used in both the Equatorial Pacific (that covered the eastern part of the South Pacific gyre; Buck et al., 2018) and in the North Atlantic (Buck et al., 2015). We relate the distribution observed in [L] and  $\log K_{\text{FeL,Fe}'}^{\text{cond}}$  to other parameters such as DFe, apparent oxygen utilization (AOU) and dissolved organic carbon (DOC) in an attempt to identify the processes impacting Fe-binding ligands and their importance to DFe distribution in the WTSP. To further constrain the composition of the Fe-binding ligand pool, the fate of the eHS and HS-like FDOM is also discussed, as well as the unusual coincidences of high [L] and tryptophan-like FDOM.

## **5.2. Material and methods**

### **5.2.1. Sampling strategy during the TONGA cruise**

Samples were collected during the TONGA French GEOTRACES process study in the western tropical south Pacific (WTSP; GPpr14). The cruise transect consisted of 12 main stations between the Melanesian basin and the South Pacific gyre (Figure 5.1), with additional stations focussed around two known volcanic sites, ST5 and ST10. ST5 was not investigated in this study and will not be discussed. ST10 (stations ST10-T1, T2 and T3) shown in red was situated in the Eastern Lau basin on the Tonga arc, approximately 30 km south west of the Late'iki island. Two stations in the Melanesian basin on the western side of the transect (ST2 and ST3, in green) were sampled to evaluate the impact of diazotrophy and hydrothermal activity on surrounding waters (Tilliette et al., 2022). The Western Lau basin was sampled at ST4, ST11 and ST12, shown in orange. Three further sampling stations (ST6, ST7 and ST8, in blue) were in the oligotrophic South Pacific gyre, with ST6 on the East of the Tonga arc but on the western side of the Tonga trench, where water exchanges between the South Pacific gyre and the Lau basin is thought to be limited by the topography (Talley et al., 2011). Further data are available for complementary parameters and stations (e.g. Dulaquais et al., in prep.; Tedetti et al., in prep.; Tilliette et al., 2022).

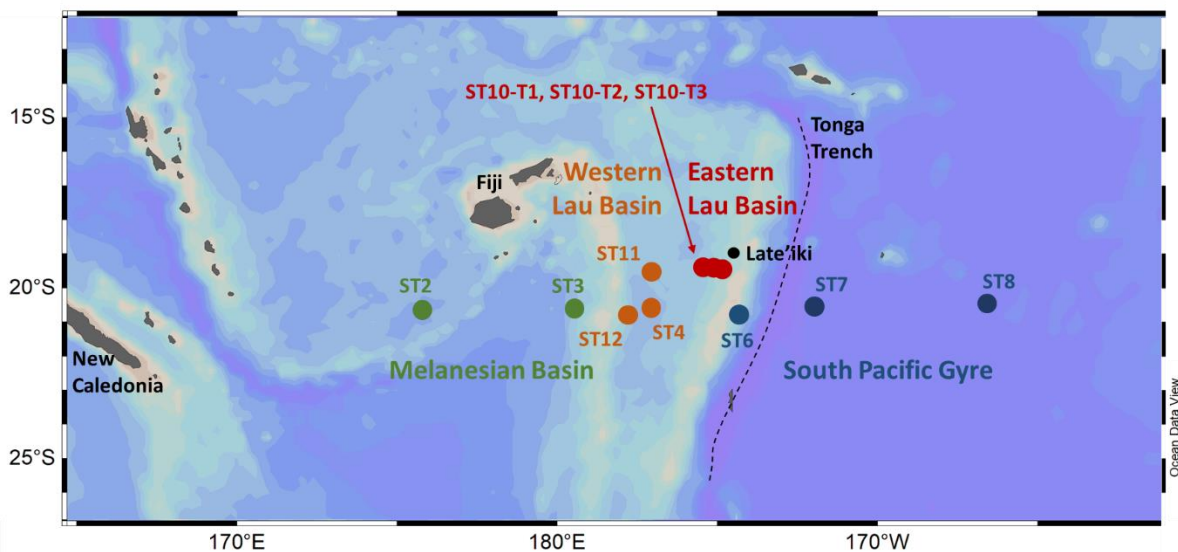


Figure 5.1. Map of sampling station of the TONGA cruise (GPpr14) for which FeL characteristics have been measured. The colour of the stations corresponds to the region (coloured labels on the map). Geographic features (in black) such as the main islands, the Tonga trench and the location of the Late'iki islands are also noted.

### 5.2.2. Sample collection and storage

The seawater samples for DFe and Fe-binding ligand analyses were collected using GO-FLO bottles mounted on a Trace Metal Clean Rosette (TMR; General Oceanics Inc., Model 1,018 Intelligent Rosette) transferred into a trace metal clean container (class-100) and pressurised with 0.2  $\mu\text{m}$ -filtered nitrogen (Air Liquide™) for sub-sampling. Dissolved fractions for the analysis of DFe and Fe-binding ligands were sampled through 0.45  $\mu\text{m}$  acid-cleaned polyethersulfone filters (Supor™). For DFe, the cleaning procedure of the bottles used for seawater collection, sample storage, handling and analyses are detailed in Tilliette et al. (2022).

For Fe-binding ligands, 250 mL low-density polyethylene (LDPE) Nalgene™ bottles were left to soak for one week in a 2% surfactant bath (Decon™), one week in a 1 mol.L<sup>-1</sup> HCl bath (laboratory reagent grade 32 %, FisherScientific™) and one week in a 0.1 mol.L<sup>-1</sup> HCl bath (laboratory reagent grade 32 %, FisherScientific™), before being left to dry under a laminar flow hood (Class-100) and double-bagged. Between each step, the bottles were rinsed 5-times with Milli-Q water (resistivity > 18.2 M $\Omega$ .cm). The samples were collected after rinsing the bottles 3 times with around 20 mL of filtered sample and frozen to -20 °C immediately after sampling. Samples were defrosted in the dark at room temperature and swirled before analysis.

The seawater samples for O<sub>2</sub> and DOC analyses as well as DOM fluorescence and absorption measurements were collected in glass bottles from a classical rosette equipped with twenty-four 12 L Niskin bottles. The samples were immediately filtered under low vacuum (< 50 mmHg) through 25-mm glass fibre filters (GF/F, size pore: ~0.7 µm, Whatmann) using glass filtration apparatus. For DOC analyses, filtered samples were transferred into 10-mL glass ampoules. Samples were acidified with 20 µL of sulphuric acid (H<sub>2</sub>SO<sub>4</sub>, 95-98%, Sigma-Aldrich), then the ampoules were flame sealed and stored in the dark at 4 °C before analysis. For DOM fluorescence and absorption measurements, filtered samples were transferred into 100 mL amber glass bottles with clean Teflon-lined caps and stored at -20 °C in the dark before analysis. Before use, all glassware was left to soak for 24 h in a 1 mol.L<sup>-1</sup> HCl bath, rinsed thoroughly with Milli-Q water, then combusted at 450 °C for 6 h, and finally rinsed three times with the respective sample before filling. GF/F filters were also combusted before use.

### **5.2.3. Analyses**

Detailed description of the analysis and distributions of DFe (Tillette et al., 2022) and eHS (Dulaquais, in prep.) can be found in the respective papers.

#### **5.2.3.1. O<sub>2</sub> and AOU**

Dissolved oxygen concentration (O<sub>2</sub>) was measured following the Winkler method (Winkler, 1888) modified by Carpenter (1965) and Carrit and Carpenter (1966), with potentiometric endpoint detection using a Titrino 716 DMS (Metrohm™; Oudot et al., 1988). For sampling, reagent preparation and analysis, the recommendations from Langdon (2010) were carefully followed. The thiosulfate solution was calibrated by titrating it against a potassium iodate certified standard solution of 0.0100 N (CSK standard solution; WAKO™). The reproducibility, expressed as the standard deviation of replicates samples was 0.8 µmol kg<sup>-1</sup> (n = 15, mean = 195.4 µmol kg<sup>-1</sup>). Apparent Oxygen Utilisation (AOU, in µmol.kg<sup>-1</sup>) was calculated from the difference between oxygen solubility concentration (at P = 0 dbar) estimated with the Benson and Krause coefficients (Garcia and Gordon, 1992) and *in-situ* O<sub>2</sub>.

#### **5.2.3.2. DOC**

DOC concentrations were measured in two ampoule replicates on a Shimadzu TOC-V analyser according to Sohrin and Sempéré (2005) and Fourrier et al. (2022). Before injection, the GF/F-filtered and acidified samples were bubbled for 2 min with CO<sub>2</sub>-free air to purge inorganic carbon. The accuracy and system blank of the instrument were determined by the analysis of certified water references (batch 19, lot #03–19, Hansell Laboratory, Miami, USA). The nominal precision of the analysis procedure was within 2%.

### 5.2.3.3. FDOM

The GF/F-filtered samples were left to return to room temperature (20°C) in the dark before transferring into to a 1 cm suprasil quartz cuvette (170-2600 nm; HELMA) for fluorescence measurements on a Hitachi F-7000 spectrofluorometer. Excitation-emission matrices (EEMs) were conducted over an excitation wavelength ( $\lambda_{\text{Ex}}$ ) range of 200-500 nm with a 5-nm step, and an emission wavelength ( $\lambda_{\text{Em}}$ ) range of 280-550 nm with a 2-nm step, with a scan speed of 1200 nm min<sup>-1</sup> and slit widths of 5 nm (Dupouy et al., 2020; Martias et al., 2018; Tedetti et al., 2012; 2020). EEMs were blank-corrected, Raman-normalized and converted into quinine sulphate unit (QSU), where 1 QSU corresponds to the fluorescence of 1 µg.L<sup>-1</sup> quinine sulfate in 0.05 mol.L<sup>-1</sup> of sulfuric acid at  $\lambda_{\text{Ex}}/\lambda_{\text{Em}}$  of 350/450 nm. EEMs were then treated with parallel factor analysis (PARAFAC) executed using the DOMFluortoolbox v1.6 273 (Stedmon and Bro, 2008) running under Matlab 7.10.0 for the identification of the main fluorescent components present in the EEM dataset. Three fluorescent components were identified: one tryptophan-like ( $\lambda_{\text{Ex1}}, \lambda_{\text{Ex2}}/\lambda_{\text{Em}}$ : 230, 300/340 nm), one tyrosine-like ( $\lambda_{\text{Ex1}}, \lambda_{\text{Ex2}}/\lambda_{\text{Em}}$ : 225, 275/304 nm) and one HS-like ( $\lambda_{\text{Ex1}}, \lambda_{\text{Ex2}}/\lambda_{\text{Em}}$ : 235, 315/436 nm). Tryptophan-like and tyrosine-like were not specifically addressed in this study and are presented elsewhere (Tedetti et al., in prep.).

### 5.2.3.4. Iron-binding ligands

The theory of the CLE-ACSV approach can be found elsewhere (e.g. Abualhaija and van den Berg, 2014; Gerringa et al., 2014; Gledhill and van den Berg, 1994; Pižeta et al., 2015; Rue and Bruland, 1995; Chapter 2). We used the added ligand salicylaldehyde (SA; 98% Acros Organics<sup>TM</sup>) at 25 µmol.L<sup>-1</sup> using the side reaction coefficient ( $\beta_{\text{FeSA}_2}$ ) of 11.1 (Buck et al., 2018, 2015, 2007) leading to a



detection window (D) of 79 (Buck et al., 2007), following the procedure described in Chapter 4. A borate buffer (boric acid, analytical reagent grade, Fisher Scientific™) at 1 mol.L<sup>-1</sup> in 0.35 mol.L<sup>-1</sup> of ammonia (NH<sub>4</sub>OH; 29% Laporte™), was used at 10 mmol.L<sup>-1</sup> for a final pH of 8.2 in the sample (Abualhaija and van den Berg, 2014; Buck et al., 2018, 2015, 2007; Rue and Bruland, 1995; Chapter 4). The following equilibration procedure was applied: natural ligands were left to equilibrate with increasing levels of DFe additions in the presence of the buffer for a minimum of 2 h, with SA added at least 15min before the start of the analysis. The titrations were performed with 16 aliquots, with DFe additions of 0, 0, 0.75, 1.5, 2.25, 3, 3.5, 4, 4.5, 5, 6, 7, 8, 10, 12 and 15 nmol.L<sup>-1</sup>. The DFe additions were adjusted from Buck et al. (2018) after preliminary tests showed emergence of the FeSA reduction current around 3 nmol.L<sup>-1</sup> of DFe added (nmoleqFe.L<sup>-1</sup>).

The same apparatus as described in Chapter 4 of this Thesis was used. Briefly, two voltammetric systems were used, each composed of a 663 VA stand (Metrohm™) installed in a laminar flow hood (class-100), supplied with nitrogen and equipped with a mercury drop electrode (MDE, Metrohm™) as single-use working electrode. For both systems, a glassy carbon counter electrode and a silver/silver chloride reference electrode were each placed in glass bridges filled with UV-irradiated 3M KCl cleaned with manganese oxides (Yokoi and van den Berg, 1992). The three electrodes were controlled with a potentiostat/galvanostat Type III (μAutolab) monitored by the software NOVA 2.5 (Metrohm™). Measurements were carried out in custom-made Teflon cells allowing analyses in 5 mL aliquots (Gourain, 2020; Chapter 3, 4). Due to the smaller cell, a home-made vibrating device was designed to replace the standard stirring system. It consisted of a 150 Hz small vibrating rotor connected to a paddle plastic tip immersed in the solution (Chapter 3, 4). The HMDE and home-made stirring devices were controlled by an Autolab IME 663 (Metrohm) interface, whereas the mercury drop size was selected on the 663 VA stand and optimized at the value of 3. During the voltammetric measurement, the sample was kept oxygenated by a constant air-flow at the surface of the sample through an aquarium pump (Sanvito et al., 2019; Sanvito and Monticelli, 2020; Chapter 3, 4). In addition, the nitrogen gas flow above the sample was stopped by tightening the screw on the right side of the 663 VA stand (Chapter 3, 4). Further details of the experimental set up, method validation and the conditioning procedure of

cells and tubes (Trace Metal Free, Labcon<sup>TM</sup>) used to prepare aliquots of the samples are described in Chapter 4.

The preconcentration of the FeSA complex on the MDE was performed by applying a potential of 0.05 V for a duration ranging from 20s to 120s. Then, the home-made stirrer was stopped for 3s and the stripping was performed from -0.25 V until -0.6 V by differential pulse (steps: -0.006 V; modulation amplitude: 0.05 V; modulation time 0.035s; interval time 0.2s). The second derivative of the FeSA reduction peak height was determined using the software ECDSOFT following the procedure described in Chapter 4 (Annex 2). Fitting of the titration was performed using the software ProMCC with the complete complexation fitting model. A step-by-step procedure for quality control of the data aiming to limit the subjectivity of the analyst during the interpretation of the titrations has been developed and is described in Chapter 4 (Annex 3, 4). The software ECDSOFT and ProMCC are freely available online (<https://sites.google.com/site/daromasoft>).

#### **5.2.4. Statistical treatment**

The variables considered in this study were not following a normal distribution, and were inter-dependent and non-linear, calling for the application of a non-parametric method. The Spearman rank correlation analysis ( $\rho$ ; Spearman, 1904) was used here as it has been previously used for the investigation of Fe-binding ligands and fluorescence of the DOM (e.g. Genovese et al., 2018; Heller et al., 2013). It is adapted to monotonic relationship between variables and is not limited to linear relationships. The calculation was performed using the function ‘`scipy.stats.spearmanr`’ in Python (version 3.9). The Spearman correlation matrix was prepared with the entire dataset, and  $\rho$  were considered significant for  $p < 0.0001$  and indicated in bold in Table 1. It was decided to not differentiate the mixed layer and the deeper waters as the dataset for the mixed layer was not large enough to established significant relationships. The comparison of the matrix from the whole dataset and from a reduced dataset excluding the mixed layer slightly impacted the correlations related to DFe and Fe-binding ligand characteristics (focus of this study) by less than 0.1 and did not impact the significance of the correlations, except for EHS that did not show any correlation in the reduced dataset. It was,

therefore, not necessary to discard any part of the dataset. For Spearman test, strong correlation corresponds to absolute  $\rho$  above 0.9, moderate correlation to  $\rho$  between 0.7 and 0.9, moderate correlation to  $\rho$  between 0.5 and 0.3, and absence of correlation to  $\rho$  below 0.3. We considered the correlation to be significant for  $p < 0.0001$ , at least one order of magnitude lower than in other studies discussing Spearman correlation matrixes including Fe-binding ligands data to ensure a strong level of confidence in the interpretation of the dataset (e.g. Genovese et al., 2018; Heller et al., 2013).

## 5.3. Results

### 5.3.1. Hydrography

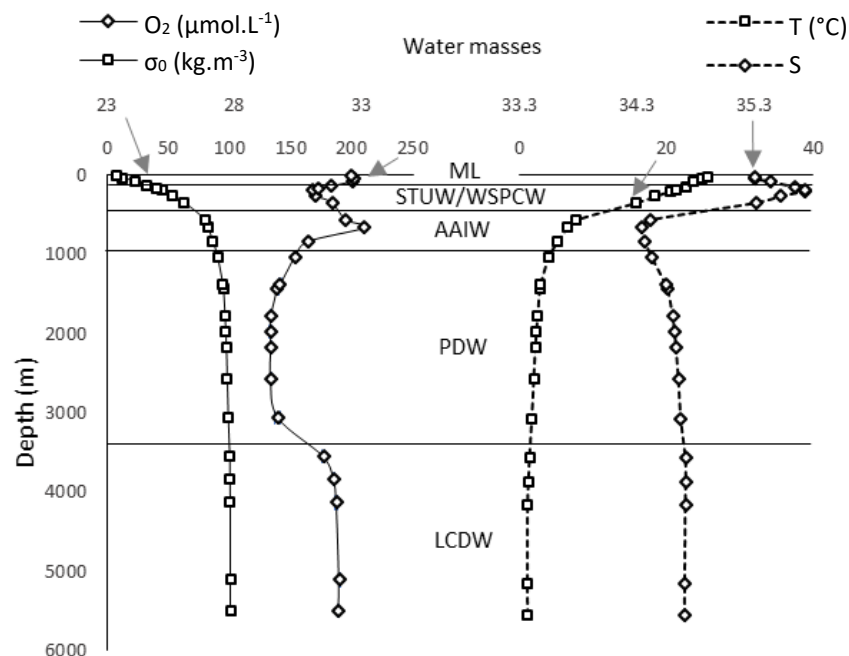


Figure 5.2. Profile of  $\sigma_0$  (full line, square), O<sub>2</sub> (full line, diamond), T (temperature, dot line, square), and S (salinity, dot line, diamond) at ST7 with the water mass separations applied in this study. The WSPCW, not present at ST7, is also mentioned to not omit any water mass investigated in this work.

The water mass composition and circulation have been thoroughly described by Tilliette et al. (2022). Briefly, O<sub>2</sub> fluctuation appeared to better describe the water masses than the physical variables related to seawater density classically used (such as potential density anomaly ( $\sigma_0$ ); Figures 5.2). During the TONGA transect, surface waters were characterised by high O<sub>2</sub> due to primary production and atmospheric exchange enhanced by physical mixing in the mixed layer, which ranged from 70 to 140

m deep during the cruise. The water mass below the mixed layer corresponds to the Subtropical Under Water (STUW) in the South Pacific gyre, and to the Western South Pacific Central Water (WSPCW) in the Melanesian and Lau basins. Both STUW and WSPCW are characterised around 200 m by a maximum of salinity (S) and minimum of O<sub>2</sub>, the latter being due to the mineralisation of the organic matter. Below these two water masses in the three basins is the Antarctic Intermediate Water (AAIW), which showed at around 650 m a S minimum and an O<sub>2</sub> maximum also corresponding to the thermocline (Kawabe and Fujio, 2010; Talley et al., 2011). Below the AAIW, salinity increases and temperature decreases. The O<sub>2</sub> is below 150  $\mu\text{mol.L}^{-1}$  and is characteristic of the Pacific Deep Water (PDW) originating from the upwelling of Antarctic Bottom Water (AABW) in the middle of the Pacific, mixing with the O<sub>2</sub> depleted waters from the Pacific Minimum Oxygen Zone and with the deep waters from the oxygen minimum zone off Chile in the Eastern South Pacific (Silva et al., 2009). AAIW and PDW are supposedly reaching the Lau and Melanesian basins from a branch of the South Pacific gyre flowing from the North of the Lau basin (Summers and Watling, 2021), as the water is flowing south-westward in the area (Tilliette et al., 2022). However, the circulation in and between the Lau and the Melanesian basins is more variable, as the currents are relatively weak in the Lau basin (Wang et al., 2022) and currents flowing northeast have been observed in the Melanesian basin (Komaki and Kawabe, 2007). In the South Pacific gyre, deeper than 3500 m, O<sub>2</sub> increases to around 190  $\mu\text{mol.L}^{-1}$  due to the intrusion of Lower Circumpolar Deep Water (LCDW) from the southeast (Kawabe and Fujio, 2010). O<sub>2</sub> concentration ranged from 121  $\mu\text{mol.kg}^{-1}$  in the PDW of the Western Lau basin, to 211  $\mu\text{mol.kg}^{-1}$  in the AAIW of the South Pacific gyre (Figure 5.3a).

### 5.3.2. DOC

The distribution and range of DOC concentrations measured in this study are typical to what was previously reported in the Tropical South Pacific (e.g. Buck et al., 2018; Fourrier et al., 2022). DOC concentrations ranged from 36 to 80  $\mu\text{mol.L}^{-1}$ , with the highest values observed in the mixed layer and related to biological activity, ranging from 60 to 80  $\mu\text{mol.L}^{-1}$ . DOC concentration were decreasing with depth due microbial mineralization to reach typical deep water values, ranging from 35 to 45  $\mu\text{mol.L}^{-1}$  in the PDW (and LCDW at ST7 and ST8). Typical deep values were reached within the

STUW/WSPCW in line with the microbial consumption of O<sub>2</sub> at most stations (Figure 2, 3), except at ST3, ST4 and ST7, where the gradient of concentration is reaching as deep as 1000 m.

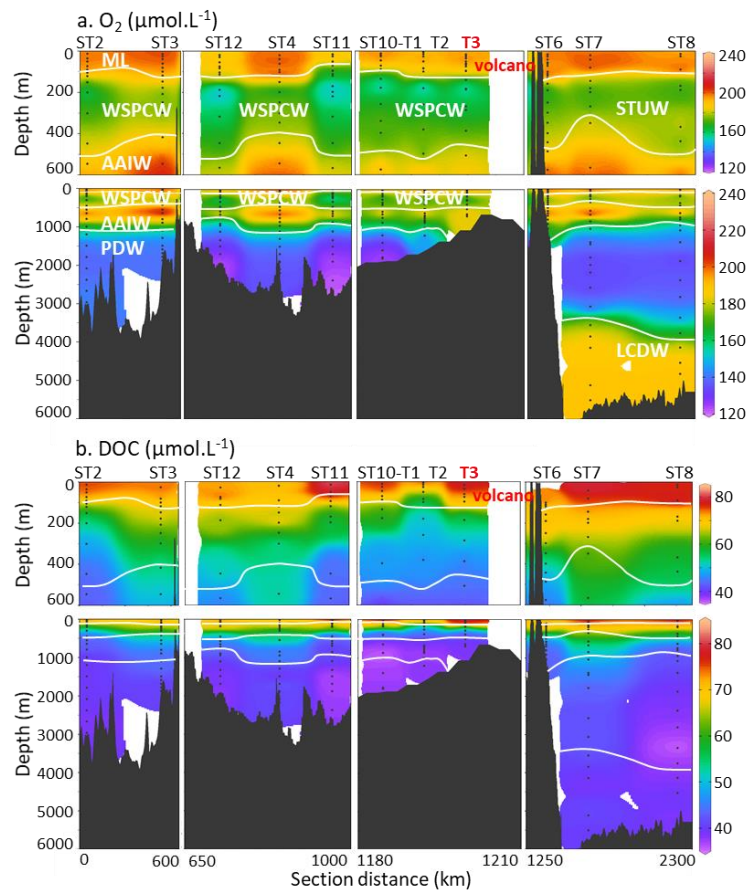


Figure 5.3. Top 600 m and full depth distribution of a) O<sub>2</sub> and b) DOC concentrations for the Tonga cruise (GEOTRACES GPpr14). The approximate water mass boundaries are defined by O<sub>2</sub> (see Figure 5.2). The section is separated in 4 segments with, from left to right, the Melanesian basin (ST2 and ST3), the Western Lau basin (ST12, ST4, ST11), the Eastern Lau basin (ST10-T1, ST10-T2, ST10-T3) and the South Pacific gyre (ST6, ST7, ST8). See Figure 5.1 for more details on the sampling locations.

### 5.3.3. FDOM

The tryptophan-like FDOM component ( $\lambda_{Ex1}$ ,  $\lambda_{Ex2}/\lambda_{Em}$ : 230, 300/340 nm) is indicative of the presence of protein-like compounds, principal component of organisms and precursor of HS-like material (Hedges, 1988). Tryptophan-like FDOM showed low values in most samples from the Lau Basin and the South Pacific gyre, in line with previously reported values in coastal and open-ocean systems (< 1.5 QSU; Figure 5.4a; Catalá et al., 2016; Yamashita and Tanoue, 2004, 2003). Several stations showed

abnormally high values, notably ST3 and ST6 with tryptophan-like FDOM content up to 8.6 and 7.6 QSU, respectively, and coincided to HS-like FDOM content increase.

The HS-like fluorescent component identified here ( $\lambda_{Ex1}, \lambda_{Ex2}/\lambda_{Em}$ : 235, 315/436 nm) referred to as peaks A + M/C (Coble, 2007, 1996; Hudson et al., 2007) or component 3 (Ishii and Boyer, 2012) in different DOM fluorophore classifications has been reported in various coastal and marine environments (Ferretto et al., 2017; Tedetti et al., 2020). HS-like fluorescence intensity ranged from 0.7 QSU in the mixed layer of the Western Lau Basin to 4.1 QSU in the PDW of the Melanesian Basin (Figure 5.4b). HS-like fluorescence systematically increased with depth, characteristic of photobleaching in the photic layer and increasing aromaticity with mineralisation (Heller et al., 2013; Nelson et al., 2010; Yamashita et al., 2017). The depth profiles of DOC (higher values in surface waters, lower at depth) and HS-like fluorescence intensity (lower values in surface waters, higher at depth) along the transect are commonly observed and have been reported for the Atlantic and North Pacific oceans (Cao et al., 2020; Omori et al., 2010; Stedmon and Álvarez-Salgado, 2011; Yamashita et al., 2017) and in the South Pacific gyre at our sampling location, at ST8 (Fourrier et al., 2022). The higher content observed in the deep waters at ST2, ST3, ST4, ST10-T1, ST10-T2, and ST6 were suggesting either benthic or hydrothermal sources of HS-like FDOM. The higher HS-like FDOM content observed at ST8 compared to ST7 was not coupled to an increase in DOC, suggesting different composition of the DOM between these two stations.

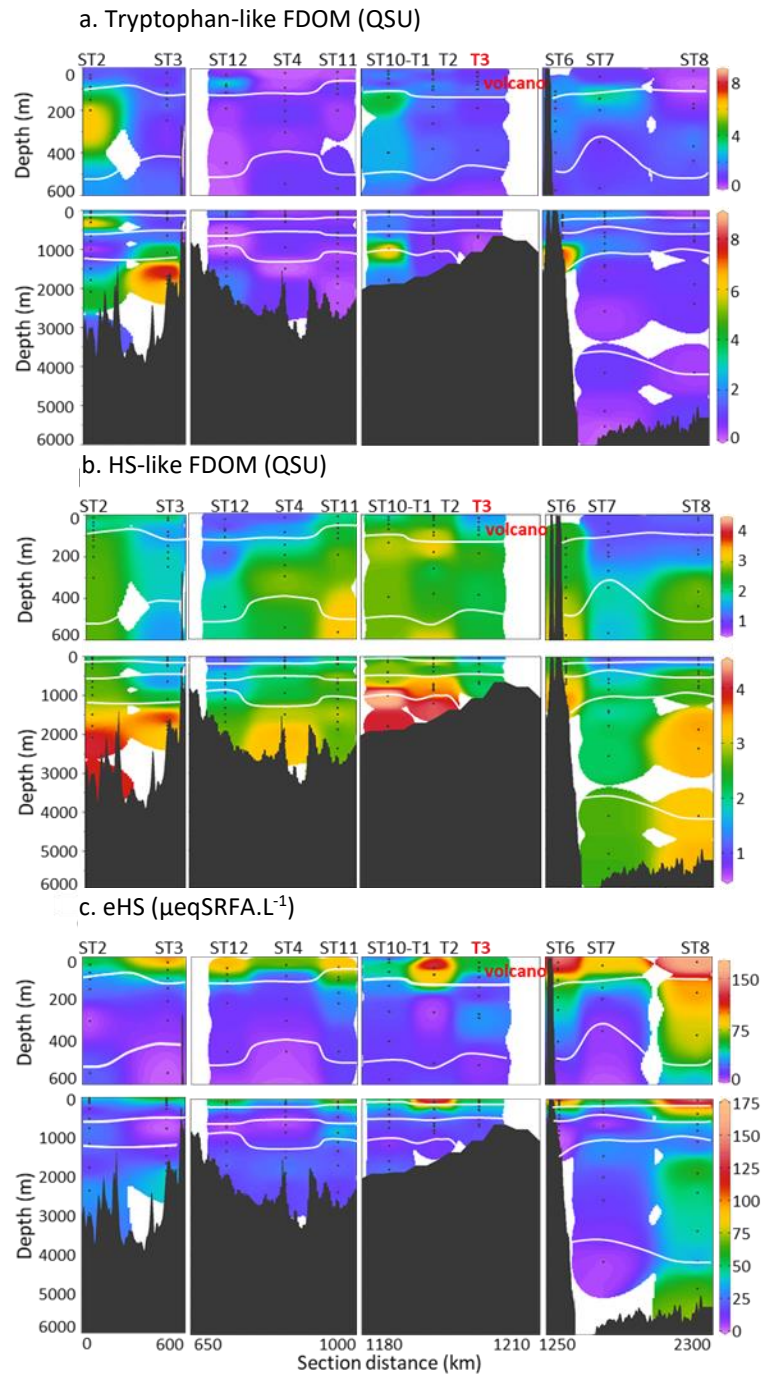


Figure 5.4. Top 600 m and full depth distribution of a) tryptophan-like FDOM, b) HS-like FDOM and b) eHS for the TONGA cruise (GEOTRACES GPpr14). The approximate water mass boundaries are defined by  $\text{O}_2$  (see Figure 2). The section is separated in four segments with, from left to right, the Melanesian basin (ST2 and ST3), the Western Lau basin (ST12, ST4, ST11), the Eastern Lau basin (ST10-T1, ST10-T2, ST10-T3) and the South Pacific gyre (ST6, ST7, ST8). See Figure 1 for more details on the sampling locations.

### 5.3.4. eHS

Details on the distribution, sources and sinks of eHS in the area are fully described elsewhere (Dulaquais et al., in prep.; Portlock et al., in prep.); Fe-eHS are shown here (Figure 5.4c) for comparison with Fe-binding ligands and HS-like FDOM. For the dataset considered in this work, eHS concentrations ranged from 10 to 163  $\mu\text{geqSRFA.L}^{-1}$  with a mean value of  $43 \pm 35 \mu\text{geqSRFA.L}^{-1}$  ( $n = 106$ ; Figure 5.5b). The highest values were observed in the mixed layer at all stations. Comparatively high eHS concentrations were detected through the entire water column of the oligotrophic ST8 in the South Pacific gyre.

### 5.3.5. DFe

DFe distribution has been thoroughly described elsewhere (Tilliette et al., 2022). For the dataset considered in this work, DFe concentrations ranged from 0.13  $\text{nmol.L}^{-1}$  in the mixed layer of the Western Lau basin to 3.13  $\text{nmol.L}^{-1}$  in the mixed layer of the Eastern Lau basin (Figure 5.5a). Higher DFe concentrations up to 50  $\text{nmol.L}^{-1}$  were observed in samples from station 5 (Tilliette et al., 2022), however we do not have data for Fe-binding ligand characteristics for those samples. The Melanesian basin and the South Pacific gyre showed DFe depletion in surface waters due to biological uptake, and an increase at depth with mineralisation in the range of previously reported open-ocean values (e.g. Resing et al., 2015; Tagliabue et al., 2012; Tonnard et al., 2020). The Western Lau basin showed similar DFe depletion in subsurface waters with the exception of a strong enhancement in the WSPCW at Station 11. Another strong DFe was enhancement observed in the mixed layer of the Eastern Lau basin, the highest values of the transect, attesting of to a source of DFe of hydrothermal origin (Benavides et al., 2022; Tilliette et al., 2022). Deep waters of the Eastern and Western Lau basin showed signs of DFe enrichment, related to mineralisation, benthic fluxes and/or hydrothermal activity, in the concentration range of previously reported values for similar bottom enrichment related to hydrothermal and shelf input (e.g. Klunder et al., 2012, 2011; Resing et al., 2015; Tonnard et al., 2020).



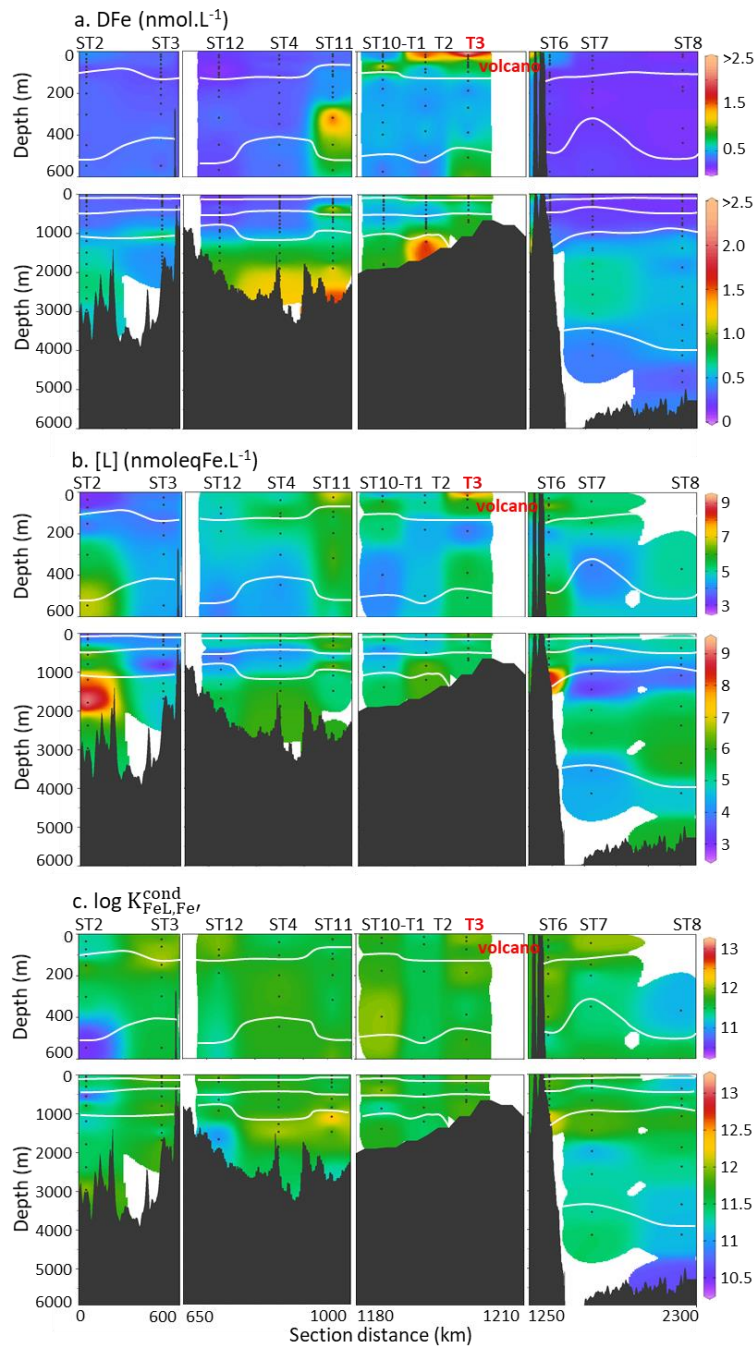


Figure 5.5. Top 600 m and full depth distribution of a) DFe, b) [L] and c)  $\log K_{FeL,Fe}^{cond}$  for the Tonga cruise (GEOTRACES GPpr14). The approximative water mass boundaries are defined by  $O_2$  (see Figure 5.2). The section is separated in 4 segments with, from left to right, the Melanesian basin (ST2 and ST3), the Western Lau basin (ST12, ST4, ST11), the Eastern Lau basin (ST10-T1, ST10-T2, ST10-T3) and the South Pacific gyre (ST6, ST7, ST8). See Figure 5.1 for more details on the sampling locations.

### 5.3.6. Iron-binding ligands

A single class of Fe-binding ligand was detected in all samples, with a mean  $[L]$  of  $5.2 \pm 1.2$  nmoleqFe.L<sup>-1</sup> and mean  $\log K_{FeL,Fe'}^{cond}$  of  $11.6 \pm 0.4$  (n = 103 samples; Figure 5.5b and Figure 5.5c, respectively).  $\log K_{FeL,Fe'}^{cond}$  ranged from 10.5 in the AAIW of the Melanesian basin to 12.7 in the PDW of the Western Lau basin, encompassing the 3 ligand classes defined by Gledhill and Buck (2012). 84% of our samples fell in the L<sub>2</sub> class, 13% in the L<sub>1</sub> class, and 4% in the L<sub>3</sub> class.  $[L]$  ranged from  $2.8 \pm 0.4$  nmoleqFe.L<sup>-1</sup> in the mixed layer of the Melanesian Basin to  $9.3 \pm 1.0$  nmoleqFe.L<sup>-1</sup> in the PDW of the Melanesian basin. Values of  $[L]$  reaching around 9.0 nmoleqFe.L<sup>-1</sup> were observed at two other locations, in the AAIW above the Tonga ridge in the South Pacific gyre (ST6) and in the mixed layer in the Lau basin (ST10-T3). At ST2 and ST6, higher  $[L]$  coincided with tryptophan-like and (in a lower extent) with HS-like FDOM (Figure 5.4a, b). In all samples,  $[L]$  was in large excess compared to DFe, with excess ligand ( $[L]_{ex}$ ) ranging from 2.6 to 8.6 nmoleqFe.L<sup>-1</sup> and a mean  $[L]_{ex}$  of  $4.6 \pm 1.1$  nmoleqFe.L<sup>-1</sup> (n = 103).

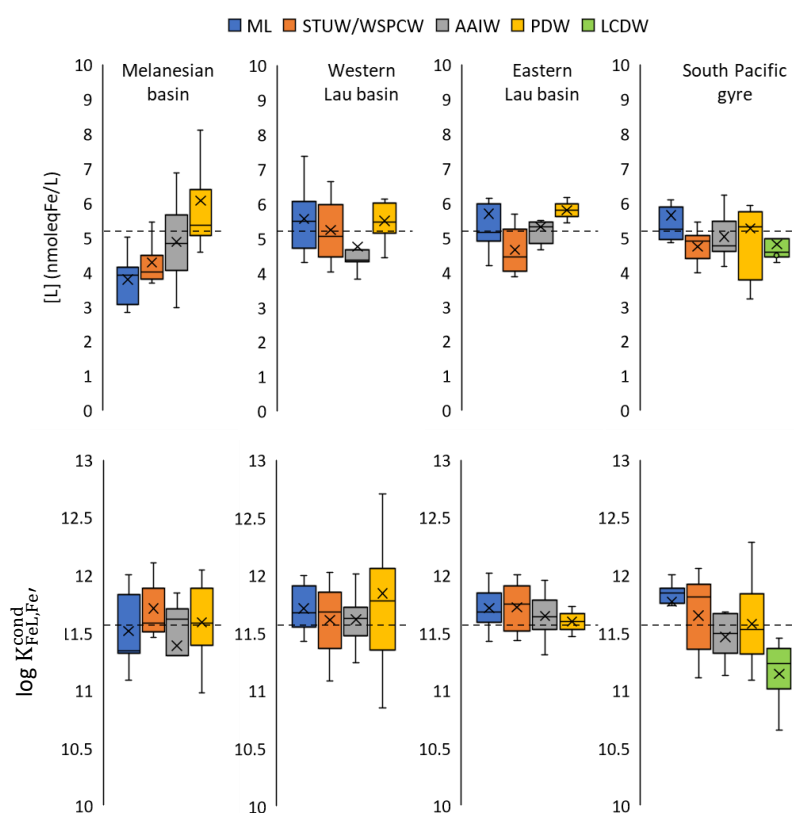


Figure 5.6. Box and Whiskers plot of a)  $[L]$  and b)  $\log K_{FeL,Fe'}^{cond}$ , split by the regions and water masses. The mean values of the entire dataset are represented (black dot line). Please refer to Figure 2 regarding the acronyms of the water masses.

The mixed layer showed lower [L] and  $\log K_{\text{FeL,Fe}'}^{\text{cond}}$  in the Melanesian basin than in other regions, suggesting lower production of Fe-binding ligands (Figure 5.6). The Western Lau basin showed relatively higher [L] in the STUW/WSPCW than other regions, potentially due to higher remineralization of sinking particles. The Western Lau basin also showed lower [L] in the AAIW than other regions, suggesting stronger Fe-binding ligand scavenging compared to other regions. Overall, the distribution of [L] and  $\log K_{\text{FeL,Fe}'}^{\text{cond}}$  was relatively homogenous regionally, except for the increase in [L] and decrease in  $\log K_{\text{FeL,Fe}'}^{\text{cond}}$  along water mass deepness in the Melanesian basin and South Pacific gyre, respectively.

## 5.4. Discussion

### 5.4.1. [L] and $\log K_{\text{FeL,Fe}'}^{\text{cond}}$ distribution in the WTSP

Contrasting with previous studies using similar CLE-ACSV application in other regions, we found even distribution of high [L] along basins and water masses, most of them falling in the L<sub>2</sub> class (84%). In comparison, in the Eastern and Central TSP, L<sub>1</sub> class ligands were detected in 54%, L<sub>2</sub> in 62%, and L<sub>3</sub> in 23% of the samples (Buck et al., 2018). These authors found that L<sub>1</sub> ligands were generally in excess compared to DFe in the first 1000 m, while excess L<sub>2</sub> and L<sub>3</sub> increased in deeper water. This distribution traduced the biological production of strong L<sub>1</sub> in upper waters, and the loss and saturation of these L<sub>1</sub> ligands with mineralization of the dissolved and organic material, responsible for increasing DFe and weaker ligands L<sub>2</sub> and L<sub>3</sub>. In our study, a decrease in  $\log K_{\text{FeL,Fe}'}^{\text{cond}}$  with depth was observable in the South Pacific gyre (Figure 6), but without change of ligand class, and no change in  $\log K_{\text{FeL,Fe}'}^{\text{cond}}$  were found in the Melanesian and Lau basins. The predominance of L<sub>2</sub> all along the water column, including surface waters, suggested that the mineralization was the main driver of the Fe-binding characteristics of the DOM.

A single ligand class was determined for all the titration performed in WTSP samples, as opposite to other studies using the same added ligand at the same concentration (e.g. Buck et al., 2018, 2015). This phenomenon could partly be explained by the large [L] being titrated. It is acknowledged that the

heterogeneity of the DOM composition is responsible for a continuum of  $\log K_{\text{FeL,Fe}'}^{\text{cond}}$  across the diverse compounds present in a seawater sample (Gledhill and Buck, 2012; Town and Filella, 2000). This is a well-known limitation of the CLE-ACSV approach, which provides an average  $\log K_{\text{FeL,Fe}'}^{\text{cond}}$  of the ligand pool. The presence of a large amount of [L], presumably proportional to the diversity in  $\log K_{\text{FeL,Fe}'}^{\text{cond}}$ , could therefore dilute and mask distinctive ligand classes.

In the WTSP, the difference between the relatively high [L] and low DFe was responsible for large  $[\text{L}]_{\text{ex}}$  compared to previous studies, even in the western part of the South Pacific gyre. In the Eastern and Central TSP, the  $[\text{L}]_{\text{ex}}$  was of  $1.86 \pm 1.05 \text{ nmoleqFe.L}^{-1}$  ( $n = 548$ ; Buck et al., 2018), more than twice lower than what was measured in the WTSP and South Pacific gyre. The difference between the Eastern and Central TSP and the western part of the South Pacific gyre in terms of  $[\text{L}]_{\text{ex}}$  and ligand classes suggested different biogeochemical processes driving the Fe-binding ligand cycling. The same analytical method was employed between these two studies, and the oligotrophy of the South Pacific gyre is highly contrasted with the Lau basin (Guieu et al., 2018). It would be of interest to analyze samples from a section crossing the Lau basin, and the whole the South Pacific gyre to evaluate the changes in biogeochemical regimes. A latitudinal transect in the Pacific included a sampling location near the Tonga trench but with a different analytical method and found  $[\text{L}]_{\text{ex}}$  of  $0.31 \pm 0.40 \text{ nmoleqFe.L}^{-1}$  ( $n = 46$ ) falling in the  $L_1$  class (Kondo et al., 2012), more than ten-fold lower than our values. They found excess of ligands in surface waters and excess of DFe in deep waters, contrasting with our large  $[\text{L}]_{\text{ex}}$  presumably due to the analytical method employed. Kondo et al. (2012) employed TAC, as added ligand, used at a higher detection window and, therefore, focusing on fewer Fe-binding ligands of higher  $\log K_{\text{FeL,Fe}'}^{\text{cond}}$ . TAC is also known as interfering with the detection of HS-like material of riverine origin (Laglera et al., 2011), missing a fraction of ligands falling in the  $L_2$  class. The detection of lower [L] than DFe using TAC could, therefore, be due to the missed HS fraction.

The difference in [L] and  $[\text{L}]_{\text{ex}}$  between the use of SA and TAC could also be impacted by colloidal material. Colloidal material is operationally defined between 0.02 and 0.2  $\mu\text{m}$ , and is composed of inorganic, organic, and combined material. In this study, the use of SA at 25  $\mu\text{mol.L}^{-1}$  results in a much

lower detection window than the use of TAC. The absorption of the Fe added to titrate organic ligands onto inorganic and organic colloids is therefore more plausible (Kondo et al., 2021), and would result in an over estimation of [L] and [L]<sub>ex</sub>. The importance of the colloidal fraction on the [L] determination was shown in the Western Subarctic Pacific using SA (Kondo et al., 2021), where the [L] of the colloidal fraction could represent as much as 75% of the total [L] in subsurface samples. The mechanisms at play are still not fully understood, but flocculation and precipitation of the colloidal fraction could be an important sink of DFe in the WTSP. It would be of great interest to measure Fe and [L] in the soluble fraction to define the potential of the colloidal fraction to scavenge DFe in the WTSP.

#### **5.4.2. Control on Fe-binding ligand distribution and DFe stabilization**

Despite the strong [L]<sub>ex</sub> and the apparent homogeneity of Fe-binding characteristics, weak but significant correlation was found between [L] and DFe (Table 1). Interestingly, either of [L] nor  $\log K_{\text{FeL,Fe}'}^{\text{cond}}$  were correlated to AOU or DOC. The strong correlation observed between AOU and DOC is typical of the microbial mineralization of dissolved and particulate material with depth (Nelson et al., 2010), while  $\log K_{\text{FeL,Fe}'}^{\text{cond}}$  values suggested mineralization to mainly drive Fe-binding ligand characteristics. The homogeneity of Fe-binding ligand characteristics could be explained by the physics of the area. Tilliette et al. (2022) attributed the depletion of DFe in surface waters to their low residence time compared to deep waters. We suggest that quicker removal than production of [L] in surface waters and production by mineralization in deep waters were balancing each other and explained the homogeneity of Fe-binding ligand characteristic in the WTSP. This hypothesis is complementary to the suggestion of intense production of Fe-binding ligands by the abnormally large [L]<sub>ex</sub> and homogenous  $\log K_{\text{FeL,Fe}'}^{\text{cond}}$ .

Table 5.1. Table of the Spearman rank correlation ( $\rho$ ) of investigated parameters for the Tonga transect. Blue corresponds to negative correlation, red to positive correlation, and white to absence of correlation. The intensity of the color is proportional to the strength of the correlation. Bold values correspond to  $p < 0.0001$  (higher level of confidence compared to studies discussing Spearman correlation matrixes and including Fe-binding ligands data, e.g. Genovese et al., 2018; Heller et al., 2013).

	AOU ( $\mu\text{mol.L}^{-1}$ )	DOC ( $\mu\text{mol.L}^{-1}$ )	DFe ( $\mu\text{mol.L}^{-1}$ )	[L] ( $\text{nmoleqFe.L}^{-1}$ )	$\log K_{\text{FeL,Fe}}^{\text{cond}}$	eHS ( $\mu\text{geqSRFA.L}^{-1}$ )	Humic-like FDOM (QSU)
DOC ( $\mu\text{mol.L}^{-1}$ )	<b>-0.93</b> n = 169						
DFe ( $\mu\text{mol.L}^{-1}$ )	<b>0.52</b> n = 238	<b>-0.55</b> n = 159					
[L] ( $\text{nmoleqFe.L}^{-1}$ )	0.20 n = 103	-0.18 n = 70	<b>0.40</b> n = 103				
$\log K_{\text{FeL,Fe}}^{\text{cond}}$	-0.18 n = 103	0.18 n = 70	-0.08 n = 103	-0.22 n = 103			
eHS ( $\mu\text{geqSRFA.L}^{-1}$ )	<b>-0.47</b> n = 120	<b>0.48</b> n = 83	-0.23 n = 119	-0.04 n = 94	0.11 n = 94		
HS-like FDOM (QSU)	<b>0.67</b> n = 130	<b>-0.72</b> n = 130	<b>0.43</b> n = 122	0.17 n = 56	-0.13 n = 56	-0.25 n = 67	
Tryptohan-like FDOM (QSU)	-0.03 n = 91	0.05 n = 91	-0.18 n = 88	0.02 n = 42	0.08 n = 42	0.21 n = 46	0.26 n = 91

The correlations of eHS with DFe, DOC, and AOU were somehow lower than previously reported in other regions (Dulaquais et al., 2018; Fourrier et al., 2022; Whitby et al., 2020b), while a weak but significant correlation was found between DFe and HS-like FDOM. DFe and HS-like FDOM were also correlated to AOU and DOC, but their distribution cannot be simply attributed to mineralization in the WTSP. Even if the moderate correlation between HS-like FDOM and AOU demonstrated the production of HS-like FDOM with mineralization of sinking particles (Nelson et al., 2010), HS-like FDOM and DOC are usually not correlated. This is due to the stability of the HS-like FDOM content compared to DOC depletion in deep waters (Nelson et al., 2010 and references within). Here, the high negative correlation between HS-like FDOM and DOC suggested the occurrence of specific processes responsible for increased HS-like FDOM content in deep and bottom waters. Further work should aim at defining if these processes are associated to the hydrothermal activity of the area. The potential for hydrothermal activity to impact the eHS fraction is also yet to be addressed.

### 5.4.3. Humic contribution to the Fe-binding ligand pool

Similar to previous studies in this region, we found L<sub>2</sub> ligands to dominate the water column (Buck et al., 2018; Cabanes et al., 2020). The L<sub>2</sub> ligand class is often considered to be humic-like (Gledhill and Buck, 2012; Hassler et al., 2017) and our averaged  $\log K_{\text{FeL,Fe}'}^{\text{cond}}$  corresponded to  $\log K_{\text{FeL,Fe}'}^{\text{cond}}$  values reported for Suwannee River humic-acid standards (SRHA; 11.1-11.6; Abualhaija et al., 2015; Abualhaija and van den Berg, 2014; Laglera and van den Berg, 2009). Around half of DOM is composed of HS-like material (Zigah et al., 2017), and around 5% can act as Fe-binding HS (Dulaquais et al., 2018; Laglera and van den Berg, 2009). DFe has been shown to correlate with eHS (Dulaquais et al., 2018; Whitby et al., 2020b) and Fe solubility has been shown to correlate with AOU and humic-like fluorescence (Cao et al., 2020; Hioki et al., 2014; Tani et al., 2003; Yamashita et al., 2017). The electroactive and fluorescent properties of HS have been thoroughly investigated in the samples from ST8 in the oligotrophic subtropical gyre (Fourrier et al., 2022). These authors observed similar HS properties in terms of Fe-eHS concentrations, Fe-binding properties, and fluorescence as previously reported in the Pacific Ocean (Fourrier et al., 2022 and references therein). However, the importance of the HS-like contribution to the Fe-binding DOM in waters impacted by diazotrophy and hydrothermalism is currently unknown. The Fe-binding ability determined for humic and fulvic standards by Laglera and van den Berg (2009), updated by Sukekava et al. (2018), allows an estimation of the amount of Fe that can be bound by the eHS. Most studies use the Fe-binding ability of the IHSS fulvic acid (FA) standard, as it is considered the most representative of marine HS (Cabanes et al., 2020; Dulaquais et al., 2018; Whitby et al., 2020a). A higher Fe binding capacity based instead on the Fe-binding ability of the humic acid standard (HA) has been previously used as an upper limit of eHS Fe-binding ability in marine systems (Laglera and van den Berg, 2009; Whitby et al., 2020b). We included here the results obtained with the two conversion factors and compared them to [L] and DFe concentrations (Table 5.2).

Table 5.2. Mean values of DFe, extremum ability of eHS to bind DFe, and [L] for the mixed layer and deeper waters.

Considered data	DFe (nmol.L <sup>-1</sup> )	Minimum Fe-eHS (nmoleqFe.L <sup>-1</sup> )	Maximum Fe-eHS (nmoleqFe.L <sup>-1</sup> )	[L] (nmoleqFe.L <sup>-1</sup> )
Mixed layer	0.45 ± 0.50 n = 60	1.3 ± 0.7 n = 31	2.5 ± 1.3 n = 31	5.3 ± 1.4 n = 24
Deeper waters	0.51 ± 0.30 n = 178	0.5 ± 0.3 n = 75	0.9 ± 0.6 n = 75	5.2 ± 1.1 n = 79

Note. Upper and lower estimates of Fe-binding equivalent concentrations for EHS were calculated using 16.4 nmo[L].mgFA-1 from Sukekava et al. (2018; minimum Fe-eHS), and 32.0 nmo[L].mgHA-1 from Laglera and van den Berg (2009; maximum Fe-eHS).

With regards to the eHS transects, we decided to separate the mixed layer, where eHS maximum and HS-like FDOM minimum were observed, and deeper waters, depleted in eHS and with higher HS-like FDOM content (Figure 5). The Fe-binding potential of the whole ligand pool (e.g. [L]) was explained by eHS from 20 to 40% in surface waters and from 8 to 18% in deep waters (Table 2). Both [L] and eHS were in excess compared to DFe in all samples investigated in our study. More information on eHS saturation can be found in Dulaquais et al. (in prep.). In contradiction to the eHS unsaturation in the deep waters of the WTSP, hydrothermal transformation of the DOM was recently shown to promote the formation of HA in sediments (Sarma et al., 2018), previously suggested as having a higher Fe-binding potential than FA. It was shown that the unsaturation of eHS could be proportional to the aging of the inorganic fraction of Fe under the form of oxyhydroxides (Dulaquais et al., in prep.), however, the hydrothermal activity of the area and potential relation with the abundance of HS-like FDOM suggested a complementary explanation. Hydrothermally derived HS, showing FA characteristics, have been shown able to bind Fe<sup>2+</sup> (Aquilina et al., 2015), while the electrochemical determination of the Fe bound to eHS is specific to Fe<sup>3+</sup>. The distinct distributions of eHS and HS-like FDOM suggested different fractions of HS are detected with each operationally-defined method, which could have specificities toward specific ionic form of Fe they are able to bind. It would be of major interest to estimate the HS-like FDOM ability to stabilize Fe<sup>2+</sup> and Fe<sup>3+</sup> through quenching experiments to define



its role in the dispersion of hydrothermally sourced DFe, specifically in cases where DFe is transported over long distances. However, here, DFe was relatively quickly scavenged from the water column (Tilliette et al., 2022), and the Fe-binding ligands including eHS were largely unsaturated (Dulaquais et al., in prep.; this study), attesting of the predominance of removal processes in the Fe cycle in the WTSP.

#### 5.4.4. Interpretation of [L] enhancements

Several samples showed substantial increase in [L] along the transect. We compared the profiles of [L] with complementary variables owing to explain these higher values and understand their implication for carbon and Fe cycling in the WTSP (Figure 7). Enhanced [L] were observed at ST2, ST6 and ST10-T3 (Figure 7a, b, and c, respectively). At ST2, [L] variations were somehow coinciding with tryptophan-like FDOM variations. The correlation between [L] and the abnormally high tryptophan-like FDOM content observed in surface and deep waters at ST2 could not be depicted further because of the mismatch in analysis depths and the lack of resolution comparatively to the variability observed, pressing for better resolution and coordination of the analyses in future work. Tryptophan-like FDOM is produced by phytoplankton, such as diatoms and cyanobacteria (Henderson et al., 2008), and form weak complexes with  $\text{Fe}^{2+}$  (Limson et al., 1998). It was recently shown that significant increase of tryptophan-like FDOM could be related to the presence of sinking photosynthetic colonies of cyanobacterium *Trichodesmium* and other diazotrophs in the Eastern Lau basin, able to fix nitrogen even in waters as deep as 1000 m (Benavides et al., 2022). However, very low density of *Trichodesmium* were observed in the Melanesian basin (Lory et al., 2022), while very high concentration of thiols was observed along the entire water column at ST2 (Portlock et al., this issue). Thiols are sulphur-containing compounds able to bind toxic metals such as copper, and their production as detoxifying agents has been shown during incubation experiments performed during the Tonga cruise (Tilliette et al., in press.). This suggests that the enhanced [L] and tryptophan-like FDOM were related to the biological activity associated to the toxicity of hydrothermal fluids. There was no discernable impact of [L] and tryptophan-like FDOM enhancement on either DFe, HS content,  $\log K_{\text{FeL,Fe}'}^{\text{cond}}$ , nor DOC.

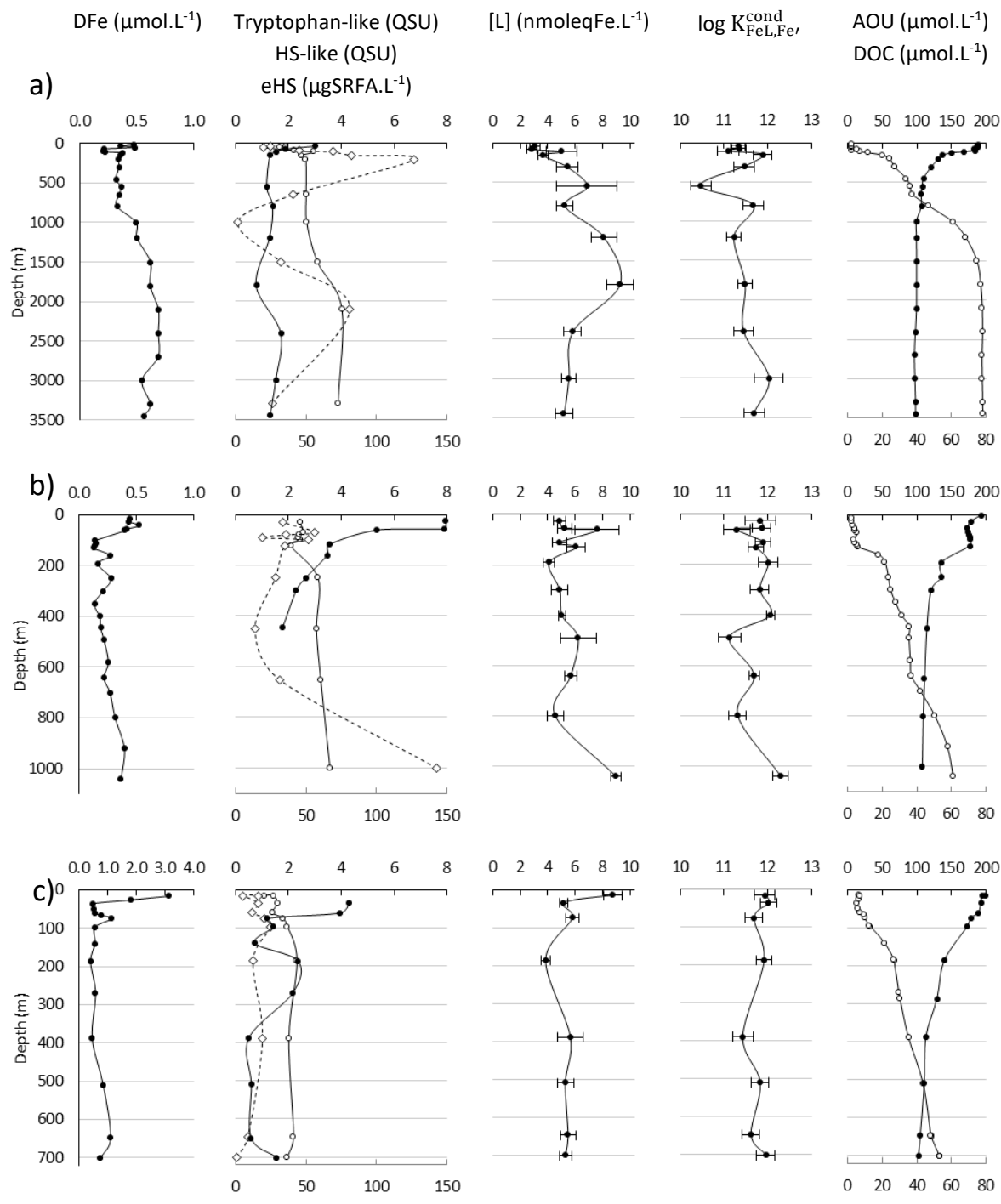


Figure 5.7. Profiles with depth at a) ST2, b) ST6, and c) ST10-T3. The profiles are showing (from left to right) DFe, tryptophan-like FDOM (dotted line, open circles), HS-like FDOM (full line, open circles), eHS (full line, full circles, bottom axis), [L],  $\log K_{FeL,Fe}^{cond}$ , AOU (open circles), and DOC (full circles, bottom axis).

Stronger relationship between [L] and tryptophan-like FDOM content emerged at ST6 where analysis depth were closer than at ST2. On the other hand, tryptophan-like FDOM, [L] and  $\log K_{FeL,Fe}^{cond}$  showed contrasted relationship between surface and deep waters (Figure 7b). The tryptophan-like FDOM content showed a smaller range of variability in the surface waters of ST6 (1.0 to 2.8 QSU) compared

to deep waters (0.7 to 7.6 QSU), of similar range that the variability observed at ST2 (0.1 to 6.8 QSU). In surface waters, the variations in  $\log K_{\text{FeL,Fe}'}^{\text{cond}}$  were inversely proportional to [L] and tryptophan-like FDOM, which were covarying. In deep waters,  $\log K_{\text{FeL,Fe}'}^{\text{cond}}$ , [L] and tryptophan-like FDOM were all covarying, with extensive increase of the tryptophan-like FDOM. FDOM measurements are not compounds specific; several compounds can be excited and emit at similar wavelength, but with different fluorescent abilities. Therefore, the emission quantified can be compound dependent and not quantitative. The contrast between surface and deep waters covariation between [L] and tryptophan-like FDOM suggested the implication of different compounds in the tryptophan-like FDOM identified. Surface tryptophan-like FDOM seemed to contribute to the Fe-binding ligand pool in term of binding-sites and impacted more sensitively [L] than in deep waters, and with regards to  $\log K_{\text{FeL,Fe}'}^{\text{cond}}$ , seemed to fell in the L<sub>2</sub> class or below. Deep tryptophan-like FDOM were showing lower contribution to [L], but these compounds had comparatively higher  $\log K_{\text{FeL,Fe}'}^{\text{cond}}$ . The reason for [L] and tryptophan-like FDOM enhancement remain uncertain at this location, but could be related to benthic processes, sinking diazotroph colonies, or hydrothermal activity. The implication of the latter was suggested by the range of variability experienced by the tryptophan-like FDOM, similar to ST2, despite the absence of thiol enhancement (Portlock et al., this issue). Interestingly, DFe seemed to covary with eHS in surface waters and with HS-like FDOM in deep waters at ST6.

Table 5.3. Values in surface sample (depth < 20 m) with distance to the hydrothermal site.

	ST10-T3 – 2 km	ST10-T2 – 8 km	ST10-T1 – 15 km
DFe (nmol.L <sup>-1</sup> )	3.20	1.52	0.38
[L] (nmoleqFe.L <sup>-1</sup> )	8.8 ± 0.7	4.7 ± 0.9	4.2 ± 0.6
$\log K_{\text{FeL,Fe}'}^{\text{cond}}$	11.9 ± 0.2	11.4 ± 0.3	11.8 ± 0.2
eHS (µgSRFA.L <sup>-1</sup> )	79	163	86
HS-like FDOM (QSU)	1.3	2.1	1.8
Tryptophan-like FDOM (QSU)	0.6	1.5	1.3

A relatively strong DFe enhancement of hydrothermal origin was observed in the mixed layer at ST10-T3, coinciding with enhanced [L] (Figure 7c; Tilliette et al., 2022). This station was part of a distal transect performed at a hydrothermal site, where repeated casts were performed at 2 km (ST10-T3), 8 km (ST10-T2) and 15 km (ST10-T1). Surface waters showed a DFe gradient decreasing linearly with distance to the hydrothermal source, while [L] was high only at the closest station to the vent (Table 3). [L] was the only variable showing positive covariation with DFe along the distal transect, and no significant differences in  $\log K_{FeL,Fe}^{cond}$  were observed between the stations, which fell into the L<sub>2</sub> class. This [L] enhancement was contrasting with the observations from ST2 and ST6 in its ability to stabilize DFe, and to not show covariation with tryptophan-like FDOM. This specificity could be partly related to the abundance of colonial diazotrophs observed in the Lau basin and (Benavides et al., 2022; Lory et al., 2022). Strong tryptophan-like FDOM signal were measured in diazotroph cultures corresponding to the species present at this location (Benavides et al., 2022), suggesting that there was no tryptophan-like FDOM diffusing from the diazotroph colonies responsible for enhanced [L] or that the FDOM was subject to photobleaching/light attenuation. In absence of diffusion of tryptophan-like FDOM from diazotroph colonies, and in view of the absence of specific HS signature, we must consider other candidates to explain the enhanced [L] in response to hydrothermally sourced toxic metals, such as the production of specialized metal binding compounds. Our results could suggest the production by diazotroph of metal binding ligands comparable to siderophores (Bundy et al., 2018) or to domoic acid (Pan et al., 1998). The identification of these compounds using recent analytical developments (Boiteau and Repeta, 2022; Bundy et al., 2018) would lead to a better understanding of the defense mechanisms and Fe acquisition strategies of the hydrothermally fueled diazotrophs flourishing observed in the WTSP. Overall, the processes at play at the three locations showing local [L] enhancement are calling for further investigation in the area and development of laboratory-based experiments, notably regarding the entanglement between tryptophan-like FDOM and [L] variations, if owing to explain carbon and Fe cycling in hydrothermal systems.

## 5.4.5. Future and perspective for Fe-binding ligands detection

### 5.4.5.1. In hydrothermal waters

The comparison of our results with previous studies on hydrothermal systems shows possibilities to refine the methodological approach to constrain the identification and quantification of Fe-binding ligands by CLE-ACSV in future work. The different CLE-ACSV methodologies are showing discrepancies in terms of  $[L]$  and/or  $\log K_{FeL,Fe}^{cond}$  (Ardiningsih et al., 2021; Buck et al., 2012; Gerringa et al., 2021), and even if it can be complicated to disentangle the natural variability of the Fe-binding ligand characteristics from the technically induced differences, it is essential to compare the dataset obtained to better understand these technical differences and the Fe-binding ligand cycle.

Fe-binding ligands have been previously investigated in hydrothermal fluids sourced in the Melanesian basin with (Kleint et al., 2016) and in the Lau basin (Wang et al., 2022) by CLE-ACSV, but following different approaches. Kleint et al. (2016) used SA at  $100 \mu\text{mol.L}^{-1}$  for a single aliquot equilibrated overnight, with, the following day, five DFe spikes equilibrating for ten minutes each. Wang et al. (2022) used 1-nitroso-2-naphtol (NN) following the reverse titration approach (RT-CLE-ACSV) consisting of titrating hydrothermal fluids with NN additions instead of DFe additions (Hawkes et al., 2013a). The importance of the added ligand used and of its concentration has been previously addressed for the detection of HS-like ligands by Laglera et al. (2011). The authors concluded that the added ligand SA was best suited for detection of HS by CLE-ACSV, and that NN outcompeted HS in the concentration range required for optimal sensitivity. Despite the need of further studies, we hypothesize that the added ligands and their detection window could explain the  $[L_{ex}]$  when using SA in hydrothermal plumes (Kleint et al., 2016; this study), and the excess of DFe when using NN (Hawkes et al., 2013b; Wang et al., 2022, 2019). The NN additions being relatively high with the RT-CLE-ACSV approach (higher than the concentrations that outcompeted HS in classic CLE-ACSV methods; Hawkes et al., 2013a), the contribution of HS-like ligands to the Fe-binding ligand pool could be missed. This, however, contradicts with the  $\log K_{FeL,Fe}^{cond}$  determined with NN by RT-CLE-ACSV, which are usually

lower than those determined with SA in hydrothermal plumes (e.g. Hawkes et al., 2013b; Kleint et al., 2016; Wang et al., 2022, 2019).

More systematic comparison of the different approaches in place is needed to identify the reason of the diverging results observed. We also strongly suggest to titrate HS-like and tryptophan-like FDOM with  $\text{Fe}^{2+}$  and  $\text{Fe}^{3+}$  as well. Such quenching experiment would allow the determination of the amount and speciation of DFe that can be bond to these fractions, to be compared to the to the amount bond by eHS (Dulaquais et al., this issue) and by the whole pool of Fe-binding ligands (this study).

#### **5.4.5.2. Deposition potential with depth and by basins**

In this study, during the treatment of the voltammograms recorded by ACSV, a shift in the reduction potential of the Fe-added ligand complex was observed. The reduction potential ranged from -413 mV to -445 mV within the first 200 m (mixed layer and most of the STUW/WSPCW), decreasing further with depth down to 1200 m to reach a stable mean value of -473 mV from 1200 m to the bottom (Figure 8a). The first 200 m correspond to well oxygenated waters, and the decrease in reduction potential started occurring in the bottom sample of the STUW/WSPCW where  $\text{O}_2$  started decreasing, characteristic of mineralization.

The reduction of the metal complexed by the added ligands during ACSV analysis happens at a specific potential following the Nernst equation (Nernst, 1889). The value of this potential is driven by i) the conditions of temperature, pH, and salinity, and ii) the activity of the redox species, which, in the case of a metal-ligand complex, can be translated to its binding strength. Here, the temperature in the laboratory was controlled, the pH fixed by the addition of a buffer, and no correlation was found between the reduction potential and the salinity. The CLE-ACSV method using SA takes advantage of a catalytic loop involving the reduction of the dissolved  $\text{O}_2$  present in the sample, re-oxidizing the  $\text{Fe}^{2+}$  back into  $\text{Fe}^{3+}$ , enhancing the signal (Laglera et al., 2016; Mahieu, 2023). The link between the efficiency of the catalytic loop and the  $\text{O}_2$  concentration was shown to impact the reduction potential with the added ligand NN (Mahieu, 2023), but in the present work, the  $\text{O}_2$  concentration was kept stable by a constant flow of air above the sample (Mahieu, 2023). It was shown for HS that a decrease in pH

led to a decrease in the strength of the Fe-HS complexes, through an increase in the reduction potential (Laglera et al., 2007). Following this theory, the Fe-added ligand complex was more easily reduced in surface waters than in the deep waters. However, here, the pH was fixed by buffering.

The change in reduction potential could be related to the characteristics of the DOM. Fe-binding ligands are known to limit Fe<sup>3+</sup> hydrolysis and to enhance Fe solubility, and studies have shown the potential of the DOM to enhance or slow down Fe oxidoreduction kinetics (Rijkenberg et al., 2006; Rose and Waite, 2003; Santana-Casiano et al., 2022), potentially enhancing or slowing down the catalytic process benefiting the ACSV measurement. The remineralization of DOM has been shown to impact the sensitivity of CLE-ACSV using SA, showing decreasing sensitivity with depth, attributed to the mineralization of the DOM (Buck et al., 2018, 2015, 2007; Mahieu 2023) and the production of surfactant compounds adsorbing on the working electrode (van den Berg and Huang, 1984; van den Berg et al., 1991). However, the effect of DOM composition on the reduction potential and the sensitivity is yet to be fully addressed. At the moment, we can conclude that the fresh DOM produced in (sub)surface waters show lower surfactant content and higher reduction potential than the DOM in deep waters.

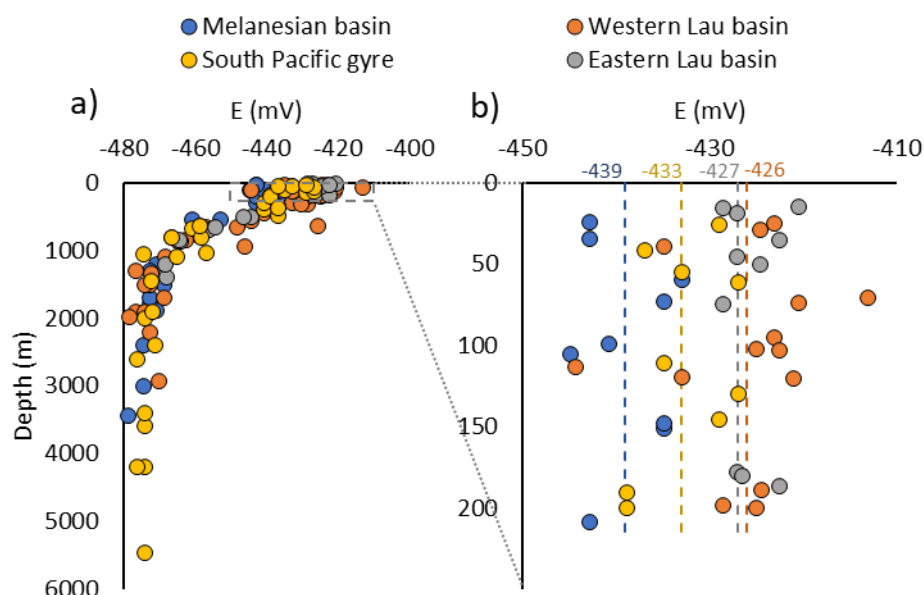


Figure 8. Reduction potential (E) of the Fe-added ligand peak with depth for a) the entire water column and b) 200 m.

Interestingly, the reduction potential showed regional differences in the well oxygenated first 200 m depth (Figure 8b). The Western Lau basin showed a reduction potential of  $-426 \text{ mV} \pm 5 \text{ mV}$  ( $n = 12$ ), the Eastern Lau basin of  $-427 \text{ mV} \pm 5 \text{ mV}$  ( $n = 11$ ), the South Pacific gyre of  $-433 \pm 5 \text{ mV}$  ( $n = 11$ ), and the Melanesian basin of  $-439 \text{ mV} \pm 5 \text{ mV}$  ( $n = 9$ ). Based on our hypothesis, the Lau basin and its intense diazotrophic activity seemed to produce DOM facilitating the ACSV measurement, while the Melanesian basin and its depletion of [L] in surface waters was the least facilitating. The South Pacific gyre fell in between, and we hypothesize the oligotrophic South Pacific gyre to be a reference of neutral impact on the reduction process and potential. Our conclusions are limited with regard of the lack of complementary information to confirm our hypothesis and compare this novel data. These results, however, suggest it would be beneficial to include the reduction potential of the peak within Fe-binding ligand datasets, as it could lead to a new understanding of the DOM properties if constrained by laboratory experiments. We recommend measuring the reduction potential in UV-irradiated seawater spiked with SA and different compounds known to either facilitate or slow down the oxidation of  $\text{Fe}^{2+}$  (e.g. bipyridyl, gallic acid) and DOM reference materials such as for HS and siderophores. Ideally, this information could be compared with Fe oxidation kinetic data, or with other methods of characterization of the DOM targeting specific chemical functions.

#### **5.4.5.3. An unexplored role of iron-sulphides in volcanic arc systems**

Compared to mid-ocean ridges, volcanic arcs are characterised by higher  $\text{CO}_2$ ,  $\text{SO}_2$  and  $\text{H}_2\text{S}$  enrichments, responsible for higher DFe removal by formation of Fe-oxyhydroxides and Fe-sulphide. Such gas enrichment and DFe removal have been observed at several locations along the Tonga-Kermadec volcanic arc (de Ronde et al., 2007; Kleint et al., 2022; Massoth et al., 2003; Neuholz et al., 2020; Resing et al., 2011). The role of Fe-sulphide formation in the Fe cycle has long been considered as a sink of hydrothermal DFe only, but recent work highlighted that the soluble ( $< 0.02 \mu\text{m}$ ) and dissolved fractions contain nanoparticulate and colloidal Fe-sulphide that could only be retrieved with nitric acid treatment. Therefore, the usual method of acidifying the sample with HCl before DFe analysis could be responsible for the underestimation of hydrothermal DFe fluxes (Yücel et al., 2021). This potential underestimation of the DFe could propagate as far as the hydrothermal influence can be



observed, and calls for the definition of a specific DFe fraction. The difference between the DFe determined by solubilisation by HCl and nitric acid could allow the determination of a dissolved Fe-sulphide fraction, pushing forward the understanding of hydrothermal Fe speciation.

The definition of the DFe fraction is of major importance in the determination of  $[L]$  and  $\log K_{FeL,Fe}^{cond}$  as DFe is implicitly incorporated in the calculation of these values. Some Fe-binding ligands are able to irreversibly bind DFe, and the crystalline structure of some Fe-oxyhydroxides is able to sterically isolate Fe from the added ligand (Kraemer et al., 2005). It is very plausible that the acidification of the samples for dissolved trace metal analysis with HCl is able to dissociate complexes that are inert at seawater pH and to dissolve Fe-hydroxide crystalline structure (Liu and Millero, 2002). While seawater collected for Fe-binding ligands analysis is not acidified, using DFe concentrations from acidified samples could over-estimate the amount of DFe the added ligand is competing for, changing the apparent Fe organic speciation values obtained ( $[L]$  and  $\log K_{FeL,Fe}^{cond}$ ). This effect has been observed in hydrothermal plumes by Kleint et al. (2016) by comparing the DFe values obtained by acidifying the samples with values of the labile Fe fraction that the added ligand was able to retrieve at natural pH. They showed that up to 90% of DFe was non-labile in the buoyant plume, but this value was down to 15% in the non-buoyant plume. It is worth noting that the hydrothermal fluids investigated by Kleint et al (2016) had DFe concentrations in the range of  $\mu\text{mol.L}^{-1}$  so the overestimation of DFe had a considerable impact on  $[L]$  and  $\log K_{FeL,Fe}^{cond}$  calculations. Overall, in the transect presented here, hydrothermal fluids were very diluted, and 90% of DFe concentrations were  $< 1 \text{ nmol.L}^{-1}$ , which represents 20% of the average  $[L]$  measured for our dataset, thus the error related to the potential overestimation of DFe in our samples is likely negligible. Nevertheless, whether sulphides, oxyhydroxides and other small particulate material that can pass through the filter, and are thus classed as dissolved by the traditional operational definition, should be considered as contributors to the ligand pool, is worth further consideration.

The definition of an Fe-sulphide fraction could be valuable not only to constrain the hydrothermal Fe speciation (Yücel et al., 2021) but the carbon cycle as well, as it can be a driver of the sulfurization of the DOM (Ma et al., 2022). Abiotic sulfurization (i.e. creation of sulphur-bonds) of the DOM by

hydrothermal sulphides was attested in the Eastern Mediterranean (Gomez-Saez et al., 2016). These authors showed that the sulfurization process consisted of the replacement of an oxygen atom by a sulphur atom in the molecule experiencing this process (Gomez-Saez et al., 2016). The sulfurization of organic matter is well known to contribute to its stabilization in soil and sediments (Sinninghe Damsté et al., 1989; Sinninghe Damsté and De Leeuw, 1990), but its role in seawater is still to be assessed (Dittmar, 2015). Abiotic and microbial sulfurization of organic matter has been shown on lipids and exopolymeric substances in sinking marine particles (Raven et al., 2021a, 2021b) as well as in algal material (Kok et al., 2000), suggesting the potential for sulfurization of Fe-binding ligands. In addition to the modification of Fe-binding ligands, the link between DOM, S and C cycles within the process of sulfurization is even tighter as it directly involves Fe-oxyhydroxides and Fe-sulphides through multiple and understudied processes. Indeed, the sulfurization process can lead to the conversion of Fe-oxyhydroxides into Fe-sulphides (Raven et al., 2021a) with unknown consequences on Fe distribution in hydrothermal systems. On the other hand, the oxidation of Fe-sulphides can lead to sulfurization of the DOM (Ma et al., 2022). The gradients in oxygen and sulphur concentration associated with hydrothermal fluids could lead to specific interplays between organic and inorganic Fe speciation, but the impact of sulfurization on the electroactivity, fluorescence, and Fe-binding ability of the DOM is yet to be investigated. With regards to the potential co-occurrence of organic matter sulfurization at hydrothermal system and in sinking diazotroph colonies, the Western South Tropical Pacific could be an ideal location to address these questions.

## 5.5. Conclusion

The comparison of the Fe-binding ligand characteristics ( $[L]$  and  $\log K_{FeL,Fe}^{cond}$ ) with HS determined by both fluorescence and voltammetry helped to constrain the processes impacting the DOM characteristics in the WTSP, although highlighted further questions. Our results suggested that the hydrothermal activities firstly identified in the Lau basin was also impacting the Melanesian basin, and potentially the western part of the South Pacific gyre, extending the biogeochemical implications of the processes at play in the area. Our data suggested DOM mineralization lead to relatively homogenous

distribution of the Fe-binding ligands in terms of [L] and  $\log K_{\text{FeL,Fe}'}^{\text{cond}}$ , while the influence of hydrothermal activity lead to enhanced HS-like FDOM content. [L] and HS-like FDOM seemed to be independently correlated to DFe, encouraging further implementation of fluorescence analysis while investigating Fe-binding ligands and its role in DFe distribution. Additional encouragement toward such practice lied on the comparison of tryptophan-like FDOM, [L] and  $\log K_{\text{FeL,Fe}'}^{\text{cond}}$  distribution at stations showing [L] maximal values. While tryptophan-like FDOM has been previously shown to bind with  $\text{Fe}^{2+}$ , CLE-ACSV focuses on  $\text{Fe}^{3+}$  and, therefore, our results suggest potential binding of  $\text{Fe}^{3+}$  with tryptophan-like compounds as well. It would be of great interest to implement quenching experiments to estimate the amount of DFe that can be complexed by the FDOM fractions and to compare with the amount determined by voltammetry for eHS and the overall [L]. Notably, such comparison could help identify the apparent defense mechanisms to hydrothermally fueled toxic metals. The WTSP could be of specific interest to address this question, with regards of the diversity of the processes highlighted in this study, regionally and along profiles.

## 5.6. References

- Ababou, F.-E., Le Moigne, F.A.C., Grosso, O., Guigue, C., Nunige, S., Camps, M., Bonnet, S., 2023. Mechanistic understanding of diazotroph aggregation and sinking: “A rolling tank approach.” *Limnol. Oceanogr.* n/a. <https://doi.org/10.1002/lno.12301>
- Abualhaija, M.M., van den Berg, C.M.G., 2014. Chemical speciation of iron in seawater using catalytic cathodic stripping voltammetry with ligand competition against salicylaldehyde. *Mar. Chem.* 164, 60–74. <https://doi.org/10.1016/j.marchem.2014.06.005>
- Abualhaija, M.M., Whitby, H., van den Berg, C.M.G., 2015. Competition between copper and iron for humic ligands in estuarine waters. *Mar. Chem.* 172, 46–56. <https://doi.org/10.1016/j.marchem.2014.06.00510.1016/j.marchem.2015.03.010>
- Aquilina, A., Homoky, W.B., Hawkes, J.A., Lyons, T.W., Mills, R.A., 2015. Hydrothermal sediments are a source of water column Fe and Mn in the Bransfield Strait, Antarctica. *Geochimica et Cosmochimica Acta* 137, 64–80. <https://doi.org/10.1016/j.gca.2014.04.003>
- Avendaño, L., Gledhill, M., Achterberg, E.P., Rérolle, V.M.C., Schlosser, C., 2016. Influence of Ocean Acidification on the Organic Complexation of Iron and Copper in Northwest European Shelf Seas; a Combined Observational and Model Study. *Front. Mar. Sci.* 3. <https://doi.org/10.3389/fmars.2016.00058>
- Benavides, M., Bonnet, S., Le Moigne, F.A.C., Armin, G., Inomura, K., Hallstrøm, S., Riemann, L., Berman-Frank, I., Poletti, E., Garel, M., Grosso, O., Leblanc, K., Guigue, C., Tedetti, M., Dupouy, C., 2022. Sinking Trichodesmium fixes nitrogen in the dark ocean. *ISME J.* 16, 2398–2405. <https://doi.org/10.1038/s41396-022-01289-6>
- Boiteau, R.M., Repeta, D.J., 2022. Slow Kinetics of Iron Binding to Marine Ligands in Seawater Measured by Isotope Exchange Liquid Chromatography-Inductively Coupled Plasma Mass Spectrometry. *Environ. Sci. Technol.* 56, 3770–3779. <https://doi.org/10.1021/acs.est.1c06922>
- Bonnet, S., Benavides, M., Le Moigne, F.A.C., Camps, M., Torremocha, A., Grosso, O., Dimier, C., Spungin, D., Berman-Frank, I., Garczarek, L., Cornejo-Castillo, F.M., 2023. Diazotrophs are overlooked contributors to carbon and nitrogen export to the deep ocean. *ISME J.* 17, 47–58. <https://doi.org/10.1038/s41396-022-01319-3>
- Bonnet, S., Caffin, M., Berthelot, H., Grosso, O., Benavides, M., Helias-Nunige, S., Guieu, C., Stenegren, M., Foster, R.A., 2018. In-depth characterization of diazotroph activity across the western tropical South Pacific hotspot of N<sub>2</sub> fixation (OUTPACE cruise). *Biogeosciences* 15, 4215–4232. <https://doi.org/10.5194/bg-15-4215-2018>
- Bonnet, S., Caffin, M., Berthelot, H., Moutin, T., 2017. Hot spot of N<sub>2</sub> fixation in the western tropical South Pacific pleads for a spatial decoupling between N<sub>2</sub> fixation and denitrification. *Proc. Natl. Acad. Sci.* 114, E2800–E2801. <https://doi.org/10.1073/pnas.1619514114>
- Buck, K.N., Lohan, M.C., Berger, C.J.M., Bruland, K.W., 2007. Dissolved iron speciation in two distinct river plumes and an estuary: Implications for riverine iron supply. *Limnol. Oceanogr.* 52, 843–855. <https://doi.org/10.4319/lo.2007.52.2.0843>
- Buck, K.N., Sedwick, P.N., Sohst, B., Carlson, C.A., 2018. Organic complexation of iron in the eastern tropical South Pacific: Results from US GEOTRACES Eastern Pacific Zonal Transect (GEOTRACES cruise GP16). *Mar. Chem., The U.S. GEOTRACES Eastern Tropical Pacific Transect (GP16)* 201, 229–241. <https://doi.org/10.1016/j.marchem.2017.11.007>
- Buck, K.N., Sohst, B., Sedwick, P.N., 2015. The organic complexation of dissolved iron along the U.S. GEOTRACES (GA03) North Atlantic Section. *Deep Sea Res. Part II Top. Stud. Oceanogr.* 116, 152–165. <https://doi.org/10.1016/j.dsr2.2014.11.016>
- Bundy, R.M., Abdulla, H.A.N., Hatcher, P.G., Biller, D.V., Buck, K.N., Barbeau, K.A., 2015. Iron-binding ligands and humic substances in the San Francisco Bay estuary and estuarine-influenced shelf regions of coastal California. *Mar. Chem., SCOR WG 139: Organic Ligands – A Key Control on Trace Metal Biogeochemistry in the Ocean* 173, 183–194. <https://doi.org/10.1016/j.marchem.2014.11.005>

- Bundy, R.M., Biller, D.V., Buck, K.N., Bruland, K.W., Barbeau, K.A., 2014. Distinct pools of dissolved iron-binding ligands in the surface and benthic boundary layer of the California Current. *Limnol. Oceanogr.* 59, 769–787. <https://doi.org/10.4319/lo.2014.59.3.0769>
- Bundy, R.M., Boiteau, R.M., McLean, C., Turk-Kubo, K.A., McIlvin, M.R., Saito, M.A., Van Mooy, B.A.S., Repeta, D.J., 2018. Distinct Siderophores Contribute to Iron Cycling in the Mesopelagic at Station ALOHA. *Front. Mar. Sci.* 5. <https://doi.org/10.3389/fmars.2018.00061>
- Bundy, R.M., Jiang, M., Carter, M., Barbeau, K.A., 2016. Iron-Binding Ligands in the Southern California Current System: Mechanistic Studies. *Front. Mar. Sci.* 3. <https://doi.org/10/gf9rj2>
- Butler, A., 2005. Marine Siderophores and Microbial Iron Mobilization. *Biometals* 18, 369–374. <https://doi.org/10.1007/s10534-005-3711-0>
- Cabanes, D.J.E., Norman, L., Bowie, A.R., Strmečki, S., Hassler, C.S., 2020. Electrochemical evaluation of iron-binding ligands along the Australian GEOTRACES southwestern Pacific section (GP13). *Mar. Chem.* 219, 103736. <https://doi.org/10.1016/j.marchem.2019.103736>
- Cao, F., Zhu, Y., Kieber, D.J., Miller, W.L., 2020. Distribution and photo-reactivity of chromophoric and fluorescent dissolved organic matter in the Northeastern North Pacific Ocean. *Deep Sea Res. Part Oceanogr. Res. Pap.* 155, 103168. <https://doi.org/10.1016/j.dsr.2019.103168>
- Carpenter, J.H., 1965. The Accuracy of the Winkler Method for Dissolved Oxygen Analysis I. *Limnol. Oceanogr.* 10, 135–140. <https://doi.org/10.4319/lo.1965.10.1.0135>
- Carritt, D.E. & J.H. Carpenter. 1966. Comparison and evaluation of currently employed modifications of the Winkler method for determining dissolved oxygen in sea-water; a NASCO report. *J. Mar. Res.* 24, 286-318
- Coble, P.G., 2007. Marine Optical Biogeochemistry: The Chemistry of Ocean Color. *Chem. Rev.* 107, 402–418. <https://doi.org/10.1021/cr050350+>
- Coble, P.G., 1996. Characterization of marine and terrestrial DOM in seawater using excitation-emission matrix spectroscopy. *Mar. Chem.* 51, 325–346. [https://doi.org/10.1016/0304-4203\(95\)00062-3](https://doi.org/10.1016/0304-4203(95)00062-3)
- Coble, P.G., Lead, J., Baker, A., Reynolds, D.M., Spencer, R.G.M., 2014. *Aquatic Organic Matter Fluorescence*. Cambridge University Press.
- Croot, P.L., Heller, M.I., 2012. The Importance of Kinetics and Redox in the Biogeochemical Cycling of Iron in the Surface Ocean. *Front. Microbiol.* 3. <https://doi.org/10/ggr9x2>
- de Ronde, C.E.J., Baker, E.T., Massoth, G.J., Lupton, J.E., Wright, I.C., Sparks, R.J., Bannister, S.C., Reyners, M.E., Walker, S.L., Greene, R.R., Ishibashi, J., Faure, K., Resing, J.A., Lebon, G.T., 2007. Submarine hydrothermal activity along the mid-Kermadec Arc, New Zealand: Large-scale effects on venting. *Geochem. Geophys. Geosystems* 8. <https://doi.org/10.1029/2006GC001495>
- Dittmar, T., 2015. Chapter 7 - Reasons Behind the Long-Term Stability of Dissolved Organic Matter, in: Hansell, D.A., Carlson, C.A. (Eds.), *Biogeochemistry of Marine Dissolved Organic Matter (Second Edition)*. Academic Press, Boston, pp. 369–388. <https://doi.org/10.1016/B978-0-12-405940-5.00007-8>
- Dittmar, T., Lennartz, S.T., Buck-Wiese, H., Hansell, D.A., Santinelli, C., Vanni, C., Blasius, B., Hehemann, J.-H., 2021. Enigmatic persistence of dissolved organic matter in the ocean. *Nat. Rev. Earth Environ.* 2, 570–583. <https://doi.org/10.1038/s43017-021-00183-7>
- Dulaquais, G., Waeles, M., Gerringa, L.J.A., Middag, R., Rijkenberg, M.J.A., Riso, R., 2018. The Biogeochemistry of Electroactive Humic Substances and Its Connection to Iron Chemistry in the North East Atlantic and the Western Mediterranean Sea. *J. Geophys. Res. Oceans* 123, 5481–5499. <https://doi.org/10.1029/2018JC014211>
- Dulaquais, G., Fourrier, P., Tilliette, C., Guieu, C., Riso, R., in prep. The role of humic type ligands in the bioavailability and stabilization of dissolved iron in the Western Tropical South Pacific Ocean.

- Fellman, J.B., Hood, E., Spencer, R.G.M., 2010. Fluorescence spectroscopy opens new windows into dissolved organic matter dynamics in freshwater ecosystems: A review. *Limnol. Oceanogr.* 55, 2452–2462. <https://doi.org/10.4319/lo.2010.55.6.2452>
- Ferretto, N., Tedetti, M., Guigue, C., Mounier, S., Raimbault, P., Goutx, M., 2017. Spatio-temporal variability of fluorescent dissolved organic matter in the Rhône River delta and the Fos-Marseille marine area (NW Mediterranean Sea, France). *Environ. Sci. Pollut. Res.* 24, 4973–4989. <https://doi.org/10.1007/s11356-016-8255-z>
- Fourrier, P., Dulaquais, G., Guigue, C., Giamarchi, P., Sarthou, G., Whitby, H., Riso, R., 2022. Characterization of the vertical size distribution, composition and chemical properties of dissolved organic matter in the (ultra)oligotrophic Pacific Ocean through a multi-detection approach. *Mar. Chem.* 240, 104068. <https://doi.org/10.1016/j.marchem.2021.104068>
- Garcia, H.E., Gordon, L.I., 1992. Oxygen solubility in seawater: Better fitting equations. *Limnol. Oceanogr.* 37, 1307–1312. <https://doi.org/10.4319/lo.1992.37.6.1307>
- Genovese, C., Grotti, M., Pittaluga, J., Ardini, F., Janssens, J., Wuttig, K., Moreau, S., Lannuzel, D., 2018. Influence of organic complexation on dissolved iron distribution in East Antarctic pack ice. *Mar. Chem.* 203, 28–37. <https://doi.org/10.1016/j.marchem.2018.04.005>
- German, C.R., Baker, E.T., Connelly, D.P., Lupton, J.E., Resing, J., Prien, R.D., Walker, S.L., Edmonds, H.N., Langmuir, C.H., 2006. Hydrothermal exploration of the Fonualei Rift and Spreading Center and the Northeast Lau Spreading Center. *Geochem. Geophys. Geosystems* 7. <https://doi.org/10.1029/2006GC001324>
- Gerringa, L.J.A., Rijkenberg, M.J.A., Schoemann, V., Laan, P., de Baar, H.J.W., 2015. Organic complexation of iron in the West Atlantic Ocean. *Mar. Chem., Cycles of metals and carbon in the oceans - A tribute to the work stimulated by Hein de Baar* 177, 434–446. <https://doi.org/10.1016/j.marchem.2015.04.007>
- Gerringa, L.J.A., Rijkenberg, M.J.A., Thuróczy, C.-E., Maas, L.R.M., 2014. A critical look at the calculation of the binding characteristics and concentration of iron complexing ligands in seawater with suggested improvements. *Environ. Chem.* 11, 114–136. <https://doi.org/10.1071/EN13072>
- Gledhill, M., Achterberg, E.P., Li, K., Mohamed, K.N., Rijkenberg, M.J.A., 2015. Influence of ocean acidification on the complexation of iron and copper by organic ligands in estuarine waters. *Mar. Chem., Cycles of metals and carbon in the oceans - A tribute to the work stimulated by Hein de Baar* 177, 421–433. <https://doi.org/10.1016/j.marchem.2015.03.016>
- Gledhill, M., Buck, K.N., 2012. The Organic Complexation of Iron in the Marine Environment: A Review. *Front. Microbiol.* 3. <https://doi.org/10.3389/fmicb.2012.00069>
- Gledhill, M., van den Berg, C.M.G., 1994. Determination of complexation of iron(III) with natural organic complexing ligands in seawater using cathodic stripping voltammetry. *Mar. Chem.* 47, 41–54. [https://doi.org/10.1016/0304-4203\(94\)90012-4](https://doi.org/10.1016/0304-4203(94)90012-4)
- Gomez-Saez, G.V., Niggemann, J., Dittmar, T., Pohlabein, A.M., Lang, S.Q., Noowong, A., Pichler, T., Wörmer, L., Bühring, S.I., 2016. Molecular evidence for abiotic sulfurization of dissolved organic matter in marine shallow hydrothermal systems. *Geochim. Cosmochim. Acta* 190, 35–52. <https://doi.org/10.1016/j.gca.2016.06.027>
- Guieu, C., Bonnet, S., 2019. TONGA 2019 cruise, L'Atalante R/V. <https://doi.org/10.17600/18000884>
- Guieu, C., Bonnet, S., Petrenko, A., Menkes, C., Chavagnac, V., Desboeufs, K., Maes, C., Moutin, T., 2018. Iron from a submarine source impacts the productive layer of the Western Tropical South Pacific (WTSP). *Sci. Rep.* 8, 9075. <https://doi.org/10.1038/s41598-018-27407-z>
- Hassler, C.S., Berg, V.D., G, C.M., Boyd, P.W., 2017. Toward a Regional Classification to Provide a More Inclusive Examination of the Ocean Biogeochemistry of Iron-Binding Ligands. *Front. Mar. Sci.* 4. <https://doi.org/10.3389/fmars.2017.00019>
- Hassler, C.S., Legiret, F.-E., Butler, E.C.V., 2013. Measurement of iron chemical speciation in seawater at 4°C: The use of competitive ligand exchange–adsorptive cathodic stripping voltammetry. *Mar. Chem.* 149, 63–73. <https://doi.org/10.1016/j.marchem.2012.12.007>

- Hassler, C.S., Norman, L., Mancuso Nichols, C.A., Clementson, L.A., Robinson, C., Schoemann, V., Watson, R.J., Doblin, M.A., 2015. Iron associated with exopolymeric substances is highly bioavailable to oceanic phytoplankton. *Mar. Chem., SCOR WG 139: Organic Ligands – A Key Control on Trace Metal Biogeochemistry in the Ocean* 173, 136–147. <https://doi.org/10.1016/j.marchem.2014.10.002>
- Hassler, C.S., Schoemann, V., Nichols, C.M., Butler, E.C.V., Boyd, P.W., 2011. Saccharides enhance iron bioavailability to Southern Ocean phytoplankton. *Proc. Natl. Acad. Sci.* 108, 1076–1081. <https://doi.org/10.1073/pnas.1010963108>
- Hawkes, J. A., Connelly, D.P., Gledhill, M., Achterberg, E.P., 2013. The stabilisation and transportation of dissolved iron from high temperature hydrothermal vent systems. *Earth Planet. Sci. Lett.* 375, 280–290. <https://doi.org/10.1016/j.epsl.2013.05.047>
- Hawkes, Jeffrey A., Gledhill, M., Connelly, D.P., Achterberg, E.P., 2013. Characterisation of iron binding ligands in seawater by reverse titration. *Anal. Chim. Acta* 766, 53–60. <https://doi.org/10.1016/j.aca.2012.12.048>
- Heller, M., Gaiero, D., Croot, P., 2013. Basin scale survey of marine humic fluorescence in the Atlantic: Relationship to iron solubility and H<sub>2</sub>O<sub>2</sub>. *Glob. Biogeochem. Cycles* 27. <https://doi.org/10.1029/2012GB004427>
- Henderson, R.K., Baker, A., Parsons, S.A., Jefferson, B., 2008. Characterisation of algogenic organic matter extracted from cyanobacteria, green algae and diatoms. *Water Res.* 42, 3435–3445. <https://doi.org/10.1016/j.watres.2007.10.032>
- Hioki, N., Kuma, K., Morita, Y., Sasayama, R., Ooki, A., Kondo, Y., Obata, H., Nishioka, J., Yamashita, Y., Nishino, S., Kikuchi, T., Aoyama, M., 2014. Laterally spreading iron, humic-like dissolved organic matter and nutrients in cold, dense subsurface water of the Arctic Ocean. *Sci. Rep.* 4, 1–9. <https://doi.org/10/ggr9zs>
- Hudson, N., Baker, A., Reynolds, D., 2007. Fluorescence analysis of dissolved organic matter in natural, waste and polluted waters—a review. *River Res. Appl.* 23, 631–649. <https://doi.org/10.1002/rra.1005>
- Ishii, S.K.L., Boyer, T.H., 2012. Behavior of Reoccurring PARAFAC Components in Fluorescent Dissolved Organic Matter in Natural and Engineered Systems: A Critical Review. *Environ. Sci. Technol.* 46, 2006–2017. <https://doi.org/10.1021/es2043504>
- Jia, K., Manning, C.C.M., Jollymore, A., Beckie, R.D., 2021. Technical note: Effects of iron(II) on fluorescence properties of dissolved organic matter at circumneutral pH. *Hydrol. Earth Syst. Sci.* 25, 4983–4993. <https://doi.org/10.5194/hess-25-4983-2021>
- Kawabe, M., Fujio, S., 2010. Pacific ocean circulation based on observation. *J. Oceanogr.* 66, 389–403. <https://doi.org/10.1007/s10872-010-0034-8>
- Kleint, C., Bach, W., Diehl, A., Fröhberg, N., Garbe-Schönberg, D., Hartmann, J.F., de Ronde, C.E.J., Sander, S.G., Strauss, H., Stucker, V.K., Thal, J., Zitoun, R., Koschinsky, A., 2019. Geochemical characterization of highly diverse hydrothermal fluids from volcanic vent systems of the Kermadec intraoceanic arc. *Chem. Geol.* 528, 119289. <https://doi.org/10.1016/j.chemgeo.2019.119289>
- Kleint, C., Hawkes, J.A., Sander, S.G., Koschinsky, A., 2016. Voltammetric Investigation of Hydrothermal Iron Speciation. *Front. Mar. Sci.* 3, UNSP 75. <https://doi.org/10.3389/fmars.2016.00075>
- Kleint, C., Pichler, T., Koschinsky, A., 2017. Geochemical characteristics, speciation and size-fractionation of iron (Fe) in two marine shallow-water hydrothermal systems, Dominica, Lesser Antilles. *Chem. Geol.* 454, 44–53. <https://doi.org/10.1016/j.chemgeo.2017.02.021>
- Kleint, C., Zitoun, R., Neuholz, R., Walter, M., Schnetger, B., Klose, L., Chiswell, S.M., Middag, R., Laan, P., Sander, S.G., Koschinsky, A., 2022. Trace Metal Dynamics in Shallow Hydrothermal Plumes at the Kermadec Arc. *Front. Mar. Sci.* 8.

- Klunder, M.B., Laan, P., Middag, R., Baar, H.J.W. de, Bakker, K., 2012. Dissolved iron in the Arctic Ocean: Important role of hydrothermal sources, shelf input and scavenging removal. *J. Geophys. Res. Oceans* 117. <https://doi.org/10/ggr9xx>
- Klunder, M.B., Laan, P., Middag, R., De Baar, H.J.W., van Ooijen, J.C., 2011. Dissolved iron in the Southern Ocean (Atlantic sector). *Deep Sea Res. Part II Top. Stud. Oceanogr., Physics, Carbon Dioxide, Trace Elements and Isotopes in the Southern Ocean: The Polarstern Expeditions ANT XXIV-3 (2008) and ANT XXIII/3 (2006)* 58, 2678–2694. <https://doi.org/10.1016/j.dsr2.2010.10.042>
- Kok, M.D., Schouten, S., Sinninghe Damsté, J.S., 2000. Formation of insoluble, nonhydrolyzable, sulfur-rich macromolecules via incorporation of inorganic sulfur species into algal carbohydrates. *Geochim. Cosmochim. Acta* 64, 2689–2699. [https://doi.org/10.1016/S0016-7037\(00\)00382-3](https://doi.org/10.1016/S0016-7037(00)00382-3)
- Komaki, K., Kawabe, M., 2007. Structure of the upper deep current in the Melanesian Basin, western North Pacific. *Mer* 45, 15–22.
- Kowalczyk, P., Tilstone, G.H., Zabłocka, M., Röttgers, R., Thomas, R., 2013. Composition of dissolved organic matter along an Atlantic Meridional Transect from fluorescence spectroscopy and Parallel Factor Analysis. *Mar. Chem.* 157, 170–184. <https://doi.org/10.1016/j.marchem.2013.10.004>
- Kraemer, S.M., Butler, A., Borer, P., Cervini-Silva, J., 2005. Siderophores and the Dissolution of Iron-Bearing Minerals in Marine Systems. *Rev. Mineral. Geochem.* 59, 53–84. <https://doi.org/10/ffz3vv>
- Laglera, L.M., Battaglia, G., van den Berg, C.M.G., 2011. Effect of humic substances on the iron speciation in natural waters by CLE/CSV. *Mar. Chem.* 127, 134–143. <https://doi.org/10.1016/j.marchem.2011.09.003>
- Laglera, L.M., Battaglia, G., van den Berg, C.M.G., 2007. Determination of humic substances in natural waters by cathodic stripping voltammetry of their complexes with iron. *Anal. Chim. Acta* 599, 58–66. <https://doi.org/10.1016/j.aca.2007.07.059>
- Laglera, L.M., Caprara, S., Monticelli, D., 2016. Towards a zero-blank, preconcentration-free voltammetric method for iron analysis at picomolar concentrations in unbuffered seawater. *Talanta* 150, 449–454. <https://doi.org/10.1016/j.talanta.2015.12.060>
- Laglera, L.M., Sukekava, C., Slagter, H.A., Downes, J., Aparicio-Gonzalez, A., Gerringa, L.J.A., 2019. First Quantification of the Controlling Role of Humic Substances in the Transport of Iron Across the Surface of the Arctic Ocean. *Environ. Sci. Technol.* 53, 13136–13145. <https://doi.org/10/ggr9mn>
- Laglera, L.M., van den Berg, C.M.G., 2009. Evidence for geochemical control of iron by humic substances in seawater. *Limnol. Oceanogr.* 54, 610–619. <https://doi.org/10/bjw89d>
- Langdon, C., 2010. Determination of Dissolved Oxygen in Seawater by Winkler Titration Using The Amperometric Technique. <https://doi.org/10.25607/OBP-1350>
- Limson, J., Nyokong, T., Daya, S., 1998. The interaction of melatonin and its precursors with aluminium, cadmium, copper, iron, lead, and zinc: An adsorptive voltammetric study. *J. Pineal Res.* 24, 15–21. <https://doi.org/10.1111/j.1600-079X.1998.tb00361.x>
- Liu, X., Millero, F.J., 2002. The solubility of iron in seawater. *Mar. Chem.* 77, 43–54. [https://doi.org/10.1016/S0304-4203\(01\)00074-3](https://doi.org/10.1016/S0304-4203(01)00074-3)
- Lory, C., Van Wambeke, F., Fourquez, M., Barani, A., Guieu, C., Tilliette, C., Marie, D., Nunige, S., Berman-Frank, I., Bonnet, S., 2022. Assessing the contribution of diazotrophs to microbial Fe uptake using a group specific approach in the Western Tropical South Pacific Ocean. *ISME Commun.* 2, 1–11. <https://doi.org/10.1038/s43705-022-00122-7>
- Ma, H., Wang, P., Thompson, A., Xie, Q., Zhu, M., Teng, H.H., Fu, P., Liu, C., Chen, C., 2022. Secondary Mineral Formation and Carbon Dynamics during FeS Oxidation in the Presence of Dissolved Organic Matter. *Environ. Sci. Technol.* 56, 14120–14132. <https://doi.org/10.1021/acs.est.1c08727>



- Massoth, G.J., De Ronde, C.E.J., Lupton, J.E., Feely, R.A., Baker, E.T., Lebon, G.T., Maenner, S.M., 2003. Chemically rich and diverse submarine hydrothermal plumes of the southern Kermadec volcanic arc (New Zealand). *Geol. Soc. Lond. Spec. Publ.* 219, 119–139. <https://doi.org/10.1144/GSL.SP.2003.219.01.06>
- Mawji, E., Gledhill, M., Milton, J.A., Tarran, G.A., Ussher, S., Thompson, A., Wolff, G.A., Worsfold, P.J., Achterberg, E.P., 2008. Hydroxamate Siderophores: Occurrence and Importance in the Atlantic Ocean. *Environ. Sci. Technol.* 42, 8675–8680. <https://doi.org/10.1021/es801884r>
- Mentges, A., Feenders, C., Seibt, M., Blasius, B., Dittmar, T., 2017. Functional Molecular Diversity of Marine Dissolved Organic Matter Is Reduced during Degradation. *Front. Mar. Sci.* 4. <https://doi.org/10.3389/fmars.2017.00194>
- Millero, F.J., Sotolongo, S., Izaguirre, M., 1987. The oxidation kinetics of Fe(II) in seawater. *Geochim. Cosmochim. Acta* 51, 793–801. [https://doi.org/10.1016/0016-7037\(87\)90093-7](https://doi.org/10.1016/0016-7037(87)90093-7)
- Moore, C.M., Mills, M.M., Arrigo, K.R., Berman-Frank, I., Bopp, L., Boyd, P.W., Galbraith, E.D., Geider, R.J., Guieu, C., Jaccard, S.L., Jickells, T.D., La Roche, J., Lenton, T.M., Mahowald, N.M., Marañón, E., Marinov, I., Moore, J.K., Nakatsuka, T., Oschlies, A., Saito, M.A., Thingstad, T.F., Tsuda, A., Ulloa, O., 2013. Processes and patterns of oceanic nutrient limitation. *Nat. Geosci.* 6, 701–710. <https://www.nature.com/articles/ngeo1765>
- Nelson, N.B., Siegel, D.A., Carlson, C.A., Swan, C.M., 2010. Tracing global biogeochemical cycles and meridional overturning circulation using chromophoric dissolved organic matter. *Geophys. Res. Lett.* 37. <https://doi.org/10.1029/2009GL042325>
- Neuholz, R., Kleint, C., Schnetger, B., Koschinsky, A., Laan, P., Middag, R., Sander, S., Thal, J., Türke, A., Walter, M., Zitoun, R., Brumsack, H.-J., 2020. Submarine Hydrothermal Discharge and Fluxes of Dissolved Fe and Mn, and He Isotopes at Brothers Volcano Based on Radium Isotopes. *Minerals* 10, 969. <https://doi.org/10.3390/min10110969>
- Norman, L., Worms, I.A.M., Angles, E., Bowie, A.R., Nichols, C.M., Ninh Pham, A., Slaveykova, V.I., Townsend, A.T., David Waite, T., Hassler, C.S., 2015. The role of bacterial and algal exopolymeric substances in iron chemistry. *Mar. Chem., SCOR WG 139: Organic Ligands – A Key Control on Trace Metal Biogeochemistry in the Ocean* 173, 148–161. <https://doi.org/10.1016/j.marchem.2015.03.015>
- Ohno, T., Amirbahman, A., Bro, R., 2008. Parallel Factor Analysis of Excitation–Emission Matrix Fluorescence Spectra of Water Soluble Soil Organic Matter as Basis for the Determination of Conditional Metal Binding Parameters. *Environ. Sci. Technol.* 42, 186–192. <https://doi.org/10.1021/es071855f>
- Omori, Y., Hama, T., Ishii, M., Saito, S., 2010. Relationship between the seasonal change in fluorescent dissolved organic matter and mixed layer depth in the subtropical western North Pacific. *J. Geophys. Res. Oceans* 115. <https://doi.org/10.1029/2009JC005526>
- Oudot, C., Gerard, R., Morin, P., Gningue, I., 1988. Precise shipboard determination of dissolved oxygen (Winkler procedure) for productivity studies with a commercial system1. *Limnol. Oceanogr.* 33, 146–150. <https://doi.org/10.4319/lo.1988.33.1.0146>
- Pan, Y., Bates, S.S., Cembella, A.D., 1998. Environmental stress and domoic acid production by *Pseudo-nitzschia*: a physiological perspective. *Nat. Toxins* 6, 127–135. [https://doi.org/10.1002/\(SICI\)1522-7189\(199805/08\)6:3/4<127::AID-NT9>3.0.CO;2-2](https://doi.org/10.1002/(SICI)1522-7189(199805/08)6:3/4<127::AID-NT9>3.0.CO;2-2)
- Pernet-Coudrier, B., Waeles, M., Filella, M., Quentel, F., Riso, R.D., 2013. Simple and simultaneous determination of glutathione, thioacetamide and refractory organic matter in natural waters by DP-CSV. *Sci. Total Environ.* 463–464, 997–1005. <https://doi.org/10.1016/j.scitotenv.2013.06.053>
- Pižeta, I., Sander, S.G., Hudson, R.J.M., Omanović, D., Baars, O., Barbeau, K.A., Buck, K.N., Bundy, R.M., Carrasco, G., Croot, P.L., Garnier, C., Gerringa, L.J.A., Gledhill, M., Hirose, K., Kondo, Y., Laglera, L.M., Nuester, J., Rijkenberg, M.J.A., Takeda, S., Twining, B.S., Wells, M., 2015. Interpretation of complexometric titration data: An intercomparison of methods for estimating models of trace metal complexation by natural organic ligands. *Mar. Chem., SCOR WG 139:*

- Organic Ligands – A Key Control on Trace Metal Biogeochemistry in the Ocean 173, 3–24. <https://doi.org/10.1016/j.marchem.2015.03.006>
- Plank, S., Marchese, F., Genzano, N., Nolde, M., Martinis, S., 2020. The short life of the volcanic island New Late'iki (Tonga) analyzed by multi-sensor remote sensing data. *Sci. Rep.* 10, 22293. <https://doi.org/10.1038/s41598-020-79261-7>
- Portlock, G., Tilliette, C., Bonnet, S., Guieu, C., Whitby, H., Salaun, P., in prep. Distribution and behaviour of thiols and humic-like substances in the oligotrophic and hydrothermal waters of the Western South Tropical Pacific
- Raven, M.R., Keil, R.G., Webb, S.M., 2021a. Rapid, Concurrent Formation of Organic Sulfur and Iron Sulfides During Experimental Sulfurization of Sinking Marine Particles. *Glob. Biogeochem. Cycles* 35, e2021GB007062. <https://doi.org/10.1029/2021GB007062>
- Raven, M.R., Keil, R.G., Webb, S.M., 2021b. Microbial sulfate reduction and organic sulfur formation in sinking marine particles. *Science* 371, 178–181. <https://doi.org/10.1126/science.abc6035>
- Resing, J.A., Rubin, K.H., Embley, R.W., Lupton, J.E., Baker, E.T., Dziak, R.P., Baumberger, T., Lilley, M.D., Huber, J.A., Shank, T.M., Butterfield, D.A., Clague, D.A., Keller, N.S., Merle, S.G., Buck, N.J., Michael, P.J., Soule, A., Caress, D.W., Walker, S.L., Davis, R., Cowen, J.P., Reysenbach, A.-L., Thomas, H., 2011. Active submarine eruption of boninite in the northeastern Lau Basin. *Nat. Geosci.* 4, 799–806. <https://doi.org/10.1038/ngeo1275>
- Resing, J.A., Sedwick, P.N., German, C.R., Jenkins, W.J., Moffett, J.W., Sohst, B.M., Tagliabue, A., 2015. Basin-scale transport of hydrothermal dissolved metals across the South Pacific Ocean. *Nature* 523, 200–203. <https://doi.org/10.1038/nature14577>
- Rickard, D., Luther, G.W., 2007. Chemistry of Iron Sulfides. *Chem. Rev.* 107, 514–562. <https://doi.org/10.1021/cr0503658>
- Rijkenberg, M.J.A., Gerringa, L.J.A., Carolus, V.E., Velzeboer, I., de Baar, H.J.W., 2006. Enhancement and inhibition of iron photoreduction by individual ligands in open ocean seawater. *Geochimica et Cosmochimica Acta* 70, 2790–2805. <https://doi.org/10.1016/j.gca.2006.03.004>
- Rochelle-Newall, E.J., Fisher, T.R., 2002. Production of chromophoric dissolved organic matter fluorescence in marine and estuarine environments: an investigation into the role of phytoplankton. *Mar. Chem.* 77, 7–21. [https://doi.org/10.1016/S0304-4203\(01\)00072-X](https://doi.org/10.1016/S0304-4203(01)00072-X)
- Romera-Castillo, C., Sarmiento, H., Álvarez-Salgado, X.A., Gasol, J.M., Marrasé, C., 2011. Net Production and Consumption of Fluorescent Colored Dissolved Organic Matter by Natural Bacterial Assemblages Growing on Marine Phytoplankton Exudates. *Appl. Environ. Microbiol.* 77, 7490–7498. <https://doi.org/10.1128/AEM.00200-11>
- Rose, A.L., Waite, T.D., 2003. Effect of Dissolved Natural Organic Matter on the Kinetics of Ferrous Iron Oxygenation in Seawater. *Environ. Sci. Technol.* 37, 4877–4886. <https://doi.org/10.1021/es034152g>
- Rue, E.L., Bruland, K.W., 1995. Complexation of iron(III) by natural organic ligands in the Central North Pacific as determined by a new competitive ligand equilibration/adsorptive cathodic stripping voltammetric method. *Mar. Chem., The Chemistry of Iron in Seawater and its Interaction with Phytoplankton* 50, 117–138. [https://doi.org/10.1016/0304-4203\(95\)00031-L](https://doi.org/10.1016/0304-4203(95)00031-L)
- Sander, S.G., Koschinsky, A., 2011. Metal flux from hydrothermal vents increased by organic complexation. *Nat. Geosci.* 4, 145–150. <https://doi.org/10.1038/ngeo1088>
- Santana-Casiano, J.M., González-Santana, D., Devresse, Q., Hepach, H., Santana-González, C., Quack, B., Engel, A., González-Dávila, M., 2022. Exploring the Effects of Organic Matter Characteristics on Fe(II) Oxidation Kinetics in Coastal Seawater. *Environ. Sci. Technol.* 56, 2718–2728. <https://doi.org/10.1021/acs.est.1c04512>
- Sanvito, F., Monticelli, D., 2020. Fast iron speciation in seawater by catalytic Competitive Ligand Equilibration-Cathodic Stripping Voltammetry with tenfold sample size reduction. *Anal. Chim. Acta* 1113, 9–17. <https://doi.org/10.1016/j.aca.2020.04.002>

- Sanvito, F., Pacileo, L., Monticelli, D., 2019. Fostering and Understanding Iron Detection at the Ultratrace Level by Adsorptive Stripping Voltammetry with Catalytic Enhancement. *Electroanalysis* 31, 212–216. <https://doi.org/10.1002/elan.201800675>
- Sarma, N.S., Kiran, R., Rama Reddy, M., Iyer, S.D., Peketi, A., Borole, D.V., Krishna, M.S., 2018. Hydrothermal Alteration Promotes Humic Acid Formation in Sediments: A Case Study of the Central Indian Ocean Basin. *J. Geophys. Res. Oceans* 123, 110–130. <https://doi.org/10.1002/2017JC012940>
- Shaked, Y., Buck, K.N., Mellett, T., Maldonado, M.T., 2020. Insights into the bioavailability of oceanic dissolved Fe from phytoplankton uptake kinetics. *ISME J.* 14, 1182–1193. <https://doi.org/10.3389/fmicb.2012.00204>
- Shi, D., Xu, Y., Hopkinson, B.M., Morel, F.M.M., 2010. Effect of Ocean Acidification on Iron Availability to Marine Phytoplankton. *Science* 327, 676–679. <https://doi.org/10.1126/science.1183517>
- Silva, N., Rojas, N., Fedele, A., 2009. Water masses in the Humboldt Current System: Properties, distribution, and the nitrate deficit as a chemical water mass tracer for Equatorial Subsurface Water off Chile. *Deep Sea Res. Part II Top. Stud. Oceanogr., The Oceanography of the Eastern South Pacific II: The Oxygen Minimum Zone* 56, 1004–1020. <https://doi.org/10.1016/j.dsr2.2008.12.013>
- Sinninghe Damsté, J.S., De Leeuw, J.W., 1990. Analysis, structure and geochemical significance of organically-bound sulphur in the geosphere: State of the art and future research. *Org. Geochem., Proceedings of the 14th International Meeting on Organic Geochemistry* 16, 1077–1101. [https://doi.org/10.1016/0146-6380\(90\)90145-P](https://doi.org/10.1016/0146-6380(90)90145-P)
- Sinninghe Damsté, J.S., Rijpstra, W.I.C., Kock-van Dalen, A.C., De Leeuw, J.W., Schenck, P.A., 1989. Quenching of labile functionalised lipids by inorganic sulphur species: Evidence for the formation of sedimentary organic sulphur compounds at the early stages of diagenesis. *Geochim. Cosmochim. Acta* 53, 1343–1355. [https://doi.org/10.1016/0016-7037\(89\)90067-7](https://doi.org/10.1016/0016-7037(89)90067-7)
- Sohrin, R., Sempéré, R., 2005. Seasonal variation in total organic carbon in the northeast Atlantic in 2000–2001. *J. Geophys. Res. Oceans* 110. <https://doi.org/10.1029/2004JC002731>
- Spearman, C., 1904. The Proof and Measurement of Association between Two Things. *Am. J. Psychol.* 15, 72–101. <https://doi.org/10.2307/1412159>
- Stedmon, C., Álvarez-Salgado, X.A., 2011. Shedding light on a black box: UV–Visible spectroscopic characterization of marine dissolved organic matter. <https://doi.org/10.1126/science.opms.sb0001>
- Stedmon, C.A., Markager, S., 2005. Resolving the variability in dissolved organic matter fluorescence in a temperate estuary and its catchment using PARAFAC analysis. *Limnol. Oceanogr.* 50, 686–697. <https://doi.org/10.4319/lo.2005.50.2.0686>
- Sukekava, C., Downes, J., Slagter, H.A., Gerringa, L.J.A., Laglera, L.M., 2018. Determination of the contribution of humic substances to iron complexation in seawater by catalytic cathodic stripping voltammetry. *Talanta* 189, 359–364. <https://doi.org/10.1016/j.talanta.2018.07.021>
- Summers, N., Watling, L., 2021. Upper Bathyal Pacific Ocean biogeographic provinces from octocoral distributions. *Prog. Oceanogr.* 191, 102509. <https://doi.org/10.1016/j.pocean.2020.102509>
- Tagliabue, A., Mtshali, T., Aumont, O., Bowie, A.R., Klunder, M.B., Roychoudhury, A.N., Swart, S., 2012. A global compilation of dissolved iron measurements: focus on distributions and processes in the Southern Ocean 17. <https://doi.org/10.5194/bg-9-2333-2012>
- Talley, L.D., Pickard, G.L., Emery, W.J., Swift, J.H., 2011. Pacific Ocean, in: *Descriptive Physical Oceanography*. Elsevier, pp. 303–362. <https://doi.org/10.1016/B978-0-7506-4552-2.10010-1>
- Tani, H., Nishioka, J., Kuma, K., Takata, H., Yamashita, Y., Tanoue, E., Midorikawa, T., 2003. Iron(III) hydroxide solubility and humic-type fluorescent organic matter in the deep water column of the Okhotsk Sea and the northwestern North Pacific Ocean. *Deep Sea Res. Part Oceanogr. Res. Pap.* 50, 1063–1078. [https://doi.org/10.1016/S0967-0637\(03\)00098-0](https://doi.org/10.1016/S0967-0637(03)00098-0)

- Tedetti, M., Guigue, C., Mahieu, L., Fourier, P., Dulaquais, G., Benavides, M., Lefevre, D., in. prep. Chromophoric and fluorescent dissolved organic matter in the Western Tropical South Pacific
- Tedetti, M., Bigot, L., Turquet, J., Guigue, C., Ferretto, N., Goutx, M., Cuet, P., 2020. Influence of Freshwater Discharges on Biogeochemistry and Benthic Communities of a Coral Reef Ecosystem (La Réunion Island, Indian Ocean). *Front. Mar. Sci.* 7.
- Tilliette, C., Taillandier, V., Bouruet-Aubertot, P., Grima, N., Maes, C., Montanes, M., Sarthou, G., Vorrath, M.-E., Arnone, V., Bressac, M., González-Santana, D., Gazeau, F., Guieu, C., 2022. Dissolved Iron Patterns Impacted by Shallow Hydrothermal Sources Along a Transect Through the Tonga-Kermadec Arc. *Glob. Biogeochem. Cycles* 36, e2022GB007363. <https://doi.org/10.1029/2022GB007363>
- Timko, S., Maydanov, A., Pittelli, S., Conte, M., Cooper, W., Koch, B., Schmitt-Kopplin, P., Gonsior, M., 2015. Depth-dependent photodegradation of marine dissolved organic matter. *Front. Mar. Sci.* 2.
- Toner, B.M., Fakra, S.C., Manganini, S.J., Santelli, C.M., Marcus, M.A., Moffett, J.W., Rouxel, O., German, C.R., Edwards, K.J., 2009. Preservation of iron(II) by carbon-rich matrices in a hydrothermal plume. *Nat. Geosci.* 2, 197–201. <https://doi.org/10.1038/geo433>
- Tonnard, M., Planquette, H., Bowie, A.R., van der Merwe, P., Gallinari, M., Desprez de Gésincourt, F., Germain, Y., Gourain, A., Benetti, M., Reverdin, G., Tréguer, P., Boutorh, J., Cheize, M., Lacan, F., Menzel Barraqueta, J.-L., Pereira-Contreira, L., Shelley, R., Lherminier, P., Sarthou, G., 2020. Dissolved iron in the North Atlantic Ocean and Labrador Sea along the GEOVIDE section (GEOTRACES section GA01). *Biogeosciences* 17, 917–943. <https://doi.org/10/gm6ntr>
- Town, R.M., Filella, M., 2000. Dispelling the myths: Is the existence of L1 and L2 ligands necessary to explain metal ion speciation in natural waters? *Limnol. Oceanogr.* 45, 1341–1357. <https://doi.org/10.4319/lo.2000.45.6.1341>
- Twining, B.S., Baines, S.B., 2013. The Trace Metal Composition of Marine Phytoplankton. *Annu. Rev. Mar. Sci.* 5, 191–215. <https://doi.org/10.1146/annurev-marine-121211-172322>
- van den Berg, C.M.G., 1995. Evidence for organic complexation of iron in seawater. *Mar. Chem., The Chemistry of Iron in Seawater and its Interaction with Phytoplankton* 50, 139–157. [https://doi.org/10.1016/0304-4203\(95\)00032-M](https://doi.org/10.1016/0304-4203(95)00032-M)
- van den Berg, C.M.G., Huang, Z.Qiang., 1984. Direct electrochemical determination of dissolved vanadium in seawater by cathodic stripping voltammetry with the hanging mercury drop electrode. *Anal. Chem.* 56, 2383–2386. <https://doi.org/10.1021/ac00277a028>
- van den Berg, C.M.G., Nimmo, M., Abollino, O., Mentasti, E., 1991. The determination of trace levels of iron in seawater, using adsorptive cathodic stripping voltammetry. *Electroanalysis* 3, 477–484. <https://doi.org/10.1002/elan.1140030606>
- Vraspir, J.M., Butler, A., 2009. Chemistry of Marine Ligands and Siderophores. *Annu. Rev. Mar. Sci.* 1, 43–63. <https://doi.org/10.1146/annurev.marine.010908.163712>
- Wang, H., Resing, J.A., Yan, Q., Buck, N.J., Michael, S.M., Zhou, H., Liu, M., Walker, S.L., Yang, Q., Ji, F., 2021. The characteristics of Fe speciation and Fe-binding ligands in the Mariana back-arc hydrothermal plumes. *Geochim. Cosmochim. Acta* 292, 24–36. <https://doi.org/10.1016/j.gca.2020.09.016>
- Wang, H., Wang, W., Liu, M., Zhou, H., Ellwood, M.J., Butterfield, D.A., Buck, N.J., Resing, J.A., 2022. Iron ligands and isotopes in hydrothermal plumes over backarc volcanoes in the Northeast Lau Basin, Southwest Pacific Ocean. *Geochim. Cosmochim. Acta* 336, 341–352. <https://doi.org/10.1016/j.gca.2022.09.026>
- Wang, H., Yan, Q., Yang, Q., Ji, F., Wong, K.H., Zhou, H., 2019. The Size Fractionation and Speciation of Iron in the Longqi Hydrothermal Plumes on the Southwest Indian Ridge. *J. Geophys. Res. Oceans* 124, 4029–4043. <https://doi.org/10.1029/2018JC014713>
- Whitby, H., Bressac, M., Sarthou, G., Ellwood, M.J., Guieu, C., Boyd, P.W., 2020a. Contribution of Electroactive Humic Substances to the Iron-Binding Ligands Released During Microbial

- Remineralization of Sinking Particles. *Geophys. Res. Lett.* 47, e2019GL086685. <https://doi.org/10.1029/2019GL086685>
- Whitby, H., Planquette, H., Cassar, N., Bucciarelli, E., Osburn, C.L., Janssen, D.J., Cullen, J.T., González, A.G., Völker, C., Sarthou, G., 2020b. A call for refining the role of humic-like substances in the oceanic iron cycle. *Sci. Rep.* 10, 1–12. <https://doi.org/10.1038/s41598-020-62266-7>
- Whitby, H., van den Berg, C.M.G., 2015. Evidence for copper-binding humic substances in seawater. *Mar. Chem., SCOR WG 139: Organic Ligands – A Key Control on Trace Metal Biogeochemistry in the Ocean* 173, 282–290. <https://doi.org/10.1016/j.marchem.2014.09.011>
- Witter, A.E., Luther, G.W., 1998. Variation in Fe-organic complexation with depth in the Northwestern Atlantic Ocean as determined using a kinetic approach. *Mar. Chem.* 62, 241–258. [https://doi.org/10.1016/S0304-4203\(98\)00044-9](https://doi.org/10.1016/S0304-4203(98)00044-9)
- Wu, J., Luther, G.W., 1995. Complexation of Fe(III) by natural organic ligands in the Northwest Atlantic Ocean by a competitive ligand equilibration method and a kinetic approach. *Mar. Chem., The Chemistry of Iron in Seawater and its Interaction with Phytoplankton* 50, 159–177. [https://doi.org/10.1016/0304-4203\(95\)00033-N](https://doi.org/10.1016/0304-4203(95)00033-N)
- Yamashita, Y., Hashihama, F., Saito, H., Fukuda, H., Ogawa, H., 2017. Factors controlling the geographical distribution of fluorescent dissolved organic matter in the surface waters of the Pacific Ocean. *Limnol. Oceanogr.* 62, 2360–2374. <https://doi.org/10.1002/lno.10570>
- Yeo, I.A., McIntosh, I.M., Bryan, S.E., Tani, K., Dunbabin, M., Metz, D., Collins, P.C., Stone, K., Manu, M.S., 2022. The 2019-2020 volcanic eruption of Late’iki (Metis Shoal), Tonga. *Sci. Rep.* 12, 7468. <https://doi.org/10.1038/s41598-022-11133-8>
- Yokoi, K., van den Berg, C.M.G., 1992. The determination of iron in seawater using catalytic cathodic stripping voltammetry. *Electroanalysis* 4, 65–69. <https://doi.org/10.1002/elan.1140040113>
- Yücel, M., Gartman, A., Chan, C.S., Luther, G.W., 2011. Hydrothermal vents as a kinetically stable source of iron-sulphide-bearing nanoparticles to the ocean. *Nat. Geosci.* 4, 367–371. <https://doi.org/10.1038/ngeo1148>
- Yücel, M., Sevgen, S., Le Bris, N., 2021. Soluble, Colloidal, and Particulate Iron Across the Hydrothermal Vent Mixing Zones in Broken Spur and Rainbow, Mid-Atlantic Ridge. *Front. Microbiol.* 12.
- Zigah, P.K., McNichol, A.P., Xu, L., Johnson, C., Santinelli, C., Karl, D.M., Repeta, D.J., 2017. Allochthonous sources and dynamic cycling of ocean dissolved organic carbon revealed by carbon isotopes. *Geophys. Res. Lett.* 44, 2407–2415. <https://doi.org/10.1002/2016GL071348>





## 6. Conclusion

The understanding of the marine Fe cycle is an essential step to explain primary production and carbon fixation. The fate of the organic speciation of Fe gained increasing interest over the last decades, however, its investigation is still hampered by the technical difficulties inherent to the characterisation of the fraction of the DOM able to bind with Fe. These Fe-binding ligands can be titrated using the CLE-ACSV approach, an electrochemical technic providing an estimation of the ligand concentration and binding strength, but to date, the CLE-ACSV technique suffers from limitations. In this Thesis, I targeted several methodological limitations of the CLE-ACSV technique, aiming to improve CLE-ACSV application and data interpretation. If adopted by the community, these developments will lead to improved comparability between CLE-ACSV studies and a greater confidence in Fe-ligand data. Ultimately, the accumulation and integration of these results into multi-approach studies combining lab-based and modelling works would provide a more holistic constraint on the global Fe cycle.

### 6.1. Summary of my findings

The limiting aspects regarding the use of the ligand NN to investigate DFe were addressed in Chapter 3. I showed that the recorded signal can be enhanced by at least 10-fold by oxygen catalysis compared to deoxygenated conditions, and that optimal enhancement is reached in absence of buffering of the sample. This is solving at once the issue related to fixing the pH, impacting DFe speciation, and to the lack of sensitivity of the deoxygenated method, limiting the investigation of the pH impact on Fe organic speciation. An unfortunate limitation of our application is the presence of an interfering signal in oxygenated samples, limiting the use of the NN-Air method in the present conditions. However, the procedure to verify the presence of this interference is simple and can be easily verified by other users. If ensured free of interference, my method development could help constrain the fate of natural pH gradient and of ocean acidification on Fe organic speciation. My development regarding the preparation of the NN solution in Milli-Q water would also allow facilitate the use of lower detection window for to accurately titrate humic-substances. The performance of such analysis in unbuffered samples and in



volume as low as 0.5 mL as presented from my apparatus development is shown to be possible for deoxygenated samples, and can be verified in oxygenated conditions for enhanced sensitivity.

The Chapter 4 can be seen as an attempt to develop a ‘toolbox’ to facilitate the implementation of CLE-ACSV analysis using SA for new users. I presented detailed procedure for faster conditioning, analysis, and data extraction, that I can help new users to implement my updated SA method. I also performed replicate analyses to constrain the accuracy of its application. Most importantly, I have developed a step by step procedure for statistically-driven interpretation of the titration curves based on the freely available software ProMCC and home-made spreadsheet (Annex 4). In addition to facilitate the interpretation of the data for non-familiar users, it helps keeping track of the interpretation performed, and lowers the impact of the analyst’s subjectivity. The procedure was successfully applied in Chapter 4 and 5, and by other analysts (L. Artigue and K. Buck, pers. comm.). It is a step forward toward better comparability of complexometric titration data. The procedure is, however, still perfectible, and users should reach out to discuss the validity of its use in specific application.

The application of the development regarding the use of SA was performed on samples collected in the Western Tropical South Pacific, hotspot of diazotrophic and hydrothermal activity. On the 103 titrations performed, 84% had a  $\log K_{\text{FeL,Fe}'}^{\text{cond}}$  falling into the  $L_2$  ligand class, characteristic of humic-substances. In fact, 20 to 40% of the Fe-binding ligand concentrations measured in surface waters (mean of  $5.2 \pm 1.2 \text{ nmoleqFe.L}^{-1}$ ) were explained by electroactive humic-substances, more concentrated in the mixed layer. Electroactive substances only explained 8 to 18% of the Fe-binding ligands measured in deep waters. The fluorescence of humic-substances showed a distribution inverse to electroactive humic-substances, suggesting a shift from electroactive in surface waters to fluorescent in deep waters. The comparison of my data with electroactivity and fluorescence of humic substances helped to constrain the role of humic-substances in the composition of the DOM able to bond with Fe in waters impacted by intense diazotrophic and hydrothermal activity, and calls for more comparison of these complementary datasets in future works.

## 6.2. Future and perspectives

To date, the fate of pH on Fe organic speciation is not empirically resolved. Modelling approaches have been developed to predict the fractionation between organic and inorganic phases of Fe, but the lack of empirical constraint on the DOM binding-sites and, therefore, of their sensitivity to changes in protonation at different pH is still limiting the outputs of these models. CLE-ACSV titrations provide data that is conditional to the temperature and pH during the measurement, which are typically performed at room temperature controlled by addition of a buffer to a pH of around 8. However, it is still unclear how this data should be interpreted in the context of samples taken from very different natural conditions, particularly with relation to pH. Previous work exploring the impact of pH on CLE-ACSV titrations to estimate the fate of ocean acidification on Fe speciation were limited by the lack of sensitivity of the added ligand NN in the absence of catalytic enhancement of the signal (Avendaño et al., 2016; Gledhill et al., 2015; Zhu et al., 2021b, 2021a). The recent method development to perform catalysed CLE-ACSV titrations in unpurged and unbuffered solutions as presented by Sanvito and Monticelli (2021) for DHN and in Chapter 3 for NN could improve the characterisation of the pH impact on Fe-binding ligands properties. This is of specific interest for global biogeochemical modelling. Despite progress in integrating Fe-binding ligands into the models aiming to reproduce DFe distribution (Boyd and Tagliabue, 2015; Tagliabue and Völker, 2011; Völker and Tagliabue, 2015; Völker and Ye, 2022), to date the impact of pH on Fe-binding ability of the DOM has been difficult to implement, as there is no suitable CLE-ACSV data available. The experimental procedure suggested in Chapter 3 could help obtaining this essential data.

The characterisation of Fe-binding ligand characteristics by CLE-ACSV can provide additional constraints on the Fe cycle. The isotopy of Fe helps to constrain its sources and internal cycling (König et al., 2021) but specific processes are still poorly constrained. Notably, the isotopic signature of hydrothermally sourced DFe is not optimally constrained in biogeochemical models. This is presumably due to lack of knowledge about the interplay between dissolved and particulate fractions (König et al., 2021), itself limited by the number of observations regarding highly dynamic and variable hydrothermal systems. The determination of the isotopic fraction of DFe is notably limited by the heaviness of the

procedure (Ellwood et al., 2020), that could possibly be avoided by the characterisation of tracer of Fe isotopic fractionation in hydrothermal fluids. A linear relationship was recently shown between hydrothermal DFe isotopic signature and Fe-binding ligand (Wang et al., 2022), suggesting that the Fe-binding ligand titrations could provide valuable information regarding the DFe isotopic fractionation processes in hydrothermal fluids. Technical requirements are lighter for CLE-ACSV titrations, that are performed with cheaper equipment, could be performed at sea, and with much lower sample volume requirement (generally 250 mL for CLE-ACSV, 2 L for the determination of the isotopic fraction). The required sample volume can even be lowered in view of the technical progresses in CLE-ACSV (Sanvito and Monticelli, 2020; Chapter 3, 4). It would take some effort to verify the possibility for Fe-binding ligand strength to proxy the Fe isotopic weight in hydrothermal fluid, but this is a good example of the potential for Fe-binding ligand titration data to address gaps in our knowledge of the Fe cycle.

The production and comparison of data from multiple analytical procedures is a widely acknowledge need in oceanography to understand the complex machinery driving biogeochemical cycles. The correlation of DFe with Fe-binding ligand characteristics and complementary analyses presented in Chapter 5 highlighted the potential to describe DFe distribution from the combination of the CLE-ACSV, looking at the whole bulk of ligands, with methods targeting specific Fe-binding ligand fractions. I strongly suggest to explore further the potential of the comparison of Fe-binding ligands characteristic defined by CLE-ACSV with fluorescence analysis. Future studies should incorporate quenching experiments that could allow the quantification of the amount of DFe that can be bond to fluorescent fraction (Esteves da Silva et al., 1998). It would be of interest to compare the concentrations of DFe that can be bond by the different fractions analysed by fluorescence and voltammetry and to compare them with the ability of the whole bulk of Fe-binding ligands determined by CLE-ACSV.

Together with multiple approaches to characterise Fe organic speciation, the consideration of the inorganic side is also needed in further investigation. A convincing proof of that need was presented by (Croot and Heller, 2012) who highlighted the dynamics intricacies between the organic and inorganic phases of iron with electrochemical approaches. These authors compared the CLE-ACSV approach based on the assumption of thermodynamic equilibrium of the sample (Chapter 2) with a kinetic

approach, quantifying the association and dissociation constants of the natural Fe-binding ligands against the added ligand TAC. The results of this study showed that Fe solubility progressively decreases with time. Their interpretation of the process at play was that organically bound Fe to weak ligands was progressively removed from the dissolved phase by formation of Fe-oxyhydroxide aggregates within hours (Croot and Heller, 2012). However, even if Fe-oxyhydroxides are less reactive with aging, they can be solubilised by Fe-binding ligands while freshly formed (Kraemer et al., 2005). It is of specific interest to consider the balance between Fe organic binding to weak ligands and Fe-oxyhydroxides reactivity in further work aiming to evaluate the processes controlling the dynamic and unstable Fe cycle *in-situ*. With that regard, a kinetic approach seems to better suit this purpose than the CLE-ACSV. To date, kinetic approaches have limited time resolution due to technical limitations. I suggest to apply the recent progresses regarding the analysis time presented in Chapter 3 and Chapter 4 to perform kinetic experiments at the minute to hour scale. Tests on individual and mixture of reference compounds would help to define the optimal added ligand concentration for which the dissociation of natural Fe-binding ligand complexes will be resolved enough to distinguish different ligand classes or binding-sites. This is calling for rapid development of kinetic analysis for their future integration to collaborative multi-approach studies in the field.

To conclude, my work draws a path to reach the objectives listed above. The NN-Air method could be successfully applied in future work, the procedures I have developed are allowing better comparability between laboratories, and my updated SA application is a promising tool to investigate exchange kinetics of natural Fe-binding ligands. The currently applied methods allow the comparison of Fe-binding ligand data obtained by CLE-ACSV with analyses targeting more specific fraction of the DOM and help disentangling the processes driving DFe distribution, attesting of the interest to keep performing CLE-ACSV analysis. I believe laboratory and *in-situ* incubation experiments focusing on relating Fe solubility with DOM aging and mineralization (traced with fluorescence and voltammetry) will be an essential step if owing to better understand the global distribution of Fe.

### 6.3. References

- Avendaño, L., Gledhill, M., Achterberg, E.P., Rérolle, V.M.C., Schlosser, C., 2016. Influence of Ocean Acidification on the Organic Complexation of Iron and Copper in Northwest European Shelf Seas; a Combined Observational and Model Study. *Front. Mar. Sci.* 3. <https://doi.org/10.3389/fmars.2016.00058>
- Boyd, P.W., Tagliabue, A., 2015. Using the L\* concept to explore controls on the relationship between paired ligand and dissolved iron concentrations in the ocean. *Marine Chemistry, SCOR WG 139: Organic Ligands – A Key Control on Trace Metal Biogeochemistry in the Ocean* 173, 52–66. <https://doi.org/10.1016/j.marchem.2014.12.003>
- Croot, P.L., Heller, M.I., 2012. The Importance of Kinetics and Redox in the Biogeochemical Cycling of Iron in the Surface Ocean. *Front. Microbiol.* 3. <https://doi.org/10/ggr9x2>
- Ellwood, M.J., Strzepak, R.F., Strutton, P.G., Trull, T.W., Fourquez, M., Boyd, P.W., 2020. Distinct iron cycling in a Southern Ocean eddy. *Nat Commun* 11, 825. <https://doi.org/10/ggr9f9>
- Esteves da Silva, J.C.G., Machado, A.A.S.C., Oliveira, C.J.S., Pinto, M.S.S.D.S., 1998. Fluorescence quenching of anthropogenic fulvic acids by Cu(II), Fe(III) and UO<sub>2</sub><sup>2+</sup>. *Talanta* 45, 1155–1165. [https://doi.org/10.1016/S0039-9140\(97\)00224-5](https://doi.org/10.1016/S0039-9140(97)00224-5)
- Gledhill, M., Achterberg, E.P., Li, K., Mohamed, K.N., Rijkenberg, M.J.A., 2015. Influence of ocean acidification on the complexation of iron and copper by organic ligands in estuarine waters. *Marine Chemistry, Cycles of metals and carbon in the oceans - A tribute to the work stimulated by Hein de Baar* 177, 421–433. <https://doi.org/10.1016/j.marchem.2015.03.016>
- König, D., Conway, T.M., Ellwood, M.J., Homoky, W.B., Tagliabue, A., 2021. Constraints on the Cycling of Iron Isotopes From a Global Ocean Model. *Global Biogeochemical Cycles* 35, e2021GB006968. <https://doi.org/10.1029/2021GB006968>
- Kraemer, S.M., Butler, A., Borer, P., Cervini-Silva, J., 2005. Siderophores and the Dissolution of Iron-Bearing Minerals in Marine Systems. *Reviews in Mineralogy and Geochemistry* 59, 53–84. <https://doi.org/10/ffz3vv>
- Sanvito, F., Monticelli, D., 2021. Exploring bufferless iron speciation in seawater by Competitive Ligand Equilibration-Cathodic Stripping Voltammetry: Does pH control really matter? *Talanta* 229, 122300. <https://doi.org/10.1016/j.talanta.2021.122300>
- Sanvito, F., Monticelli, D., 2020. Fast iron speciation in seawater by catalytic Competitive Ligand Equilibration-Cathodic Stripping Voltammetry with tenfold sample size reduction. *Analytica Chimica Acta* 1113, 9–17. <https://doi.org/10.1016/j.aca.2020.04.002>
- Tagliabue, A., Völker, C., 2011. Towards accounting for dissolved iron speciation in global ocean models. *Biogeosciences* 8, 3025–3039. <https://doi.org/10.5194/bg-8-3025-2011>
- Völker, C., Tagliabue, A., 2015. Modeling organic iron-binding ligands in a three-dimensional biogeochemical ocean model. *Marine Chemistry, SCOR WG 139: Organic Ligands – A Key Control on Trace Metal Biogeochemistry in the Ocean* 173, 67–77. <https://doi.org/10.1016/j.marchem.2014.11.008>
- Völker, C., Ye, Y., 2022. Feedbacks Between Ocean Productivity and Organic Iron Complexation in Reaction to Changes in Ocean Iron Supply. *Frontiers in Marine Science* 9.
- Wang, H., Wang, W., Liu, M., Zhou, H., Ellwood, M.J., Butterfield, D.A., Buck, N.J., Resing, J.A., 2022. Iron ligands and isotopes in hydrothermal plumes over backarc volcanoes in the Northeast Lau Basin, Southwest Pacific Ocean. *Geochimica et Cosmochimica Acta* 336, 341–352. <https://doi.org/10.1016/j.gca.2022.09.026>
- Zhu, K., Birchill, A.J., Milne, A., Ussher, S., Humphreys, M.P., Carr, N., Mahaffey, C., Lohan, M.C., Achterberg, E.P., Gledhill, M., 2021a. Equilibrium calculations of iron speciation and apparent iron solubility in the Celtic Sea at ambient seawater pH using the NICA-Donnan model. *Marine Chemistry* 237, 104038. <https://doi.org/10.1016/j.marchem.2021.104038>

Zhu, K., Hopwood, M.J., Groenenberg, J.E., Engel, A., Achterberg, E.P., Gledhill, M., 2021b. Influence of pH and Dissolved Organic Matter on Iron Speciation and Apparent Iron Solubility in the Peruvian Shelf and Slope Region. *Environ. Sci. Technol.* 55, 9372–9383. <https://doi.org/10.1021/acs.est.1c02477>

## 7. Annexs

The protocol and procedures developed in this work were developed and are owned by L. Mahieu. Any publicable use of them must refer to this Thesis.

Regarding the nature of the annexs (mostly Excel spreadsheets), they were made freely available following the link below:

<https://www.dropbox.com/sh/o0zvyjnn1qn0460/AAA8QpdTomualGBbgrjcLZJ4a?dl=0>

Annex 1: Optical calibration of NN-MQ solutions

Annex 2: Data handling with the ECDSOft

Annex 3: Protocol for the interpretation of ligand titration

Annex 4: Spreadsheet for the interpretation of ligand titration

Annex 5: Link for video tutorial for the interpretation of ligand titration

